

THEORETICAL STUDIES OF CHEMISORPTION

Thesis by
Stephen Perry Walch

In Partial Fulfillment of the Requirements
for the Degree of
Doctor of Philosophy

California Institute of Technology
Pasadena, California

1977

(Submitted March 29, 1977)

ACKNOWLEDGMENTS

I wish to thank my research advisor, Dr. William A. Goddard III, for his advice and guidance during the course of my graduate studies. I also wish to thank the other members of our research group for helpful and stimulating discussions.

Financial support from the Department of Health, Education and Welfare in the form of an NDEA Title IV fellowship, from the National Science Foundation, and from the California Institute of Technology is gratefully acknowledged.

Supplementary financial assistance from the Veterans Administration is also gratefully acknowledged.

Finally, I wish to thank my wife, Madeline, for having put up with four years of the Naval Service followed by four years of graduate study.

ABSTRACT

PART A: GVB and GVB-CI wavefunctions (using a double zeta basis)

have been obtained as a function of internuclear distance for the lowest three states of NiCO. The wavefunctions lead to a qualitative description in which the Ni atom is neutral with a $(4s)^1(3d)^9$ atomic configuration. The CO lone pair delocalizes slightly onto the Ni, leading to the 4s-like orbital hybridizing away from the CO. The $d\pi$ pairs on the Ni are slightly back-bonding to the CO. The three bound states are ${}^3\Sigma^+$, ${}^3\Pi$, and ${}^3\Delta$ consisting of the singly occupied 4s-like orbital plus a single d hole in a σ , π , or δ orbital, respectively. The ground state is found to be ${}^3\Delta$ with calculated $R_e = 1.90\text{\AA}$, $D_e = 1.15\text{ eV} = 26.5\text{ kcal/mol}$, and $\omega_c(\text{Ni-C}) = 428\text{ cm}^{-1}$, all reasonable values, although direct information on NiCO is not yet available. The adiabatic excitation energies are calculated as 0.240 eV to ${}^3\Sigma^+$ and 0.293 eV to ${}^3\Pi$. The states with $(4s)^2(3d)^8$ configurations on the Ni lead to repulsive potential curves with vertical excitation energies in the range of 3.0 to 5.0 eV.

PART B: Configuration interaction calculations have been carried out for a number of positive ion states of NiCO. These calculations indicate that there are two distinct groups of ionization potentials. The first group involves ionizations out of Ni-like orbitals. The lowest states of this group involve ionization out of a Ni 4s-like orbital leading to a $3d^9$ configuration and states of symmetry ${}^2\Sigma^+$,

$^2\Pi$, and $^2\Delta$ depending on whether the 3d-hole is taken in a σ , π , or δ orbital. At the optimum geometry of NiCO, the dissociation energy of NiCO⁺ to Ni⁺(2D) and CO is calculated to be 2.26, 2.03 and 2.50 eV for the $^2\Sigma^+$, $^2\Pi$, and $^2\Delta$ states, respectively, in reasonable agreement with the value of 2.10 eV calculated from the experimental heat of formation of NiCO⁺. Other states in the first group involve ionization out of Ni 3d orbitals leading to a group of ion states with a width of 3.1 eV. This is in good agreement with the Ni d bandwidth as observed in photoemission experiments. The second group of ion states correlates at large Ni-C separation with the ground state of the Ni atom and various states of CO⁺. The principal change as compared with free CO is that the $\overline{5\sigma}$ ionization (lone pair on the CO) increases in energy by about 2.5 eV, whereas the $\overline{4\sigma}$ and $\overline{1\pi}$ ionizations change only slightly. This leads to the $\overline{5\sigma}$ and $\overline{1\pi}$ ionizations being nearly degenerate, with the $\overline{4\sigma}$ ionization about 3.0 eV higher, in agreement with the currently accepted interpretation of the photoelectron spectrum of CO chemisorbed on Ni.

PART C: Geometries for O and S overlayers on the (100) and (110) surfaces of Ni have been calculated using ab initio wavefunctions for O and S bonded to small clusters of Ni atoms (1 to 5 Ni atoms). The calculated geometries are within 0.07Å of the results of dynamic LEED intensity calculations, indicating that accurate geometries of chemisorbed atoms may be obtained from calculations using clusters including only those metal atoms within bonding distance.

PART D: Electronic wavefunctions have been obtained as a function of geometry for a S atom bonded to Ni clusters consisting of 1 to 4 atoms designed to model bonding to the Ni(100) and Ni(110) surfaces. Electron correlation effects were included using the generalized valence bond and configuration interaction methods.

Modeling the (100) surface with four Ni atoms, we find the optimum S position to be 1.33\AA above the surface, in good agreement with the value ($1.30 \pm 0.10\text{\AA}$) from dynamic LEED intensity calculations. The bonding is qualitatively like that in H_2S with two covalent bonds to one diagonal pair of Ni atoms. There is a S $p\pi$ pair overlapping the other diagonal pair of Ni atoms. [Deleting this pair the S moves in to a position 1.04\AA from the surface.] There are two equivalent such structures, the resonance leading to equivalent S atoms and a $c(2 \times 2)$ structure for the S overlayer. The Ni in the layer beneath the surface seems to have little effect ($\sim 0.03\text{\AA}$) on the calculated geometry.

The above model of the bonding suggests that for the (110) surface the S lies along the long edge of the rectangular unit cell (2 coordinate) rather than at the four coordinate site usually assumed. Our calculated position for the S of 1.04\AA is in reasonable agreement with the value from dynamic LEED intensity calculations, $0.93 \pm 0.10\text{\AA}$

Bonding the S directly above a single Ni atom leads to a much weaker bond ($D_e = 3.32 \text{ eV}$) than does bonding in a bridge position ($D_e = 5.37 \text{ eV}$).

PART E: Electronic wavefunctions have been obtained as a function of geometry for an O atom bonded to Ni clusters (consisting of 1 to 5 atoms) designed to model bonding to the Ni(100) and Ni(110) surfaces. Electron correlation effects were included using the generalized valence bond and configuration interaction methods.

For the (100) surface, we find that the charge distribution for the full O overlayer is consistent with taking a positively charged cluster. The four surface atoms in the surface unit cell and the atom beneath the surface are important in determining the geometry, leading to a Ni_5^+O cluster as the model for the (100) surface. The optimum oxygen position with this model is 0.96\AA above the surface (four-fold coordinate site) in good agreement with the value $(0.90 \pm 0.10\text{\AA})$ from dynamic LEED intensity analysis. The atom beneath the surface allows important polarization effects for the positively charged cluster. The bonding to the surface involves bridging two diagonal surface Ni atoms. There is an $\text{O}(2p\pi)$ pair which overlaps the other diagonal pair of Ni atoms leading to nonbonded repulsions which increase the distance above the surface. There are two equivalent such structures, the resonance leading to a $c(2 \times 2)$ structure for the O overlayer.

The above model suggests that for the (110) surface the O lies along the long edge of the rectangular unit cell. For this registry with the surface, calculations based on Ni_2O and Ni_3O models indicate that the oxygen is only 0.1\AA above the plane of the surface.

PART F: Generalized valence bond and configuration interaction wave-

functions have been obtained as a function of R for numerous electronic states of NiO. All the lower states are found to involve the $(4s)^1(3d)^9$ Ni atom configuration and O in the $(2s)^2(2p)^4$ configuration. There are two groups of states.

The lower group of states involves pairing singly occupied Ni(4s) and O($2p\sigma$) orbitals into a (somewhat ionic) sigma bond pair with various pairings of the Ni($3d$)⁹ and O($2p\pi$)³ configurations. This leads to a number of states including the ground state which we find to be $X^3\Sigma^-$. (The electronic structure is analogous to that of O_2 .) The calculated D_0 and R_e for the $X^3\Sigma^-$ state of NiO are 89.9 Kcal/mole and 1.60Å respectively. The bond energy is in good agreement with the experimental value 86.5 ± 5 Kcal/mole, while the R_e value is not known experimentally.

The higher group of states involve a doubly occupied O($2p\sigma$) orbital. The Ni(4s) orbital in this case is non-bonding and builds in 4p character to move away from the oxygen orbitals. The bonding mainly involves stabilization of the oxygen orbitals by the Ni($3d$)⁹ core (somewhat analogously to the bonding in NiCO). Numerous allowed transitions between these states and the states of the lower group are calculated to be in the range 1.0 to 3.0 eV where numerous bands are seen in emission.

PREFACE

The subject of this thesis is the theoretical description of the bonding of atoms and molecules to Ni surfaces. Our theoretical model replaces the semi-infinite solid by small clusters of Ni atoms. We solve for the states of the small clusters using the ab initio generalized valence bond (GVB) method [which differs from the usual Hartree-Fock (HF) method in that it includes the dominant electron correlation effects necessary to describe bond formation]. From the results we conclude that the chemisorptive bond is sufficiently localized that these calculations are applicable to the semi-infinite solid.

The results are quite encouraging. We find that geometries are very well described using small clusters. For example, using a Ni₅ cluster the geometries for O and S overlayers on the (100) surface of Ni are determined to within 0.07⁰Å of the results of dynamic LEED intensity analysis. Thus, the chemisorptive bond appears to be localized and dominated by the positions of the Ni atoms to which it is bonded.

Bond energies are less well described by small clusters since bond disruption effects involving the semi-infinite solid are not included. For purposes of comparing bond energies for various species on the Ni surface, we use a single Ni atom to model the surface for sites where the bonding is directly above a surface Ni atom (linear site) and two Ni atoms at $\sqrt{2}$ times the nearest neighbor separation [as appropriate to the (100) and (110) surfaces] for bridged sites. These

clusters have essentially zero bond energy, thus no bond disruption effects are included and the resulting bond energies may be thought of as upper bounds to the actual bond energy. Thus, we expect that relative bond energies for different species at the same site should be accurate, since comparable bond disruption effects are involved. Based on this assumption it has been possible to develop tables of bond energies for various species at bridged and linear sites leading to useful predictions about mechanisms.

We find that the bonding shifts in the photoelectron spectrum associated with chemisorption are also well described with a small cluster. For example, even the simple NiCO model leads to calculated bonding shifts in reasonable agreement with experimental values for CO chemisorbed on Ni(111). However, the relaxation shifts resulting from polarization effects involving the bulk metal are not described by such a small cluster and at the present time we have not carried out calculations for sufficiently large clusters to obtain accurate absolute values for the ionization potentials.

In addition to the utility of these results for understanding chemistry on metal surfaces, the results of some of the smaller clusters (e.g., NiO and NiCO) are of direct chemical interest, since such molecules are prototypes for the bonding in small transition metal compounds (for which experimental evidence is only now becoming available). The bonding in these simple cases is expected to be different from cases where more ligands are attached to the metal atom.

In Part A we consider the bonding in the NiCO molecule. We find that the wavefunction leads to a qualitative description in which the Ni atom has the $(4s)^1(3d)^9$ atomic configuration. The bond is due to stabilization of the CO 5σ orbital (essentially a C lone pair) from interaction with the partially exposed Ni^+3d^9 core, resulting from hybridization of the singly occupied Ni(4s) orbital away from the CO molecule.

In Part B we describe the results of configuration interaction (CI) calculations for the positive ion states of NiCO. We find that there are two groups of ion states. The first group involves ionization out of Ni-like orbitals. Ionization of the Ni(3d) orbitals leads to a group of states with a bandwidth of 3.1 eV in good agreement with the Ni d bandwidth as observed in photoemission experiments. The second group of states involves ionization out of the CO. The principal change here as compared with free CO is that the 5σ ionization (lone pair on the CO) increases in energy by about 2.5 eV, whereas the 4σ and 1π ionizations change only slightly. This leads to the 5σ and 1π ion states of the chemisorbed species being nearly degenerate, with the 4σ ion state about 3.0 eV higher, in agreement with the currently accepted interpretation of the photoelectron spectrum of CO chemisorbed on Ni.

Part C summarizes the results of cluster calculations for the geometries of O and S overlayers on the (100) and (110) surfaces of Ni, while the S and O cases are discussed in more detail in Parts D and E, respectively.

For the S case we find that modeling the surface with four Ni atoms leads to an optimum S position 1.33\AA above the surface, in good agreement with the value $(1.30 \pm 0.10\text{\AA})$ from dynamic LEED intensity analysis. The bonding is qualitatively like that in H_2S with two covalent bonds between the two singly occupied S(3p) orbitals and the singly occupied 4s orbitals of one diagonal pair of Ni atoms. There is a S p π pair overlapping the other diagonal pair of Ni atoms. [Deleting this pair the S moves in to a position 1.04\AA from the surface.] There are two equivalent such structures, the resonance leading to equivalent S atoms and a c(2x2) structure for the S overlayer. The Ni in the layer beneath the surface seems to have little effect ($\sim 0.03\text{\AA}$) on the calculated geometry.

The above model of the bonding suggests that for the (110) surface the S lies along the long edge of the rectangular unit cell (2 coordinate) rather than at the four coordinate site usually assumed. Our calculated position for the S of 1.04\AA is in reasonable agreement with the value from dynamic LEED intensity calculations, $0.93 \pm 0.10\text{\AA}$.

Bonding the S directly above a single Ni atom leads to a much weaker bond ($D_e = 3.32\text{ eV}$) than does bonding in a bridge position ($D_e = 5.37\text{ eV}$).

For the O case we find that the larger amount of ionic character in the O cluster requires that the Ni atom beneath the surface be included in the cluster, whereas only the surface Ni atoms were important in the S case. The charge distribution here is consistent with taking a positively charged cluster, leading to a Ni_5^+O cluster as the model

for the (100) surface. The optimum oxygen position with this model is 0.96\AA above the surface (four-fold coordinate site) in good agreement with the value $(0.90 \pm 0.10\text{\AA})$ from dynamic LEED intensity analysis. The atom beneath the surface allows important polarization effects for the positively charged cluster. The bonding to the surface involves bridging two diagonal surface Ni atoms. There is an $O(2p\pi)$ pair which overlaps the other diagonal pair of Ni atoms leading to nonbonded repulsions which increase the distance above the surface. There are two equivalent such structures, the resonance leading to a $c(2 \times 2)$ structure for the O overlayer.

The above model suggests that for the (110) surface the O lies along the long edge of the rectangular unit cell. For this registry with the surface, calculations based on Ni_2O and Ni_3O models indicate that the oxygen is only 0.1\AA above the plane of the surface.

In Part F we discuss the electronic states of the NiO molecule. All the lower states are found to involve the $(4s)^1(3d)^9$ Ni atom configuration and O in the $(2s)^2(2p)^4$ configuration. There are two groups of states. The lower group of states involves pairing singly occupied Ni(4s) and O(2p σ) orbitals into a (somewhat ionic) sigma bond pair with various pairings of the Ni(3d)⁹ and O(2p π)³ configurations. This leads to a number of states including the ground state which we find to be $X^3\Sigma^-$. (The electronic structure is analogous to that of O_2 .) The calculated D_0 and R_e for the $X^3\Sigma^-$ state of NiO are 89.9 Kcal/mole and 1.60\AA respectively. The bond energy is in good agreement with the experimental value 86.5 ± 5 Kcal/mole, while the R_e value is not known experimentally.

The higher group of states involve a doubly occupied $O(2p\sigma)$ orbital. The $Ni(4s)$ orbital in this case is nonbonding and builds in 4p character to move away from the oxygen orbitals. The bonding mainly involves stabilization of the oxygen orbitals by the $Ni(3d)^9$ core (somewhat analogously to the bonding in $NiCO$). Numerous allowed transitions between these states and the states of the lower group are calculated to be in the range 1.0 to 3.0 eV where numerous bands are seen in emission.

Appendix A summarizes bond energies for various atoms and molecules in bridged and linear sites and also discusses the wavefunctions for certain cases (Ni_2CO , Ni_2CH_2 , $NiCHO$, and Ni_2C) which have not been discussed elsewhere in this thesis.

Appendix B contains reprints of the following two publications by the author which are not directly related to the subject of this thesis.

1. The Generalized Valence Bond Description of the Low-Lying States of Diazomethane
S. P. Walch and W. A. Goddard III
J. Amer. Chem. Soc., 97, 5319 (1975)
2. Dipole Moments and Electric Field Gradients for Correlated Wavefunctions of NO: The $X^2\Pi$, $A^2\Sigma^+$, and $D^2\Sigma^+$ States
S. P. Walch and W. A. Goddard III
Chem. Phys. Lett., 33, 18 (1975)

TABLE OF CONTENTS

Part A.	Generalized Valence Bond Description of the Low-Lying States of NiCO	1
I.	Introduction	2
II.	The Wave Functions	2
III.	Qualitative Description of NiCO	3
IV.	More Detailed Discussion of the GVB Wave Function	5
V.	The s^2d^8 Excited States	6
VI.	The CI Calculations	7
VII.	Comparison of Results with the MEP and AIEP	10
VIII.	Summary	11
IX.	References	11
Part B.	Configuration Interaction Studies of the Positive Ion States of NiCO; Implications for the Photoelectron Spectrum of CO Chemisorbed to Nickel	12
I.	Introduction	13
II.	Calculation Details	14
III.	The Ion States of NiCO	14
IV.	NiCO as a Model for CO Chemisorbed on Ni(111)	25
V.	The Comparison of Theoretical Methods for the Ion States of NiCO	40
VI.	Details of the Configuration Interaction (CI) Calculations	47
VII.	References	59

Part C.	Theoretical Studies of the Geometries of O and S Overlayers on the (100) and (110) Surfaces of Nickel	63
I.	References	72
II.	Appendix to Part C	74
Part D.	Theoretical Studies of the Bonding of Sulfur to Models of the (100) and (110) Surfaces of Nickel	75
I.	Introduction	76
II.	Qualitative Description of the Theoretical Results	78
III.	Further Discussion of the Wavefunctions	98
IV.	Calculation Details	132
V.	Details of the CI Calculations	135
VI.	References	143
Part E.	Theoretical Studies of the Bonding of Oxygen to Models of the (100) and (110) Surfaces of Nickel	147
I.	Introduction	148
II.	Computational Details	148
III.	Qualitative Discussion	149
IV.	Further Discussion of the Wavefunctions	172
V.	References	202

Part F.	The Electronic States of the NiO Molecule	205
I.	Introduction	206
II.	Qualitative Description	207
III.	Calculation Details	247
IV.	The CI Calculations	249
V.	Summary	257
VI.	References	259
Appendix A.	Bond Energies for Bridged and Linear Sites	263
Appendix B.	Other Publications by the Author	278

PART A: GENERALIZED VALENCE BOND DESCRIPTION OF THE LOW-
LYING STATES OF NiCO^{1,2}

I. Introduction

The study of the reactions occurring at metal surfaces constitutes an important field of modern chemical research. As one step in a program directed toward understanding one such reaction, the methanation of CO on a nickel surface, we are investigating the bonding of CO to the surface. As the first step of examining the bonding of CO to a Ni surface, we have carried out extensive studies of the bonding of CO to a single Ni atom. These results will be useful in understanding how to study the bonding of CO to larger complexes and indeed already provide some useful insights into the nature of the bond to the surface.

In addition, matrix isolation experiments have provided evidence for the existence of $\text{Ni}(\text{CO})_n$, $n = 1-4$.³ It is expected that the results of the NiCO calculations will suggest some experimental tests for these model systems.

In section II we describe basic concepts of the GVB wave functions, the effective potential, and the basis set used. In section III the results obtained are discussed in qualitative terms, while section IV examines in more detail some of these concepts in terms of the GVB wave function. Section V discusses the excited states. In section VI we describe the CI calculations. Section VII compares results with the *ab initio* effective potential (AIEP) and the modified effective potential (MEP) used here.

II. The Wave Functions

A. The GVB Method. The details of the GVB method have been described elsewhere.⁴ The GVB wave function can be viewed as a normal closed-shell Hartree-Fock (HF) wave function,

$$\mathcal{A}(\phi_1\phi_1\alpha\beta\phi_2\phi_2\alpha\beta\dots)$$

in which certain doubly occupied singlet pairs

$$\phi_i\phi_i\alpha\beta \quad (1)$$

are replaced by GVB pairs

$$(\phi_{ia}\phi_{ib} + \phi_{ib}\phi_{ia})\alpha\beta = (\lambda_1\phi_{i1}^2 - \lambda_2\phi_{i2}^2)\alpha\beta \quad (2)$$

where each electron of the pair is allowed to have its own GVB orbital ϕ_{ia} or ϕ_{ib} , the overlap of which,

$$S_{ab}^i = \langle \phi_{ia} | \phi_{ib} \rangle \quad (3)$$

is in general nonzero. In the perfect pairing approximation to GVB (referred to as GVB-PP), the GVB orbitals of a given pair are taken as orthogonal to those of all other pairs (strong orthogonality restriction) and in addition the spin eigenfunction is restricted to the form where the maximum number of pairs are singlet coupled (perfect pairing restriction). For nonsinglet states we also allow n high coupled orbitals.

$$\phi_1 \dots \phi_n \alpha \alpha \dots \alpha \quad (4)$$

To simplify the variational equations, the nonorthogonal orbitals $\{\phi_{1a}, \phi_{1b}\}$ are expanded in an orthonormal set $\{\phi_{11}, \phi_{12}\}$ (referred to as the natural orbitals) as in (2).

B. The Modified Effective Potential. In order to carry out calculations of the type described here at reasonable cost, it is expedient to use an effective potential to replace the 18-electron Ar core of the transition metal. Considerable progress in this area has been made by Melius, Olafson, and Goddard⁵ in developing an effective potential for Ni which allows near ab initio accuracy, referred to as the ab initio effective potential (AIEP). However, for the Ni atom ab initio calculations themselves lead to incorrect separations of the states if carried out with the usual basis and level of correlation. For example, using the Wachter basis⁹, the $s^1d^9(^3D)$ state is calculated in the Hartree-Fock (HF) description to be 2.32 eV above the $s^2d^8(^3F)$ state, whereas the experimental separation is only 0.03 eV.^{6,7} There are three contributions to this error: (1) basis set—the s^1d^9 state requires more diffuse d functions than the s^2d^8 state for which the basis was optimized; (2) correlation effects involving s, p, and d basis functions; and (3) correlation effects involving f functions. Including effects 1 and 2 (highly correlated wave functions using an extended basis with tight p functions) leads to a decrease in the excitation energy from 2.32 to 0.22 eV,²¹ with the remaining 0.25 eV error presumably due to f functions. The level of correlation required here is impractical for molecular systems with transition metals, and we have adopted an alternative procedure for including these effects in an approximate way.

Sollenberger, Goddard, and Melius⁸ have found that these missing efforts in the atoms can be imitated by adding additional terms to the ab initio effective potential in such a way as to reproduce the correct atomic separations and orbital shapes. Thus it was anticipated that the bond lengths and geometries resulting from interaction with other atoms would be accurate. Indeed this procedure does lead to reasonable bond lengths and bond energies for NiH and FeH.⁸ The resulting potential referred to as the modified effective potential (MEP) was used for the calculations described here. Some comparisons with the results of the AIEP are made in section VII.

C. Basis Set and Geometry. The basis for Ni was selected from the set optimized for the ground states of the third-row atoms by Wachters.⁹ We have used all five d primitives (of each type) but, as discussed in ref 5, only the outer four s functions are needed for describing the coreless Hartree-Fock orbital. The inner four d primitives were contracted together and the inner two s functions were contracted together with the relative coefficients based on Hartree-Fock calculations for the $s^2d^8(^3F)$ state of the Ni atom (ref 8). In addition, a single p primitive with $\alpha = 0.12$ was added in each direction (to allow polarization effects involving the 4s orbital). The final basis for Ni (see Table I) is identical with that in ref 8 except for the p functions and slight differences in the s functions.

The basis for carbon and oxygen is the Dunning (3s2p) contraction¹⁰ of the Huzinaga (9s,5p) basis. This contraction is double ζ valence but uses a single 1s-like contracted function and leads to energies which are generally within 0.0001 hartree of those obtained with the "double ζ " contraction.¹¹

We have taken the CO bond distance as 2.17 bohr which is close to the experimental CO bond distance in Ni(CO)₄.¹² The NiC bond length was varied over the range of 3.2 to 3.8 bohr (the NiC distance is 3.48 bohr in Ni(CO)₄).¹²

III. Qualitative Description of NiCO

For the moment we will view the CO molecule as



that is, a triple bond with a C lone pair protruding from the carbon.

Table I. The Nickel Basis Set^a

	α	C
d	48.940 30	0.032 958 4
	13.716 90	0.177 800 2
	4.639 51	0.443 562 6
	1.574 33	0.565 603 9
s	0.486 41	1.000
	2.400 00	0.132 666 1
	0.940 00	0.884 440 4
	0.150 00	1.000
p	0.049 00	1.000
	0.120 00	1.000

^a The Ni basis was taken from earlier calculations on NiH (C. Melius, unpublished work). In these calculations we have not excluded the s-like ($x^2 + y^2 + z^2$) combinations of the d basis functions. Including these additional s functions in combination with the other s functions, which are slightly different from those used in ref 8, leads to atomic energies of -40.495 31 hartree for $^3D(s^1d^9)$ and -40.490 65 hartree for $^3F(s^2d^8)$ which are 0.0010 hartree lower and 0.0028 hartree higher, respectively, than with the basis used in ref 8.

The lowest state of the Ni atom is the 3F_4 state arising from the $(4s)^2(3d)^8$ configuration; however, the 3D_3 state arising from the $(4s)^1(3d)^9$ configuration is only 0.025 eV higher. Since spin-orbit coupling effects are not included, we will henceforth average together the various J states corresponding to a particular L and S. In this case we find that the ground state is $^3D(s^1d^9)$ with the $^3F(s^2d^8)$ state at 0.03 eV, the $^1D(s^1d^9)$ state at 0.33 eV, and the $^3P(s^2d^8)$ state at 1.86 eV.

Upon bringing the Ni and CO together we find that the s^1d^9 states are stabilized significantly with respect to the s^2d^8 states. As a result the three bound states of NiCO are all of s^1d^9 character on the Ni. Given the s^1d^9 configuration of Ni, we obtain three triplet states of NiCO, $^3\Sigma^+$, $^3\Pi$, and $^3\Delta$, depending upon whether we take the single d hole as σ , π , or δ in symmetry.

The orbitals of the $^3\Sigma^+$ state are shown in Figure 1 while the corresponding orbitals of Ni and CO are shown in Figures 2 and 3, respectively. From the orbitals one sees that (1) the 4s-like orbital hybridizes away from the CO, (2) the CO lone pair delocalizes (bonds) just slightly onto the Ni, (3) the Ni d π orbitals delocalize slightly (back bond) into the π system of the CO, and (4) the CO π bonds are modified slightly by the Ni. For comparison, selected orbitals of the $^3\Pi$ and $^3\Delta$ states are shown in Figures 4 and 5.

The Mulliken populations (Table II) for the $^3\Sigma^+$ state reflect the above trends, the σ donation showing up in a decreased $s + p_z$ population on carbon of 0.08 with an increase in the $4s + 4p\sigma + 3d\sigma$ population on the Ni of 0.09. In the π system, back-donation is reflected in an increase of 0.12 in the carbon p π population and a corresponding decrease of 0.08 in the nickel 3d π population.

Since the $^3\Sigma^+$ state has a d σ hole, while the $^3\Pi$ and $^3\Delta$ states have doubly-occupied d σ orbitals, one would expect the $^3\Sigma^+$ state to act as a better σ acceptor for the CO lone pairs, stabilizing the $^3\Sigma^+$ state. Since the $^3\Sigma^+$ and $^3\Delta$ states each have two doubly occupied d π pairs, whereas the $^3\Pi$ state has only three electrons in d π orbitals, the $^3\Sigma^+$ and $^3\Delta$ states are expected to obtain more π back-bonding than the $^3\Pi$ state. Putting these effects together would lead to the ordering

$$^3\Sigma^+ < ^3\Delta < ^3\Pi$$

with perhaps comparable spacings. In fact, we find that the actual ordering of states is $^3\Delta < ^3\Sigma^+ < ^3\Pi$ with the $^3\Delta$ and $^3\Sigma^+$

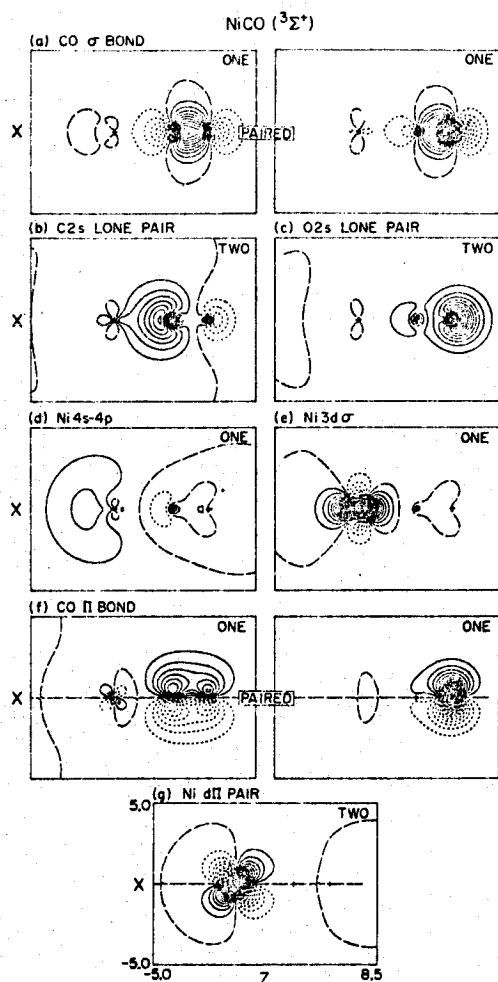


Figure 1. The GVB(3) orbitals of the ${}^3\Sigma^+$ state of NiCO. Unless otherwise noted, all plots have uniformly spaced contours with increments of 0.05 au. Nodal lines are indicated by long dashes. The same conventions are used for other figures unless otherwise stated.

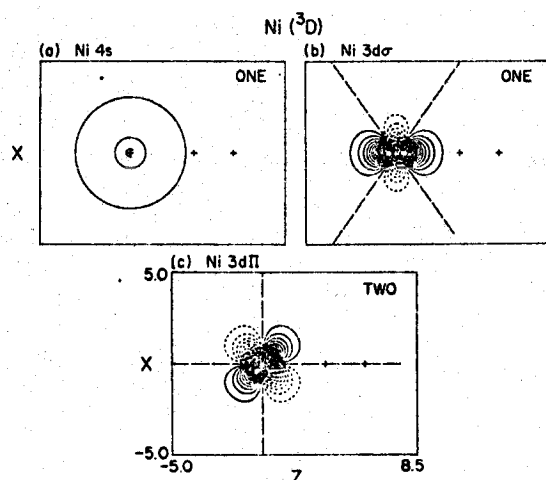


Figure 2. Selected HF orbitals of the 3D state of Ni.

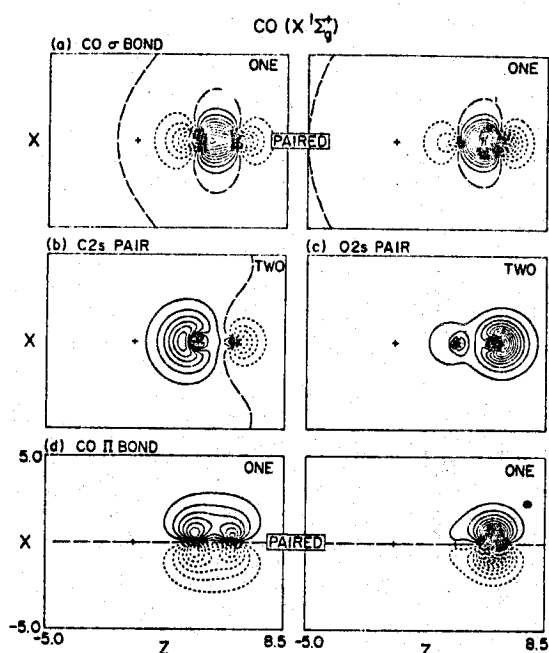


Figure 3. Selected orbitals of the GVB(3) $[\text{CO}\sigma, \pi_x, \pi_y]$ wave function of the $X\ 1\Sigma_g^+$ state of CO.

Table II. Mulliken Populations for CO and NiCO^a

		Ni(<i>s</i> ¹ <i>d</i> ⁹) + CO	NiCO		
			${}^3\Sigma^+$	${}^3\Pi$	${}^3\Delta$
C	<i>s</i>	3.8449	3.6472	3.6448	3.636 0
	<i>p_z</i>	0.9875	1.1001	1.0887	1.078 6
	<i>p_x</i>	0.5280	0.5942	0.5843	0.595 5
	<i>p_y</i>	0.5281	0.5942	0.5984	0.595 5
O	<i>s</i>	3.7846	3.8086	3.8091	3.807 4
	<i>p_z</i>	1.3830	1.3515	1.3519	1.350 7
	<i>p_x</i>	1.4720	1.4451	1.4254	1.444 4
	<i>p_y</i>	1.4719	1.4451	1.4491	1.444 4
Ni	4 <i>s</i>	1.0	0.9541	1.0327	1.077 4
	4 <i>p_σ</i>	0.0	0.2376	0.2525	0.258 1
	3 <i>d_σ</i>	1.0 or 2.0	0.9009	1.8205	1.791 8
	3 <i>d_{π_x}</i>	1.0 or 2.0	1.9600	0.9902	1.958 8
	4 <i>p_{π_x}</i>	0.0	0.0006	0.0001	0.001 3
	3 <i>d_{π_y}</i>	2.0	1.9600	1.9507	1.958 8
	4 <i>p_{π_y}</i>	0.0	0.0006	0.0017	0.001 3
	<i>d_{xy}</i>	1.0 or 2.0	2.0000	2.0000	1.000 0
	<i>d_{x²-y²}</i>	1.0 or 2.0	2.0000	2.0000	2.000 0
	<i>s</i> + <i>p_z</i>	4.8324	4.7473	4.7335	4.714 6
	<i>s</i> + <i>p_z</i>	5.1676	5.1601	5.1610	5.158 1
4 <i>s</i> + 4 <i>p_σ</i> + 3 <i>d_σ</i>	2.0 or 3.0	2.0926	3.1057	3.127 3	
Totals	Ni	10.0	10.0141	10.0484	10.047 7
	C	5.8885	5.9356	5.9162	5.905 6
	O	8.1115	8.0503	8.0355	8.046 7

^a Based on GVB wave functions at $R = 1.84 \text{ \AA}$.

states separated by 0.240 eV, whereas the ${}^3\Sigma^+$ and ${}^3\Pi$ states are separated by 0.053 eV.

Following the analysis of Melius and Goddard¹⁷ (for NiH and Ni₂), we believe that there is one additional intraatomic effect (intraatomic coupling) favoring ${}^3\Delta$ and ${}^3\Pi$. As discussed in section IV.C, rehybridizing the 4*s* and 3*d* orbitals of the *s*¹*d*⁹

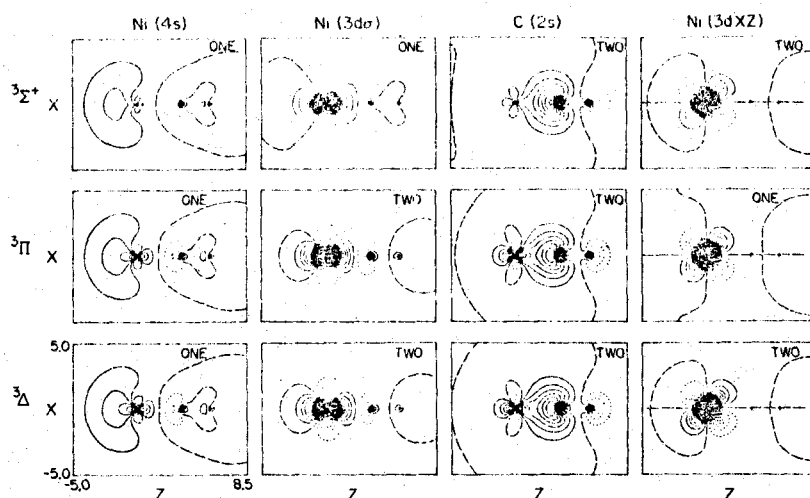


Figure 4. A comparison of selected orbitals of the GVB wave function for the $^3\Sigma^+$, $^3\Pi$, $^3\Delta$ states of NiCO.

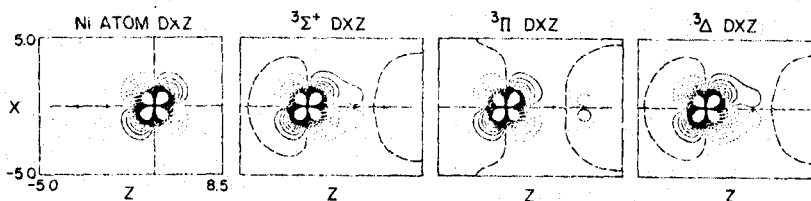


Figure 5. A comparison of the $3d_{xy}$ orbitals of Ni(2D) and the $^3\Sigma^+$, $^3\Pi$, and $^3\Delta$ states of NiCO using a contour interval of 0.025 to emphasize the differences in the amount of back-bonding.

state leads to incorporation of specific components of the s^2d^8 state. However, the energies of these components differ markedly (a range of ~ 4 eV) depending upon the specific configuration involved. The result is that the state with the δ hole is stabilized with respect to the state of the π hole which is in turn stabilized with respect to the state with a σ hole. As a result, the $^3\Delta$ state allows greater rehybridization of the σ orbitals than the $^3\Pi$ state, and the $^3\Pi$ state allows much greater rehybridization than the $^3\Sigma$ as is clear from Figures 1 and 4.

The fact that greater rehybridization of the $4s$ $3d$ orbitals is favored for the $^3\Pi$ and $^3\Delta$ states whereas the $^3\Sigma$ state is more favorable for a pure s^2d^8 configuration results in similar σ donations (CO to Ni) for all three states (see Table II), a result that would not be expected if the intraatomic coupling were not present. As expected, the singly occupied Ni($3d\pi$) orbital of the $^3\Pi$ state leads to very little back-bonding (Ni $3d\pi$ Mulliken population = 0.99 as compared with 1.96 for the $3d\pi$ orbitals of the $^3\Sigma$ and $^3\Delta$ states) so that the total π back-bonding in the $^3\Pi$ state is significantly less than for the $^3\Sigma$ and $^3\Delta$ states. (See also Figure 5.)

As discussed in section V, there are low-lying $^3\Delta$ and $^3\Pi$ states arising from s^2d^8 configurations on the Ni but no comparable $^3\Sigma^+$ state. Thus in the CI the $^3\Delta$ and $^3\Pi$ states are further stabilized relative to the $^3\Sigma^+$ state, leading to the calculated spacings.

The $^3\Sigma^+$, $^3\Pi$, and $^3\Delta$ states all lead to minima at about the same R_e . For the $^3\Delta$ ground state the calculated R_e (1.90 Å) and D_e (1.15 eV) compare reasonably well with the NiC distance (1.84 Å) and average bond energy (1.53 eV) in Ni(CO)₄.¹³ The NiC stretching constant calculated for NiCO is 428 cm^{-1} which is in the range observed for Ni(CO)₄ (423

cm^{-1})¹³ and tentatively assigned to Ni(CO)₃ (457 cm^{-1})¹³ and Ni(CO)₂ (516 cm^{-1}).¹³

IV. More Detailed Discussion of the GVB Wave Function

A. The CO Molecule. Omitting the C(2s) and O(2s) pairs and adopting a familiar notation, the ground states of C(s^2p^2) and O(s^2p^4) are represented as⁴

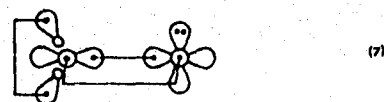


where p orbitals in the plane are represented by ∞ and p orbitals perpendicular to the plane by \circ . Coupling these so as to form a σ bond leads to two degenerate structures,



where the lines indicate bond (singlet coupled) pairs.

Considering for the moment only one of the structures (6), there is an important angular correlation of the C(2s) pair in the direction of the empty $2p\pi$ orbital (just as for the ground state of the carbon atom⁴). This leads to the description for CO,



which we will refer to as GVB(3) [C(2s), σ , π_x], to indicate which pairs are being correlated.

This single structure provides a useful description in situations where the symmetry is lowered due to bond formation. For example, (7) leads to a facile understanding of the structure of the formyl radical and of formaldehyde.¹⁴

One should keep in mind, however, that (7) does not exhibit the correct rotational symmetry. The correct symmetry is obtained by taking the sum of the two structures (6), and the resulting wave function is lower in energy than either of the individual structures (6). In the GVB method, this wave function may be described in an average sense by simultaneously correlating the σ , π_x , and π_y pairs in such a way that the two π directions are equivalent.¹⁵ This wave function is referred to as GVB(3) $\{\sigma, \pi_x, \pi_y\}$ and leads to an energy 0.413 eV lower than the wave function (7). (This is essentially the triple bond picture of CO we adopted in section III.) The self-consistent orbitals of the GVB(3) $\{\sigma, \pi_x, \pi_y\}$ wave function are those shown in Figure 3.

B. NiCO. Now consider bringing up a transition metal atom to the CO molecule in a linear arrangement. Given the empty C(2p) orbital in (6), a doubly occupied 3d π orbital would be expected to delocalize onto carbon leading to resonance structures (8) which are analogous to (6)



[Note here that d π orbitals are schematically indicated in the same way as p π orbitals, in order to keep the diagrams simple.] The delocalization of the metal 3d π orbital is expected to be more favorable if it is balanced by delocalization of the C(2s) orbital into empty metal σ orbitals, thus leading to less net transfer of charge. Thus the valence bond description leads naturally to the concept of CO as a σ donor and π acceptor in bonding to a transition metal.

As with CO the orbitals of NiCO were solved for with a three-pair wave function, GVB(3) $\{\sigma, \pi_x, \pi_y\}$, in which the π directions are kept equivalent. This wave function may be thought of as a superposition of the structures (8) in the same way that the analogous wave function for CO was described as a superposition of the structures (6).

C. The Intraatomic Coupling Effect.¹⁷ Consider the wave function for the $^3\Delta$ state of NiCO

$$\psi(s^1d^9) = \mathcal{A}[\{\text{CORE}\}(3d\sigma)^2(4s)(3d\delta)\alpha\beta\alpha\alpha] \quad (9)$$

where most orbitals (including the bonds) have been collected into [CORE]. In the GVB wave function all orbitals are solved for self-consistently; however, for the time being we restrict the 4s and 3d σ orbitals to mix only with each other (rehybridize). The result is

$$\begin{aligned} \mathcal{A}[\{\text{CORE}\}(3d\sigma - \lambda 4s)^2(4s + \lambda 3d\sigma)(3d\delta)\alpha\beta\alpha\alpha] \\ = \psi(s^1d^9) + \lambda\psi(s^2d^8) \end{aligned} \quad (10)$$

where

$$\psi(s^2d^8) = \mathcal{A}[\{\text{CORE}\}(4s)^2(3d\sigma)(3d\delta)\alpha\beta\alpha\alpha] \quad (11)$$

and where we neglected terms of order λ^2 (for the self-consistent wave function, λ is ~ 0.21). Thus rehybridizing the orbitals leads to mixing of s^2d^8 character into the wave function.

The component of s^2d^8 character in (10) has 3F symmetry; however, in the $^3\Pi$ state the term corresponding to (11) is¹⁸

$$\mathcal{A}[\{\text{CORE}\}(4s)^2(3d\sigma)(3d\pi)\alpha\beta\alpha\alpha] \quad (12)$$

Assuming a triplet d^2 state (following the holes of d^8) with $M_S = 1$, the 3F and 3P states with $M_L = 1$ are described as

$$\begin{aligned} |L = 3, M_L = 1\rangle &= \sqrt{\frac{4}{10}} |m_1 = 1, m_2 = 0\rangle \\ &\quad + \sqrt{\frac{6}{10}} |m_1 = 2, m_2 = -1\rangle \\ |L = 1, M_L = 1\rangle &= \sqrt{\frac{6}{10}} |m_1 = 1, m_2 = 0\rangle \\ &\quad - \sqrt{\frac{4}{10}} |m_1 = 1, m_2 = -1\rangle \end{aligned} \quad (13)$$

so that

$$\begin{aligned} |m_1 = 1, m_2 = 0\rangle &= \sqrt{\frac{4}{10}} |L = 3, M_L = 1\rangle \\ &\quad + \sqrt{\frac{6}{10}} |L = 1, M_L = 1\rangle \end{aligned} \quad (14)$$

Thus the configuration in (12) is 40% 3F and 60% 3P corresponding to an atomic excitation energy of 1.13 eV. As a result, rehybridization should be less important for the $^3\pi$ state than for the $^3\Delta$ state. In the $^3\Sigma$ state the s^1d^9 wave function is¹⁹

$$\mathcal{A}[\{\text{CORE}\}(3d\sigma)(4s)\alpha\alpha] \quad (15)$$

and hence *no* rehybridization is allowed (in this approximation). These expectations are borne out by the shapes of the orbitals as indicated in Figures 1 and 4.

V. The s^2d^8 Excited States

The three bound states of NiCO all arise from the $^3D(s^1d^9)$ state of the Ni atom. Higher states are derived from the 3F - and $^3P(s^2d^8)$ states of Ni. Given two holes in the d shell and classifying the *atomic states* according to their rotational symmetry relative to the molecular axis leads to five different triplet states depending on how the two holes are distributed over the d orbitals. Taking $\delta\pi$ or $\delta\sigma$ holes leads to a pure 3F state which is only 0.03 eV higher than the 3D state. Taking $\pi\pi$ holes leads to 80% 3F and 20% 3P with an excitation energy of 0.40 eV, taking $\sigma\pi$ holes leads to 40% 3F and 60% 3P corresponding to an excitation energy of 1.13 eV, and taking $\delta\delta$ holes leads to 20% 3F and 80% 3P leading to an excitation energy of 1.49 eV.¹⁶ Thus, based only on the atomic states involved, one would expect the ordering

$$\delta\pi \approx \delta\sigma < \pi\pi < \sigma\pi < \delta\delta$$

Upon bringing up a CO, the above ordering would be modified depending on the favorability for the atomic configuration to function as a σ acceptor, π donor. On this basis one would expect the state with the $\delta\sigma$ holes to be stabilized relative to the state with the $\delta\pi$ holes. Similarly, one might expect the state with the $\pi\pi$ holes to be destabilized somewhat relative to the state with the $\delta\delta$ holes. However, there is an additional important effect here. At large R the separation between the $\pi\pi$ and $\delta\delta$ $^3\Sigma^-$ states is only 1.09 eV (a separation that would be expected to decrease as R decreases), and in the CI there is a strong interaction between these pure configurations leading to a major stabilization of the state with the $\pi\pi$ holes and destabilization of the state with the $\delta\delta$ holes. (This effect involves an interpair correlation which increases the average separation between the electrons in the doubly occupied δ^+ and δ^- orbitals.) The net result is that the state with the $\pi\pi$ hole ends up below the state with the $\delta\pi$ holes leading to the ordering

$$\delta\sigma < \pi\pi < \delta\pi < \sigma\pi < \delta\delta$$

In Table III we summarize the atomic and molecular configurations of the s^2d^8 states of NiCO. The energies are from an extensive CI calculation using 24 basis functions as described in section VI.

Table III. CI Energies for the s^2d^8 and s^1d^9 States of NiCO ($R_{\text{NiC}} = 1.84 \text{ \AA}$)

Holes	Atomic states	Atomic energy, eV ^a	Dominant molecular configuration								No. ^b conf	Mol state	Energy, eV		
			O(2s)	C(2s)	3d σ	4s	σ	σ^*	π_x	π_y				δ_{xy}	$\delta_{x^2-y^2}$
s^2d^8 states															
$\delta\delta$	20% 3F , 80% 3P	1.49	2	2	2	2	2	0	2200000	2200000	10	10	1320	$2^3\Sigma^-$	5.290
$\sigma\pi$	40% 3F , 60% 3P	1.13	2	2	1	2	2	0	1200000	2200000	20	20	1192	$3^3\Pi$	4.390
$\delta\pi$	100% 3F	0.03	2	2	2	2	2	0	1200000	2200000	20	10	1320	$2^3\Pi$	3.988
$\pi\pi$	80% 3F , 20% 3P	0.40	2	2	2	2	2	0	2200000	1200000	10	20		$^3\Phi^d$	3.034
$\delta\sigma$	100% 3F	0.03	2	2	1	2	2	0	2200000	2200000	10	20	1208	$2^3\Delta$	3.020
s^1d^9 states															
π	100% 3D	0.00	2	2	2	1	2	0	1200000	2200000	20	20	1192	$1^3\Pi$	0.400
σ	100% 3D	0.00	2	2	1	1	2	0	2200000	2200000	20	20	698	$1^3\Sigma^+$	0.304
δ	100% 3D	0.00	2	2	2	1	2	0	2200000	2200000	10	20	1208	$1^3\Delta$	0.000 ^c

^a Experimental numbers. ^b Number of spin eigenfunctions. ^c The total energy is -153.34177 . All other energies are relative to this energy. ^d $^3\Phi$ corresponds to (-) phase, whereas $^3\Pi$ corresponds to (+) phase.

Table IV. Generating Configurations for the $^3\Sigma^+$, $^3\Pi$, and $^3\Delta$ CI Calculations

State	Conf set	O(2s)	C(2s)	3d σ	4s	σ	σ^*	π_x	π_y	δ_{xy}	$\delta_{x^2-y^2}$
$^3\Sigma^+$	A	2	2	1	1	2	0	2200000	2200000	2	2
		2	2	1	1	1	1	2200000	2200000	2	2
		2	2	1	1	2	0	2110000	2200000	2	2
$^3\Delta$	A	2	2	1	1	2	0	2200000	2110000	2	2
		2	2	2	1	1	1	2200000	2200000	1	2
		2	2	2	1	2	0	2110000	2200000	1	2
$^3\Delta$	B	2	2	2	1	2	0	2200000	2110000	1	2
		2	2	1	2	2	0	2200000	2200000	1	2
		2	2	1	2	1	1	2200000	2200000	1	2
$^3\Pi$	A	2	2	2	1	2	0	1200000	2200000	2	2
		2	2	2	1	1	1	1200000	2200000	2	2
		2	2	2	1	2	0	1110000	2200000	2	2
$^3\Pi$	B	2	2	2	1	2	0	1200000	2110000	2	2
		2	2	1	2	2	0	1200000	2200000	2	2
		2	2	1	2	1	1	1200000	2200000	2	2
$^3\Pi$	B	2	2	1	2	2	0	1110000	2200000	2	2
		2	2	1	2	2	0	1110000	2200000	2	2
		2	2	1	2	2	0	1200000	2110000	2	2

Of the states listed in Table III, the dipole-allowed transitions involving only a single one-electron transition (for the dominant configuration) are: $1^3\Delta \rightarrow 2^3\Delta$ ($3d\sigma \rightarrow 4s$) at 3.02 eV, $1^3\Delta \rightarrow ^3\Phi$ ($3d\pi_x \rightarrow 4s$) at 3.03 eV, $1^3\Delta \rightarrow 2^3\Pi$ ($3d\pi_x \rightarrow 4s$) at 3.99 eV, $1^3\Sigma^+ \rightarrow 3^3\Pi$ ($3d\pi_x \rightarrow 4s$) at 4.09 eV, $1^3\Pi \rightarrow 1^3\Sigma^-$ ($3d\pi_y \rightarrow 4s$) at 2.73 eV, $1^3\Pi \rightarrow 3^3\Pi$ ($3d\sigma \rightarrow 4s$) at 3.99 eV, $1^3\Pi \rightarrow ^3\Phi$ ($3d\delta_{x^2-y^2} \rightarrow 4s$) at 2.63 eV, and $1^3\Pi \rightarrow 2^3\Pi$ ($3d\delta_{x^2-y^2} \rightarrow 4s$) at 3.59 eV. All of these transitions involve $3d \rightarrow 4s$ atomic transitions which are parity forbidden ($g \rightarrow g$) for the atom and consequently are not expected to be strong.

VI. The CI Calculations

A. The $^3\Sigma^+$, $^3\Pi$, $^3\Delta$ States. GVB-CI calculations were carried out for the $^3\Sigma^+$, $^3\Pi$, $^3\Delta$ states of NiCO using as a basis the self-consistent GVB orbitals for each state. Preliminary CI calculations including all single and double excitations from the dominant configuration for each state indicated that all the important configurations are obtained by allowing all single excitations from the A configurations in Table IV. In addition, for the $^3\Delta$ and $^3\Pi$ states we found that significant energy lowerings (~ 0.2 eV) resulted if the B configurations, which describe the $3^3\Pi$, $2^3\Delta$ states (of s^2d^8 character), were added

to the list of generating configurations. (No comparable s^2d^8 state exists for the $^3\Sigma^+$ state.)

To allow for possible readjustment effects due to relaxation of the perfect pairing and strong orthogonality restrictions, the π space was augmented by adding three π virtuals in each direction chosen as the more diffuse atomic basis function of Ni($3d\pi$), C($2p\pi$), and O($2p\pi$) type, respectively (subsequently orthogonalized to the valence orbitals for the CI). The presence of these functions in the CI allows the π orbitals (in the CI) to change their radial extent on the three centers. The final CI included all single excitations from the A and B configurations in Table III into the full CI basis (20 functions after eliminating the CIs- and OIs-like functions by appropriate readjustment of the one-electron integrals). This CI thus includes the important configurations from the single and double excitation GVB-CI, the orbital readjustment effects within the full π space, and the effects from mixing in s^2d^8 character. This procedure resulted in 112, 180, and 172 spatial configurations (538, 852, 988 spin eigenfunctions; 833, 1312, 1564 determinants) for the $^3\Sigma^+$, $^3\Pi$, and $^3\Delta$ states, respectively.

In order to determine the relative importance of each configuration in the CI, the energy lowering is computed according to the formula

Table V. Energy Contribution of Dominant Configurations^a of the GVB-CI Wave Functions for the $^3\Sigma^+$, $^3\Pi$, and $^3\Delta$ States of NiCO ($R_{\text{NiCO}} = 1.84 \text{ \AA}$)

State	No.	Character ^b	Configuration										Energy contribution, mh ^c
			O(2s)	C(2s)	3d σ	4s	σ	σ^*	π_x	π_y	δ_{xy}	$\delta_{x^2-y^2}$	
$^3\Sigma^+$	1	HF	2	2	1	1	2	0	220000	220000	2	2	
	2	I(π_x, π_y)	2	2	1	1	2	0	211000	211000	2	2	17.8
	3	C(π_x)	2	2	1	1	2	0	202000	220000	2	2	14.5
	4	C(π_y)	2	2	1	1	2	0	220000	202000	2	2	14.5
	5	I(σ, π_y)	2	2	1	1	1	1	220000	211000	2	2	12.2
	6	I(σ, π_x)	2	2	1	1	1	1	211000	220000	2	2	12.2
	7	C(σ)	2	2	1	1	0	2	220000	220000	2	2	7.5
$^3\Pi$	1	HF	2	2	2	1	2	0	120000	220000	2	2	
	2	I(π_x, π_y)	2	2	2	1	2	0	111000	211000	2	2	17.9
	3	C(π_x)	2	2	2	1	2	0	102000	220000	2	2	15.1
	4	C(π_y)	2	2	2	1	2	0	120000	202000	2	2	14.3
	5	I(σ, π_x)	2	2	2	1	1	1	110000	220000	2	2	12.3
	6	I(σ, π_y)	2	2	2	1	1	1	120000	211000	2	2	12.1
	7	C(σ)	2	2	2	1	0	2	120000	220000	2	2	7.4
	8	R(1 $\pi_x, 2\pi_x$)	2	2	2	1	2	0	210000	220000	2	2	2.2
	9	M, R(1 $\pi_y, 4\pi_y$)	2	2	1	2	2	0	120000	120100	2	2	1.0
$^3\Delta$	1	HF	2	2	2	1	2	0	220000	220000	1	2	
	2	I(π_x, π_y)	2	2	2	1	2	0	211000	211000	1	2	18.3
	3	C(π_x)	2	2	2	1	2	0	202000	220000	1	2	14.4
	4	C(π_y)	2	2	2	1	2	0	220000	202000	1	2	14.4
	5	I(σ, π_y)	2	2	2	1	1	1	220000	211000	1	2	12.3
	6	I(σ, π_x)	2	2	2	1	1	1	211000	220000	1	2	12.3
	7	C(σ)	2	2	2	1	0	2	220000	220000	1	2	7.4
	8	M	2	2	1	2	2	0	220000	220000	1	2	2.5
	9	M, R(1 $\pi_x, 4\pi_x$)	2	2	1	2	2	0	120100	220000	1	2	1.7
	10	M, R(1 $\pi_y, 4\pi_y$)	2	2	1	2	2	0	220000	120100	1	2	1.7

^a All configurations contributing 1 mhartree or more are listed. ^b R indicates an orbital readjustment effect (single excitation); C indicates correlation of a particular doubly occupied orbital; I indicates an interpair correlation effect; M indicates mixing in of s^2d^8 character. ^c 1 mhartree = 10^{-3} hartree = 0.027 eV.

Table VI. Energy Contribution of the Dominant Configuration of the GVB-CI Wave Function for the X $^1\Sigma_g^+$ State of CO

No.	Character ^a	Configuration						Energy contribution, mhartrees
		O(2s)	C(2s)	σ	σ^*	π_x	π_y	
1	HF	2	2	2	0	2000	2000	
2	I(π_x, π_y)	2	2	2	0	1100	1100	21.4
3	C(π_x)	2	2	2	0	0200	2000	13.9
4	C(π_y)	2	2	2	0	2000	0200	13.9
5	I(σ, π_x)	2	2	1	1	1100	2000	13.8
6	I(σ, π_y)	2	2	1	1	2000	1100	13.8
7	C(σ)	2	2	0	2	2000	2000	7.2

^a The same notation as Table V is used here.

Table VII. Energies for the $^3\Sigma^+$, $^3\Pi$, and $^3\Delta$ States of NiCO^a

		$R = 3.20a_0$ (1.69 \AA)	$R = 3.48a_0$ (1.84 \AA)	$R = 3.80a_0$ (2.01 \AA)
$^3\Sigma^+$	GVB	-153.258 51	-153.271 61	-153.272 82
	CI	-153.318 77	-153.331 48	-153.332 48
$^3\Delta$	GVB	-153.262 19	-153.272 29	-153.271 12
	CI	-153.326 77	-153.336 16	-153.334 20
$^3\Pi$	GVB	-153.239 69	-153.258 36	-153.263 55
	CI	-153.302 94	-153.320 49	-153.324 71

^a At $R = \infty$ the energies for Ni(3D) + CO X $^1\Sigma_g^+$ are -153.243 11 and -153.300 56 hartrees for the GVB and CI wave functions, respectively.

$$\Delta E_\mu = C_\mu^2(E - H_{\mu\mu}) / (1 - C_\mu^2) \quad (16)$$

This is the energy increase that would result if configuration μ were deleted while keeping all other CI coefficients fixed. In cases where there is more than one spin eigenfunction for a

Table VIII. Potential Curve Parameters from the CI Calculations on NiCO

	$R_e, \text{ \AA}$	$D_e, \text{ eV}^a$	$\omega_e, \text{ cm}^{-1}$
$^3\Delta$	1.901	1.145	427.5
$^3\Sigma^+$	1.937	0.905	441.3
$^3\Pi$	1.968	0.852	477.5

^a We have included in D_e the additional energy lowering obtained in the 24 basis function CI at $R = 1.84 \text{ \AA}$. With the 20 basis function CI for each R, we obtained D_e of 0.992, 0.905, and 0.671 eV for these states.

given spatial configuration, we have simply added the separate contributions due to each spin eigenfunction. The ΔE_μ provides an indication of the relative importance of configurations, although the sum of the ΔE_μ does not equal the total energy lowering.

Table V shows the dominant configurations in the CI wave

Table IX. Generating Configurations for the 24 Basis Function CI

State	O(2s)	C2(s)	3d σ	4s	σ	σ^*	3d σ'	4s'	π_x	π_y	δ_{xy}	$\delta_{x^2-y^2}$
$^3\Sigma^+$	2	2	1	1	2	0	0	0	220000	220000	20	20
	2	2	1	1	1	1	0	0	220000	220000	20	20
	2	2	1	1	2	0	0	0	211000	220000	20	20
	2	2	1	1	2	0	0	0	220000	211000	20	20
$^3\Phi^a$	2	2	2	2	2	0	0	0	120000	220000	20	10
	2	2	2	2	1	1	0	0	120000	220000	20	10
	2	2	2	2	2	0	0	0	111000	220000	20	10
	2	2	2	2	2	0	0	0	120000	211000	20	10
	2	2	2	2	2	0	0	0	220000	120000	10	20
	2	2	2	2	2	1	0	0	220000	120000	10	20
	2	2	2	2	2	2	0	0	220000	111000	10	20
	2	2	2	2	2	2	0	0	211000	120000	10	20
$^3\Pi$	2	2	2	1	2	0	0	0	120000	220000	20	20
	2	2	2	1	1	1	0	0	120000	220000	20	20
	2	2	2	1	2	0	0	0	111000	220000	20	20
	2	2	2	1	2	0	0	0	120000	211000	20	20
	2	2	2	1	2	0	0	0	120000	220000	20	20
	2	2	2	1	2	1	1	0	120000	220000	20	20
	2	2	2	1	2	2	0	0	111000	220000	20	20
	2	2	2	1	2	2	0	0	120000	211000	20	20
$^3\Sigma^-$	2	2	2	2	2	0	0	0	120000	120000	20	20
	2	2	2	2	2	1	1	0	120000	120000	20	20
	2	2	2	2	2	0	0	0	111000	120000	20	20
	2	2	2	2	2	0	0	0	120000	111000	20	20
	2	2	2	2	2	0	0	0	220000	220000	10	10
	2	2	2	2	2	1	1	0	220000	220000	10	10
	2	2	2	2	2	2	0	0	211000	220000	10	10
	2	2	2	2	2	2	0	0	220000	211000	10	10
$^3\Delta$	2	2	2	1	2	0	0	0	220000	220000	10	20
	2	2	2	1	1	1	0	0	220000	220000	10	20
	2	2	2	1	2	0	0	0	211000	220000	10	20
	2	2	2	1	2	0	0	0	220000	211000	10	20
	2	2	1	2	2	0	0	0	220000	220000	10	20
	2	2	1	2	1	1	0	0	220000	220000	10	20
	2	2	1	2	2	0	0	0	211000	220000	10	20
	2	2	1	2	2	0	0	0	220000	211000	10	20

^a This group of configurations leads to both $^3\Phi$ and $^3\Pi$ states. Thus these configurations should be combined with the $^3\Pi$ configurations, leading to 2512 spin eigenfunctions. However, the $1^3\Pi$ and $3^3\Pi$ states are well described by excitations from the configurations listed under $^3\Pi$ while the $2^3\Pi$ state is well described by excitations from the configurations listed under $^3\Phi$. Hence we calculated these states separately, leading to slight errors for the $2^3\Pi$ and $3^3\Pi$ energies.

functions for the $^3\Sigma^+$, $^3\Pi$, $^3\Delta$ states of NiCO (at $R = 1.84 \text{ \AA}$). Table VI gives the same information for a comparable CI on CO. The configurations are characterized according to the notation explained in footnote *b* of Table IV. In general the three states of NiCO show correlation effects very similar to those seen in CO, but the $^3\Pi$ and $^3\Delta$ states show some mixing in of s^2d^8 character from the higher s^2d^8 state. The energies for the GVB and CI wave functions of the three states as a function of NiC separation are given in Table VII. For each state a parabola was fit through the three points to obtain the D_e , R_e , and ω_e values given in Table VIII.²⁰

B. The s^2d^8 States. A procedure for generating configurations similar to that used for the s^1d^9 states was used. The generating configurations are given in Table IX. As a CI basis the GVB orbitals of the $^3\Delta$ state (s^1d^9) were used. In order to describe readjustment effects, the π space was augmented as previously described for the s^1d^9 states and, in addition, functions were added which correspond to the more diffuse component of the $3d\delta_{xy}$, $3d\delta_{x^2-y^2}$, and $3d\sigma$ atomic orbitals. To describe the contraction of the 4s orbital appropriate to a $(4s)^2$ state the 4s orbital from an SCF calculation on the $^3\Phi$ state ($\delta\pi$ holes) was added as a virtual orbital. The resulting basis consisted of 24 functions.

All singles from the generating configurations in Table IX

were included in the CI (with the restriction that excitations into the $3d\delta$ and $4s$ virtuals were allowed only for configurations of s^2 character and only from the $4s$, $3d\sigma$, and $C(2s)$ -like orbitals which would be expected to change in character for s^2 states). This leads to 144, 236, 236, 236, and 212 spatial configurations (698, 1320, 1192, 1320, and 1208 spin eigenfunctions; 1081, 2082, 1854, 2082, and 1910 determinants) for the $^3\Sigma^+$, $^3\Phi$, $^3\Pi$, $^3\Sigma^-$, and $^3\Delta$ CI's, respectively.

The CI energies have been presented in Table III. In Table X we show the dominant configurations and energy lowerings for each of the states. For the s^1d^9 states the energy contributions for each important configuration are generally the same as for the smaller 20 basis function CI (used to derive the properties of the potential curves). A notable exception is for the $1^3\Delta$ state where configuration 5 (which describes mixing in of s^2d^8 character) contributes 11.9 mhartrees for the larger CI, whereas it contributed only 2.5 mhartrees in the smaller CI. This effect is due to a better description of the $2^3\Delta$ state which lowers this state by 1.21 eV relative to the 20 basis function CI; as a result there is greater interaction with the $1^3\Delta$ state, leading to an additional energy lowering of 0.153 eV. Adding this lowering (at 1.84 \AA) to the D_e obtained with the smaller CI at the optimum R ($R_e = 1.90 \text{ \AA}$) leads to 1.145 eV as our best estimate of D_e for the $^3\Delta$ state.

Table X. Energy Contributions of the Dominant Configurations ($\Delta E > 10$ mhartree) for each of the Roots of the 24 Basis Function CI^a

State	No.	Character	Configuration											Energy contribn mhar- trees	
			O(2s)	C(2s)	3d α	4s	σ	σ^*	3d σ'	4s'	π_x	π_y	δ_y		$\delta_{x^2-y^2}$
1 ³ Δ	1	HF	2	2	2	1	2	0	0	0	220000	220000	10	20	
	2	I(2 π_x , 2 π_y)	2	2	2	1	2	0	0	0	211000	211000	10	20	17.7
	3	C(2 π_x)	2	2	2	1	2	0	0	0	202000	220000	10	20	13.9
	4	C(2 π_y)	2	2	2	1	2	0	0	0	220000	202000	10	20	13.9
2 ³ Δ	5	M	2	2	1	2	2	0	0	0	220000	220000	10	20	11.9
	1	HF	2	2	1	2	2	0	0	0	220000	220000	10	20	
	2	I(2 π_x , 2 π_y)	2	2	1	2	2	0	0	0	211000	211000	10	20	17.0
	3	R(4s)	2	2	1	1	2	0	0	1	220000	220000	10	20	13.4
	4	C(2 π_y)	2	2	1	2	2	0	0	0	220000	202000	10	20	12.8
	5	C(2 π_x)	2	2	1	2	2	0	0	0	202000	220000	10	20	12.8
	6	R(1 π_y)	2	2	1	2	2	0	0	0	220000	121010	10	20	12.2
	7	R(1 π_x)	2	2	1	2	2	0	0	0	121010	220000	10	20	12.2
3 ³ Σ^+	8	I(σ , 2 π_y)	2	2	1	2	1	1	0	0	220000	211000	10	20	10.9
	9	I(σ , 2 π_x)	2	2	1	2	1	1	0	0	211000	220000	10	20	10.9
	1	HF	2	2	1	1	2	0	0	0	220000	220000	20	20	
	2	R(C(2s), 3d σ)	2	1	2	1	2	0	0	0	220000	220000	20	20	17.5
	3	I(2 π_x , 2 π_y)	2	2	1	1	2	0	0	0	211000	211000	20	20	16.9
	4	C(2 π_y)	2	2	1	1	2	0	0	0	220000	202000	20	20	13.7
	5	C(2 π_x)	2	2	1	1	2	0	0	0	202000	220000	20	20	13.7
	6	I(σ , 2 π_y)	2	2	1	1	1	1	0	0	220000	211000	20	20	11.7
	7	I(σ , 2 π_x)	2	2	1	1	1	1	0	0	211000	220000	20	20	11.7
	1 ³ Π	1	HF	2	2	2	1	2	0	0	0	120000	220000	20	20
2		I(2 π_x , 2 π_y)	2	2	2	1	2	0	0	0	111000	211000	20	20	17.5
3		C(2 π_x)	2	2	2	1	2	0	0	0	102000	220000	20	20	14.8
4		C(2 π_y)	2	2	2	1	2	0	0	0	120000	202000	20	20	13.9
5		I(σ , 2 π_x)	2	2	2	1	1	1	0	0	111000	220000	20	20	12.0
6		I(σ , 2 π_y)	2	2	2	1	1	1	0	0	120000	211000	20	20	11.7
3 ³ Π	1	HF	2	2	1	2	2	0	0	0	120000	220000	20	20	
	2	I(2 π_x , 2 π_y)	2	2	1	2	2	0	0	0	111000	211000	20	20	16.8
	3	R(4s)	2	2	1	1	2	0	0	1	120000	220000	20	20	14.9
	4	C(2 π_x)	2	2	1	2	2	0	0	0	102000	220000	20	20	13.4
	5	C(2 π_y)	2	2	1	2	2	0	0	0	120000	202000	20	20	13.2
	6	R(1 π_y)	2	2	1	2	2	0	0	0	120000	120100	20	20	11.8
	7	R(3d σ)	2	2	0	2	2	0	1	0	120000	220000	20	20	11.0
	8	I(σ , 2 π_x)	2	2	1	2	1	1	0	0	111000	220000	20	20	11.0
	9	I(σ , 2 π_y)	2	2	1	2	1	1	0	0	120000	211000	20	20	11.0
	10	R(2 π_x)	2	2	1	2	2	0	0	0	201000	220000	20	20	10.2
1 ³ Σ^-	1	HF	2	2	2	2	2	0	0	0	120000	120000	20	20	
	2	I(π , δ)	2	2	2	2	2	0	0	0	220000	220000	10	10	99.8
	3	R(3d σ)	2	2	1	2	2	0	1	0	120000	120000	20	20	15.1
	4	I(2 π_x , 2 π_y)	2	2	2	2	2	0	0	0	111000	111000	20	20	13.1
	5	R(4s)	2	2	2	1	2	0	0	1	120000	120000	20	20	12.7
2 ³ Σ^-	1	HF	2	2	2	2	2	0	0	0	220000	220000	10	10	
	2	I(π , δ)	2	2	2	2	2	0	0	0	120000	120000	20	20	61.4
	3	I(2 π_x , 2 π_y)	2	2	2	2	2	0	0	0	211000	211000	10	10	15.4
	4	R(1 π_y)	2	2	2	2	2	0	0	0	220000	120100	10	10	12.2
	5	R(1 π_x)	2	2	2	2	2	0	0	0	120100	220000	10	10	12.2
	6	R(4s)	2	2	2	1	2	0	0	1	220000	220000	10	10	10.5
	7	R(3d σ)	2	2	1	2	2	0	1	0	220000	220000	10	10	10.2
3 ³ Φ	1	HF	2	2	2	2	2	0	0	0	220000	120000	10	20	^b
	2	HF	2	2	2	2	2	0	0	0	120000	220000	20	10	
2 ³ Π	1	HF	2	2	2	2	2	0	0	0	220000	120000	10	20	
	2	HF	2	2	2	2	2	0	0	0	120000	220000	20	10	

^a The notation for describing the character of each configuration is the same as for Tables V and VI. ^b The coefficients are equal in magnitude but opposite in phase. ^c The coefficients are of the same magnitude and phase.

VII. Comparison of Results with the MEP and AIEP

In Table XI we show the GVB bond energies for selected states of NiCO for which calculations using the AIEP are available. The results from the AIEP are expected to be quite close (within 0.2 eV) to what would be obtained from corresponding ab initio calculations. Here we see that at $R = 1.84$ Å the best state (2³ Δ) has (4s)²(3d)⁸ character and is 2.2 eV above the energy for ground state atoms. Thus we obtain the

wrong character and no bond. The 3³ Σ^+ state has (4s)¹(3d)⁹ character and one might argue that its energy should be compared with that of the corresponding atomic state (since the ab initio HF wave function discriminates against this state by 2.3 eV). However, even in this case the calculated bond energy is negative although only by 0.2 eV.

The problem here is clearly related to the fact that the AIEP (in conjunction with the usual basis set) leads to an incorrect bias toward s²d⁸ states for the Ni atom. Thus for molecular

Table XI. Bond Energies at $R_{\text{NiC}} = 1.84 \text{ \AA}$ from GVB(3) Calculations on Selected States of NiCO Using the AIEP

O(2s)	C(2s)	Dominant configuration								Corresponding State using the MEP	Bond energy, eV rel to	
		3d σ	4s	σ	σ^*	π_x	π_y	δ_{xy}	$\delta_{x^2-y^2}$		^3D	^3F
2	2	1	2	2	0	2 2 0	2 2 0	1	2	$2^3\Delta$	+0.11	-2.18
2	2	1	1	2	0	2 2 0	2 2 0	2	2	$3^3\Sigma^+$	-0.17	-2.47
2	2	2	2	2	0	1 2 0	2 2 0	1	2	$3^3\Phi$	-1.21	-3.50

systems there is a comparable bias toward s^2d^8 states which are unfavorable for bonding in NiCO. One might hope to correct this error by adding additional s, p, d, and f basis functions on the Ni and including the appropriate correlation effects; however, to carry out a comparable CI would involve an enormously increased number of configurations. At the present time such calculations of potential curves for numerous excited states are not practical and we conclude that use of the MEP, which *does* lead to reasonable results, is a better alternative.

VIII. Summary

Since the 4s orbital has a significant overlap with the CO lone pair, the $(4s)^2$ state of Ni leads to strong repulsive interaction when the CO is pushed close enough to overlap the d orbitals of the Ni. As a result, the three bound states of NiCO all have s^1d^9 character on the Ni. We find similar results for bonding of CO to two and three Ni and expect these conclusions to apply also to CO bonded to the Ni surface.

Of the three bound states a strong intraatomic coupling effect leads to stabilization of the $^3\Delta$ state (δ hole) over the $^3\Sigma^+$ (σ hole) and $^3\Pi$ (π hole) states. The $^3\Delta$ and $^3\Sigma^+$ states exhibit greater π back-bonding than $^3\Pi$ and consequently lie lower. The resulting bond energies are 1.15 eV ($^3\Delta$), 0.91 eV ($^3\Sigma^+$), and 0.85 eV ($^3\Pi$). The optimum NiC bond length ($^3\Delta$) is found to be 1.90 \AA which is slightly longer than that of $\text{Ni}(\text{CO})_4$, 1.84 \AA . The vibrational frequency is calculated at 428 cm^{-1} .

Ab initio HF calculations (using the usual basis set) on the states of Ni put the $^3\text{D}(s^1d^9)$ state 2.3 eV above the $^3\text{F}(s^2d^8)$ state, whereas experimentally these states are essentially degenerate. In order to obtain the correct atomic separations, additional basis functions and correlation effects must be included, a procedure which is not practical for molecules. Use of the ab initio effective potential (AIEP) should yield results in close agreement (errors <0.2 eV) with the ab initio results. However, because the bonding in NiCO involves the $^3\text{D}(s^1d^9)$ state, which is very poorly described with the AIEP, use of the AIEP for NiCO leads to no bond whatsoever. In the calculations reported here we have used a modified effective potential (MEP) which is adjusted so as to yield the correct separation of the atomic states while not modifying the sizes of the orbitals. The results obtained for NiCO with the MEP are in

agreement with the fragmentary experimental information available and provide evidence for the efficacy of this approach.

References and Notes

- (1) Supported by a grant (DMR74-04965) from the National Science Foundation with some support from a grant (PRF No. 7683-AC6) from the donors of the Petroleum Research Fund, administered by the American Chemical Society.
- (2) Partially supported by a grant (CHE73-05 132) from the National Science Foundation.
- (3) R. L. De Kock, *Inorg. Chem.*, **10**, 1205 (1971).
- (4) W. A. Goddard III, T. H. Dunning, Jr., W. J. Hunt, and P. J. Hay, *Acc. Chem. Res.*, **6**, 368 (1973).
- (5) C. F. Melius, B. D. Olafson, and W. A. Goddard III, *Chem. Phys. Lett.*, **28**, 457 (1974); C. F. Melius and W. A. Goddard III, *Phys. Rev. A*, **10**, 1528 (1974).
- (6) The quoted atomic separations are obtained by taking a weighted average over the spectral levels corresponding to a given L and S (spin-orbit interactions are not included in our calculation). The values are from ref 7.
- (7) C. E. Moore, "Atomic Energy Levels", Vol. II, National Bureau of Standards, 1952.
- (8) M. J. Sollenberger, W. A. Goddard III, and C. F. Melius, manuscript to be submitted.
- (9) A. J. H. Wachters, *J. Chem. Phys.*, **52**, 1033 (1970).
- (10) T. H. Dunning, Jr., unpublished work. The p functions are the same as in ref 11, the tightest seven s basis functions are contracted into a single basis function based on the 1s HF orbital, the second and third most diffuse are contracted into a basis function based on the 2s HF orbital; the most diffuse function is uncontracted.
- (11) T. H. Dunning, Jr., *J. Chem. Phys.*, **53**, 2823 (1970).
- (12) F. A. Cotton and G. Wilkinson, "Advanced Inorganic Chemistry", 3rd ed, Interscience, New York, N.Y., 1972, p 684.
- (13) See ref 3 and references cited therein.
- (14) L. B. Harding and W. A. Goddard III, *J. Am. Chem. Soc.*, **97**, 6293 (1975).
- (15) The second natural orbital of each π pair is similar to the orbital that would be used to correlate angularly the C(2s) pair. Thus, since all of the natural orbitals must be orthogonal in a GVB-PP calculation, we cannot simultaneously obtain optimal correlation of the C(2s) and π pairs in a given direction. Since the π pair leads to a larger energy lowering, a better energy is obtained by correlating both π pairs. In a CI calculation over these orbitals, configurations can be included that describe simultaneous correlation of the C(2s) and π pairs.
- (16) The percentage of ^3P and ^3F corresponding to each determinant was determined in a manner analogous to the derivation of eq 14 in section IV.C.
- (17) The analysis of this section is based on the analysis by C. F. Melius and W. A. Goddard III of the states of NiH and Ni₂.
- (18) In (12) [CORE] is different from (11) since [CORE] includes all the doubly occupied orbitals.
- (19) Again, [CORE] contains all doubly occupied d π and d δ orbitals.
- (20) The energy of the separated limits was taken as the Ni(^3D) HF energy plus the energy for a comparable CI on CO. At $R = \infty$ the procedure for selecting configurations results in only single excitations involving the Ni; thus the CI leads to just the HF wave function for the Ni atom.
- (21) T. Smedley and W. A. Goddard III, unpublished calculations.

PART B: CONFIGURATION INTERACTION STUDIES OF THE POSITIVE ION
STATES OF NiCO; IMPLICATIONS FOR THE PHOTOELECTRON
SPECTRUM OF CO CHEMISORBED TO NICKEL [1],[2],[3]

1. Introduction

There have been numerous experimental studies of the chemisorption of CO on nickel surfaces. Using low energy electron diffraction (LEED), structural information has been obtained on the location of CO molecules relative to each other on the surface [4]. In addition, photoelectron spectroscopy has given information on the electronic energy levels of CO bonded to Ni films and to the (111) surface [8]. Without reliable theoretical calculations as a guide, it has been difficult to assign unambiguously the photoelectron spectrum--a situation resulting in considerable controversy. In addition, analysis of the LEED data has not yet provided information about the relative positioning of CO with respect to the surface Ni atoms.

As part of a program directed toward obtaining a detailed theoretical model for the surface sites associated with chemisorption and catalysis, we have recently completed a series of ab initio generalized valence bond (GVB) and configuration interaction (CI) calculations on NiCO [9]. In Ref. 9 (henceforth referred to as paper I), the low-lying states of NiCO were described. In this paper we describe CI calculations for the positive ion states of NiCO. The results for the ion states are used as a model for interpreting the photoelectron spectrum of CO chemisorbed on Ni.

Some of the calculational details are described in Section 2. In Section 3 we discuss the various ion states of NiCO and compare with the photoelectron spectrum of CO chemisorbed to Ni. Section 4 compares the results for NiCO with those obtained for larger clusters and with results expected for the semi-infinite solid. Section 5

compares this CI description with results obtained using the Koopmans' theorem and compares our results with those obtained from other calculations. The CI calculations are described in Section 6.

2. Calculation Details

The basis set and effective potential used are described in paper I. All calculations for the positive ions reported here use a Ni-C distance of 1.84\AA which is the experimental Ni-C distance in $\text{Ni}(\text{CO})_4$ [10] and is close to the optimum bond length of 1.90\AA found for the $^3\Delta$ ground state of NiCO (see paper I).

3. The Ion States of NiCO

3.1 Calculations

The three bound states of NiCO neutral are derived from the s^1d^9 (3D) state of the Ni atom, leading to $^3\Sigma^+$, $^3\Pi$, and $^3\Delta$ states depending on whether the single 3d hole is taken in a σ , π , or δ orbital, respectively. As discussed in paper I, the ordering of these states is found to be $^3\Delta < ^3\Sigma^+ < ^3\Pi$ with spacings of 0.240 eV between $^3\Delta$ and $^3\Sigma^+$ and 0.053 eV between $^3\Sigma^+$ and $^3\Pi$.

The qualitative picture of the bonding from the calculations is that the bond is due to stabilization of the CO 5σ orbital [essentially a C lone pair which we will henceforth refer to as C(2s)] from interaction with the partially exposed Ni^+3d^9 core, resulting from hybridization of the singly occupied Ni(4s) orbital away from the CO molecule. Because the CO 5σ orbital is more tightly bound than the Ni $3d\sigma$ orbital [the ionization potentials (IP's) are 14.01 and 8.70 eV

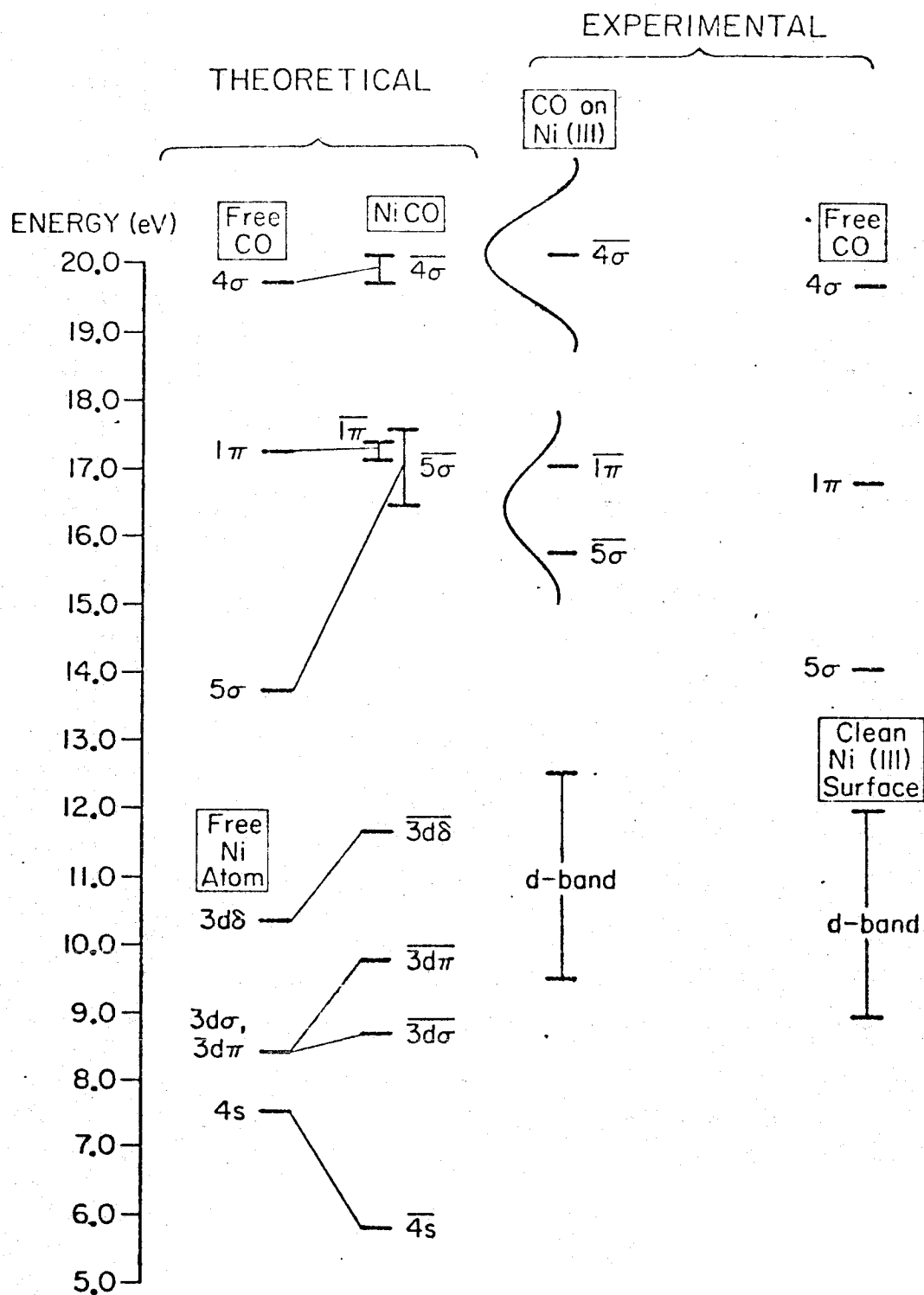
respectively], the CO 5σ orbital builds in only a small amount of Ni $3d\sigma$ character and the Ni $3d\pi$ orbitals delocalize (back bond) only slightly. Since the orbitals of NiCO are very similar to the corresponding orbitals of free CO and free Ni, we will denote the NiCO orbitals in terms of the corresponding designations for the free CO and Ni orbitals but with a bar (e.g., $\overline{5\sigma}$, $\overline{\pi}$, $\overline{3d\sigma}$).

From this qualitative picture of the bonding one expects that upon forming NiCO the main changes will be to make the $\overline{4s}$ orbital more easily ionized while the $\overline{5\sigma}$ orbital will be more difficult to ionize. In the following, we will concentrate on ionization from the ground $^3\Delta$ state (the $^3\Sigma^+$ and $^3\Pi$ states lead to very similar results).

The overall picture is illustrated in Fig. 1. Here we compare (i) the IP's (derived from the CI calculations) for the ion states which arise by removing a single electron from the $^3\Delta$ (i.e., $3d\delta$ hole) ground state of NiCO, (ii) the corresponding experimental IP's for CO and the Ni (111) surface, respectively, and (iii) the experimental IP's for CO chemisorbed on Ni. In the following, we will distinguish the NiCO ion states as to whether they are of Ni^+ or CO^+ character.

Concentrating first on the states of Ni^+ character, we find (just as for the Ni atom) that the lowest state of Ni^+CO involves removing the $\overline{4s}$ electron. However, since the $\overline{4s}$ orbital of NiCO is antibonding (it built in a substantial amount of $4p$ character to move out of the way of the CO orbitals), the IP for the $\overline{4s}$ orbital is only 5.96 eV as compared with 7.53 eV for the $4s$ orbital of the free Ni

Fig. 1. Comparison of calculated and experimental ionization potentials for i) CO, ii) NiCO and CO chemisorbed on Ni(111), iii) the free Ni atom and clean Ni(111). The experimental IP's for CO on Ni(111) and the d-band of Ni have been shifted toward higher binding energy by 3.6 eV to account for relaxation shifts not included in the one Ni atom "cluster".



atom. Given this destabilization of the $\overline{4s}$ orbital, one expects that the NiCO^+ state arising from ionization of the $\overline{4s}$ orbital should lead to a stronger bond than for NiCO neutral. Indeed, from table 1 one sees that the ${}^2\Delta$ ground state of NiCO^+ has a bond energy (D_e) of 2.50 eV as compared with 1.15 eV for the ground state of NiCO . Ionizing the $\overline{4s}$ orbital of the ${}^3\Sigma^+$ and ${}^3\Pi$ excited states of NiCO leads to the ${}^2\Sigma^+$ and ${}^2\Pi$ states of NiCO^+ with bond energies of 2.26 and 2.03 eV, respectively, somewhat smaller than for the ${}^3\Delta$ state, while the corresponding IP's, 5.88 and 5.93 eV, respectively, are very close to those obtained for the ${}^3\Delta$ state. Using the experimental heat of formation of NiCO^+ [11], one calculates a dissociation energy of 2.07 eV [12], somewhat smaller than the calculated value.

The other states of NiCO^+ in table 1 all correlate with states of Ni^+ arising from the s^1d^8 excited configuration of Ni^+ . The ordering of these states is as predicted by the atomic energies except for the state with $\pi\pi$ holes which is stabilized by interaction in the CI with the state having $\delta\delta$ holes. (A very similar effect was found for s^2d^8 states of NiCO .) The spectrum of s^1d^8 -like ion states obtained by ionizing from the ground state of NiCO covers a range of 3.1 eV in good agreement with the d-bandwidth (3.0 eV) observed in photoemission experiments (vide infra). Of this group of states only one, the s^1d^8 state with $\delta\sigma$ holes, appears to be bound with respect to dissociation to $\text{Ni}(^4F)$. The bond energies for these s^1d^8 states of NiCO^+ are smaller than for the $3d^9$ states for two reasons: (i) the hybridization of the $\overline{4s}$ orbital away from the CO leads to stabilization of the $\text{Ni } \overline{3d}$ orbitals thus making them more difficult to ionize, (ii) splitting of the $d\sigma$

Table 1
 Calculated energies for NiCO^+ involving ionization from Ni-like orbitals

NiCO^+ State	Multiplicity	Energy(eV) ^a	Ni^+ State ^b	Ni^+ Energy(eV) ^c	D Ni^+ - CO (eV)
$s^1 d^8 \delta \delta$ holes	quartet	10.78	20% ^4F , 80% ^4P	10.44	-2.32 ^d
$s^1 d^8 \sigma \pi$ holes	quartet	9.18	40% ^4F , 60% ^4P	9.95	-0.72 ^d
$s^1 d^8 \pi \pi$ holes	quartet	8.51	80% ^4F , 20% ^4P	8.96	-0.05 ^d
$s^1 d^8 \delta \pi$ holes	quartet	8.94	^4F	8.46	-0.48
$s^1 d^8 \delta \sigma$ holes	quartet	7.76	^4F	8.46 ^e	+ .70
$d^9 \sigma$ hole	doublet	5.27	^2D	7.53	2.26
$d^9 \pi$ hole	doublet	5.50	^2D	7.53	2.03
$d^9 \delta$ hole	doublet	5.03	^3D	7.53	2.50

^a The zero point of energy is taken as $\text{Ni} + \text{CO}$ at $R = \infty$ which corresponds to -153.2533. The energies of the $^3\Delta$, $^3\Sigma^+$, and $^3\Pi$ states are then -0.932, -0.606, and -0.429 eV, respectively, using a consistent CI treatment.

^b This is the mixture of pure atomic states of Ni^+ which correspond at $R = \infty$ to the Ni^+ CO configuration.

^c This corresponds to the energy of CO plus the appropriate mixture of Ni^+ states using the same basis as for the NiCO^+ calculations (M. J. Sollenberger, M.S. Thesis, California Institute of Technology, 1975).

^d Dissociation energy relative to Ni^+ (^4F).

^e The experimental values for ^2D , ^4F , and ^4P are 7.62, 8.70, and 10.63 eV, respectively, whereas the calculated value for ^4P (not shown) is 10.94 eV.

$d\pi$, and $d\delta$ orbitals due to the CO tends to mix $4p$ character into the $4F$ ground state of Ni^+ . (The only exception is for the case of $\sigma\delta$ holes which leads to pure $4F$ atom states.) It is this latter effect which is responsible for the lack of binding of four of the s^1d^8 states.

Looking now at the ion states of CO^+ character, we see from Fig. 1 that the $\overline{4\sigma}$ and $\overline{1\pi}$ ionization potentials have changed only slightly, whereas the $\overline{5\sigma}$ ionization has increased in energy by 2.49 eV. This effect derives from stabilization of the $\overline{5\sigma}$ orbital by interaction with the $3d^9 Ni^+$ core (which was partially exposed due to the $\overline{4s}$ orbital hybridizing away from the CO orbitals). The ionization potentials for the $^3\Pi$ and $^3\Sigma^+$ states of $NiCO$ (which involve a $3d\pi$ and $3d\sigma$ hole, respectively) differ only slightly from the corresponding ionization potentials for the $^3\Delta$ states (see table 2).

For ionizations from the CO-like orbitals, the results shown in table 2 and Fig. 1 are derived from extensive CI calculations for the quartet states which arise from high spin coupling the $\overline{4s}$, $\overline{3d}$, and \overline{CO} (ion) orbitals. However, for each such quartet state there are two doublet states which will be somewhat higher in energy, depending on the size of the exchange integrals involved. Since the $\overline{4s}$ and $\overline{3d}$ orbitals are triplet coupled in $NiCO$, only that spin state of $NiCO^+$ which also has these orbitals high spin coupled has a non-zero oscillator strength. However, we find that for the ionizations considered, both doublet states contain a component of the allowed spin function and thus both have a finite oscillator strength. The result is that the transitions are broadened by the quartet-doublet splitting. These splittings (estimated from a small CI over all the dominant ion state

Table 2

Calculated ionization potential (eV) for quartet states of NiCO⁺ involving ionization of CO-like orbitals.^a

NiCO State		Ionized Orbital		
Sym.	Hole ^c	$\overline{5\sigma}$	$\overline{4\sigma}$	$\overline{1\pi}$
³ Π	dπ	16.83	20.06	17.17 ^b
³ Σ ⁺	dσ	16.24	19.90	16.80
³ Δ	dδ	16.50	19.75	17.09

^aThe quoted energies are relative to the energy of the corresponding NiCO state. Using a CI consistent with the ion state CI, we find -153.26906, -153.27556, and -153.28755 for ³Π, ³Σ⁺, and ³Δ, respectively.

^bFor π ionizations out of the ³Π state there are four states within an energy range of 0.17 eV depending on which π orbital is ionized. The value quoted is obtained by averaging the energy of these states.

^cThe Ni character is (4s)(3d)⁹ with the hole as indicated. The ³Δ state is the ground state of NiCO.

configurations) are 1.06, 0.38, and 0.22 eV for the $\overline{5\sigma}$, $\overline{4\sigma}$, and $\overline{1\pi}$ ionizations, respectively. (The width of the bands shown in Fig. 1 corresponds to these splittings.) The result is that the $\overline{5\sigma}$ ionization (which for the quartet spin coupling is at 16.50 eV) extends from 16.50 to 17.56 eV and similarly the $\overline{1\pi}$ and $\overline{4\sigma}$ ionizations extend from 17.09 to 17.29 eV and 19.75 to 20.13 eV, respectively (not including the Franck-Condon width). Thus the $\overline{5\sigma}$ and $\overline{1\pi}$ ionizations overlap and lead to a total combined width of 1.06 eV, whereas the $\overline{4\sigma}$ ionization is 0.38 eV wide and 2.96 eV higher (taking the difference between the centers of the bands).

In the following, we compare the results for NiCO with experimental results on the Ni(111) surface. [As discussed in Section 4, it is probable that the Ni-CO bonding orbitals for the (110) and (100) surfaces are quite different from those of NiCO, whereas the NiCO orbitals for the Ni(111) surface are similar to those of NiCO. Hence, it is the (111) surface that our NiCO calculations model.]

3.2 Experimental Results

For CO on Ni(111) two CO derived bands are observed. The P_2 band at 7.6 eV (IP = 13.6 eV) is quite broad and asymmetric, while the P_1 band at 10.7 eV (IP = 16.7 eV) is sharper. (The values in parentheses are corrected to vacuum using a value of $E_f = 6.0$ eV as suggested by Eastman [8b].) Since there was a close correspondence between these values and the gas phase 1π and 5σ levels (14.0 and 16.9 eV, respectively) of CO, and since the 4σ ionization cross

section is small at an incident photon energy of 21.2 eV, it was at first thought that the P_1 band corresponds to the 1π level of CO and the P_2 band to the 5σ level with the 4σ level too weak to be seen [8a]. However, reexamination of the system using variable photon energies (in the range of 20.0 to 100.0 eV) and comparing the change in cross sections with incident photon energy for free CO and chemisorbed CO showed that the P_1 band is the $\overline{4\sigma}$ level and that the P_2 band is a mixture of the $\overline{5\sigma}$ and $\overline{1\pi}$ levels [8c]. For CO chemisorbed to Ni(111) the P_2 band was resolved (from the angular dependence of the photoemission) into two bands centered at 6.2 eV (IP = 12.2 eV) and 7.5 eV (IP = 13.5 eV), which are associated with the $\overline{5\sigma}$ and $\overline{1\pi}$ levels, respectively [8b].

In addition to bands due to the CO, the Ni d-bands which involve ionization from the Ni 3d orbitals extend from ~ 5.4 eV to ~ 8.4 eV for the clean Ni(111) surface. (The top of the conduction band is close to the top of the d-band for the free metal, thus it is assumed that the top of the d-band relative to the vacuum level corresponds to the work function.) Upon absorbing CO the work function increases by ~ 0.6 eV, thus the d-band is shifted upward by 0.6 eV and extends from ~ 6.0 eV to ~ 9.0 eV.

Photoelectron spectra of chemisorbed molecules are often analyzed with reference to the gas phase spectrum of the free molecule. The shifts in the ionization potentials upon chemisorption are then divided into two classes:

1. bonding shifts which depend on the nature of the bonding to the surface and normally lead to higher ionization potentials for the bonding orbitals; and
2. relaxation shifts which result from polarization of the metal by the positive ion hole. The relaxation shifts normally result in a somewhat uniform decrease of all the ionization potentials (typically by 2-3 eV) [8c].

3.3 Comparison

Our calculations indicate that only the $\overline{5\sigma}$ orbital shows a significant bonding shift (~ 2.5 eV), leading to the $\overline{5\sigma}$ and $\overline{1\pi}$ ionizations being nearly degenerate. These bands are broadened by quartet-doublet splitting, leading to a combined bandwidth of about 1.0 eV. (For the actual surface the bands should be further broadened due to coupling to the ion states of the metal and also due to unresolved vibrational structure.) The $\overline{4\sigma}$ ionization is predicted to be about 3.0 eV higher and considerably sharper (bandwidth ~ 0.4 eV).

Shifting our calculated IP's by 3.6 eV (*vide infra*) leads to IP's of 12.9 ($\overline{5\sigma}$), 13.5 ($\overline{1\pi}$), and 16.2 ($\overline{4\sigma}$) eV in good agreement with the experimental values 12.2 ($\overline{5\sigma}$), 13.5 ($\overline{1\pi}$), and 16.7 ($\overline{4\sigma}$) from the recent angular resolved studies [8b]. Thus the pattern of the bonding shifts for CO on the Ni surface is well reproduced with the simple NiCO model, indicating that the essential features of the bonding to the surface are localized in nature.

Applying the same shift to the ionizations involving 3d electrons leads to levels at 4.86 eV and 6.84 eV for the free Ni atom and

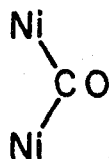
at 5.07 eV, 6.27 eV, and 8.11 eV for ionizations involving the $\overline{3d}$ orbitals of NiCO. Since the 3d electrons of the metal should not be strongly modified from the atom (the 3d orbitals have small overlaps at the separations involved in the bulk metal), these levels should provide a reasonable representation of the effects of CO adsorption on the d-band of the metal. Thus, our calculations predict that the d-band should be shifted somewhat toward higher binding energies, as is observed (see Fig. 1). This effect derives from stabilization of the Ni $\overline{3d}$ orbitals due to the Ni $\overline{4s}$ orbital hybridizing away from the CO orbitals.

As shown in Fig. 1, comparison of calculated and experimental ionization potentials requires that the experimental spectrum be shifted upward by about 3.6 eV (depending on the value used for E_f) to obtain the best correspondence for CO derived levels. Clearly such shifts are expected since our Ni model is not large enough to include polarization effects responsible for the relaxation shift in the IP's. However, such effects are expected to shift all the NiCO ionization potentials by nearly the same amount and thus we expect that larger clusters would lead to essential features similar to the NiCO. This point is treated in more detail in the next section.

4. NiCO as a Model for CO Chemisorbed on Ni(111)

4.1 The Bonding to the Surface

Chemisorbed CO molecules on metal surfaces such as Ni are commonly assumed to be in either bridged sites



or linear sites



with the bridged sites usually assumed to involve greater bonding. For bridge bonding to Ni atoms that are second nearest neighbors [as on the (100) surface] we find stronger bonds ($D_e = 1.42$ eV) than for the linear site ($D_e = 1.15$ eV) and a significantly different bonding (significantly more charge transfer for the bridged bond). On the other hand, for nearest neighbor Ni atoms as on the (111) surface, we find the bridge bonding to be similar in character to the linear bond (the calculations indicate a weaker bond) [14].

Our calculated bond energies are in reasonable agreement with experimental D_0 values of 1.15 eV for Ni(111), where we expect linear bonding, and 1.30 eV to 1.39 eV for Ni(100) and Ni(110), where we expect bridged bonding (between second nearest neighbor Ni atoms). Thus, we will assume that the character of CO bonding on the (111) surface is as found for the linear site, while the character for the (100) and (110) surfaces is as found for the bridged site.

The LEED data for CO on Ni(111) are consistent with the superposition of the three possible domain orientations of a $\sqrt{3} \times \sqrt{3}/R$ 30°

structure [7]. In Ref. 7, a structure model is suggested in which the CO molecules are bridged; however, as shown in Fig. 2, a structure in which the CO molecules are bonded directly above surface Ni atoms is also consistent with the LEED data.

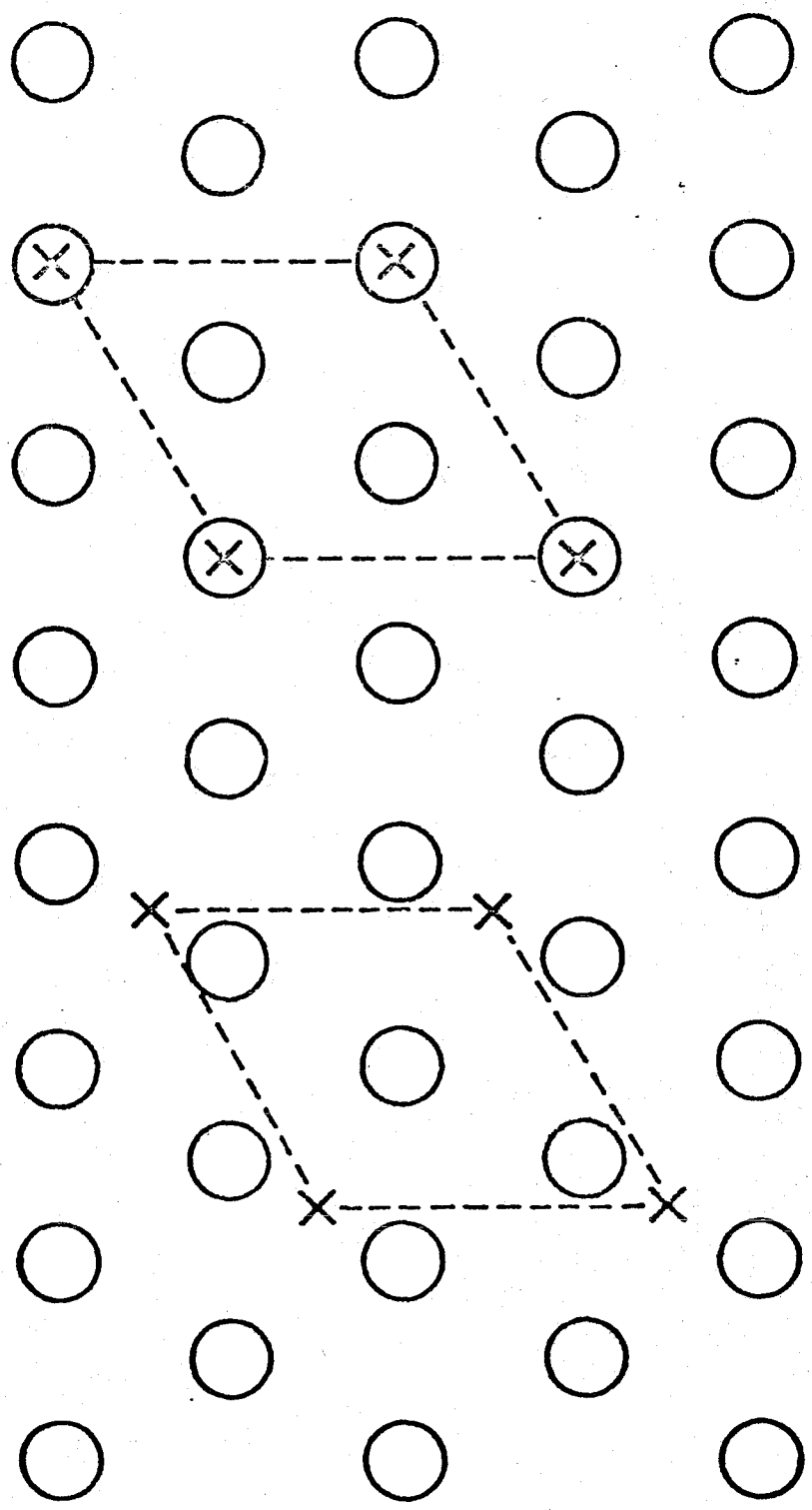
For NiCO, we found that the Ni atom has a $(4s)^1(3d)^9$ configuration and calculations on a number of metal clusters also indicate a ground state in which each Ni is effectively of $(4s)^1(3d)^9$ character. Thus, the main change between NiCO and the bonding of CO to the Ni surface is that the latter case has the $\overline{4s}$ orbital involved in the states of the conduction band (involved in metal-metal bonding) so that it will respond differently to the CO. For the Ni(111) surface each surface atom has six nearest neighbors in the surface and three nearest neighbors below the surface. In this case, we expect that the three nearest neighbors below the surface are most important in the bonding of the CO since they are in the direction the $\overline{4s}$ orbital has to hybridize to move out of the way of the CO orbitals.

To study this possibility we carried out calculations for the bonding of CO to one apex of a tetrahedral Ni_4 cluster (i.e., we added to the NiCO calculation the three nearest neighbors below the surface). In order to simplify the calculations, a d-averaged potential [15] was used for the three Ni atoms below the surface. [The d-averaged potential replaces the Ar core plus a weighted average over the various components of the $3d^9$ configuration, thus leaving only a singly-occupied valence orbital ($4s$ for the free atom); this orbital is given full variational freedom to rehybridize or shift to other centers.] For the apex Ni atom we used the same potential and basis set as for the NiCO calculation.

Fig. 2. Comparison of bonding models (involving superposition of three possible domain orientations of a $\sqrt{3} \times \sqrt{3}/R30^\circ$ structure) for bridged structures as suggested by Ref. 7 (a), with bonding consistent with a site where the CO is bonded directly above a surface Ni atom (b).

(a) Bridged site

(b) Linear site



Classifying the orbitals of the Ni_4 cluster with respect to the C_{3v} symmetry of the Ni_4CO cluster leads to three low-lying configurations for the Ni_4 cluster,

$$a_1^2 e_x^1 e_y^1, \quad (1)$$

$$a_1^2 e_x^1 2a_1^1, \quad (2)$$

and

$$a_1^2 e_y^1 2a_1^1, \quad (3)$$

which are the three degenerate components of the 3T_1 state in the full T_d symmetry of the Ni_4 cluster. [Using C_{3v} symmetry, we find that (2) and (3) are degenerate and (1) is 0.004 eV higher.] [In the following the hole in the 3d shell of the surface Ni atom is taken as a 3d δ orbital.]

Bringing up a CO molecule to the Ni_4 cluster we find that the Ni_4CO state with configuration (1) is considerably stabilized relative to the Ni_4CO states related to (2) or (3), leading to a bond energy, $D_e(\text{Ni}_4\text{-CO})$, of 2.25 eV for the Ni_4CO state from (1) as compared with 1.07 eV for the Ni_4CO state from (2) or (3) and 0.79 eV for the NiC bond in NiCO (at the same level of calculation and Ni-C distance). The large difference in bond energy between these two configurations can be understood in terms of differences in the charge distributions induced into the Ni_4 cluster for the two configurations. For the free Ni_4 cluster the radical orbitals e_x and e_y have zero density on the surface Ni atom while the paired $1a_1$ orbital has significant amplitudes on all four centers and the radical $2a_1$ orbital has large amplitude on the

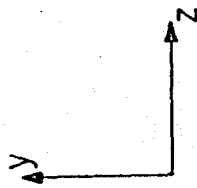
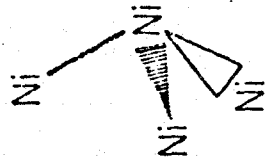
surface Ni (like a 4s orbital hybridized away from the bulk metal). Thus (1) has a positive charge on the surface Ni (total Mulliken population 0.73) and leads to a large bond energy for the same reason that bonding CO to the $3d^9$ configuration of Ni^+ leads to a larger bond energy than did bonding to Ni neutral. On the other hand, (2) or (3) have a slight negative charge on the surface Ni atom (Mulliken population 1.14) and thus lead to a bond energy comparable to that for NiCO.

For the real surface the three Ni atoms below the surface should be bonded to other atoms and we expect that configuration (1) is not a good model. (For the solid, states of this sort will be high in energy.) On the other hand, (2) and (3) seem to be reasonable models and hence we will compare the bonding in NiCO with this state of the Ni_4CO cluster.

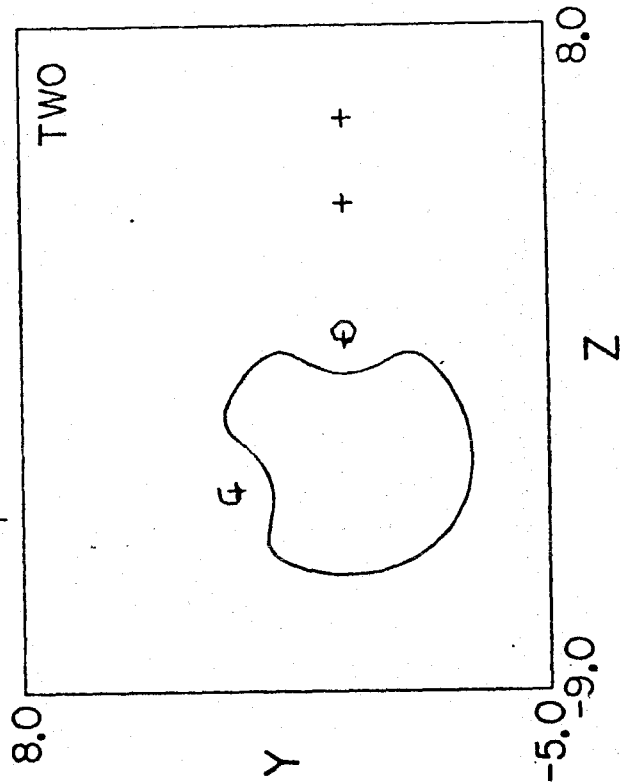
In Fig. 3 we show the orbitals of (2). Here one sees that the $1a_1$ orbital is a bonding orbital that extends over all four centers, whereas the $2a_1$ orbital is essentially a $\overline{4s}$ orbital on the surface Ni atom and has hybridized away from the bulk solid. Thus, the surface Ni atom has essentially a $4s^1 3d^9$ configuration (the actual population for the 4s basis function is 1.081) and is bonded to the solid by delocalization of the $1a_1$ orbital onto the surface atom. Bringing up a CO to the surface Ni atom requires that the $2a_1$ orbital hybridize so as to move away from the CO (i.e., into the solid) leading to stabilization of the CO 5σ orbital by interaction with the partially exposed $Ni^+ 3d^9$ configuration as in NiCO. These expectations are borne out by the shapes of the Ni_4CO orbitals (Fig. 4), where one sees a striking

Fig. 3. Selected orbitals of the 3E state of Ni_4 . Unless otherwise noted, all plots have uniformly spaced contours with increments of 0.05 a.u. Positive contours are indicated by solid lines, negative contours are indicated by short dashes, and nodal lines are indicated by long dashes. The same conventions are used for other figures.

SELECTED ORBITALS OF Ni_4



(a) The $1a_1$ Orbital



(b) The $2a_1$ Orbital

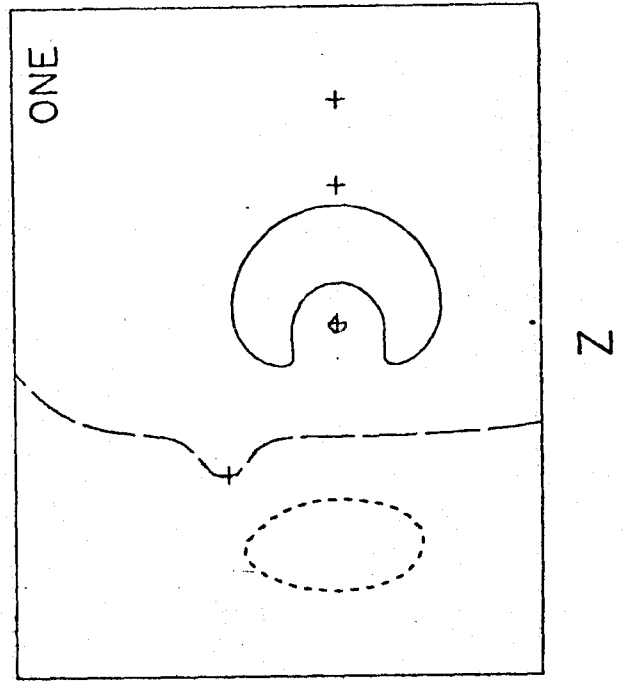


Fig. 4. Selected orbitals of the Ni_4CO state derived from the ${}^3\text{E}$ state of Ni_4 .

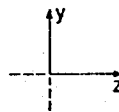
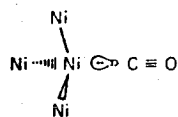
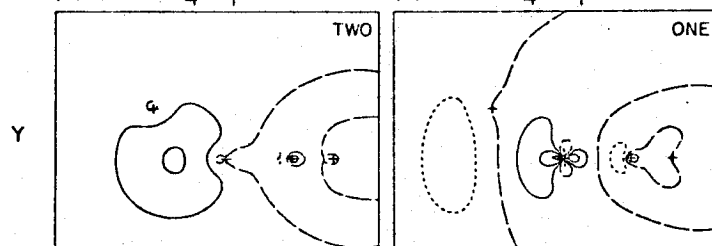
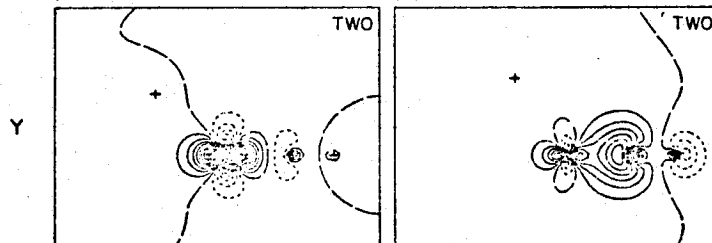
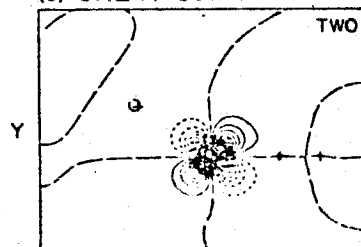
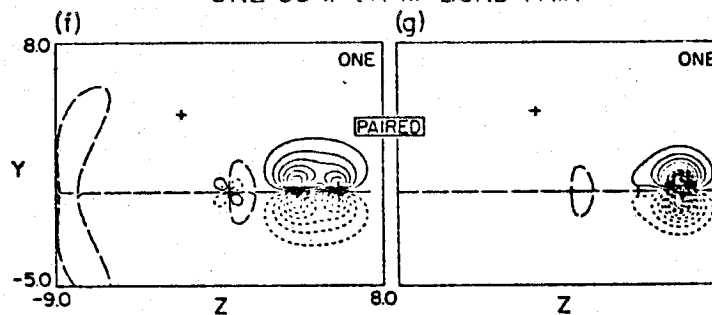
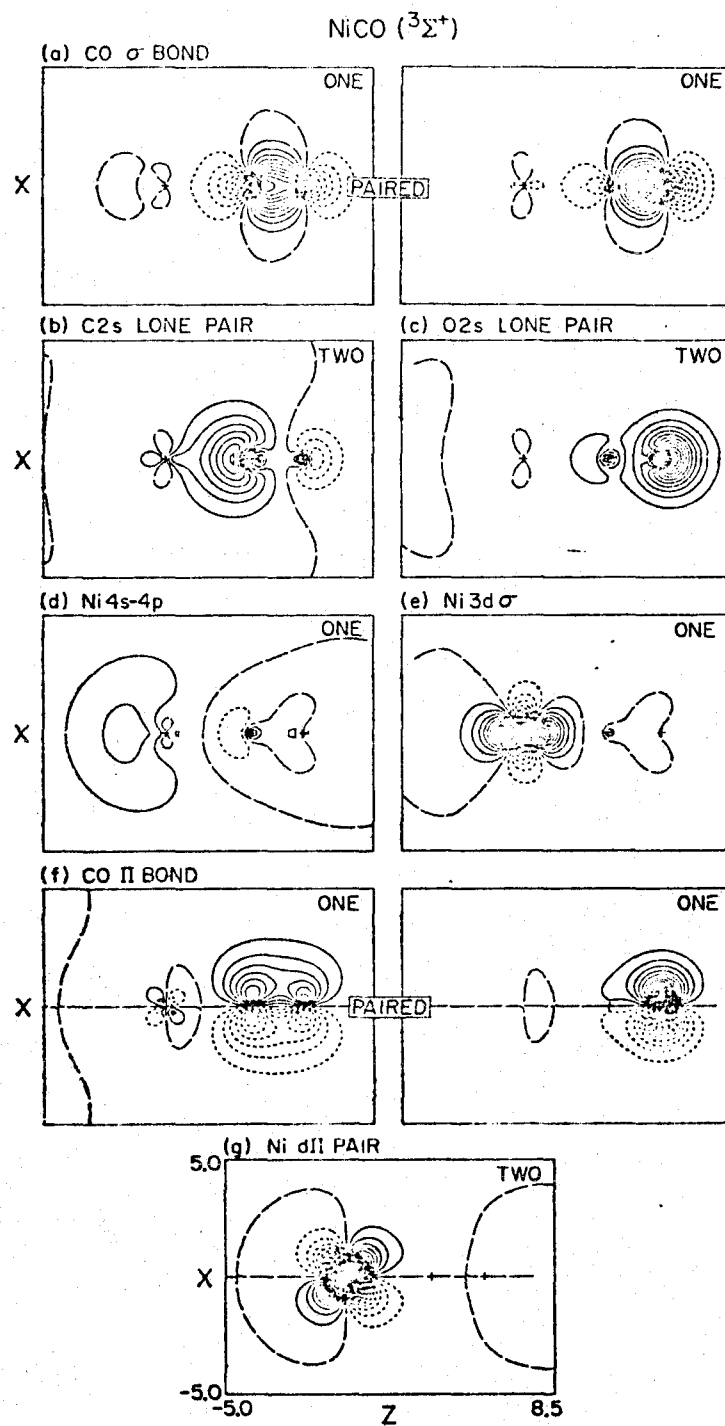
SELECTED ORBITALS OF Ni₄CO(a) THE Ni₄ $\bar{1}a_1$ ORBITAL (b) THE Ni₄ $\bar{2}a_1$ ORBITAL(c) THE Ni 3d σ ORBITAL (d) THE C 2s OR 5 σ PAIR(e) ONE Ni 3d π PAIRONE CO π OR $\bar{1}\pi$ BOND PAIR

Fig. 5. Selected orbitals of the NiCO ${}^3\Sigma^+$ state.



similarity to the NiCO orbitals (Fig. 5). Thus it appears that the basic effects involved in the bonding of CO to a single Ni atom are reproduced by the appropriate state of the Ni₄ cluster and should apply to the bulk metal as well.

4.2 The Photoelectron Spectrum

Whereas the basic nature of the bonding to the surface is probably not strongly affected by adding more Ni atoms to the NiCO cluster, the ion levels of NiCO are expected to be strongly modified by the presence of additional Ni atoms. Specifically, one expects a strong polarization effect which involves mixing the ion states of the Ni cluster with the CO ion states (sometimes termed a relaxation shift). For NiCO the ion states were described in terms of two distinct groups of states, the first of which involved ionizations out of the Ni-like orbitals, and the second of which involved ionizations out of CO-like orbitals. For NiCO these sets of states are well separated in energy and do not interact strongly in the CI. For larger clusters the d levels of the Ni atoms should not be strongly modified (since the d orbitals have very small overlaps at the interatomic separations involved here); however, the 4s orbitals will combine into new orbitals such that the bonding orbitals are much more tightly bound than for the free atom (some nonbonding orbitals may increase in energy). Thus some ion states of the cluster will be much higher in energy than for a single Ni atom. In the CI calculations the CO⁺ states would couple more strongly with the higher Ni

ion states of the cluster (i.e., build in Ni^+ character) leading to mixed states which are CO^+ in character but lower in energy than for the comparable NiCO^+ states. In addition, these states would be expected to split due to d orbital interactions. Thus the overall picture would be a decrease in energy of the CO^+ -like ion states of NiCO and some broadening of the levels as more Ni atoms are added to the cluster.

At the present time, calculations for the ion states of CO bonded to large Ni clusters are not feasible for the extensive level of CI used in NiCO^+ . Thus, for the purpose of comparing the NiCO ion states to experiment, we resort to a different type of correction which is based on simple classical electrostatics. Here one simply assumes that all polarization effects have been included within a sphere of radius r_0 into the metal, which in this case we take as 2.35 bohr (one-half the nearest neighbor distance in Ni metal). The problem then reduces to the classical one of finding the interaction energy for a charge a distance h from the metal with the metal surface (i.e., with the image charge) but with a hemisphere of radius r_0 cut out of the metal (directly below the charge). The result in atomic units is simply

$$\Delta E = -\frac{1}{4h} \left\{ \frac{h}{r_0 + h} - \ln \left(\frac{\sqrt{r_0^2 + h^2}}{r_0 + h} \right) \right\} \quad (4)$$

This type of approach has worked well for corrections in the IP's for Si clusters [16]. In the metal this type of correction is less reasonable since the dielectric constant of the metal is infinite.

In table 3 we give the values of h (computed from the CI wavefunction as the center of charge for each electronic state of NiCO^+) and the ionization potentials for the states of NiCO corrected using formula (4). While the correction (4) is in the right direction, the magnitude of the correction is not large enough to account for the full magnitude of the relaxation shift. Thus, it appears that to obtain an adequate model of the surface (for IP's) we must include in the cluster at least the nearest neighbor Ni atoms with the dominant polarization effects included explicitly. The use of (4) to correct for image charge effects outside the larger sphere might provide accurate absolute IP's. We have not carried out such CI calculations for the ion states, and hence we will simply assume that the levels from the NiCO^+ calculations would be shifted by amounts proportional to the above estimates.

5. The Comparison of Theoretical Methods for the Ion States of NiCO

5.1 Comparison of the CI Method with Koopmans' Theorem

It is well known that the orbital energies from the usual Hartree-Fock (HF) wavefunction correspond to the energy change that would occur if an electron were removed from that orbital, keeping all the other orbitals fixed (Koopmans' theorem). One might expect IP's calculated in this way to be high since the ground state orbitals are not optimum for the ion. However, the ion, which has one less electron than the neutral, has a smaller electron correlation error (in the HF approximation) and this differential correlation error tends to partially cancel the readjustment error, often leading to results in good agreement (10%)

Table 3

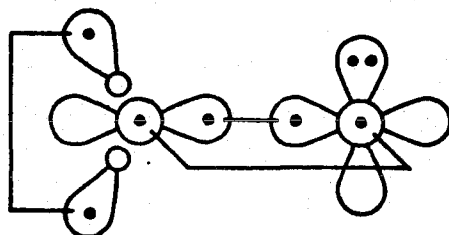
Electrostatic corrections for ionizations out of the CO-like orbitals of NiCO.
 h is the height (in bohr) of the charge center with respect to the Ni

	Orbital			State
	$\overline{5\sigma}$	$\overline{4\sigma}$	$\overline{1\pi}$	
h ^a	4.536	4.819	5.221	} ³ Π
ΔE (eV)	1.436	1.359	1.263	
Corrected I. P. (eV)	15.39	18.70	15.91	
h	4.414	5.365	4.810	} ³ Σ ⁺
ΔE (eV)	1.471	1.231	1.361	
Corrected I. P. (eV)	14.77	18.67	15.44	
h	4.254	3.923	5.009	} ³ Δ
ΔE (eV)	1.520	1.632	1.312	
Corrected I. P. (eV)	14.98	18.12	15.78	

^a The nuclei are at 0.000, 3.480, and 5.650 for Ni, C, and O, respectively.

with experiment.

In a localized description the ground state of CO may be described as



(5)

where the C lone pair has been angularly correlated in the direction of the empty carbon p orbital. In this picture, there is no comparable correlation effect of the O(2s) pair because there is an occupied p orbital in each direction [17]. Thus, at this level of description, if comparable readjustment effects were involved, one would expect the error in the Koopmans' theorem ionization potentials to be larger for ionization from the O(2s) [or (4 σ)] orbital than from the C(2s) [or (5 σ)] or 1 π orbitals. In fact, the actual errors in using Koopmans' theorem for CO are 2.12 (4 σ), 0.98 (5 σ), and 0.45 (1 π) eV, respectively, all high [19]. This is consistent with the fact that the π correlation error is much larger than the C(2s) correlation error (see table 4).

Examining table 4 in more detail, one sees that at the Koopmans' theorem level the addition of d functions has a relatively small effect on the ionization potentials. We conclude that Koopmans' theorem ionization potentials are unreliable for CO and thus should be unreliable for NiCO.

Now consider the CI results. Here one sees that at the valence double zeta (VDZ) level the agreement with experiment is fair (errors

Table 4

Comparison of theoretical methods for calculating ionization potentials for CO and NiCO

	Koopmans' Theorem			CI		Exp.	
	VDZ Basis	VDZd Basis	DZd Basis [23]	VDZ Basis	VDZd Basis		
CO	3 σ	42.46	41.42	41.08	---	---	38.9
	4 σ	21.73	21.84	21.80	19.41	19.72	19.72
	1 π	17.63	17.36	17.12	17.17	17.25	16.91
	5 σ	15.07	14.99	15.15	13.09	13.76	14.01
NiCO	3 σ	43.54	---	42.09	---	---	---
	4 σ	23.41	---	22.97	19.75	---	16.7 ^b
	1 π	18.88	---	18.26	17.09	---	12.2 ^b
	5 σ	19.66	---	18.42	16.50	---	13.5 ^b
	3d δ_{xy}	17.83	---	---	11.71	---	---
	3d $\delta_{x^2-y^2}$	16.24	---	---	---	---	---
	3d π	14.95	---	---	9.87	---	---
		14.95	---	---	---	---	---
	3d σ	13.64	---	---	8.69	---	---
	4s	6.18	---	---	5.96	---	---

^a The VDZ basis is the same as the CO basis used in paper I. The VDZd basis was augmented with a single set of d primitives on C and O ($\alpha_C = 0.60$ and $\alpha_O = 1.04$).

^b Experimental values for CO bonded to Ni (111).

of -0.31 and $+0.26$ eV, respectively) for the 4σ and 1π levels but quite poor (-0.92 eV error) for the 5σ level. We find that this problem results from an inadequate description of the C(2s) angular correlation of CO neutral at the VDZ level [20].

Including d polarization functions, the CI leads to substantially better results for the 5σ level (-0.25 eV error) and 4σ level (0.00 eV error) while the 1π level is slightly worse ($+0.34$ eV error).

More insight into the problem may be obtained by looking at the CI energy contributions of configurations involving the C(2s) pair for the ground state and each of the ion states. In the VDZ basis, we find that such configurations contribute 15.6 mh for the ground state, 3 mh for the 5σ ion state, 22.5 mh for the 4σ ion state, and 26.9 mh for the 1π ion state. The much lower contribution for the 5σ ion state, as compared with the 4σ ion state of course simply reflects the fact that for CO the 5σ ion state corresponds to ionization from the C(2s) orbital. For the 4σ ion state, the correlation of the C(2s) pair is actually more important than for the ground state. This may be understood by noticing that this state involves ionization out of a combination of the O(2s) and bond orbitals, and hence the center of charge is toward the O. This leads to a shift of the π orbitals toward the O and decreases the π density at the carbon. The net effect is that there is more π -hole character at C, which increases the angular correlation of the C(2s) pair. A similar effect is involved for the 1π ion. Thus, for CO there are very important differential correlation effects involving the C(2s) pair, and addition

of d functions, which improves the description of this pair, becomes essential [22].

For NiCO, on the other hand, we find that correlation of the C(2s) pair leads to energy contributions of 10.0 mh for the ground state, 3.0 mh for the $\bar{5}\sigma$ ion state, 3.0 mh for the $\bar{4}\sigma$ ion state, and 10.3 mh for the $\bar{1}\pi$ ion state. Thus, angular correlation of the C(2s) pair is less significant and the differential errors are much smaller. This effect is mainly a result of π donation from the Ni $d\pi$ orbitals into the partial π hole on C. In addition, for NiCO, as we saw in Section 3, the C(2s)-like orbital is more tightly bound. Thus, the $\bar{4}\sigma$ and $\bar{5}\sigma$ ions are much closer in energy and mix strongly in the CI. This effect leads to both of these orbitals containing essentially the same amount of C(2s) ion character and thus there is a similar amount of C(2s) correlation in the CI. The net effect is that $d\pi$ orbitals in the basis are expected to be much less important for NiCO ion states than they were for CO ion states, and they were not included in the calculations reported here.

5.2 Comparison with Other Calculations

Recently Bagus et al. [23] have carried out ab initio Hartree-Fock (HF) calculations on NiCO which to some extent parallel the work reported here. Although the calculations reported in Ref. 23 lead to similar qualitative conclusions relative to the bonding shifts of CO on Ni as reached in the present paper, and although the HF wavefunctions were solved for carefully using excellent basis sets, the present calculations are different in two important respects which lead us to believe that our results are substantially more reliable.

The first difference has to do with the method of calculating ionization potentials. Bagus et al. calculate ionization potentials as differences between the HF energies of the ion state and the neutral molecule--a method which for CO is clearly less reliable than Koopmans' theorem (see the discussion in Section 5.1), which is in turn not reliable for the systems discussed here.

In addition, Bagus et al. neglect a serious deficiency in the usual HF description of the electronic states of the Ni atom. The problem, as discussed in paper I, is that HF calculations for the Ni atom with the usual basis and level of correlation lead to the s^2d^8 (3F) state of the Ni atom being 2.3 eV below the s^1d^9 (3D) state, whereas experimentally the two states are essentially degenerate. Since the poorly described s^1d^9 state is the state involved in the bonding of NiCO, whereas the s^2d^8 state leads to repulsive potential curves, the net effect is that the NiCO wavefunction incorporates excessive amounts of s^2d^8 character with the consequence that NiCO is not bound relative to the lower (in this approach) s^2d^8 state and is bound by only 0.2 eV relative to the s^1d^9 state. As discussed in paper I, a correct description of the atom levels requires a greatly extended basis and greatly extended CI which is currently not practical for molecules. In our calculations we have avoided this problem by modifying the effective potential such that the correct atomic separations are obtained while leaving the shapes of the orbitals unchanged. Our approach leads both to a correct description of the atoms and a bond energy for NiCO ($D_e = 1.15$ eV) in reasonable agreement with experimental values (1.15 eV).

The effects of the incorrect description of the Ni atom states in the ab initio calculations of Ref. 23 are apparent in the Koopmans' theorem ionization potentials as shown in table 4. Looking first at the CO numbers, one sees that our VDZd basis gives results very comparable (within 0.3 eV) to the DZd basis used by Bagus et al. For NiCO, on the other hand, the sigma orbital energies reported by Ref. 23 are all smaller than for the calculation reported here. In particular, the $\bar{5}\sigma$ orbital, which is responsible for the bonding in NiCO, is 1.24 eV less tightly bound than in our calculation. These effects result, we believe, from excessive incorporation of s^2d^8 character for the wavefunction of Ref. 23. These differences seem to be responsible for the negative Ni-CO bond energy obtained by Bagus et al. (comparable ab initio calculations carried out by us show similar results). Clearly, this problem also affects the bonding shift for CO bonded to Ni.

6. Details of the Configuration Interaction (CI) Calculations

6.1 NiCO⁺ States

The major problem in doing CI calculations for the ion states of NiCO is that states which involve ionization out of Ni-like orbitals are in general not separated by symmetry from states which involve ionization out of CO-like orbitals. Since the former are lower in energy, a good description of the latter set of states requires that the CI simultaneously describe both sets of states. This requires the use of a large basis set with configurations appropriate for both sets of states and the solution of all the lower roots even though only the higher roots are of interest.

In these calculations the CI basis consisted of 24 functions. The starting point for the CI basis was the 16 generalized valence bond (GVB) orbitals of the $^3\Delta$ state of NiCO. The two 1s-like orbitals were eliminated from the CI by appropriate modification of the one-electron integrals. To describe readjustment effects, the resulting 14 functions were augmented by adding (1) three π virtuals in each direction chosen as the more diffuse component of the Ni(3d π), C(2p π), and O(2p π) atomic orbitals, respectively (six functions); (2) virtuals corresponding to the more diffuse Ni(3d $_{xy}$) and Ni(3d $_{x^2-y^2}$) atomic orbitals, respectively (two functions); (3) virtuals corresponding to the more diffuse Ni(3d σ) atomic function and an orbital appropriate to Ni(4s) from an s^2d^8 state of NiCO (two functions). These latter ten functions were orthogonalized to the 14 GVB orbitals leading to a CI basis of 24 functions.

In table 5 the dominant configurations for each symmetry type (based on C_{2v} symmetry) are listed. This list was generated by considering states which could arise from low-lying states of CO($^1\Sigma_g^+$) + Ni $^+$ and the three low-lying states of Ni(3D) + CO $^+$.

For ionizations involving CO, the spin state was restricted to be quartet. In addition, since the quartet spin state involves at least three open shell orbitals and our present CI program allows a maximum of six open shell orbitals, consistent levels of CI for various spin states require a maximum of two, three, four, and five open spin orbitals for singlet, doublet, triplet, and quartet spin states, respectively.

Within the above restrictions, double excitations were allowed from each of the dominant configurations, which consisted of products

Table 5
 Dominant configurations for the NiCO⁺ CI calculations

State Character	Symmetry in C _{2v}	O(2s)	C(2s)	3dσ	4s	σ	σ*	π _x	π _y	δ _{xy}	δ _{x²-y²}
σ ionization	$\left\{ \begin{array}{l} {}^4A_1 \\ {}^4A_1 \\ {}^4A_1 \end{array} \right.$	2	1	1	1	2	0 0 0	2 2 0 0 0 0	2 2 0 0 0 0	2 0	2 0
from ${}^3\Sigma^+$ state		1	2	1	1	2	0 0 0	2 2 0 0 0 0	2 2 0 0 0 0	2 0	2 0
		2	2	1	1	1	0 0 0	2 2 0 0 0 0	2 2 0 0 0 0	2 0	2 0
π ionization	$\left\{ \begin{array}{l} {}^4A_1 \\ {}^4A_1 \end{array} \right.$	2	2	2	1	2	0 0 0	1 1 0 0 0 0	2 2 0 0 0 0	2 0	2 0
from ${}^3\Pi$ state		2	2	2	1	2	0 0 0	2 2 0 0 0 0	1 1 0 0 0 0	2 0	2 0
Ni (s ¹ d ⁸) δσ holes	4A_2	2	2	1	1	2	0 0 0	2 2 0 0 0 0	2 2 0 0 0 0	1 0	2 0
Ni (s ¹ d ⁸) ππ holes	4A_2	2	2	2	1	2	0 0 0	1 2 0 0 0 0	1 2 0 0 0 0	2 0	2 0
Ni (s ¹ d ⁸) δδ holes	4A_2	2	2	2	1	2	0 0 0	2 2 0 0 0 0	2 2 0 0 0 0	1 0	1 0
σ ionization	$\left\{ \begin{array}{l} {}^4A_2 \\ {}^4A_2 \\ {}^4A_2 \end{array} \right.$	2	1	2	1	2	0 0 0	2 2 0 0 0 0	2 2 0 0 0 0	1 0	2 0
from ${}^3\Delta$ state		1	2	2	1	2	0 0 0	2 2 0 0 0 0	2 2 0 0 0 0	1 0	2 0
		2	2	2	1	1	0 0 0	2 2 0 0 0 0	2 2 0 0 0 0	1 0	2 0

Table 5 (continued)

State Character	Symmetry in C_{2v}	O(2s)	C(2s)	3d σ	4s	σ	σ^*	π_x	π_y	δ_{xy}	$\delta_{x^2-y^2}$
π ionization	$\left\{ \begin{array}{l} {}^4A_2 \\ {}^4A_2 \end{array} \right.$	2	2	2	1	2	0 0 0	1 2 0 0 0 0	2 1 0 0 0 0	2 0	2 0
from ${}^3\Pi$ state		2	2	2	1	2	0 0 0	2 1 0 0 0 0	1 2 0 0 0 0	2 0	2 0
Ni (s^1d^8) σ π holes	4B_1	2	2	1	1	2	0 0 0	1 2 0 0 0 0	2 2 0 0 0 0	2 0	2 0
σ ionization	$\left\{ \begin{array}{l} {}^4B_1 \\ {}^4B_1 \\ {}^4B_1 \end{array} \right.$	2	1	2	1	2	0 0 0	1 2 0 0 0 0	2 2 0 0 0 0	2 0	2 0
from ${}^3\Pi$ state		1	2	2	1	2	0 0 0	1 2 0 0 0 0	2 2 0 0 0 0	2 0	2 0
π ionization from ${}^3\Sigma^+$ state		2	2	2	1	1	0 0 0	1 2 0 0 0 0	2 2 0 0 0 0	2 0	2 0
π ionization from ${}^3\Delta$ state	4B_2	2	2	1	1	2	0 0 0	2 1 0 0 0 0	2 2 0 0 0 0	2 0	2 0
Ni (s^1d^8) $\delta\pi$ holes	4B_2	2	2	2	1	2	0 0 0	1 2 0 0 0 0	2 2 0 0 0 0	1 0	2 0
Ni (d^9) δ hole	2A_2	2	2	2	0	2	0 0 0	2 2 0 0 0 0	2 2 0 0 0 0	1 0	2 0
Ni (d^9) π hole	2B_1	2	2	2	0	2	0 0 0	1 2 0 0 0 0	2 2 0 0 0 0	2 0	2 0
Ni (d^9) σ hole	2A_1	2	2	1	0	2	0 0 0	1 2 0 0 0 0	2 2 0 0 0 0	2 0	2 0

of up to double excitations within the natural orbitals of each GVB pair, and up to doubles were allowed overall. These configurations allow an essentially consistent description of the dominant correlations for each state over the ground state orbitals. To allow for readjustment effects, all single excitations over the full space were allowed from the same set of dominant configurations. In addition, configurations were included which describe angular correlation of the C(2s) pair. The resulting CI for the quartet states led to (211, 592, 719); (306, 858, 1042); (191, 518, 627); and (79, 217, 263) (spatial configurations, spin eigenfunctions, determinants) for the 4A_1 , 4A_2 , 4B_1 , 4B_2 symmetries, respectively.

The CI's for the doublet states were mainly directed toward describing the three states involving an Ni^+d^9 configuration. Thus, we included in the CI only configurations describing these three states (i.e., Ni^+d^9 with the single hole in the d shell in a σ , π , or δ orbital leading to ${}^2\Sigma^+$, ${}^2\Pi$, and ${}^2\Delta$, respectively). These CI's lead to (45, 77, 109); (43, 75, 107); and (42, 77, 112) (configurations, spin eigenfunctions, determinants) for the ${}^2\Sigma^+$, ${}^2\Pi$, and ${}^2\Delta$ states, respectively. For comparison, comparable CI calculations were carried out for the ${}^3\Sigma^+$, ${}^3\Pi$, and ${}^3\Delta$ states of NiCO and for the ${}^1\Sigma_g^+$ ground state of CO.

In order to determine the relative importance of each configuration in the CI, the energy lowering is computed according to the formula

$$\Delta E_{\mu} = C_{\mu}^2(E - H_{\mu\mu}) / (1 - C_{\mu}^2) \quad (6)$$

In cases where there is more than one spin eigenfunction for a given spatial configuration, the separate contributions due to each spin eigenfunction are simply added [24].

In table 6 we list those configurations with energy contributions of 10 mh or more in the CI calculations on NiCO^+ . In table 7 we list similar information for CI calculations on CO^+ . The energies of the various roots have been given in tables 1 and 2.

Close examination of tables 6 and 7 reveals several interesting points. As observed previously, the first ionization out of CO predominantly involves the C(2s) orbital and in the CI one sees that the dominant configuration involves ionization from this orbital, whereas for NiCO^+ the dominant configuration for the first sigma ionization involves the CO bonding orbital, thus indicating a significant difference in character. This effect of course derives from the stabilization of the C(2s)-like ($\bar{5}\sigma$) orbital of NiCO as compared with the similar CO orbital. Additionally, one sees that for symmetry types where states of Ni^+ and CO^+ character are both present, there is no mixing of these states (at least involving configurations with energy contributions larger than 10 mh); thus, the single Ni has allowed relatively little polarization. With a larger cluster one would expect these states to be closer in energy, leading to stabilization of the CO^+ -like ion states.

Table 6
Energy contributions by configuration for the NiCO^+ CI calculations

State Character	Symmetry in C_{2v}	Configuration Number	Configurations										Energy Lowering(mh)							
			O(2s)	C(2s)	3d	4s	σ	σ^*	π_x	π_y	δ_{xy}	$\delta_{x^2-y^2}$								
σ ionization from $^3\Sigma^+$ state	1^4A_1	1	2	2	1	1	1	1	1	0	2	2	0	0	0	0	2	0	263.2	
		2	2	1	1	2	0	0	2	2	0	0	0	2	2	0	0	0	2	158.1
		3	1	2	1	1	2	0	0	2	2	0	0	2	2	0	0	0	2	150.0
		4	2	1	2	1	1	0	0	2	2	0	0	2	2	0	0	0	2	18.7
		5	2	1	1	1	2	0	0	2	2	0	0	2	2	0	0	0	2	16.8
		6	2	1	1	1	2	0	0	2	2	0	0	2	2	0	0	0	2	16.8
		7	2	1	1	0	2	0	0	1	2	2	0	0	2	2	0	0	2	11.2
π ionization from $^3\Pi$ state	2^4A_1	1	2	2	2	1	2	0	0	1	1	0	0	2	2	0	0	2	0	119.3
		2	2	2	2	1	2	0	0	2	2	0	0	1	1	0	0	2	0	117.6
		1	2	2	2	1	2	0	0	2	2	0	0	1	1	0	0	2	0	119.6
		2	2	2	2	1	2	0	0	1	1	0	0	2	2	0	0	2	0	117.7
σ ionization from $^3\Sigma^+$ state	4^4A_1	1	1	2	1	1	2	0	0	2	2	0	0	2	2	0	0	2	0	168.8
		2	2	2	1	1	1	0	0	2	2	0	0	2	2	0	0	2	0	112.9
		3	2	1	1	1	2	0	0	2	2	0	0	2	2	0	0	2	0	94.4
		4	1	2	1	1	2	0	0	2	1	1	0	0	2	2	0	0	2	27.2
		5	1	2	1	1	2	0	0	2	2	0	0	2	1	1	0	0	2	27.2
		6	2	2	1	1	1	0	0	2	1	1	0	0	2	2	0	0	2	13.4
		7	2	2	1	1	1	0	0	2	2	0	0	2	1	1	0	0	2	13.4
		8	2	1	1	1	2	0	0	2	2	0	0	2	2	0	0	2	0	10.6
		9	2	1	1	1	2	0	0	2	2	0	0	2	2	0	0	2	0	10.6

Table 6 (continued)

State Character	Symmetry Configuration in C_{2v}	Configuration Number	Configurations										Energy Lowering(mh)					
			O(2s)	C(2s)	3d σ	4s	σ^*	π_x	π_y	δ_{xy}	$\delta_{x^2-y^2}$							
Ni (sd^8) with $\delta\sigma$ holes	1^4A_2	1	2	2	1	1	2	0	0	2	2	0	0	0	0	1	0	1462.2
		2	2	2	1	1	2	0	0	2	2	0	0	0	1	0	0	25.9
		3	2	2	1	1	2	0	0	2	2	0	0	0	1	0	0	25.9
		4	2	2	1	1	2	0	0	2	2	0	0	0	1	0	0	16.4
		5	2	2	1	1	2	0	0	1	2	0	0	0	1	0	0	16.4
		6	2	2	1	1	2	0	0	2	2	0	0	0	1	0	1	12.2
		7	2	2	1	1	0	2	0	2	2	0	0	0	1	0	0	10.2
		8	2	2	0	1	2	0	1	2	2	0	0	0	1	0	0	10.2
Ni (sd^8) with $\pi\pi$ holes	2^4A_2	1	2	2	2	1	2	0	0	1	2	0	0	0	2	0	0	484.0
		2	2	2	2	1	2	0	0	2	2	0	0	0	1	0	0	78.3
		3	2	2	2	1	2	0	0	1	0	2	0	0	2	0	0	19.4
		4	2	2	2	1	2	0	0	1	2	0	0	0	2	0	0	19.4
		5	2	2	2	1	1	2	0	1	1	2	0	0	2	0	0	17.7
Ni (sd^8) with $\delta\delta$ holes	3^4A_2	1	2	2	2	1	2	0	0	2	2	0	0	0	1	0	0	476.5
		2	2	2	2	1	2	0	0	1	2	0	0	0	2	0	0	42.0
		3	2	2	2	1	2	0	0	2	0	2	0	0	1	0	0	19.1
		4	2	2	2	1	2	0	0	2	2	0	0	0	1	0	0	19.1
		5	2	2	2	1	2	0	0	1	2	0	0	0	1	0	0	14.3
		6	2	2	2	1	2	0	0	2	2	0	0	0	1	0	0	14.3
		7	2	2	2	1	1	2	0	1	2	0	0	0	1	0	0	12.2
σ ionization from $^3\Delta$ state	4^4A_2	1	2	2	2	1	1	0	0	2	2	0	0	0	1	0	0	244.0
		2	2	1	2	1	2	0	0	2	2	0	0	0	1	0	0	158.1
		3	1	2	2	1	2	0	0	2	2	0	0	0	1	0	0	145.9
		4	2	1	2	1	2	0	0	2	2	0	0	0	1	0	0	16.9
		5	2	1	2	1	2	0	0	2	2	0	0	0	1	0	0	16.9
		6	2	1	2	0	2	0	0	1	2	0	0	0	1	0	0	11.4

Table 8 (continued)

State Character	Symmetry in C_{2v}	Configuration Number	Configurations										Energy Lowering (mh)						
			O(2s)	C(2s)	3d	4s	σ^*	π_x	π_y	δ_{xy}	$\delta_{x^2-y^2}$								
π ionization from $^3\Pi$ state	5^4A_2	1	2	2	2	1	2	0	0	2	1	0	0	0	0	2	0	119.0	
		2	2	2	2	1	2	0	0	1	2	0	0	0	0	2	0	118.9	
π ionization from $^3\Pi$ state	6^4A_2	1	2	2	2	1	2	0	0	1	2	0	0	0	2	0	0	99.7	
		2	2	2	2	1	2	0	0	1	2	0	0	0	2	0	0	99.6	
		3	2	2	2	1	2	0	0	1	1	0	0	0	2	0	0	13.2	
		4	2	2	2	1	2	0	0	1	1	0	0	0	2	0	0	12.5	
σ ionization from $^3\Delta$ state	7^4A_2	1	1	2	2	1	2	0	0	2	2	0	0	0	1	0	0	75.5	
		2	2	2	1	1	2	0	0	2	1	0	0	0	1	0	0	61.4	
		3	2	2	1	1	2	0	0	2	2	0	0	0	1	0	0	61.3	
		4	2	2	2	1	1	0	0	2	2	0	0	0	1	0	0	58.6	
		5	2	2	1	2	1	2	0	0	2	2	0	0	0	1	0	0	28.1
		6	2	2	2	1	1	2	0	0	2	1	0	0	0	1	0	0	17.2
		7	2	2	2	1	1	2	0	0	2	2	0	0	0	1	0	0	17.2
Ni (sd^8) with $\sigma\pi$ holes	1^4B_1	8	1	2	2	1	2	0	0	2	2	0	0	0	1	0	0	16.3	
		9	1	2	2	1	2	0	0	2	1	0	0	0	1	0	0	16.3	
		10	2	2	2	1	1	0	0	2	1	0	0	0	1	0	0	12.4	
		11	2	2	2	1	1	0	0	2	2	0	0	0	1	0	0	12.4	
		1	2	2	1	1	2	0	0	1	2	0	0	0	2	0	0	1203.9	
		2	2	2	1	1	2	0	0	1	0	2	0	0	0	2	0	0	25.9
		3	2	2	1	1	2	0	0	1	2	0	0	0	2	0	0	25.8	
		4	2	2	1	1	2	0	0	1	2	0	0	0	2	0	0	14.8	
		5	2	2	2	1	1	0	0	1	2	0	0	0	2	0	0	12.2	
		6	2	2	2	0	1	2	0	0	1	2	0	0	0	2	0	0	12.2
		7	2	2	2	1	1	2	0	0	2	0	0	0	2	0	0	11.4	
8	2	2	1	0	2	0	0	1	1	2	0	0	0	2	0	0	10.1		
9	2	2	1	1	0	2	0	0	1	2	0	0	0	2	0	0	10.0		

Table 6 (continued)

State Character	Symmetry in C_{2v}	Configuration Number	Configurations										Energy Lowering (mh)					
			O(2s)	C(2s)	3d σ	4s	σ^*	π_x	π_y	δ_{xy}	$\delta_{x^2-y^2}$	δ_{yz}						
π ionization from $^3\Sigma^+$	2^4B_1	1	2	2	1	1	2	0	0	2	1	0	0	0	0	2	0	192.1
		2	2	2	2	1	1	0	0	1	2	0	0	0	0	2	0	80.6
		3	1	2	2	1	2	0	0	1	2	0	0	0	0	2	0	53.6
		4	2	1	2	1	2	0	0	1	2	0	0	0	0	2	0	44.1
		5	2	1	2	1	2	0	0	2	1	0	0	0	0	2	0	17.2
		6	2	2	1	1	2	0	0	1	1	0	0	0	0	2	0	10.6
σ ionization from $^3\Pi$ state	3^4B_1	1	2	2	2	1	1	0	0	1	2	0	0	0	2	0	120.0	
		2	2	2	1	1	2	0	0	2	1	0	0	0	2	0	85.9	
		3	2	1	2	1	2	0	0	1	2	0	0	0	2	0	82.2	
		4	1	2	2	1	2	0	0	1	2	0	0	0	2	0	79.4	
		5	2	1	2	1	2	0	0	1	0	2	0	0	2	0	10.5	
		6	2	1	2	1	2	0	0	1	2	0	0	0	2	0	10.3	
σ ionization from $^3\Pi$ state	4^4B_1	1	1	2	2	1	2	0	0	1	2	0	0	0	2	0	128.8	
		2	2	2	2	1	1	0	0	1	2	0	0	0	2	0	92.2	
		3	2	1	2	1	2	0	0	1	2	0	0	0	2	0	63.3	
		4	1	2	2	1	2	0	0	1	2	0	0	0	2	0	23.8	
		5	1	2	2	1	2	0	0	1	1	0	0	0	2	0	23.2	
		6	2	2	1	1	2	0	0	1	2	0	0	0	2	0	23.1	
		7	2	2	1	1	2	0	0	1	1	0	0	0	2	0	18.4	
		8	2	2	2	1	1	0	0	1	2	0	0	0	2	0	14.0	
		9	2	2	2	1	1	0	0	1	1	0	0	0	2	0	13.5	

Table 6 (continued)

State Character	Symmetry in C_{2v}	Configuration Number	Configurations								Energy Lowering (mh)							
			O(2s)	C(2s)	3d σ	4s	σ	σ^*	π_x	π_y		δ_{xy}	$\delta_{x^2-y^2}$					
Ni (sd) $\delta\pi$ holes	1^1B_2	1	2	2	2	1	2	0	0	1	2	0	0	0	0	10	20	1448.0
		2	2	2	2	1	2	0	0	1	2	0	0	0	0	10	20	25.0
		3	2	2	2	2	1	2	0	0	1	2	0	0	0	10	20	25.0
		4	2	2	2	1	1	2	0	1	1	2	0	0	0	10	20	19.2
		5	2	2	2	2	1	2	0	0	1	2	0	0	0	10	20	17.4
		6	2	2	2	2	1	2	0	0	1	2	0	0	0	10	11	15.6
		7	2	2	2	2	1	2	0	0	1	2	0	0	0	10	20	13.3
		8	2	2	2	2	1	0	2	0	1	2	0	0	0	10	20	10.1
π ionization from $^3\Delta$	2^1B_2	1	2	2	2	1	2	0	0	1	2	0	0	0	10	20	816.3	
		2	2	2	2	1	2	0	0	1	2	0	0	0	10	20	12.5	
		3	2	2	2	2	1	2	0	0	1	2	0	0	10	20	11.1	
		4	2	2	2	2	1	2	0	0	1	2	0	0	10	20	11.0	
Ni (d^9) with o hole	1^2A_1	1	2	2	1	0	2	0	0	1	2	0	0	0	20	20	1028.3	
		2	2	2	1	0	2	0	0	1	2	0	0	0	20	20	27.3	
		3	2	2	1	0	2	0	0	1	2	0	0	0	20	20	27.3	
		4	2	2	1	2	0	2	0	0	1	2	0	0	20	20	13.5	
		5	2	2	1	0	0	2	0	0	1	2	0	0	20	20	11.2	
Ni (d^9) with δ hole	1^2A_2	1	2	2	2	0	2	0	0	1	2	0	0	0	10	20	1123.6	
		2	2	2	2	0	2	0	0	1	2	0	0	0	10	20	28.9	
		3	2	2	2	0	2	0	0	1	2	0	0	0	10	20	28.9	
		4	2	2	2	0	0	2	0	0	1	2	0	0	10	20	11.5	
Ni (d^9) with π hole	1^2B_1	1	2	2	2	0	2	0	0	1	2	0	0	0	20	20	1028.0	
		2	2	2	2	0	2	0	0	1	2	0	0	0	20	20	28.5	
		3	2	2	2	0	2	0	0	1	2	0	0	0	20	20	28.3	
		4	2	2	2	0	0	2	0	0	1	2	0	0	20	20	11.3	

Table 7

Energy contributions by configuration for the CO and CO⁺ CI calculations^a

State	Configuration Number	Configurations						Energy Lowering (mh)
		O(2s)	C(2s)	σ	σ^*	π_x	π_y	
CO	1	2	2	2	0	2 0 0 0	2 0 0 0	Dom
$x^1\Sigma^+$	2	2	2	2	0	1 1 0 0	1 1 0 0	21.0
	3	2	2	1	1	1 1 0 0	2 0 0 0	13.7
	4	2	2	1	1	2 0 0 0	1 1 0 0	13.7
	5	2	2	2	0	0 2 0 0	2 0 0 0	13.0
	6	2	2	2	0	2 0 0 0	0 2 0 0	13.0
	CO ⁺	1	2	1	2	0	2 0 0 0	2 0 0 0
$1^2\Sigma^+$	2	2	2	1	0	2 0 0 0	2 0 0 0	224.7 ^b
	3	1	2	2	0	2 0 0 0	2 0 0 0	96.6
	4	2	1	2	0	1 1 0 0	1 1 0 0	16.0
	5	2	1	2	0	2 0 0 0	1 1 0 0	14.1
	6	2	1	2	0	1 1 0 0	2 0 0 0	14.1
	7	2	1	2	0	0 2 0 0	2 0 0 0	13.1
	8	2	1	2	0	2 0 0 0	0 2 0 0	13.1
	9	2	1	2	0	2 0 0 0	1 0 0 1	11.0
	10	2	1	2	0	1 0 0 1	2 0 0 0	11.0
	CO ⁺	1	1	2	2	0	2 0 0 0	2 0 0 0
$2^2\Sigma^+$	2	2	2	1	0	2 0 0 0	2 0 0 0	158.5 ^b
	3	2	1	2	0	2 0 0 0	2 0 0 0	35.6
	4	1	2	2	0	2 0 0 0	1 1 0 0	34.2
	5	1	2	2	0	1 1 0 0	2 0 0 0	34.2
	6	2	2	1	0	2 0 0 0	1 1 0 0	17.0
	7	2	2	1	0	1 1 0 0	2 0 0 0	17.0
	CO ⁺	1	2	2	2	0	1 0 0 0	2 0 0 0
$^2\Pi$	2	2	2	2	0	0 1 0 0	2 0 0 0	15.1
	3	2	2	1	1	1 0 0 0	1 1 0 0	13.3
	4	2	2	2	0	1 0 0 0	0 2 0 0	10.1

a) Configurations with contributions less than 10 mh are not listed.

b) See ref. [24].

References

- [1] Partially supported by a grant (DMR74-04965) from the National Science Foundation.
- [2] Partially supported by National Science Foundation Fellowship (energy-related) during the summer of 1975.
- [3] Partially supported by a grant (CHE73-05132) from the National Science Foundation.
- [4] The LEED data for the (100), (110), and (111) surfaces are discussed in Refs. 5, 6 and 7, respectively.
- [5] J. C. Tracy, J. Chem. Phys. 56 (1972) 2736.
- [6] H. H. Madden, J. Koppers and G. Ertl, J. Chem. Phys. 58 (1973) 3401.
- [7] J. Christmann, O. Schober and G. Ertl, J. Chem. Phys. 60 (1974) 4719.
- [8] (a) D. E. Eastman and J. K. Cashion, Phys. Rev. Lett. 27 (1971) 1520.
(b) D. E. Eastman and J. E. Demuth, Jap. J. Appl. Phys. Suppl. 2, 52 (1974) 827.
(c) T. Gustafson, E. W. Plummer, D. E. Eastman and J. L. Freeouf, Solid State Commun. 17 (1975) 391.
- [9] S. P. Walch and W. A. Goddard III, J. Am. Chem. Soc. 98 (1976) 7908.
- [10] F. A. Cotton and G. Wilkinson, Advanced Inorganic Chemistry (Wiley-Interscience, New York, 1972), 3rd ed., p. 684.
- [11] G. Distefano, J. Res. Natl. Bur. Stand. (U.S.) A 74 (1970) 233.

[12] The calculated dissociation energy is based on

$$\Delta H_f^0[\text{NiCO}^+] = 203.8 \pm 2 \text{ kcal/mole} \quad (\text{Ref. 11})$$

$$\Delta H_f^0[\text{Ni}^+] = 278.7 \pm 2 \text{ kcal/mole} \quad (\text{Ref. 11})$$

$$\text{and } \Delta H_f^0[\text{CO}] = -27.20 \pm 0.04 \text{ kcal/mole} \quad (\text{Ref. 13})$$

[13] JANAF Thermochemical Tables (The Dow Chemical Company, Midland, Michigan, 1970), NSRDS-NBS37.

[14] S. P. Walch and W. A. Goddard III, unpublished results.

[15] T. H. Upton and W. A. Goddard III, unpublished results.

[16] W. A. Goddard III, A. Redondo and T. C. McGill, Solid State Commun. 18 (1976) 981.

[17] For the ground (3P) state of the carbon atom, the HF wavefunction is

$$a[\phi_s^2 \phi_x \phi_y \alpha\beta\alpha\alpha]$$

Thus we may angularly correlate the 2s pair using the p_z orbital leading to the wavefunction

$$a[(\phi_s^2 - \lambda\phi_z^2) \phi_x \phi_y \alpha\beta\alpha\alpha]$$

which is equivalent to

$$a[(\phi_{s_z} \phi_{s_z} + \phi_{s_z} \phi_{s_z}) \phi_x \phi_y \alpha\beta\alpha\alpha],$$

where $\phi_{s_z} = \phi_s - \lambda\phi_z$ (apart from normalization). However, because of the Pauli principle, the analogous wavefunction for $O(^3P)$ leads to only the HF wavefunction. Thus, angular correlation of the 2s pair is important for carbon but not for oxygen, an effect which persists in the CO molecule. See also Ref. 18.

[18] a) W. A. Goddard III, T. H. Dunning, Jr., W. J. Hunt and P. J. Hay, Accts. Chem. Res. 6 (1973) 368.

- (b) P. J. Hay, W. J. Hunt and W. A. Goddard III, Chem. Phys. Lett. 13 (1972), 30.
- (c) W. A. Goddard III and R. J. Blint, Chem. Phys. Lett. 14 (1972) 616.
- [19] This calculation uses a valence double zeta basis with d polarization functions (VDZd).
- [20] The CI calculations using the VDZ basis are based on a wavefunction in which the two π pairs and the sigma bond are correlated [21]. In an average sense, this wavefunction may be thought of as a superposition of the structure (5) and an equivalent structure rotated by 90° . However, with the VDZ basis it is not possible at the SCF level to effectively introduce angular correlation of the C(2s) pair, because the correlating orbitals that would be used are essentially the same as those used to correlate the π pairs. Adding d functions to the basis, it is possible to simultaneously correlate the C(2s) and π pairs.
- [21] This wavefunction leads to an energy 0.41 eV lower than the wavefunction (5) where one π pair, the C(2s) pair, and a sigma bond are correlated.
- [22] At the SCF level, addition of d functions decreases the separation between (5) and the case where both π pairs are correlated to 0.270 eV, indicating the importance of d functions for describing the correlation of the C(2s) pair.
- [23] (a) P. S. Bagus and K. Hermann, Solid State Commun. 20 (1975) 5.
- (b) P. S. Bagus and K. Hermann, "Model Studies of the Binding and the Energy Level Shifts of Carbon Monoxide Adsorbed on Nickel," to be published.

[24] The ΔE_{μ} , while providing an indication of the relative importance of configurations are of little significance for the dominant configuration(s). (The sum of the ΔE_{μ} does not equal the total energy.)

PART C: THEORETICAL STUDIES OF THE GEOMETRIES OF O AND S
OVERLAYERS ON THE (100) AND (110) SURFACES OF NICKEL[†]

A first step in understanding the mechanisms of heterogeneous catalysis at transition metal surfaces is to investigate the nature of the bonding of atoms and molecules to the surface.

Experimentally, geometric information is obtained by detailed analysis of low energy electron diffraction (LEED) intensities.¹ Because the theoretical analysis involves some severe approximations, these geometries cannot be described as purely experimental, however with high quality LEED intensities it appears that the determination of geometric spacings of atomic overlayers to within $\sim 0.1\text{\AA}$ is possible (in the direction perpendicular to the surface).

We are in the process of developing theoretical techniques for solving directly for the geometries of chemisorbed species. Such theoretical procedures, if reliable, would be extremely valuable, since one could consider special surface defects (e.g., steps) and reaction intermediates, both of which are relevant for studying catalysis. In our theoretical model we solve for the states of finite clusters representing the semi-infinite solid, using the ab initio generalized valence bond (GVB) method;² this differs from the usual Hartree-Fock (HF) method in that we include the dominant electron correlation (many body) effects. We feel that the chemisorptive bond is sufficiently localized that our description of the chemisorbed species is valid for the real metal, however detailed comparison to experiment would be valuable.

As a test of our theoretical methods, we have chosen to examine the geometries of O and S overlayers on the Ni(100) surface, a case

which has been thoroughly studied with LEED and dynamic intensity calculations.¹ The results of these calculations also lead to predictions for the (110) surface.

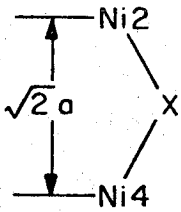
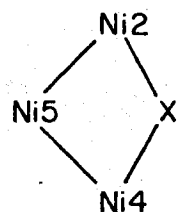
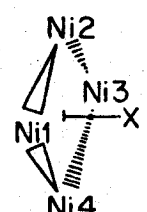
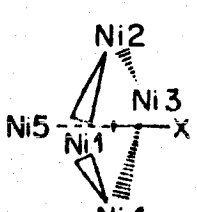
Table I summarizes the results for S. For the (100) surface we denote the four surface atoms at the corners of the surface unit cell as Ni1, Ni2, Ni3, and Ni4 and we denote as Ni5 the atom in the second layer below the center of this cell. Including the four Ni atoms (Ni1, Ni2, Ni3, and Ni4) to which the S bonds, we calculate an optimum position of the S, 1.33\AA above the surface. This is in excellent agreement with the results from dynamic LEED intensity calculations which lead to $1.30 \pm 0.10\text{\AA}$.¹

We find that the bonding in this cluster is across one diagonal (say Ni2-Ni4) somewhat analogous to the bonding in H_2S .³ There is a repulsive interaction between the S($3p\pi$) lone pair and the other diagonal atoms (Ni1-Ni3). The extent of this repulsive interaction was tested by removing Ni1 and Ni3 and recalculating the optimum S position; the S moved to a position 1.04\AA above the surface. We tested the effect of Ni5 using the Ni2, Ni4, Ni5 complex, finding the optimum S position at 1.07\AA above the surface. The conclusion here was that Ni5 does not affect the S position.

The calculated D_e for Ni_2S is 5.37 eV as compared to 3.32 eV for NiS, indicating that bridging is much more favorable than bonding directly above a surface Ni atom (as is generally presumed).

Qualitatively the electronic configuration of the Ni_4S cluster is as shown in the diagram at the top of Fig. 1.

Table I. Optimum Geometries for the 0 and S Overlayers

Cluster	Geometry	Model for	Distance ^o Above Plane (Å)	
			x = 0	x = S
NiX	Ni—X		1.60	1.91
Ni ₂ X			0.31	1.04
Ni ₃ X		(110)	0.08	1.07
Ni ₄ X			(0.75) ^c	1.33
Ni ₅ X		(100)	0.96 ^a	(1.36) ^b

^aBased on the positive ion calculation as described in the text. For the neutral 0.65Å is obtained.

^bObtained from Ni₄S using the Ni₂S to Ni₃S correction.

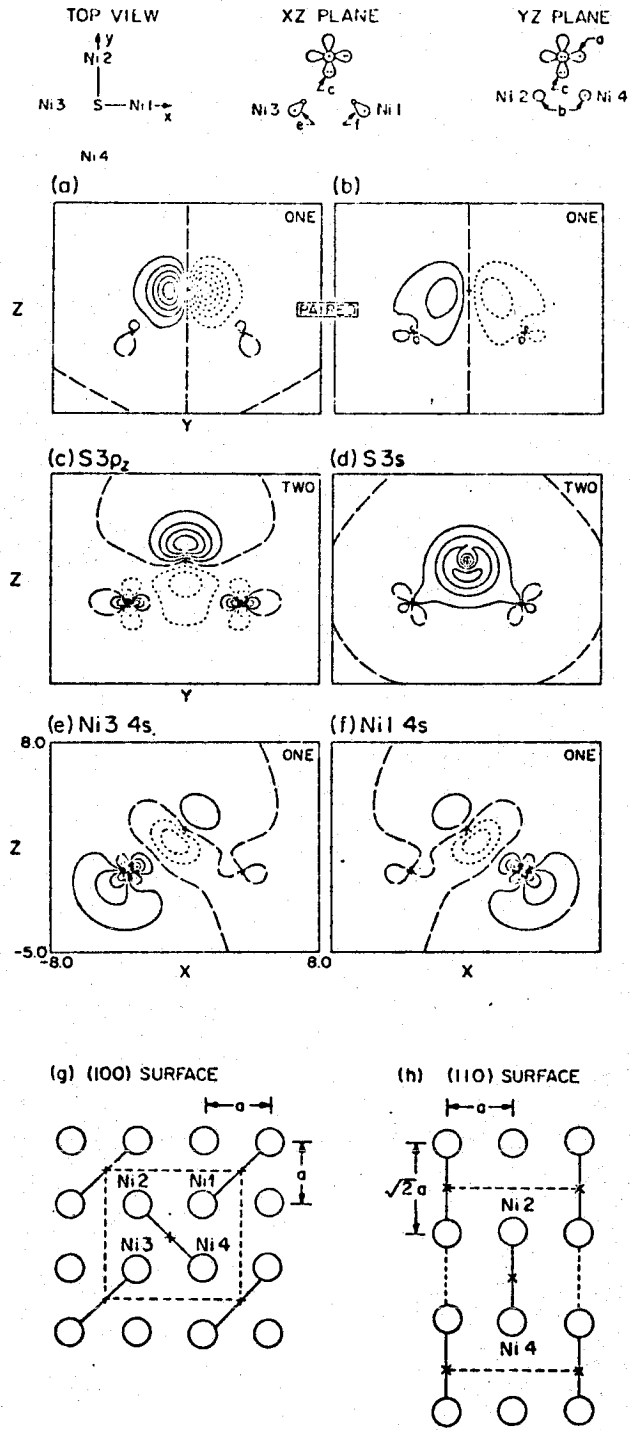
^cEstimated for the positive ion using Koopmans' theorem. For the neutral 0.56Å is obtained.

Figure Caption

(a)-(f): Selected orbitals of the GVB(1/pp) wavefunction for the Ni_4S cluster. These plots have uniformly spaced contours with a separation of 0.05 a.u. Positive contours are indicated by solid lines, negative contours are indicated by dashed lines, and nodal surfaces are indicated by long dashes.

(g),(h): Bonding patterns for $c(2 \times 2)$ overlayers on the (100) surface (g) and on the (110) surface (h). The circles represent surface Ni atoms, while the S and O atoms are indicated by crosses. The solid lines represent the bonding orbitals, while the unit cell is outlined by dashed lines.

Ni₄S GVB (I/PP)



The important orbitals of the Ni_4S cluster are shown in Figure 1a-f. One bonding pair (Fig. 1ab) involves one component (Fig. 1a) which is essentially a $S(3p_y)$ orbital, while the other component (Fig. 1b) corresponds approximately to $\text{Ni}2(4s)\text{-Ni}4(4s)$. The other bonding orbital (Fig. 1c) is essentially $S(3p_z)$ -like, but has built in a bonding combination of $\text{Ni}(4s)$ character on all four Ni atoms.

The 4s orbitals of the remaining two Ni atoms (Fig. 1ef) are triplet paired and have significant nonbonded repulsions with the doubly occupied $S(3p_x)$ orbital. These orbitals are involved in bonds to adjacent S atoms for the full overlayer, as illustrated in Fig. 1g. The localized bonds shown in Fig. 1g suggest a $p(2 \times 2)$ structure, with the center and corner atoms connected by a glide plane. However, there is a degenerate structure with all the bond directions rotated by 90° and these two structures are expected to have a strong interaction (resonance), leading to all the S atoms being equivalent. This results in $c(2 \times 2)$, as observed.

The wavefunctions for the (100) cluster suggest that on the (110) surface the S is along the long side of the rectangle as indicated in Fig. 1h. Thus, the simplest model for the (110) surface is the Ni_2 cluster with the Ni atoms separated by $\sqrt{2}$ times the nearest neighbor separation. The calculations lead to an optimum S position 1.04\AA away from the Ni surface, in fair agreement with the results of dynamic LEED intensity analysis which leads to $0.93 \pm 0.10\text{\AA}$.¹ The LEED calculations assumed the S to be centered in alternative

rectangular cells, however these calculations are not sensitive to lateral displacement of the overlayer.⁴

The geometries for bonding of an O atom to the various Ni clusters are also summarized in Table I. The principal differences between the S and O results have to do with i) the smaller size of the oxygen atom and ii) the larger electronegativity for O.⁵ We found here that the presence of Ni5 has a significant effect on the O position due to the much greater charge transfer. Consequently, Ni5 was included for both the (100) and (110) models.

The calculated D_e for Ni_2O is 4.37 eV as compared with 3.95 eV for NiO, indicating that bridging is more favorable than bonding directly above a surface Ni atom. The smaller energy difference here as compared with the S case results mainly from loss of π bonding effects (which are more important for NiO than for NiS) upon forming Ni_2O and Ni_2S .

Considering the full oxygen overlayer, Ni atoms 1 and 3 are involved in bonds to adjacent O atoms (see Fig. 1g). Here the ionic NiO bonds lead to a total charge of 0.92 electrons on Ni atoms 1 and 3, as compared with the S case where the total charge was only 0.62. In order to include effects resulting from this charge distribution, we examined the positive ion state of the Ni_5^+O cluster (involving removal of one of the 4s electrons from Ni1 and Ni3).⁶ We find that the Ni_5^+ cluster has a higher effective electronegativity, resulting in more covalent bonding. The net effect is an increase in the bond energy along with a 0.40\AA vertical displacement away from the surface to

0.96\AA for the Ni_5^+O cluster. This value is in good agreement with the distance from the LEED intensity analysis, $0.90 \pm 0.10\text{\AA}$.¹

Using the Ni_2O cluster to model the (110) surface leads to an optimum O position only 0.31\AA above the surface (for bonding along the long edge of the surface unit cell). However, the calculations on the Ni_3O cluster indicate that the two Ni atoms in the next layer down will have attractive interactions with the oxygen, leading to the O being even closer to the surface (0.08\AA) and perhaps penetrating it. LEED studies have not been carried out for O on Ni(110), however for O on Fe(100)⁷ [which involves a more open structure (BCC lattice with $a = 2.87\text{\AA}$ as compared with FCC with $a = 2.49\text{\AA}$ for Ni), and appears to be intermediate between Ni(100) and Ni(110)] the O is found to be $0.53 \pm 0.06\text{\AA}$ from the surface, intermediate between our results for the (100) and (110) surfaces of Ni.

We conclude that reliable geometric information for chemisorbed species on transition metal surfaces can be obtained using small clusters including only those atoms within bonding distance. This encouraging result opens the way for theoretical studies of other chemisorbed species and reactive intermediates, systems that may well be impossible to study experimentally (due to lack of long range order).

References

- † Supported by a grant (DMR74-04965) from the National Science Foundation.
1. (a) J. E. Demuth, D. W. Jepsen and P. M. Marcus, Phys. Rev. Lett. 32(21), 1182 (1974); (b) J. E. Demuth, D. W. Jepsen and P. M. Marcus, Phys. Rev. Lett. 31(8), 540 (1973).
 2. (a) W. A. Goddard III, T. H. Dunning, Jr., W. J. Hunt and P. J. Hay, Accts. Chem. Res. 6, 368 (1973).
 (b) The basis sets for the Ni^c, O^c, and S^d are valence double zeta (allowing for contraction and delocalization effects) and should lead to good geometries. In order to obtain accurate bond energies for NiX and Ni₂X, we also included d polarization functions on the O^c and S^d. Since the Ni configuration is 4s¹3d⁹ in all clusters, we simplified the calculations for Ni₃X, Ni₄X, and Ni₅X by contracting the Ni basis to [2s,1p,1d] based on the (4s)¹(3d)⁹ state of the Ni atom.
 (c) See e.g., S. P. Walch and W. A. Goddard III, J. Amer. Chem. Soc. 98, 7908 (1976).
 (d) R. A. Bair and W. A. Goddard III, J. Amer. Chem. Soc., in press.
 3. For the clusters considered here, the Ni atom has the character of the 4s¹3d⁹ configuration, leading to bonds between the singly occupied S(3p) orbitals and the singly occupied Ni(4s) orbitals.
 4. For example, for S on Ni(111) there are two possible three-fold coordinate sites. The LEED intensities are quite similar for these two sites, but change significantly if the distance to the surface is changed.^{1a}

5. The electronegativities involved are 3.5 for O, 2.5 for S, and 1.8 for Ni, respectively. L. Pauling, The Nature of the Chemical Bond (Cornell University Press, New York, 1972), 3d ed., p. 93.
6. For O on Ni the positively charged cluster is consistent with the overall charge distribution, while the neutral cluster is not. For S on Ni the charge distribution is intermediate between a neutral cluster and the positively charged cluster, and we have used a neutral cluster as a model. We expect that charge transfer effects will be less important for the S case than for the O case, since the bonding of S to the surface is more covalent.
7. K. O. Legg, F. P. Jona, D. W. Jepsen, and P. M. Marcus, J. Phys. C8, L492 (1975).

Appendix to Part C

The following table contains supplementary information on vibrational constants for the Ni_nX clusters:

Table 1. Vibrational Constants for Ni_nX Clusters (cm^{-1})^a

	X = O	X = S
NiX	841	483
Ni_2X	170	298
Ni_3X	525	-
Ni_4X	303	315
Ni_5X	302	-
Ni_5^+X	325	-

^aUsing masses of 12 for C, 16 for O, 32 for S, and 58 for Ni.

PART D: THEORETICAL STUDIES OF THE BONDING OF SULFUR TO MODELS
OF THE (100) AND (110) SURFACES OF NICKEL [1],[2]

1. Introduction

A first step in understanding the mechanisms of heterogeneous catalysis at transition metal surfaces is to understand the nature of the bonding of atoms and molecules to the surface.

Experimentally, geometric information is obtained by detailed analysis of low energy electron diffraction (LEED) intensities [3]. Because the theoretical analysis involves some severe approximations, these geometries cannot be described as purely experimental, however with high quality LEED intensities, it appears that the determination of geometric spacings of atomic overlayers to within $\sim 0.1\text{\AA}$ is possible (in the direction perpendicular to the surface).

We are in the process of developing theoretical techniques for solving directly for the geometries of chemisorbed species. Such theoretical procedures, if reliable, would be extremely valuable, since one could consider special surface defects (e.g., steps) and reaction intermediates, both of which are relevant for studying catalysis. Our theoretical model involves replacing the semi-infinite solid by a finite cluster. We feel that the chemisorptive bond is sufficiently localized that our description of the chemisorbed species is valid for the real metal, however detailed comparison to experiment would be valuable.

As a test of the theory, we have chosen to examine the geometries for S overlayers on Ni(100) and Ni(110) surfaces, both of which have been the object of extensive LEED studies and dynamic intensity calculations [3a].

We solve for the states of the finite clusters using the ab initio generalized valence bond (GVB) method [4], which differs from the usual Hartree-Fock (HF) method in that it includes the dominant correlation effects necessary to describe bond formation.

In Section 2, we discuss qualitatively the wavefunctions for the various clusters and compare the geometry predictions from the calculations with experimental results for the Ni(100) and Ni(110) surfaces, while Section 3 discusses the wavefunctions in more detail. Section 4 describes some of the details of the basis set and effective potentials used here, while Section 5 discusses the configuration interaction (CI) calculations.

2. Qualitative Description of the Theoretical Results

2.1.1 NiS

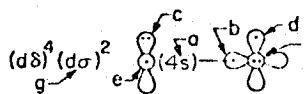
We find that for the ground state of NiS, the Ni has the character of the $\text{Ni}(4s)^1(3d)^9$ configuration, while the S has the character of the $\text{S}(3s)^2(3p)^4$ configuration. The bonding is dominated by the sigma bond which may be described qualitatively as a $\text{Ni}(4s)$ orbital paired up with a singly occupied $\text{S}(3p\sigma)$ orbital. The quantitative shape of these orbitals are given in Fig.1ab; as expected from the relative electronegativities [5a] (1.8 for Ni, 2.5 for S) there is some charge transfer to the S atom (~ 0.38 electrons [6]). For the ground state of NiS the 3d hole of the $\text{Ni}3d^9$ configuration is $3d\pi$. This orbital is paired with the $2p\pi$ hole of the S leading to a $^3\Sigma^-$ ground state which is quite analogous to the ground states of O_2 [7] and of NiO [8]. As indicated in Fig. 1, the Ni3d orbitals are only slightly affected by the bond.

As indicated in Table 1, the calculated bond distance is 1.91\AA which is substantially smaller than that of bulk Ni sulfides. (The bond length of the NiS molecule is not known experimentally.) The calculated bond energy is 3.32 eV which is in reasonable agreement with current experimental estimates 3.53 ± 0.15 eV [9].

2.1.2 Ni₂S

As a first model for both the (100) and (110) surfaces we considered two Ni atoms separated by $\sqrt{2}$ times the bulk separation [these atoms are second nearest neighbor atoms of bulk Ni but correspond to neighboring Ni atoms on the (100) and (110) surfaces]. Here we

Fig. 1 The GVB orbitals of configuration $1b$ which corresponds to the $X^3\Sigma^-$ state of NiS. Unless otherwise noted, all plots have uniformly spaced contours of 0.05 a.u. Solid lines indicate positive contours, short dashes indicate negative contours, and long dashes indicate nodal lines. The same conventions are used for other figures.

NiS $X^3\Sigma^-$ 

THE NiS SIGMA BOND

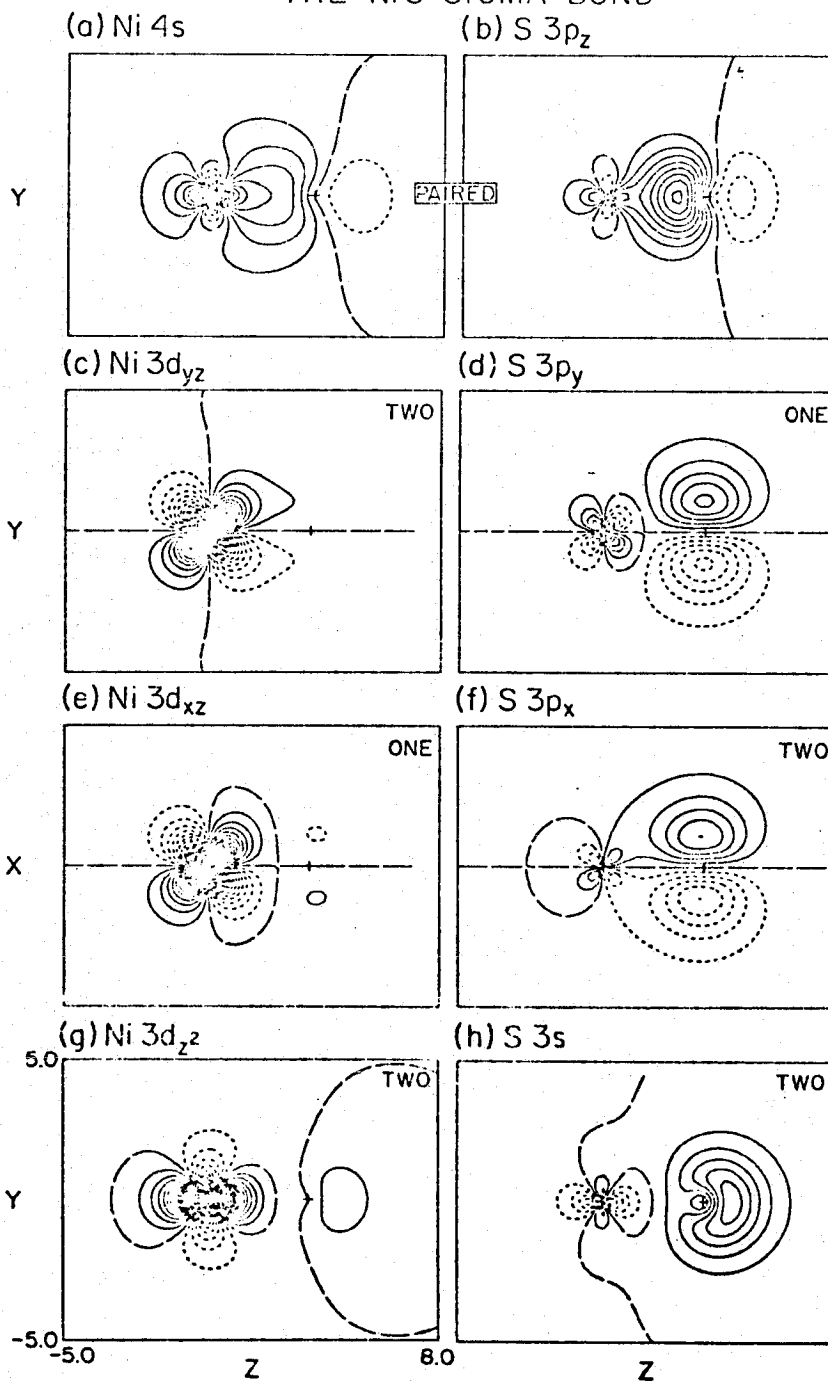
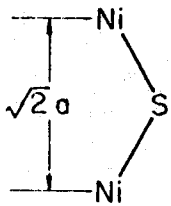
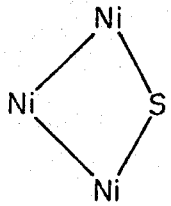
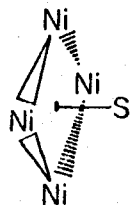


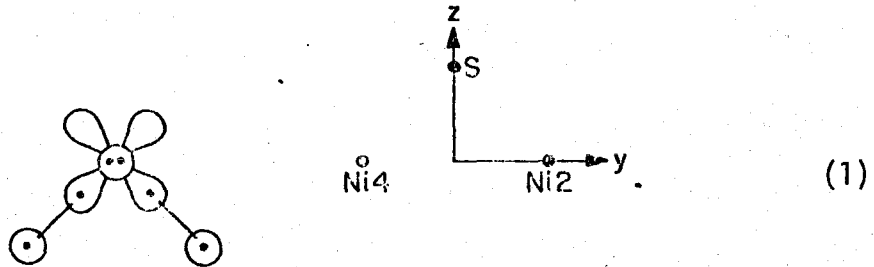
Table 1 Summary of Results for Bonding of Sulfur to the Ni Clusters

Cluster	Geometry	Model for	Distance above Plane(Å)	R_{NiS}^0 (Å)	$D(eV)$
NiS	Ni—S	-	1.91	1.91	3.32
Ni ₂ S		(110)	1.04	2.04	5.37
Ni ₃ S		-	1.07	2.06	3.89 ^a
Ni ₄ S		(100)	1.33	2.21	3.91 ^a

^aThe NiS and Ni₂S calculations used a [3s,1p,2d/3s,2p,1d] basis, while a [2s,1p,1d/3s,2p] basis was used for the Ni₃S and Ni₄S calculations. From comparisons of both types of calculations for Ni₂S we estimate that this basis leads to an error in D_e of 0.63 eV, but does not have a significant effect on the geometry. Thus, we have added 0.63 eV to the D_e values for the Ni₃S and Ni₄S calculations in order to compare with the NiS and Ni₂S calculations. (See footnote a of Table 5.)

optimized the position of the S but with the Ni atoms fixed.

Qualitatively one can visualize the electronic configuration of Ni_2S as



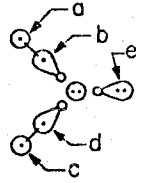
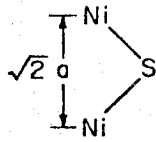
where lines connect pairs of singly occupied bonding orbitals and the remaining doubly occupied $\text{S}(3p_x)$ orbital (pointing perpendicular to the plane) is denoted with a circle containing two dots. (As discussed in Section 3.2, the lowest state corresponds to taking the 3d holes to be delta-like with respect to the NiS bond axes.)

As shown in Fig. 2, the two NiS sigma bonds (Fig. 2abcd) are somewhat ionic, much like those in diatomic NiS, leading to a total charge transfer to the S of 0.57 electrons [6]. The doubly occupied $\text{S}(3s)$ orbital (Fig. 2e) has built-in 3p character resulting in hybridization away from the Ni-S bonds.

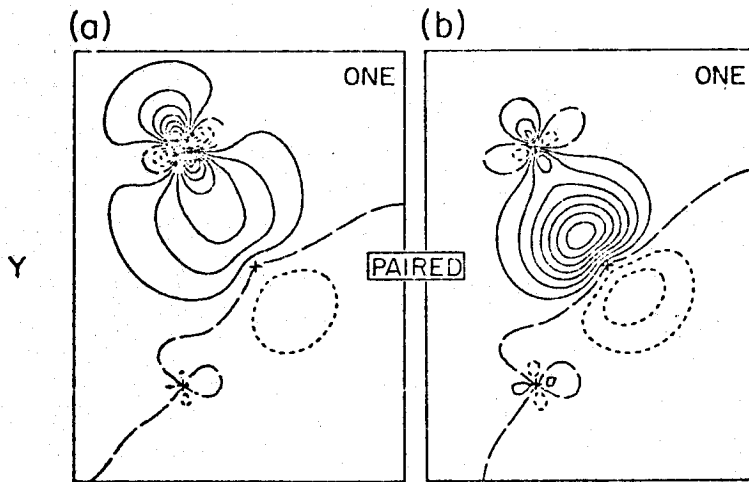
The calculated optimum NiS bond length has increased to 2.04\AA while the bond energy has increased to 5.37 eV. Thus, our calculations indicate that bridging is more favorable than bonding directly above a surface Ni atom. Comparing to the bond energy of NiS, 3.32 eV, suggests that ~ 0.64 eV of the bond energy of the NiS molecule is due to π bonding.

As discussed in Section 2.2, the Ni_2S cluster is an appropriate model for the (110) surface where the closest nonbonding Ni atoms are

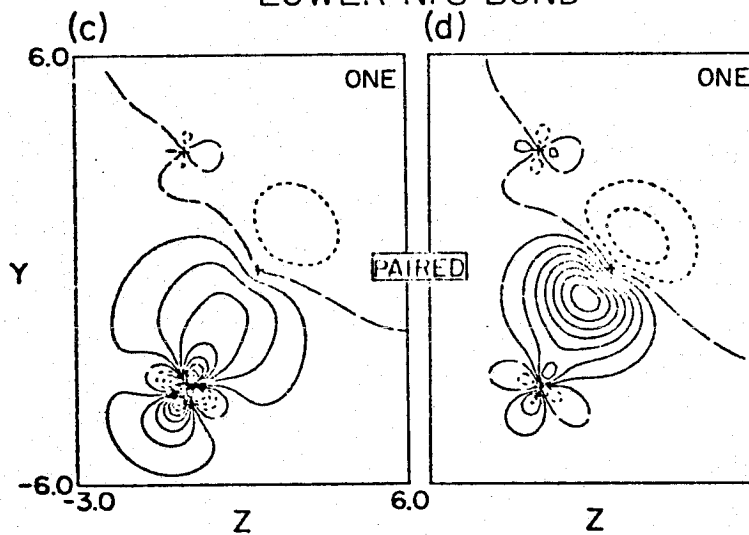
Fig. 2 Selected orbitals of the Ni₂S cluster.

Ni₂S GVB (2/PP)

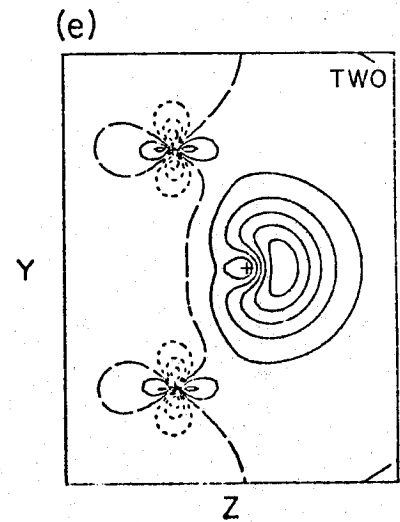
UPPER Ni S BOND



LOWER Ni S BOND



THE S 3s PAIR

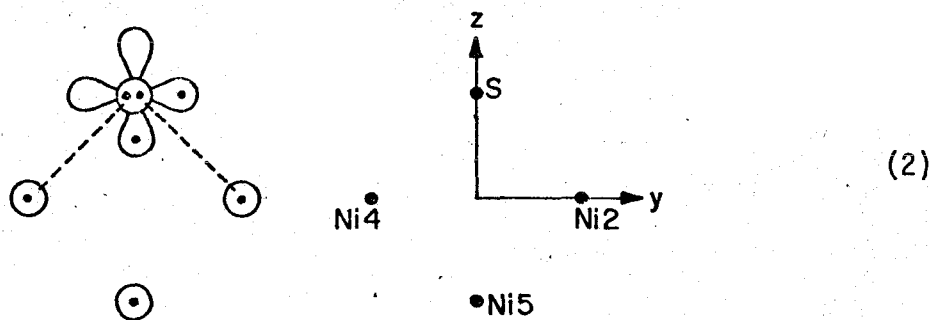


in the next layer down. However, for the (100) surface there are two nearest neighbor Ni atoms in the surface and one in the layer below close enough to affect the geometry. We examined the effect of the second layer Ni atom using a Ni_3S cluster, and the effect of the other two surface Ni atoms using a Ni_4S cluster.

2.1.3 Ni_3S

Adding a third Ni atom below the surface leads to the Ni_3S cluster. Qualitatively the bonding in Ni_3S involves Ni-S bonds to the two surface Ni atoms, as in the Ni_2S calculation, while the Ni atom below the surface is nonbonding.

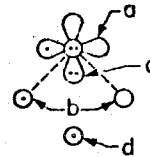
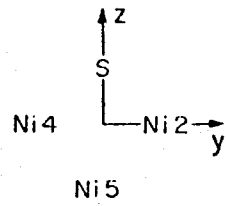
As discussed in Section 3, we did not solve for the Ni_3S wavefunction in terms of localized orbitals as in (1), but rather used the full C_{2v} symmetry of the molecule leading to a wavefunction which may be qualitatively understood in terms of bonding the S atom to the Ni_3 cluster in the following orientation:



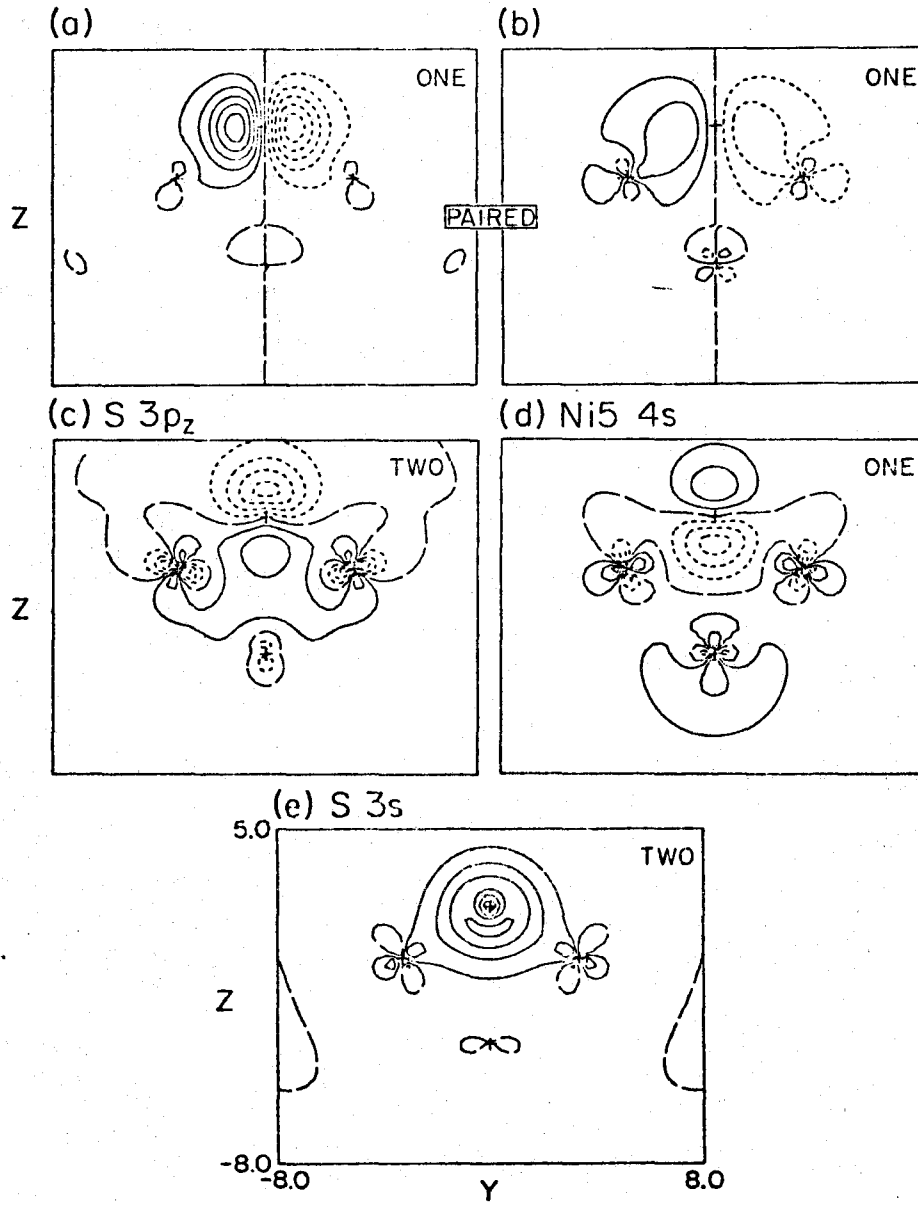
As shown in Fig. 3, the resulting wavefunction has a bond pair (Fig. 3ab) with one component (Fig. 3a) which is basically a $\text{S}(3p_y)$ orbital while the other component (Fig. 3b) corresponds qualitatively to $\text{Ni}_2(4s) - \text{Ni}_4(4s)$. The other bonding orbital (Fig. 3c) is doubly occupied and corresponds to the bonding combination of a $\text{S}(3p_z)$ orbital

Fig. 3 Selected orbitals of the Ni₃S cluster.

Ni₃S GVB (I/PP)



THE NiS BOND PAIR

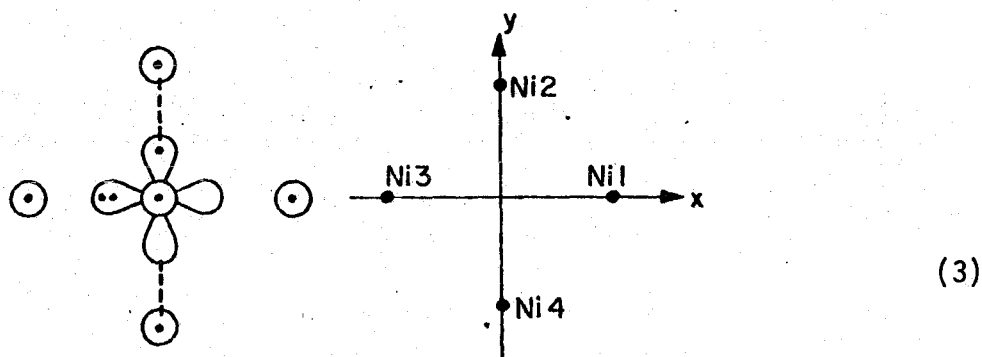


and 4s character on all three Ni atoms. The 4s orbital of Ni5 (Fig. 3d) is nonbonding and has built-in 4p character so as to hybridize toward the bulk metal. The S(3s) orbital (Fig. 3e) has hybridized slightly in the direction of Ni3.

Essentially this wavefunction corresponds to two Ni-S bonds to Ni2 and Ni4, as in Ni₂S, while Ni5 is nonbonding. Thus the geometry should be predominantly determined by the interactions between the sulfur and the surface Ni atoms (2 and 4). Indeed, the Ni₃S cluster has an optimum geometry with the S 1.07Å above the surface as compared with 1.04Å for Ni₂S, and we conclude that the second layer Ni atom has only a very small effect on the geometry. The bond energy, on the other hand, decreases to 3.89 eV, since the bonding here involves disruption of metal-metal bonds for the Ni₃ cluster.

2.1.4 Ni₄S

Considering the four surface atoms interacting with the S for the (100) surface leads to the Ni₄S cluster. Qualitatively the electronic configuration of the Ni₄S cluster is:



The bonding orbitals (Fig. 4abc) are analogous to the bond orbitals

Fig. 4 Selected orbitals of the Ni₄S cluster.

of the Ni_3S cluster. The GVB pair (Fig. 4ab) involves one component (Fig. 4a) which is essentially a $\text{S}(3p_y)$ orbital while the other component (Fig. 4b) corresponds approximately to $\text{Ni}2(4s) - \text{Ni}4(4s)$. The other bonding orbital (Fig. 4c) is essentially $\text{S}(3p_z)$ -like, but has built in a bonding combination of $\text{Ni}(4s)$ character on all four Ni atoms.

The 4s orbitals of the remaining two Ni atoms (Fig. 4ef) are high-spin coupled and have significant nonbonded repulsions with the doubly occupied $\text{S}(3p_x)$ orbital. [As discussed in Section 2.2, these orbitals are involved in bonds to adjacent S atoms for the full overlayer. Thus, we high-spin couple these orbitals to best approximate the repulsive effects between these orbitals and the $\text{S}(3p_x)$ pair.]

The 4s orbitals of Ni1 and Ni3 have hybridized away from the sulfur orbitals to minimize their overlap with the $\text{S}(3p_x)$ pair. (They must be orthogonal because of the Pauli principle.) This results in some stabilization of the $\text{S}(3s)$ orbital by interaction with the $3d^9$ cores of Ni1 and Ni3 (somewhat as for the 5σ orbital of CO upon bonding to Ni), however, the overall effect is repulsive and leads to an optimum geometry with the S atom 1.33\AA above the surface. (Compare with 1.04\AA for Ni_2S).

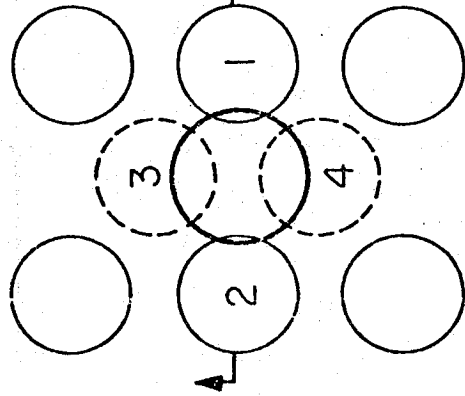
2.2 Comparison to Experimental Results

Figure 5 shows the location of the S atom relative to the nearest neighbor Ni atoms for the (100) and (110) surfaces of Ni. Figure 6 illustrates the bonding expected for $c(2 \times 2)$ overlayers on the (100) and (110) surfaces.

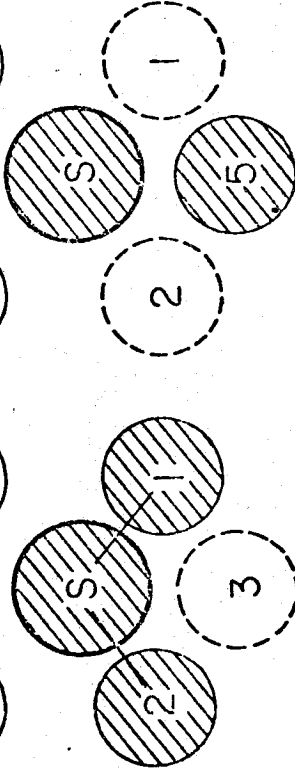
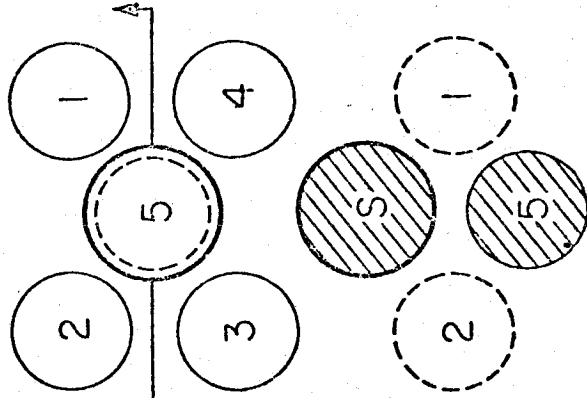
Fig. 5 The geometry of the S atom and nearest neighbor Ni atoms for the Ni(100) and Ni(110) surfaces. Ni atoms in the plane of the paper are illustrated by light circles, while those below the paper are illustrated by dashed circles and the S atom is illustrated by a somewhat larger heavy circle. For the (110) surface, geometry A is suggested by our results, while geometry B is the registry with the surface assumed for calculation of LEED intensities [3a].

Ni (110)

GEOMETRY A

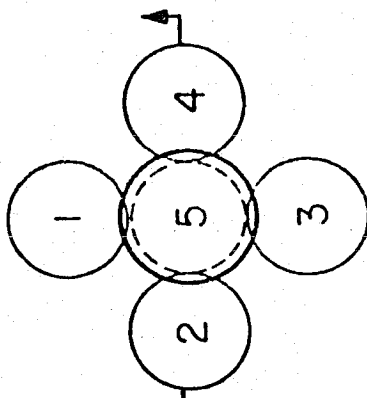


GEOMETRY B



Ni (100)

TOP VIEW



SIDE VIEW

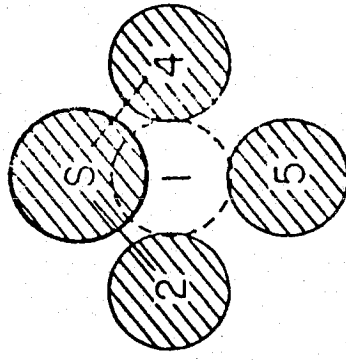
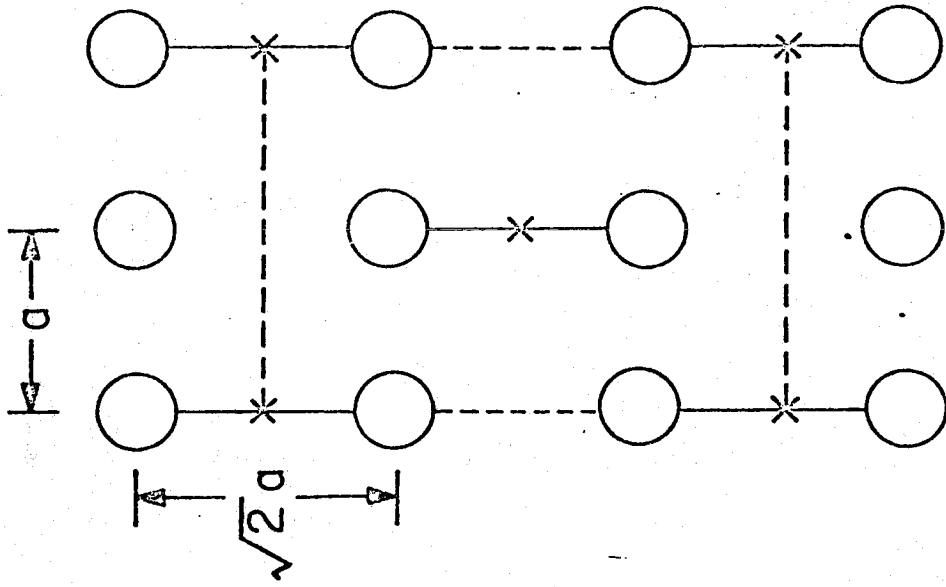
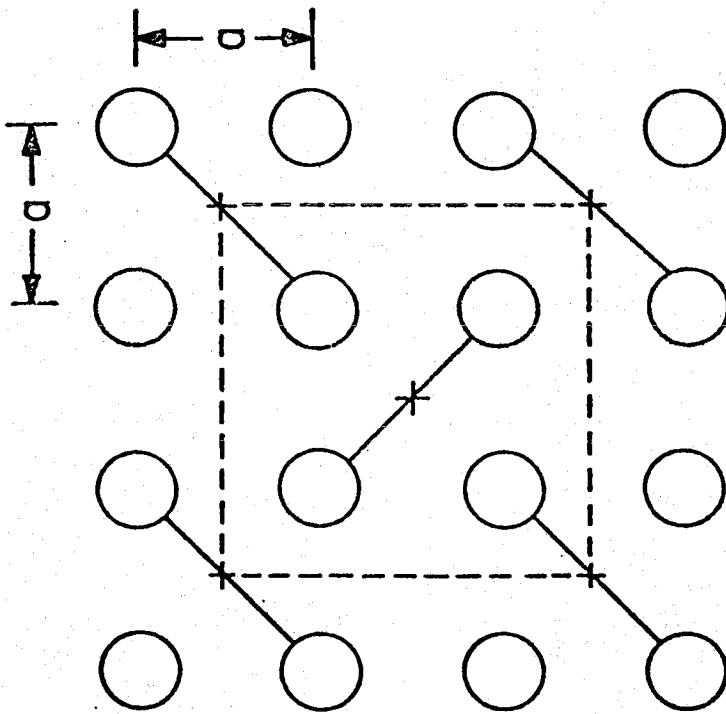


Fig. 6 The $c(2 \times 2)$ structure for S on Ni(100) and Ni(110) respectively. Circles represent surface Ni atoms, crosses represent S atoms, heavy lines represent Ni-S bonds, and dashed lines outline the unit cell.

(110) SURFACE



(100) SURFACE



2.2.1 The Ni(100) Surface

Ni atoms 2 and 4 of Fig. 5 were included in the Ni₂S calculation. Adding Ni atom 5 leads to the Ni₃ cluster, but as discussed in Section 2.1.3 the effect of Ni atom 5 on the geometry is very small (0.03Å), thus we included only the surface Ni atoms (1-4) in the final Ni₄S calculation to determine the geometry. From Fig. 6, one sees that Ni atoms 1 and 3 are involved in bonds to adjacent S atoms. These orbitals are expected to lead to nonbonded repulsions with the S orbitals, causing the S atom to be pushed up higher above the surface than for the Ni₂S complex. In the Ni₄S calculations (described in the previous section) this effect was approximated by coupling the 4s orbitals of Ni atoms 1 and 3 into a triplet state. The optimum geometry for the Ni₄S cluster has the S atom 1.33Å above the surface in excellent agreement with the distance from LEED intensity analysis, 1.30 ± 0.10Å [3a].

The bonding structure for (100) shown in Fig. 6 has the corner and center S atoms related by a glide plane; consequently it leads to a p(2 x 2) structure. However, there is a degenerate structure with all the bond directions rotated by 90°; these two structures are expected to have a strong interaction (resonance), leading to all the S atoms being equivalent. Thus, including this resonance effect, the overall symmetry is c(2 x 2).

From Fig. 6 we see that with a S in only half the four-fold sites each surface Ni atom has its 4s orbital involved in a Ni-S bond. Thus, this bonding picture suggests that the c(2 x 2) overlayer is particularly stable.

Note that the van der Waals radius of the S atom is 1.85\AA [5b], whereas half the S-S distance for the $c(2 \times 2)$ structure is 1.76\AA . Thus, higher densities of S atoms on the surface are also unfavorable due to large nonbonded repulsions between adjacent sulfur atoms.

2.2.2 The (110) Surface

For the (110) surface the LEED intensity analysis was carried out assuming a registry with the surface given by geometry B of Fig. 5b. However, as discussed in Section 3.5, geometry B involves a Ni-Ni separation of $\sqrt{3}$ times the bulk separation leading to a NiS bond length (2.35\AA) and a NiSNi angle (133.3°) which seem much less favorable than the optimum Ni-S distance and bond angle for the Ni_2S cluster 2.04\AA and 118.8° respectively (geometry A). Since the LEED intensity analysis is more sensitive to the distance above the surface than to the registry with the surface [10], we suggest that geometry A is a likely alternative. The Ni_2S cluster is appropriate to calculating the optimum geometry for a site of geometry A since the closest nonbonded Ni atoms are in the next layer down (2.61\AA away for the experimental geometry) and should not significantly influence the geometry. Thus, we predict that for the (110) surface the S atom should be 1.04\AA above the surface, which is in reasonable agreement with the distance, $0.93 \pm 0.10\text{\AA}$, found from analysis of LEED intensities [3a].

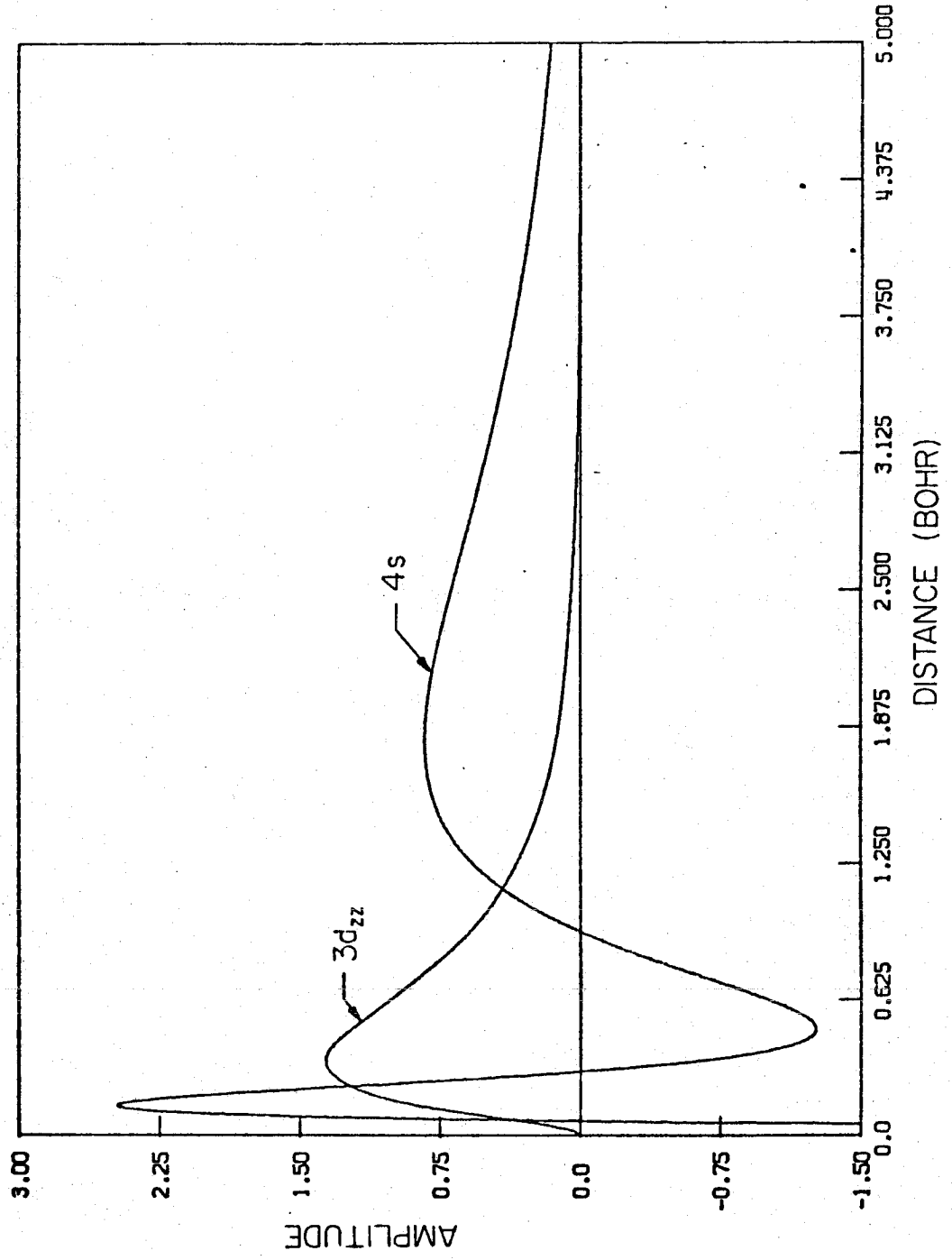
3. Further Discussion of the Wavefunctions

Before discussing the bonding of a sulfur atom to the various Ni clusters, we first consider the bonding in NiH and Ni₂ since these simple cases illustrate the basic characteristics of the bonding between Ni atoms and the bonding to a sulfur atom.

The Ni atom has two low-lying states $4s^1 3d^9 (^3D)$ and $4s^2 3d^8 (^3F)$. Ignoring spin-orbit coupling effects, the ground state is 3D with the 3F state only 0.03 eV higher [11]. Thus, both states could play a role in the bonding. However, the Ni(4s) orbital is $\sim 2-1/2$ times as large as the Ni(3d) orbitals (see Fig. 7); thus the 4s orbital dominates the bonding. Bringing up an H atom to the $4s^2 3d^8$ state of Ni leads to repulsive interactions much as for the case of HeH. The $4s^1 3d^9$ state of Ni, on the other hand, leads to a sigma bond between the Ni(4s) and H(1s) orbitals and, hence, an attractive potential curve as for H₂.

The remaining $3d^9$ configuration on the Ni then leads to $^2\Sigma^+$, $^2\Pi$, and $^2\Delta$ states depending on whether the singly occupied 3d orbital is taken as a $3d\sigma$, $3d\pi$, or $3d\delta$ orbital respectively. As discussed elsewhere [13], while the Ni configuration is basically $4s^1 3d^9$, some $4s^2 3d^8$ character is introduced in certain states. The intra-atomic coupling between $4s^1 3d^9$ and $4s^2 3d^8$ leads to a stabilization of the $4s^1 3d^9$ configuration with a singly occupied $3d\delta$ orbital. The net effect is the ordering $^2\Delta < ^2\Pi < ^2\Sigma^+$ with $^2\Delta$ 0.346 eV below $^2\Pi$ which in turn is 0.095 eV below $^2\Sigma^+$ (at R_e for the $X^2\Delta$ state)[14]. We find that these results are quite general for sigma bonds to the Ni(4s) orbital leading to an

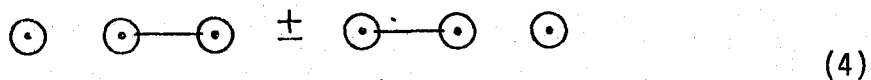
Fig. 7 Comparison of the 4s and 3d orbital sizes of the Ni atom.

NICKEL ATOM $4s^2 3d^8$ (3F)

increased stability associated with having a 3d hole which is δ -like with respect to the bond axis.



From the discussion of NiH, it is not surprising that the bonding in Ni_2 [15] involves a $4s^1 3d^9$ configuration on each Ni leading to a sigma bond between the 4s orbitals, and the lowest 3d occupation has both 3d holes taken in $3d\delta$ orbitals (other 3d orbital occupancies lead to numerous low-lying excited states).

For larger clusters of Ni atoms there is a possibility of bonding involving the $4s^2 3d^8$ configuration of the Ni atom. We illustrate this possibility for Ni_3 [16], where the central Ni atom can be taken as $4s^1 3d^9$ or $4s^2 3d^8$ in character. For the $4s^1 3d^9$ case (considering only the Ni(4s)-like orbitals), the bonding is analogous to that in linear H_3 [18] leading to resonance states of the form



For the $4s^2 3d^8$ case the lowest state involves two sigma bonds:



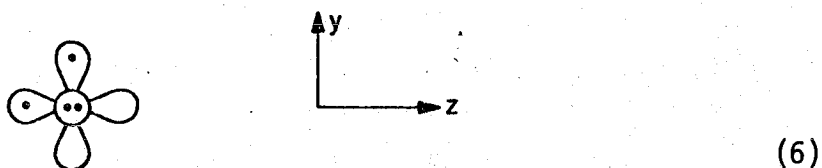
(Here the $(4s)^2$ pair of the central Ni has been angularly correlated, leading to an s_z lobe  overlapping Ni1 and an \bar{s}_z lobe  overlapping Ni2.)

Keeping the bond lengths equal, both (4) and (5) lead to linear geometries with $R = 2.28\text{\AA}$ for (4) and $R = 2.36\text{\AA}$ for (5). Using the

optimum R, the s^1d^9 state (4) is the ground state. However, if the R is fixed at the bulk value of 2.49\AA the potential curves are as in Fig. 8b. Here one sees that linear geometries favor s^2d^8 , while bent geometries favor s^1d^9 [19]. (From examination of the orbitals we find that the sz and \overline{sz} -like lobes of the central Ni in (5) remain oriented at 180° to each other as the molecule bends, leading to a decrease in the overlap of the bond pairs and a large increase in energy upon bending.) Thus, at the Ni-Ni-Ni bond angles involved in the Ni clusters considered here (90°), we expect that all Ni atoms have a $4s^13d^9$ configuration. (The energies as a function of geometry for (4) and (5) are summarized in Table 2.)

3.1 NiS

Now we consider bonding a single Ni atom to S. The sulfur atom has a $(1s)^2(2s)^2(2p)^6(3s)^2(3p)^4$ configuration, leading to a 3P ground state. Ignoring the core electrons and the $(3s)^2$ pair [since we find they are not involved in the bonding] leads to a $(3p)^4$ configuration which we represent as

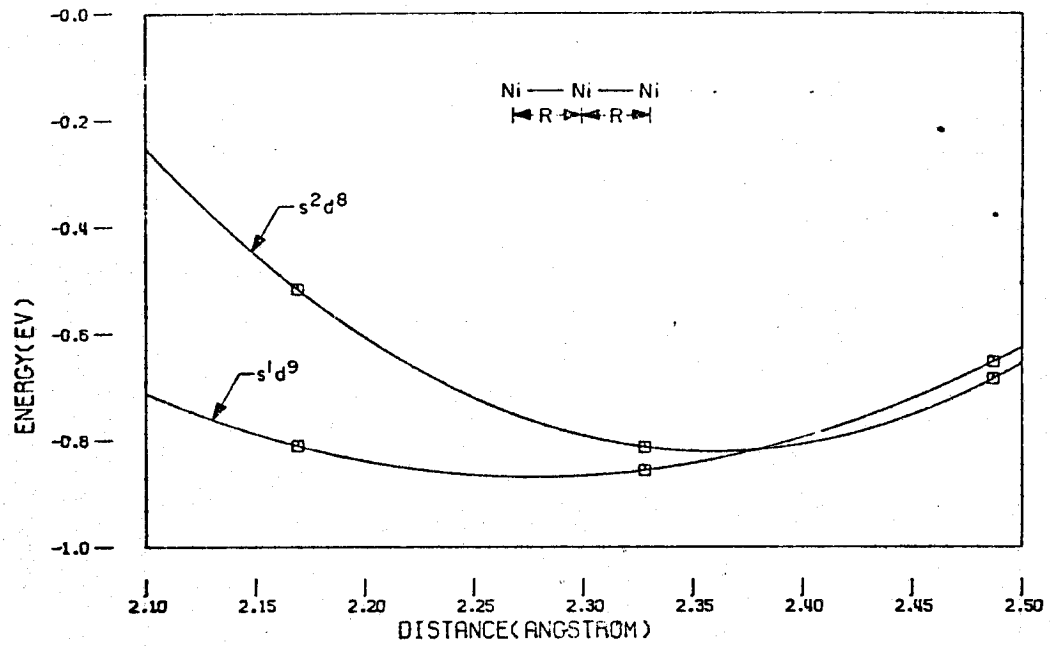


where \bigcirc represents a $3p_x$ orbital perpendicular to the plane of the paper and ∞ represents a $3p$ orbital in the plane of the paper. Bringing up a single Ni atom (along the z axis) leads to formation of a sigma bond between the Ni($4s$) and S($3p_z$) orbital.

Fig. 8 Energy of Ni_3 as a function of bond length and bond angle. The curves labeled s^1d^9 correspond to (4), while the curves labeled s^2d^8 correspond to (5). Figure 8a corresponds to optimizing the Ni-Ni length for equal Ni-Ni bond lengths, while Fig. 8b corresponds to varying the bond angle for a fixed Ni-Ni distance corresponding to the bulk separation (2.49\AA).

Ni₃ GEOMETRY VARIATION

(a) R VARIATION



(b) ANGLE VARIATION (R=2.49 Å)

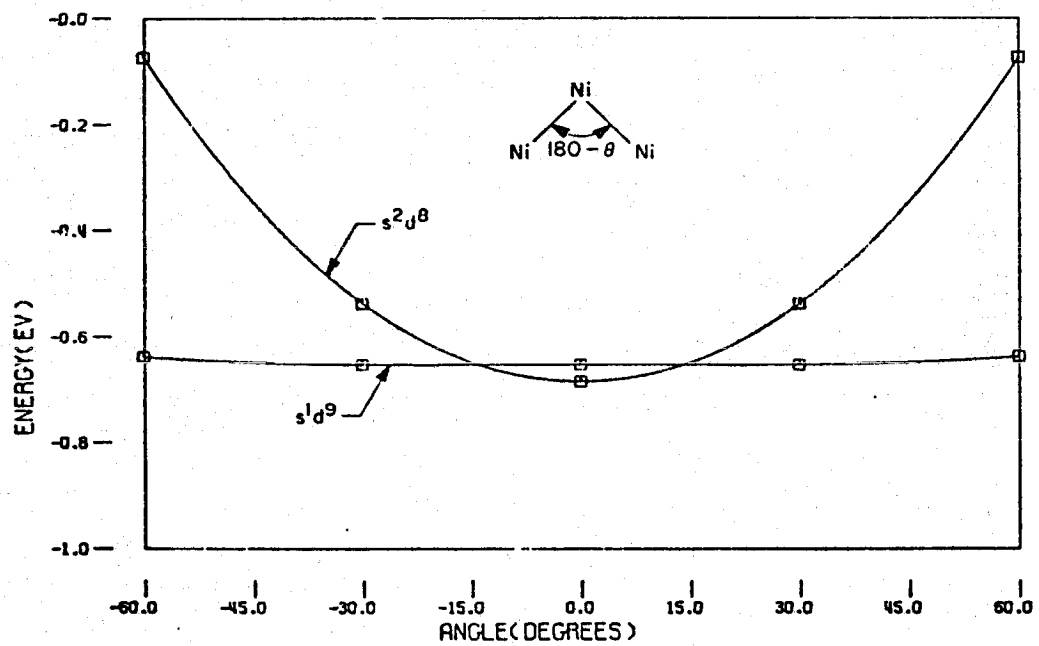
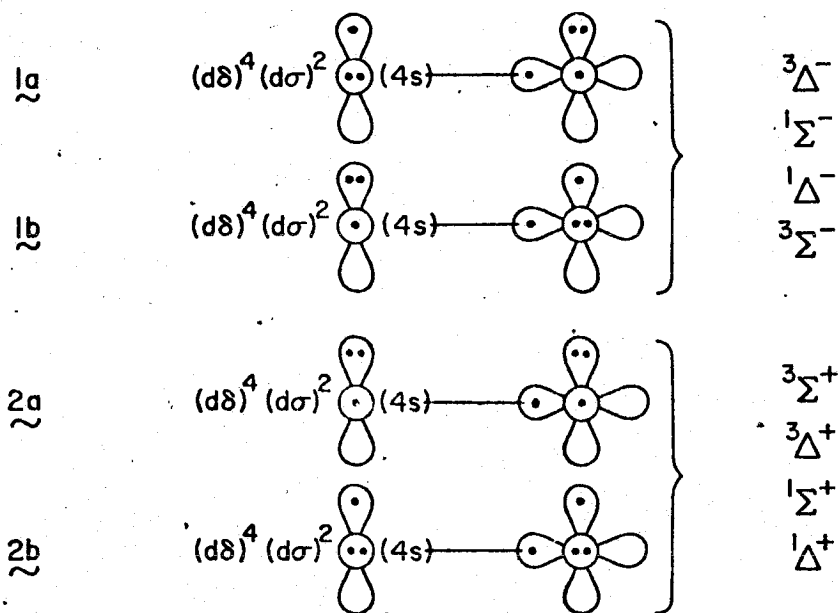
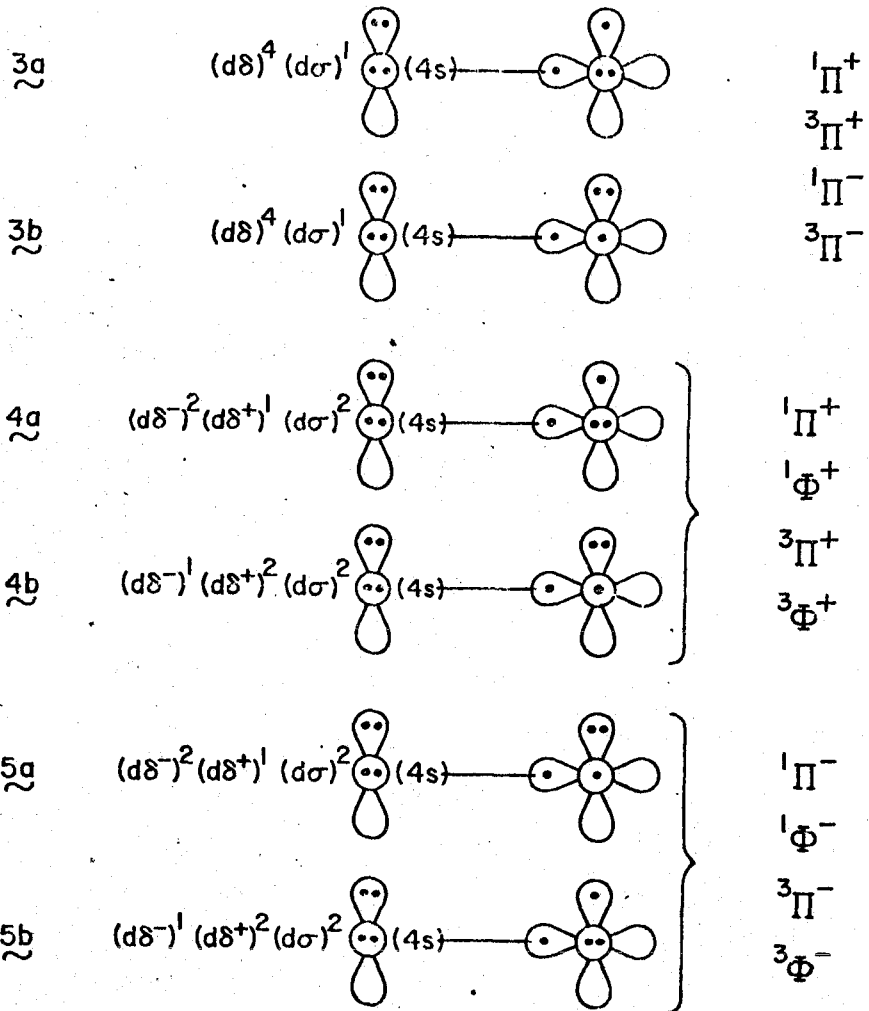


Table 2 Energies for GVB Calculations on Ni_3 as a Function of Geometry. (Always retaining equal bond lengths. As described in section 3, one state has s^1d^9 character on the central Ni while the other has s^2d^8 character.)

θ	R	4.1 a_0	4.4 a_0	4.7 a_0
180°	s^1d^9	-41.14976	-41.15143	-41.14397
	s^2d^8	-41.13894	-41.14984	-41.14515
150°	s^1d^9			-41.14398
	s^2d^8			-41.13974
120°	s^1d^9			-41.14344
	s^2d^8			-41.12270

This leaves a single 3d hole on the Ni which, together with the two possible S atom configurations, leads to the ten configurations shown below as 1a to 5b [20]. Each of these configurations involves a sigma bond between Ni(4s) and S(3p σ) orbitals and the ordering of the states is controlled mainly by differences in the π bonding. In these diagrams, we indicate the Ni(3d π) and S(3p π) orbitals schematically [using the same notation for Ni d π orbitals as was used in (6) for S p π orbitals] and include the remaining Ni atom configuration in an abbreviated form (e.g., (d δ)⁴(d σ)²).





Thus, taking a Ni(3d π) hole as in $\underline{1}$ and $\underline{2}$ leads to states $X^3_{\Sigma^-}$, $^1_{\Delta}$, $^1_{\Sigma^+}$, $^1_{\Sigma^-}$, $^3_{\Delta}$, and $^3_{\Sigma^+}$ which are analogous to the corresponding states of O₂ [7]. The 3d σ hole (as in $\underline{3}$) leads to the $2^1,^3_{\Pi}$ states and the 3d δ hole (as in $\underline{4}$ and $\underline{5}$) leads to the $1^1,^3_{\Pi}$ and $1^1,^3_{\Phi}$ states.

The potential curves for these states of NiS [CI calculations based on the $X^3_{\Sigma^-}$ state of NiS, see Section 5.1 for further discussion], are shown in Fig. 9, while the CI energies used to construct the curves are shown in Table 3.

By analogy to NiH, the states of the 3d δ hole are expected to be stabilized relative to the state of the 3d π hole, which in turn are stabilized relative to the states of the 3d σ hole. This leads to the $\underline{4}$ and $\underline{5}$ states (which involve a 3d δ hole) being below the $\underline{3}$ states (which involve a 3d σ hole). However, as was the case for NiO [8], the states having a Ni 3d π hole have additional π bonding, resulting in the $\underline{1}$ and $\underline{2}$ configurations being lowest. Thus $\underline{1,2} < \underline{4,5} < \underline{3}$. The ground state of NiS is the $^3_{\Sigma^-}(1)$ state which has an electronic structure analogous to O₂ [7]. The ordering of the remaining states is the same for the corresponding states of O₂.

The orbitals of the $X^3_{\Sigma^-}$ state of NiS are shown in Fig. 1. Looking at the sigma bond pair (Fig. 1ab) one sees that the Ni(4s)-like component (Fig. 1a) has been distorted toward the sulfur [a situation typical of a somewhat ionic bond (toward the S)]. As for NiO [8], the doubly occupied π orbitals (Fig. 1cf) have delocalized onto the opposite centers (leading to two three-electron bonds and the extra stability associated with the $^3_{\Sigma^-}$ state). However, the doubly occupied S(3p_x) orbital (Fig. 1f) has delocalized substantially more onto Ni than the

Fig. 9 Potential curves for the states of NiS. The calculated points are at 3.4, 3.5, 3.8, 4.1, and 4.4 a.u., respectively. The numbers in parentheses refer to the dominant configuration(s) for each state.

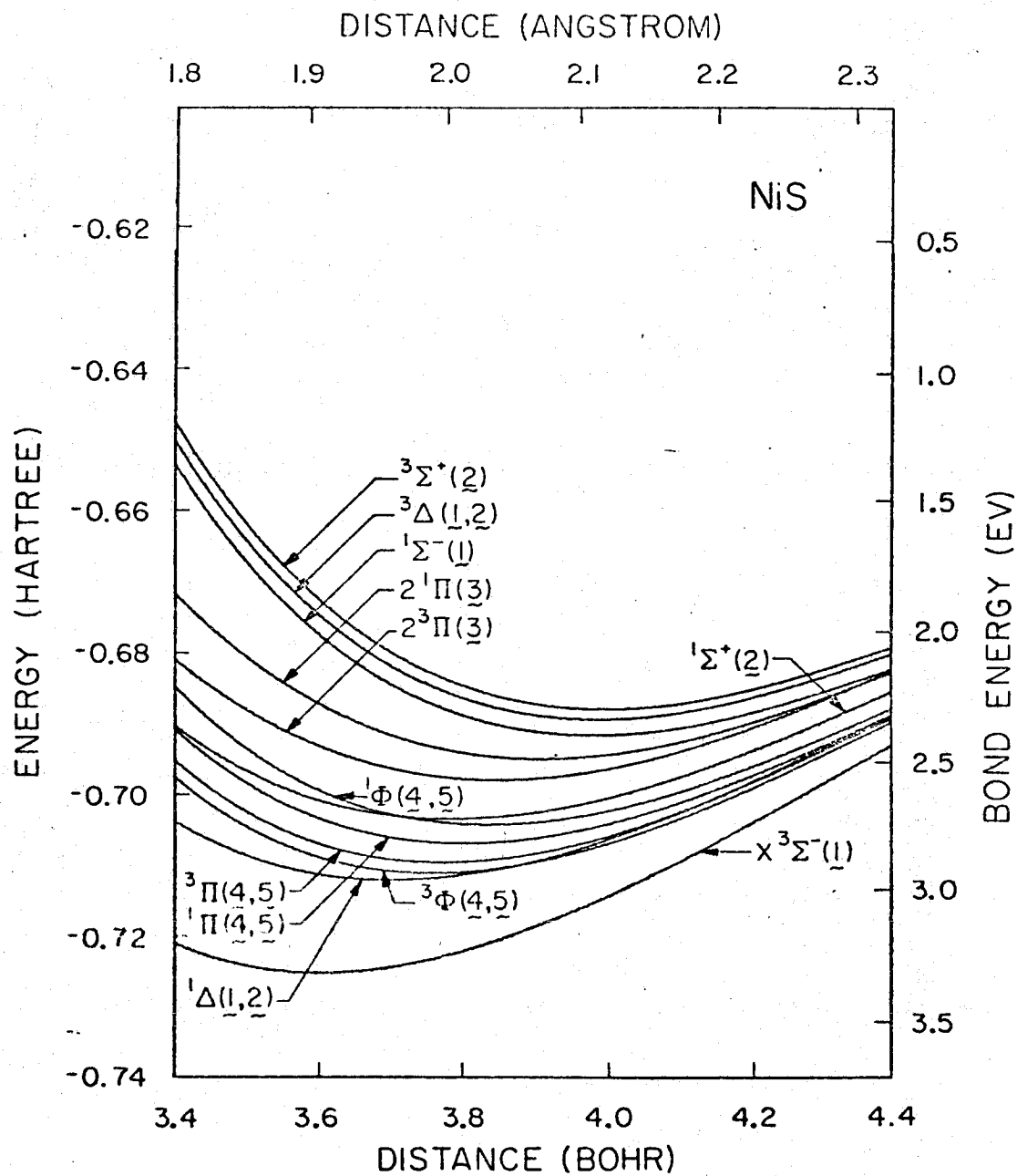


Table 3 Energies for CI Wavefunctions of N1s (Subtract the quoted energy from -50.0 to get the total energy in hartrees).

State	R =	3.4a ₀	3.5a ₀	3.8a ₀	4.1a ₀	4.4a ₀
3 $\phi(4,5)$		0.69700	0.70418	0.71071	0.70323	0.68905
2 $^3\Pi(4,5)$		0.69460	0.70200	0.70925	0.70229	0.68842
1 $^3\Pi(3)$		0.68015	0.68739	0.69729	0.69346	0.68171
1 $\phi(4,5)$		0.68406	0.68293	0.70381	0.69930	0.68712
2 $^1\Pi(4,5)$		0.69015	0.69788	0.70658	0.70089	0.68803
1 $^1\Pi(3)$		0.67077	0.67980	0.69353	0.69206	0.68192
3 $\Sigma^+(2)$		0.64615	0.66069	0.68384	0.68653	0.67833
3 $\Delta(1,2)$		0.64881	0.66311	0.68562	0.68783	0.67927
1 $\Sigma^-(1)$		0.65216	0.66618	0.68809	0.69000	0.68144
1 $\Sigma^+(2)$		0.68965	0.69618	0.70303	0.69716	0.68468
1 $\Delta(1,2)$		0.70338	0.70835	0.71115	0.70239	0.68804
X $^3\Sigma^-(1)$ ^b		0.72086	0.72411	0.72204	0.70944	0.69236

^aThe numbers in parentheses indicate the dominant configuration(s) for each state.

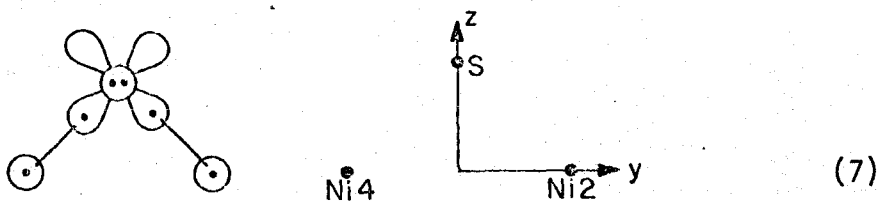
^bThe potential curve for the X $^3\Sigma^-$ state leads to D_e = 3.32 eV, R_e = 1.91Å, and ω_e = 483 cm⁻¹.

doubly occupied Ni($3d_{yz}$) orbital (Fig. 1c) did onto S, leading thus to some charge flow from S to Ni in the π system in response to charge flow from Ni to S in the sigma system. (The overall net charge transfer from the Mulliken populations is ~ 0.38 electron. For comparison the charge transfer in NiO is 0.55 electron.)

The potential curves in Fig. 9 lead to $D_e = 3.32$ eV, $R_e = 1.91\text{\AA}$ and $\omega_e = 483$ cm^{-1} for the $X^3\Sigma^-$ state. The only experimentally available information for NiS is $D_0 = 3.53 \pm 0.15$ eV [9]. The calculated R_e value, as expected, is substantially shorter than for bulk compounds (2.28, 2.34, 2.38, and 2.18\AA for Ni_3S_2 , NiS_2 , $\alpha\text{-NiS}$ and $\gamma\text{-NiS}$ respectively) [3a].

3.2 Ni_2S

Bringing up two Ni atoms to (3) and considering only the 4s electrons of the Ni atoms leads to two sigma bonds to the sulfur as in H_2S .



Given (4) one expects the lowest Ni($3d$) occupancy to correspond to taking the singly occupied Ni($3d$) orbitals to be delta-like with respect to the Ni-S bond axis [21].

In these calculations we fixed the Ni-Ni distance at $\sqrt{2}a$ (where a is the nearest neighbor distance 2.49\AA in Ni metal) as appropriate

for next nearest neighbors on the Ni(100) and Ni(110) surfaces. We then varied the NiS distance (retaining C_{2v} symmetry). The resulting potential curve is shown in Fig. 10, while the energies used to construct the curve are tabulated in Table 4. The optimum geometry from the potential curve corresponds to a distance above the surface of 1.04\AA which leads to a Ni-S bond length of 2.04\AA and a NiSNi angle of 118.8° .

Thus the NiS distance is 0.13\AA longer than for NiS, a reasonable result given that the ground state of NiS involved important π bonding effects not present in the case of Ni_2S .

Normally in bonding to sulfur one expects bond angles only slightly larger than 90° (e.g., 92.5° in H_2S [22]). However, there are two factors which tend to lead to a larger bond angle for Ni_2S than for H_2S : (i) The Ni(4s) orbital is much larger than a H(1s) orbital leading thus to larger orthogonality constraints (the orbitals of the two bond pairs must become orthogonal because of the Pauli principle). These effects are minimized by increasing the bond angle. (ii) The NiS bond is more ionic than an HS bond, leading to an increased overlap of the Ni(4s) orbitals and favoring an even larger bond angle.

In addition, the optimum bond angle in our Ni_2S complex represents to some extent a compromise between bond angle and bond length at the fixed Ni-Ni separation used [e.g., a small bond angle of 92.5° would lead to a Ni-S distance of 2.43\AA , much too large for a NiS bond].

Selected orbitals of Ni_2S (at the optimum geometry) are shown in Fig. 2 where one sees that: (i) The Ni-S sigma bonds are very similar to the corresponding bond orbitals for NiS shown in Fig. 1;

Fig. 10 Ni_2S geometry optimization. The calculated points are indicated.

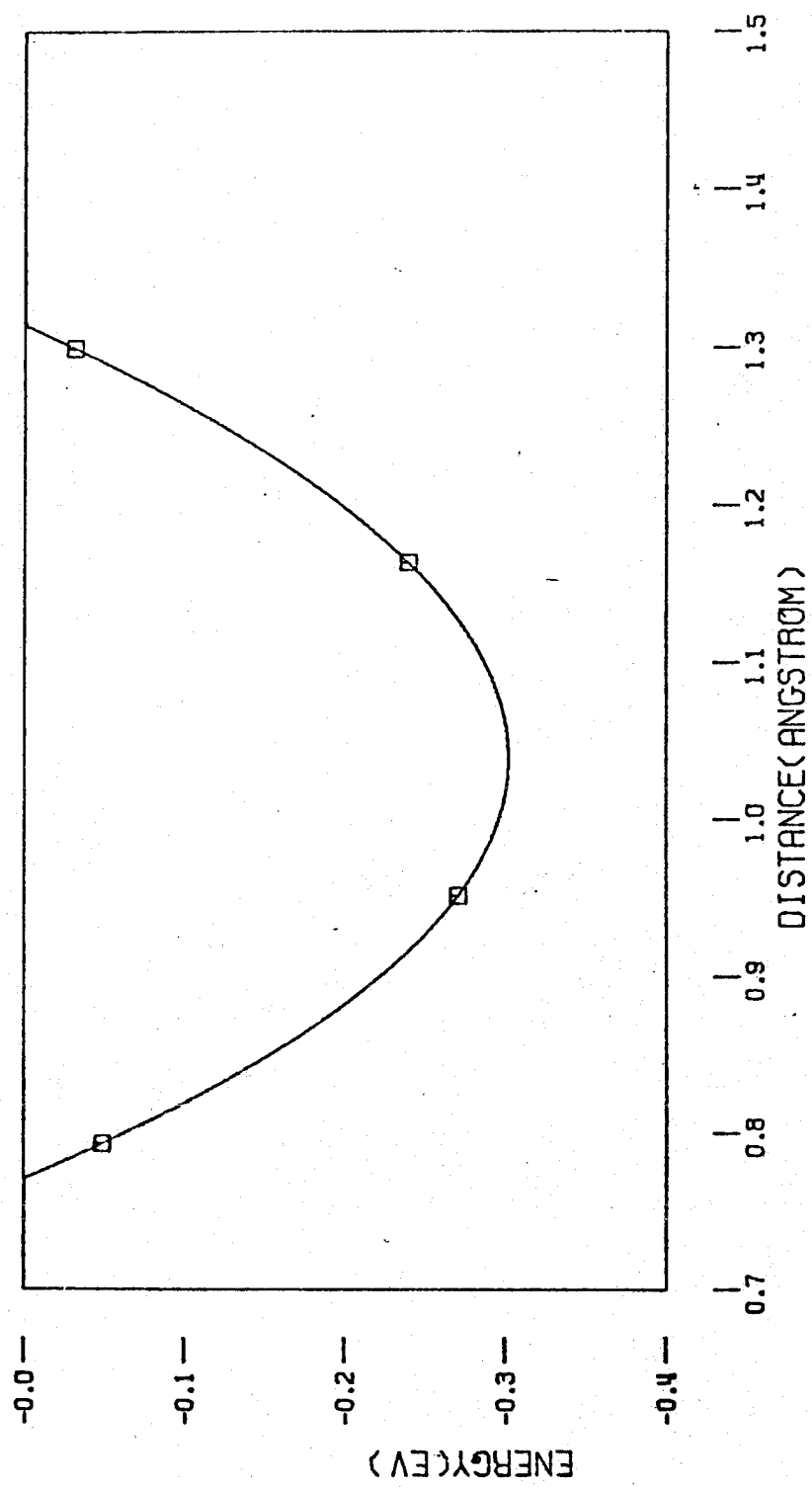
Ni₂S GEOMETRY OPTIMIZATION

Table 4 Ni_2S Geometry Optimization^a ($\text{Ni-Ni} = \sqrt{2}a$). D is the distance of the S from the Ni-Ni axis.

D (a_0)	Energy ^d (hartree)
2.4567	-91.28115
2.2000	-91.28880
1.9700 ^b	-91.29118 ^c
1.8000	-91.28995
1.5000	-91.28179

^aThe basis set is [3s,1p,2d/3s,2p,1d] (see Section 3)

^bThis is the minimum from a fit to the other 4 points

^cThe optimum geometry is with the S 1.04 \AA above the surface, which corresponds to a Ni-S distance of 2.04 \AA and a NiSNi angle of 118.8°. The bond energies (D_e) for GVB and CI wavefunctions are 5.27 eV and 5.37 eV, respectively. (The Ni_2 energy is taken as twice the HF energy of the Ni atom.)

^dGVB(2/pp) calculations

and (ii) the S(3s) pair has built-in $3p_z$ character in such a way as to move away from the bond pairs. These orbitals were used to construct a small CI wavefunction (see Section 5.2) over the occupied orbitals of the GVB wavefunction. This CI wavefunction leads to a D_e of 5.37 eV [as compared with 5.27 eV for the GVB(2/PP) wavefunction]. Comparing to the bond energy for NiS (3.32 eV) indicates that S has a strong tendency to bridge two Ni atoms for Ni-Ni separations of $\sqrt{2}a$, as on the Ni(100) and Ni(110) surfaces [23].

3.3 Ni₃S

We first consider an alternative form of the wavefunction for Ni₂S which is more appropriate to four-fold bonding sites on Ni(100). For the case of Ni₂S, the GVB(2/PP) wavefunction (7) corresponds to localized bond pairs which are represented in terms of natural orbitals as

$$(\phi_\ell^2 - \lambda\phi_\ell^{*2})(\phi_r^2 - \lambda\phi_r^{*2}) \quad , \quad (8)$$

where ϕ_ℓ is the mirror image of ϕ_r and ϕ_ℓ^* is the mirror image of ϕ_r^* , respectively. An alternative way to correlate this wavefunction using symmetry orbitals is

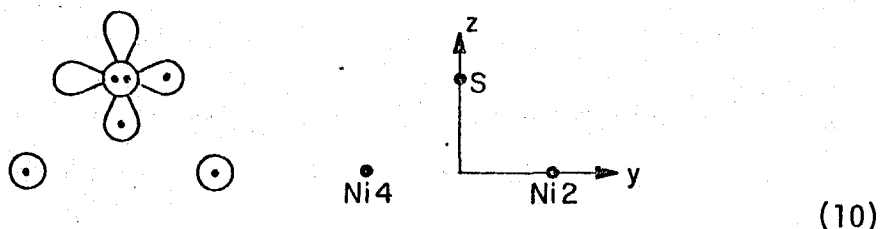
$$(1a_1^2 - \lambda 2a_1^{*2})(1b_2^2 - \lambda 2b_2^{*2}) \quad (9)$$

where $1a_1 = \phi_\ell + \phi_r$, $1b_2 = \phi_\ell - \phi_r$,

$$2a_1 = \phi_\ell^* + \phi_r^* \quad , \quad \text{and} \quad 2b_2 = \phi_\ell^* - \phi_r^* \quad .$$

For Ni_2S the wavefunction (8) leads to a lower energy than (9). However, for S in a four-fold site on the Ni(100) surface, the presence of the other nearby Ni atoms restricts the correlation effects, leading to a wavefunction of the form (9) being lower [24]. Thus, we show the orbitals of (9) in Fig. 11 for comparison to the orbitals of the Ni_3S and Ni_4S clusters to be discussed next.

The orbitals shown in Fig. 11 may be interpreted in terms of bonding the sulfur atom to the Ni_2 cluster in the following orientation



The $\text{S}(3p_z)$ orbital (Fig. 11a) is then singlet paired with the a_1 combination of the $\text{Ni}(4s)$ orbitals (Fig. 11b) and the $\text{S}(3p_y)$ orbital (Fig. 11c) is singlet paired with the b_2 combination of the $\text{Ni}(4s)$ orbitals (Fig. 11d), leading to the bond pairs shown in Fig. 11. We also show the $1a_1$ orbital of (9) (Fig. 11e), since it is appropriate to cases where this orbital is not correlated.

Considering only the $\text{Ni}(4s)$ electrons, the bonding in the Ni_3 cluster may be thought of as

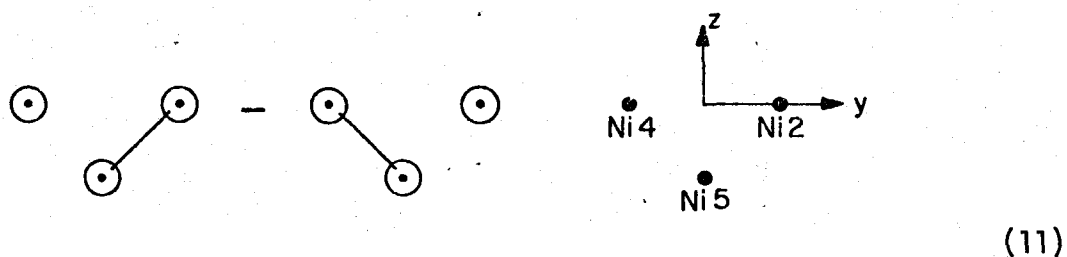
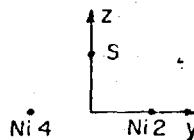
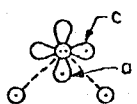


Fig. 11 The GVB orbitals for Ni_2S using the wavefunction (9).

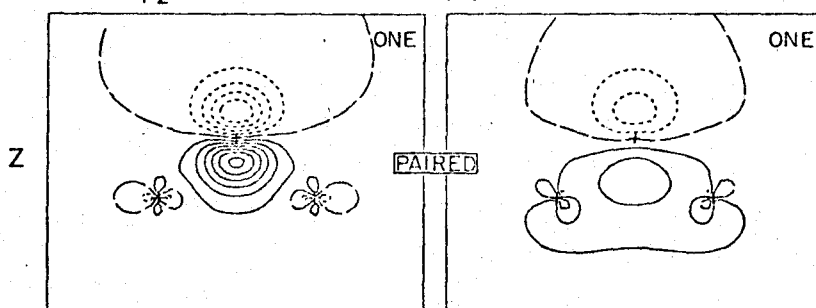
Ni_2S
GVB (2/PP), C_{2v} SYMMETRY



THE a_1 BOND PAIR

(a) S $3p_z$

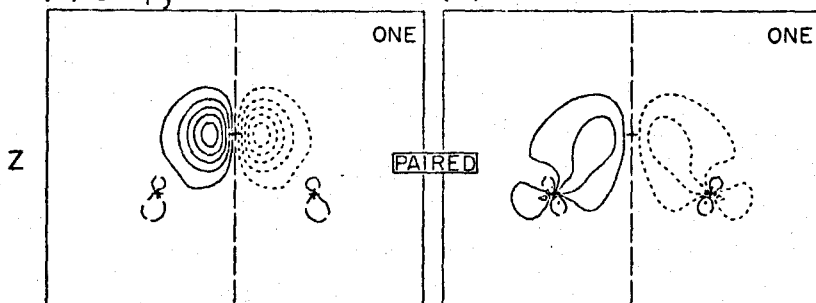
(b)



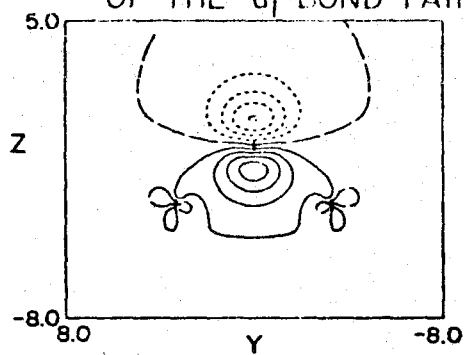
THE b_2 BOND PAIR

(c) S $3p_y$

(d)



(e) FIRST NATURAL ORBITAL
OF THE a_1 BOND PAIR

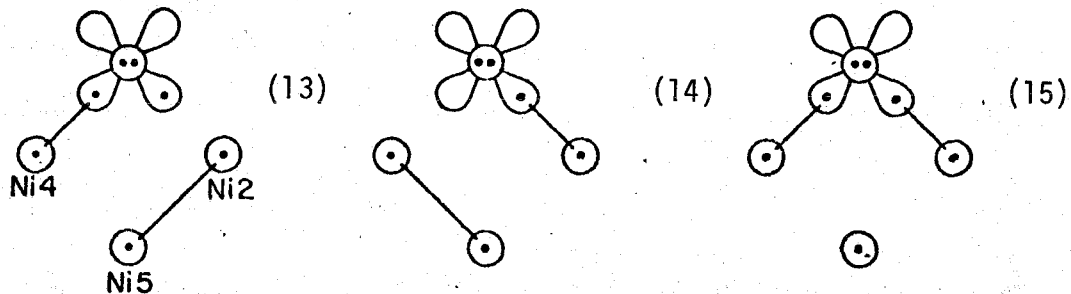


Using symmetry for the GVB wavefunction leads to

$$(1a_1^2 - \lambda 2a_1^2)1b_2^1 \quad (12)$$

The orbitals of this wavefunction are shown in Fig. 12 where one sees that the bond pair corresponds to a component localized mainly on Ni5 and a component localized mainly on Ni2 and Ni4, while the singly occupied orbital corresponds to the antibonding combination of Ni2(4s) and Ni4(4s) [25].

Given the structure of Ni₃, bonding a S atom leads to three principal resonance structures:



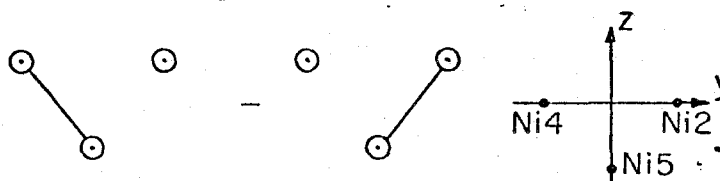
We find that the dominant configuration is (15) which involves disruption of the Ni-Ni bond leading to formation of two Ni-S bonds. [For the actual solid, the Ni5(4s) orbital of (15) is able to form bonds to other Ni atoms leading to less disruption of metal-metal bonds and further favoring (15).] The GVB wavefunction for (15) is

$$1a_1^2(1b_2^2 - \lambda 2b_2^2)1b_1^2 2a_1^1 \quad (16)$$

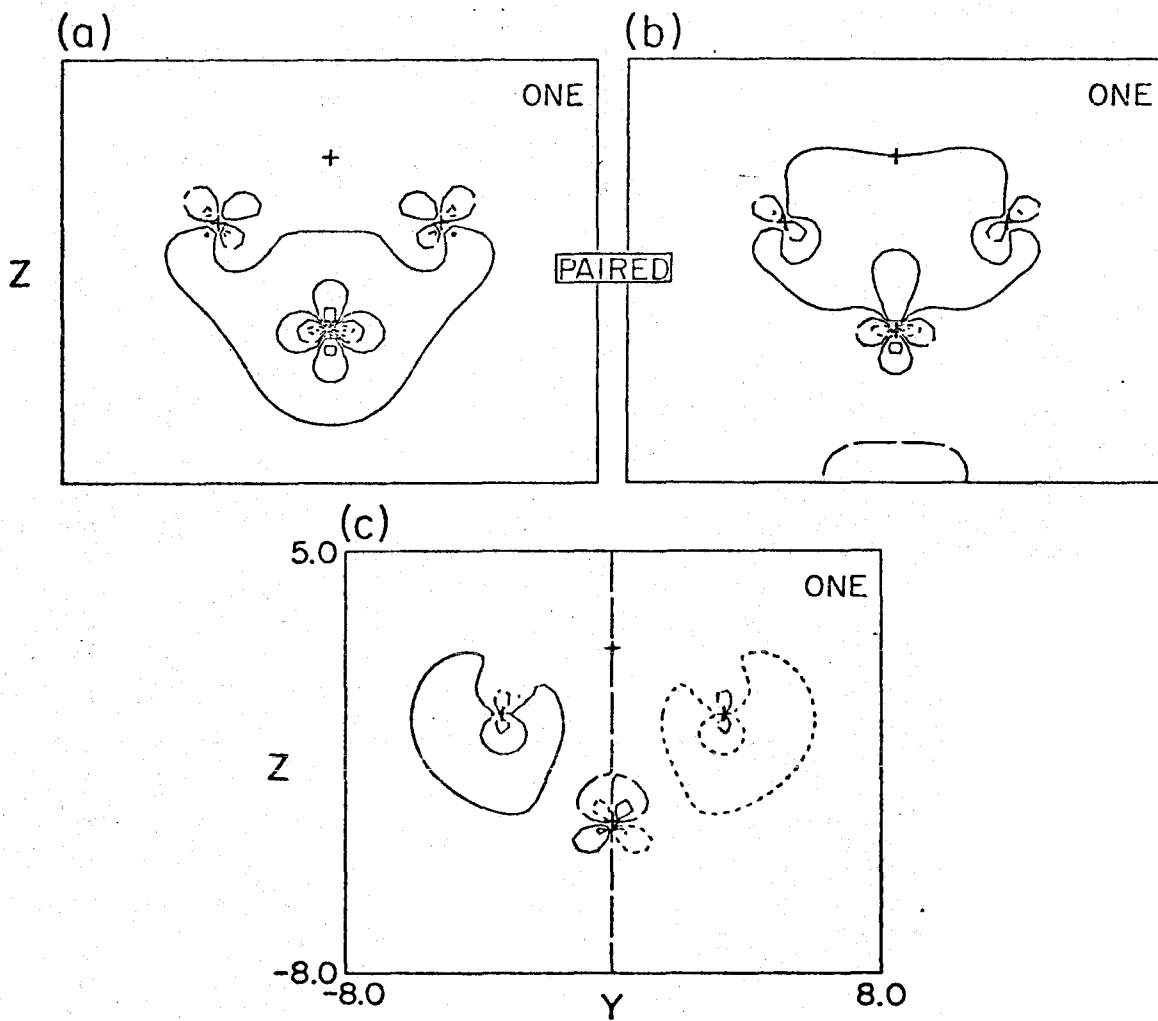
Here the $1a_1^2(1b_2^2 - \lambda 2b_2^2)$ part of the wavefunction is analogous to

Fig. 12 The orbitals of Ni_3 corresponding to the wavefunction (12).

Ni₃ GVB (I/PP)



THE BOND PAIR



the wavefunction (9) for the bond pairs of Ni_2S except that the $1a_1^2$ pair is not correlated. The $2a_1$ orbital is predominately a 4s orbital on Ni5 and the $1b_1^2$ pair corresponds to a $S(3p_x)$ pair.

We show the orbitals corresponding to (16) in Fig. 3. Here one sees that the bond pair is similar to the b_2^2 pair in (9) and has one component (Fig. 3a) which is basically $S(3p_y)$ -like, while the other component (Fig. 3b) corresponds to the b_2 combination of 4s functions on Ni2 and Ni4. The doubly occupied $1a_1$ orbital (Fig. 3c) has slightly less bonding character than for Ni_2S , largely as a result of orthogonality constraints with the $2a_1$ singly occupied orbital (Fig. 3d), which is mainly a 4s orbital on Ni5 but with substantial hybridization away from the Ni-S bonds.

Putting these effects together, orthogonality constraints between the 4s orbital of Ni5 and the bond pairs are expected to increase slightly the distance of the S above the surface, but this effect should be partially counterbalanced by the small, attractive interaction between the $S(3s)$ pair and the $3d^9$ core of Ni5. These considerations suggest that the Ni_3S cluster should lead to a geometry with the sulfur atom slightly further above the surface than for the Ni_2S cluster. Indeed, we find that the optimum distance above the surface for the Ni_3S cluster is 1.07\AA , only 0.03\AA larger than the optimum distance (1.04\AA) for the Ni_2S cluster. We conclude that the effect of Ni5 (the second layer Ni) on the geometry is negligible and the geometry of the S atom should be determined mainly by the four nearest neighbor atoms in the surface. Table 5 summarizes the Ni_3S geometry optimization.

Table 5 Ni₃S Geometry Optimization^a

D (a ₀)	Energy ^b		
	HF	GVB(1/pp)	CI ^c
2.457	0.77815	0.78581	0.79435
2.000	0.78701	0.79383	0.79999
1.800	0.78665	0.79312	0.79840
1.600	0.78335	0.78948	0.79418

^aThese calculations use the [2s,1p,1d/3s,2p] basis. For Ni₂S this basis leads to an error of 0.343 eV from removal of S d functions and an error of 0.283 eV from the single zeta contraction of the Ni(3d) basis functions.

^bSubtract the quoted value from -131.0 to get the total energy in hartree.

^cThe optimum geometry is with the S 1.07Å above the surface, which corresponds to a Ni-S distance of 2.06Å and a NiSNi angle of 117.2°. The D_e value is 3.261 eV.

For purposes of comparing to the Ni₂S and NiS calculations which use the larger [3s,1p,2d/3s,2p,1d] basis one should add the total error for the smaller basis^a (0.626 eV) leading to a D_e of 3.886 eV.

3.4 Ni₄S

In Section 2.1.4 we noted that for the Ni₄S cluster the S(3s) pair is stabilized by interaction with the 3d⁹ cores of Ni atoms 1 and 3, leading to incorporation of S(3p_z) character so as to hybridize toward the surface. [Here the S(3s) orbital energy is 2.12 eV more negative than for the atom as compared to 0.43 eV more negative in the case of the Ni₃S cluster.]

The hybridization of the S(3s) orbital toward the surface leads to correlation effects for the NiS bond pairs being substantially less important in the z direction than in the y direction [24] resulting in NiS bond pairs of the form

$$1a_1^2(1b_2^2 - \lambda 2b_2^2) \quad (17)$$

(analogous to the description of the NiS bond pairs in Ni₃S).

Combining these orbitals with the Ni1 and Ni3 4s orbitals ($2a_1^1 2b_1^1$) and the O (2p_x) pair ($1b_1^2$) leads to a total wavefunction [27]

$$1a_1^2(1b_2^2 - \lambda 2b_2^2) 1b_1^2 2a_1^1 2b_1^1 \quad (18)$$

The orbitals of (18) are shown in Fig. 4. Examining first the bond pair (Fig. 4ab) we see that one component (Fig. 4a) is essentially a S(3p_y) orbital, while the other component (Fig. 4b) corresponds to the b₂ combination of 4s orbitals on Ni2 and Ni4. The $1a_1^2$ pair (Fig. 4c) is mainly S(3p_z)-like, but has Ni-S bonding character on all four Ni atoms. The S(3s) orbital (Fig. 4d) has built in a

small amount of $3d\sigma$ character on all four Ni atoms, somewhat analogously to the small incorporation of $3d\sigma$ character for the 5σ orbital of CO bonded to Ni. Thus the a_1 bonding pair and the $S(3s)$ pair have the four-fold symmetry of the Ni_4S cluster, whereas the b_2 bond pair is localized (involving bonding to Ni2 and Ni4).

The Ni1 and Ni3 $4s$ orbitals show antibonding character on the sulfur due to orthogonality constraints with the sulfur orbitals. These effects seem to be more important than stabilization of the $S(3s)$ pair, leading to an optimum geometry with the S 1.33\AA above the surface as compared with 1.04\AA for the Ni_2S cluster.

In Fig. 6 we show the overall bonding pattern for the $c(2 \times 2)$ structure on the surface. The localized orbitals shown in Fig. 6 correspond to the b_2 bond pair of our Ni_4S cluster. Including these bonds, the S atoms are related by a glide plane and the overlayer is actually of $p(2 \times 2)$ symmetry. However, the overlayer structure shown is degenerate with an equivalent structure where all the bond pairs are rotated by 90° . For the portion of the overlayer included in our Ni_4S calculation, these two structures are actually of different symmetry (b_1 and b_2) and thus do not couple to each other. However, if the total overlayer is considered, these structures are both of a_1 symmetry and do overlap. Thus, they interact strongly (resonate) leading to all S atoms on the surface being equivalent and the total symmetry of the overlayer is $c(2 \times 2)$.

The energies of the Ni_4S cluster as a function of geometry are shown in Table 6.

Table 6 Ni₄S Geometry Optimization. D is the distance from the S to the Ni₄ plane.

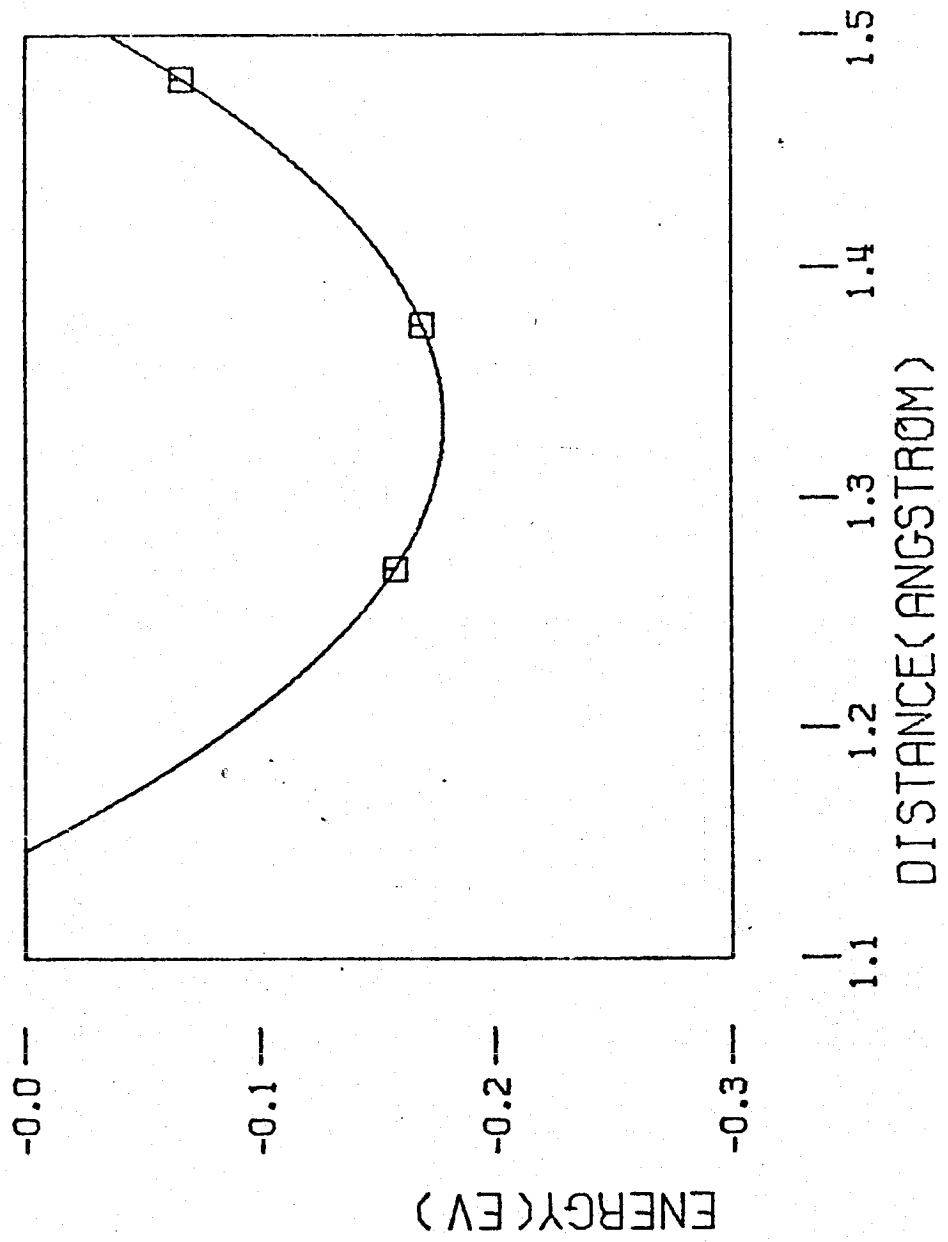
D (a ₀)	Energy ^{a,b} (hartree)
2.8	-172.34744
2.6	-172.35122
2.4	-172.35079

^aThe optimum geometry has the S atom 1.33Å above the surface, which leads to a Ni-S distance of 2.21Å and a NiS₂ angle of 105.6°.

The D_e value is 3.28eV.

^bGVB(1/pp) calculations

Fig. 13 The Ni_4S geometry optimization. The calculated points are indicated.

Ni₄S GEOMETRY OPTIMIZATION

3.5 Comparison of Bonding Geometries for the (110) Surface

In Fig. 5 we compare the bonding position currently suggested for S on Ni (110) from analysis of the LEED intensity data [3a] (geometry B) to the position we favor (geometry A). For geometry A the S is bridged across Ni atoms 1 and 2 which are separated by $\sqrt{2}a$ (as in our Ni_2S calculations). Here, there are two second nearest neighbors below the surface (Ni atoms 3 and 4), but they are 2.609\AA from the S and should not interact strongly with the S atom. We thus conclude that our Ni_2S calculations should be a good model for this surface--a conclusion which is supported by the fact that the calculated distance above the surface (1.04\AA) for the Ni_2S model is in reasonable agreement with the distance ($0.93 \pm 0.1\text{\AA}$) obtained from analysis of the LEED intensity data [3a]. (We assume here that the distance above the surface influences the fit to the LEED data more strongly than differences in the registry with the surface. [10].)

Geometry B has the S bridged across Ni atoms separated by $\sqrt{3}a$. One can imagine two bonding arrangements consistent with this geometry: i) a bonding arrangement where the S atom forms two sigma bonds to Ni atoms separated by $\sqrt{3}a$ (e.g., 2 and 4) as in our Ni_2S model; ii) a situation in which the S atom bonds to the atom directly beneath it in the layer beneath the surface (i.e., to Ni5) as in our NiS calculations.

(i) leads to a Ni-S distance of 2.35\AA which is considerably larger than the optimum NiS distance we find for Ni_2S and leads to a

NiS_{Ni} bond angle of 133.3° which seems unreasonably large. In addition there should be strong nonbonded repulsions from Ni5 (2.17Å from the S) and Ni1 and Ni3 (2.35Å from the S).

(ii) leads to a reasonable Ni-S distance (2.17Å) but suffers from the fact that there are four nearest neighbor atoms (1,2,3, and 4) only 2.35Å away which should lead to strong nonbonded repulsions. In addition, we find that bridged bonding should be stronger.

With either type of bonding geometry B would seem to have a higher energy than geometry A. (A also leads to reasonable Ni-S bond lengths and minimal nonbonded repulsions).

The assumption is often made that an adsorbed atom will occupy a position similar to that which would be occupied by a metal atom in the next layer up. However, for S we find that the character of the atomic orbitals (two singly occupied 3p orbitals oriented at 90° to each other) leads to a strong preference for forming two bonds to next nearest neighbor Ni atoms. Thus, the chemical nature of the adsorbed atom may play a role in determining the bonding site and in the case of the Ni (110) surface may result in a structure different from that obtained with a "hard sphere model".

4. Calculation Details

The effective potential used for the Ni atom has been previously reported [28]. (This potential replaces the 18 electron Ar-core of the Ni atom.) The Ni basis set was taken from the set optimized for the third row atoms by Wachters [29]. All five d primitives of each type

were used but only the outer four s functions were needed for describing the coreless Hartree-Fock orbital [30]. In addition, a single set of p functions $\alpha = 0.12$ was added to describe polarization effects involving the 4s orbital.

Two contractions of this basis set were used. The first is identical to that used in Ref. 13 and has the tightest two s primitives and the tightest four d primitives contracted together based on the $4s^2 3d^8 ({}^3F)$ state of the Ni atom. This basis then has three contracted s functions and two contracted d functions of each type and is denoted [3s,1p,2d]. This basis set was used for the NiS and Ni₂S calculations.

For the larger Ni₃S and Ni₄S calculations we contracted the basis to [2s,1p,1d]. Since the states considered here have the $4s^1 3d^9$ configuration on Ni, the contraction used was based on a (symmetry restricted) HF calculation for the $4s^1 3d^9$ state of the Ni atom [17]. The tightest three s functions were contracted together while the fourth was left free and all five d functions were contracted to a single d function. This contraction of the Ni basis led to energies about 0.3 eV higher for Ni₂S than with the [3s,1p,2d] basis. These two contractions of the Ni basis set are given in Table 7.

For the sulfur atom we used an effective potential to replace the ten electron Ne core leaving only the 3s and 3p electrons [31]. The basis set used for S was based on the (11s,7p) primitive set of Huzinaga [32]. The outer four s functions of this basis were used with the inner two contracted together based on the 3P state of the S atom. The p primitive basis consisted of three functions of each type

Table 7 The Nickel Basis Set^a

	α	[3s,1p,2d]	[2s,1p,1d]
s	2.39417	0.07894	-0.03635
	0.918169	0.93226	-0.42936
	0.130176	1.00000	1.16036
	0.046392	1.00000	1.00000
p	0.12000	1.00000	1.00000
d	48.9403	0.03296	0.02564
	13.7169	0.17780	0.13831
	4.63951	0.44356	0.34504
	1.57433	0.56560	0.43998
	0.486409	1.00000	0.39312

^aThe energy of the $^3D(4s^1 3d^9)$ state of the Ni atom using this basis is -40.4943h.

where the outer two are those given by Huzinaga, while the third was obtained by taking the geometric mean of the third and fourth primitives given by Huzinaga. The inner two of the resulting three primitives were contracted together based on the 3P state of the S atom. The resulting basis is $[3s,2p]$. For NiS and Ni₂S, we also added to the S a single set of d functions $\alpha = 0.532$. (The value of the exponent was optimized for S₂ [31].) The d functions were not found to be especially important (energy contribution 0.3 eV for Ni₂S) and were omitted for the larger Ni₃S and Ni₄S calculations. The basis set and effective potential for S are given in Table 8.

5. Details of the CI Calculations

5.1 NiS

The starting point for the basis was the GVB orbitals of configuration $\underline{1b}$ (10 orbitals including the natural orbitals of the bond pair and the S (3s)-like orbital). Because configuration $\underline{1b}$ is only one of two degenerate configurations (i.e., $\underline{1a}$ and $\underline{1b}$) which together describe the $X^3\Sigma^-$ state of NiS, the π_x and π_y orbitals from the calculation were not equivalent as is evident from Fig. 1. In order to generate an equivalent set of orbitals for the CI, the π_x orbitals were rotated and averaged with the π_y orbitals and the resulting set of two functions was used in both directions. To provide sufficient flexibility to describe the electronic states of NiS, additional orbitals (suitably orthogonalized to the occupied orbitals) referred to as virtual orbitals, were added which correspond to the more diffuse components of the Ni(3d π_x), Ni(3d π_y), S(3p π_x), S(3p π_y), Ni(3d δ_{xy}), and Ni(3d $\delta_{x^2y^2}$)-like functions. The resultant basis consisted of 16

Table 8 The Sulfur Basis Set and Effective Potential^a
 (From unpublished calculations by R. A. Bair)

<u>The Basis Set</u>		α	c
s		5.420	0.2052
		2.074	0.8203
		0.4264	1.0000
		0.1519	1.0000
p		3.345	-0.0248
		0.5218	1.0093
		0.1506	1.0000
d		0.532	1.0000

<u>The Effective Potential</u>	$(V_l = \sum_k c_k r^{n_k} e^{-\zeta_k r^2})$		
	n	ζ	c
V_{s-d}	-2	37.86817	5.5929
	0	6.86855	56.5728
	0	1.56858	5.0746
V_{p-d}	0	11.70804	95.88100
	0	1.94498	6.46433
V_d	-1	5.5318	-4.14561
	0	2.17611	-0.598214
	-1	0.34187	-0.002868

^aThe energy of the 3P ground state of the S atom is -10.1090 h using this basis set and potential.

functions.

The configurations were generated using a procedure analogous to that which had been used for O_2 by Moss and Goddard [7a]. The first step was to select a set of reference configurations corresponding to the dominant configurations for the states of interest (in this case configurations $\underline{1a-5b}$). This configuration list then defined a set of generating configurations which consisted of products of single excitations within subsets corresponding to: i) the natural orbitals of the GVB bond pair, ii) the $Ni(3d\pi_x)$ and $S(3p\pi_x)$ orbitals, and iii) the $Ni(3d\pi_y)$ and $S(3p\pi_y)$ orbitals. Single excitations from the generating configurations into the space of the above six orbitals generates all the important configurations for the states of interest. However, we also allow all single excitations from the generating configurations into the full virtual space in order to ensure inclusion of readjustment effects necessary to allow a consistent treatment of all the states.

We show the generating configurations for the NiS CI in Table 9 (based on C_{2v} symmetry). The resultant CI consisted of (130,232), (92,208), (122,326), (92,324), (158,392) and (158,626) {(spatials, spin-eigenfunctions)} for the 1A_1 , 1A_2 , 3A_1 , 3A_2 , 1B_1 and 3B_1 CI calculations, respectively.

5.2 Ni₂S

The GVB calculations were carried out in C_s symmetry (retaining

Table 9 Generating Configurations for the NiS CI

	Ni(3d σ)	σ	σ^* ^a	Ni(3d π_x)	S(3p π_x)	Ni(3d π_x)	Ni(3d π_y)	S(3p π_y)	Ni(3d δ_{xy})	Ni(3d $\delta_{x^2-y^2}$)
A1	2	$\begin{pmatrix} 2 \\ 1 \end{pmatrix}$	$\begin{pmatrix} 0 \\ 1 \end{pmatrix}$ ^b	$\begin{pmatrix} 2 \\ 1 \\ 2 \\ 2 \\ 0 \\ 2 \end{pmatrix}$	$\begin{pmatrix} 2 \\ 1 \\ 2 \\ 0 \\ 2 \\ 2 \end{pmatrix}$	$\begin{pmatrix} 1 \\ 2 \\ 2 \\ 2 \\ 2 \\ 0 \end{pmatrix}$	$\begin{pmatrix} 1 \\ 2 \\ 0 \\ 2 \\ 2 \\ 2 \end{pmatrix}$	$\begin{pmatrix} 1 \\ 2 \\ 0 \\ 2 \\ 2 \\ 2 \end{pmatrix}$	2	2
A2	2	$\begin{pmatrix} 2 \\ 1 \end{pmatrix}$	$\begin{pmatrix} 0 \\ 1 \end{pmatrix}$	$\begin{pmatrix} 2 \\ 1 \\ 1 \\ 2 \end{pmatrix}$	$\begin{pmatrix} 1 \\ 2 \\ 2 \\ 1 \end{pmatrix}$	$\begin{pmatrix} 1 \\ 2 \\ 1 \\ 2 \end{pmatrix}$	$\begin{pmatrix} 2 \\ 1 \\ 2 \\ 1 \end{pmatrix}$	$\begin{pmatrix} 2 \\ 1 \\ 2 \\ 1 \end{pmatrix}$	2	2
B1	2	$\begin{pmatrix} 2 \\ 1 \end{pmatrix}$	$\begin{pmatrix} 0 \\ 1 \end{pmatrix}$	$\begin{pmatrix} 2 \\ 1 \\ 2 \\ 2 \end{pmatrix}$	$\begin{pmatrix} 1 \\ 2 \\ 2 \\ 2 \end{pmatrix}$	$\begin{pmatrix} 2 \\ 2 \\ 1 \\ 2 \end{pmatrix}$	$\begin{pmatrix} 2 \\ 2 \\ 1 \\ 2 \end{pmatrix}$	$\begin{pmatrix} 2 \\ 2 \\ 1 \\ 2 \end{pmatrix}$	2	2
1	$\begin{pmatrix} 2 \\ 1 \end{pmatrix}$	$\begin{pmatrix} 0 \\ 1 \end{pmatrix}$	$\begin{pmatrix} 2 \\ 1 \end{pmatrix}$	$\begin{pmatrix} 1 \\ 2 \end{pmatrix}$	$\begin{pmatrix} 2 \\ 2 \end{pmatrix}$	$\begin{pmatrix} 2 \\ 2 \end{pmatrix}$	$\begin{pmatrix} 2 \\ 2 \end{pmatrix}$	$\begin{pmatrix} 2 \\ 2 \end{pmatrix}$	2	2

^a σ and σ^* are the natural orbitals of the sigma bond pair.

^b The parentheses indicate that we take products of the configurations in the left parentheses with those in the right parentheses (e.g., for the A1 case there are $2 \times 6 = 12$ configurations.)

the molecular plane) which led to localized bond pairs as in (8). However, in the CI we did not use these orbitals but rather used orbitals corresponding to (9) which have the full C_{2v} symmetry of the molecule and are generated by projecting the localized orbitals of (8) onto the wavefunction (9). In addition, the remaining occupied orbitals (which were essentially of C_{2v} symmetry) were projected, leading to a total of 16 basis functions.

The configurations were generated in a manner analogous to the NiS CI using the generating configuration shown in Table 10.

The CI calculations were carried out only at the optimum geometry found from the GVB calculations. Since we found the CI energy to be only ~ 0.1 eV below the GVB energy (at this R), we concluded that CI effects would have only negligible effects on the geometry.

5.3 Ni_3 and Ni_3S

For Ni_3 the CI basis consisted of the orbitals of (12) plus all the occupied a_2 and b_1 orbitals (which were included to allow readjustment effects involving reorientation of the 3d holes of the Ni atoms). The generating configurations used are given in Table 11.

For Ni_3S the CI basis consisted of the orbitals of (16) plus the $S(3s)$ -like orbital, additional virtuals having the character of the more diffuse components of the $S(3p_x)$ and $S(3p_y)$ -like functions, and all the occupied a_2 and b_1 orbitals (which were included to allow readjustment of the 3d holes for the Ni atoms, as for the Ni_3 calculation). The

Table 10 Generating Configurations for the Ni₂S CI Calculation

1a ₁	2a ₁	1b ₂	2b ₂ ^a
$\begin{pmatrix} 2 \\ 1 \end{pmatrix}$	$\begin{pmatrix} 0 \\ 1 \end{pmatrix}^b$	$\begin{pmatrix} 2 \\ 1 \end{pmatrix}$	$\begin{pmatrix} 0 \\ 1 \end{pmatrix}$

^aThese orbitals correspond to the bond orbitals of Ni₂S projected on C_{2v} symmetry.

^bSee footnote b of Table 9.

generating configurations are given in Table 11. As can be seen from the energies in Table 5, the CI led to only small energy lowerings as compared to the GVB wavefunction.

Table 11 Generating Configurations for the Ni_3 and Ni_3S CI Calculations

Ni_3^a

$$\begin{array}{ccc} 1a_1 & 2a_1 & 1b_2 \\ \left(\begin{array}{c} 2 \\ 1 \end{array} \right) & \left(\begin{array}{c} 0 \\ 1 \end{array} \right) & 1 \end{array}$$

Ni_3S^b

$$\begin{array}{cccc} 1a_1 & 2a_1 & 1b_2 & 2b_2 \\ \left(\begin{array}{c} 2 \\ 1 \end{array} \right) & \left(\begin{array}{c} 1 \\ 2 \end{array} \right)^c & \left(\begin{array}{c} 2 \\ 1 \end{array} \right) & \left(\begin{array}{c} 0 \\ 1 \end{array} \right) \end{array}$$

^aThese configurations correspond to wavefunction (12).

^bThese configurations correspond to wavefunction (16).

^cSee footnote b of Table 9.

References

- [1] Partially supported by a grant (DMR74-04965) from the National Science Foundation.
- [2] Partially supported by a grant (EX-76-G-03-1305) from the Energy Research and Development Administration.
- [3] (a) J. E. Demuth, D. W. Jepsen and P. M. Marcus, Phys. Rev. Lett. 32(21) (1974) 1182; (b) J. E. Demuth, D. W. Jepsen and P. M. Marcus, Phys. Rev. Lett. 31(8) (1973) 540.
- [4] W. A. Goddard III, T. H. Dunning, Jr., W. J. Hunt and P. J. Hay, Accts. Chem. Res. 6 (1973) 368.
- [5] (a) L. Pauling, The Nature of the Chemical Bond (Cornell University Press, New York, 1972), 3rd ed., p. 93; (b) *ibid*, p. 260.
- [6] This is from Mulliken populations. Generally, these populations indicate a greater charge transfer than would be indicated, for example, by the dipole moment. Thus, the populations although indicative of charge transfer should not be taken too literally.
- [7] (a) B. J. Moss and W. A. Goddard III, J. Chem. Phys. 63 (1975) 3523; (b) B. J. Moss, F. W. Bobrowicz and W. A. Goddard III, *ibid* 63 (1975) 4632.
- [8] S. P. Walch and W. A. Goddard, III, J. Amer. Chem. Soc., to be published.
- [9] Spectroscopic Constants for Selected Heteronuclear Diatomic Molecules (Air Force Report No. SAMSO-TR-74-82), Vol. II, p. N102.
- [10] For example, for S on Ni(111) there are two possible three-fold sites. The LEED intensities are quite similar for these two sites but change significantly if the distance to the surface is changed [3a].

- [11] The quoted atomic separations are obtained by taking a weighted average over the spectral levels corresponding to a given L and S (spin-orbit interactions are not included in our calculations). The values are from Ref. 12.
- [12] C. E. Moore, "Atomic Energy Levels", Vol. II, National Bureau of Standards (1952).
- [13] S. P. Walch and W. A. Goddard III, J. Amer. Chem. Soc. 98 (1976) 7908.
- [14] M. J. Sollenberger, M. S. Thesis, California Institute of Technology, 1975.
- [15] T. H. Upton, W. A. Goddard III and C. F. Melius, J. Amer. Chem. Soc., to be submitted.
- [16] In these calculations we have used the [3s,1p,2d] contraction of the Ni basis (see Section 4) for the central Ni atom in conjunction with the MEP. For the other two Ni atoms, we have used an effective potential which replaces the 18 electron Ar core and a weighted average over the various $3d^9$ configurations (referred to as the d-averaged potential [17]). The remaining 4s orbital is then expanded in an sp basis identical to that used on the central Ni atom.
- [17] T. H. Upton and W. A. Goddard III, unpublished results.
- [18] Here we are referring to a linear geometry with equal bond lengths.
- [19] For (5) the GVB (2/PP) wavefunction was used. However, for (4) the perfect pairing approximation (see Ref. 4) is not applicable and we used the SOGVB method (F. W. Bobrowicz, Ph.D Thesis, California Institute of Technology, 1974) which retains strong orthogonality but relaxes the perfect pairing restriction.

- [20] Configurations 1a to 5b are analogous to the group I configurations of NiO [8].
- [21] There are two possible choices for the delta-like orbitals on each Ni. Their energies are within ~ 0.04 eV and we chose to solve self-consistently for the case where each Ni 3d hole is asymmetric with respect to the molecular plane, since this choice simplifies the SCF calculations.
- [22] G. Herzberg, *Electronic Spectra and Electronic Structure of Polyatomic Molecules* (Van Nostrand Reinhold, N.Y., 1966), p. 585.
- [23] The Ni and Ni₂ clusters [which correspond to the NiS and Ni₂S clusters] have zero bond energy. Thus, effects arising from disruption of metal-metal bonds are not included. These effects should be more important for the bridged case and comparisons of the NiS and Ni₂S bond energies is expected to overestimate the favorability of bridged sites over linear sites.
- [24] For Ni₂S we find that (8) is 0.083 eV below (9). For (9) the correlation energies due to the a₁ and b₂ pairs are 0.26 eV and 0.19 eV, respectively. For Ni₃S and Ni₄S the b₂ pairs have comparable correlation energies but the a₁ pairs contribute only 0.12 eV and 0.12 eV for Ni₃S and Ni₄S, respectively.
- [25] The 3d holes for Ni2 and Ni4 were taken in orbitals of the form xz+yz and xz-yz which are thus delta-like with respect to the bond axes while the 3d hole for Ni5 was taken in a 3d_{xy} orbital (which represents a compromise between delta character with respect to the two bond axes.)

- [26] We show here the orbitals which involve the Ni(4s) orbitals and the orbitals of the S(3p⁴) configuration. The remaining 3d occupation is the same as for the Ni₃ cluster [25].
- [27] The Ni(3d) holes for Ni atoms 2 and 4 (involved in Ni-S bonds) were taken to be delta-like with respect to the NiS bond axis and asymmetric with respect to the yz plane (containing Ni₂, Ni₄, and the S) which is the same orientation as for the Ni₂S calculation. The Ni(3d) holes for Ni₁ and Ni₃ were taken in 3d_{yz} orbitals which are delta-like with respect to the x axis, which passes through Ni₁ and Ni₃.
- [28] The numerical potential is reported in Ref. 14. See also the discussion in Ref. 13.
- [29] A.J.H. Wachters, J. Chem. Phys. 52 (1970) 1033.
- [30] C. F. Melius, B. O. Olafson and W. A. Goddard III, Chem. Phys. Lett. 28 (1974) 457; C. F. Melius and W. A. Goddard III, Phys. Rev. A 10 (1974) 1528.
- [31] R. A. Bair and W. A. Goddard III, unpublished results.
- [32] S. Huzinaga, unpublished.

PART E: THEORETICAL STUDIES OF THE BONDING OF OXYGEN TO MODELS
OF THE (100) AND (110) SURFACES OF NICKEL [1],[2]

1. Introduction

Previously, we reported calculations for the bonding of S to Ni clusters designed to model the (100) and (110) surfaces of Ni [3]. Here, we report similar cluster calculations for O on Ni. We find that the main differences between the O and S calculations have to do with (i) the smaller size of the oxygen atom, and (ii) the higher electronegativity of O (3.5 for O as compared with 2.5 for S [4a]). The larger amount of ionic character in the O clusters requires that the atom beneath the surface be included in the cluster for the O case, whereas only the surface Ni atoms were important in the S case.

In section 2, we describe the basis set and other calculational details. Section 3 describes the qualitative nature of the wavefunctions for the various Ni clusters and (i) compares the calculated geometry for the (100) surface with results of dynamic LEED intensity calculations [5] and (ii) predicts the geometry for the (110) surface for which no LEED intensity analysis has been carried out. Section 4 discusses the wavefunctions for the clusters in somewhat more detail.

2. Computational Details

The basis set and effective potential used for Ni have been reported previously [3]. (The Ni basis is based on the set optimized for the third row atoms by Wachters [6].) The [3s,1p,2d] contraction of the Ni basis was used for the NiO and Ni₂O calculations, while for the larger Ni₃O, Ni₄O, and Ni₅O calculations the [2s,1p,1d] contraction was used [3]. The basis for oxygen is the Dunning [3s,2p]

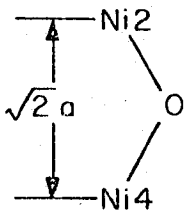
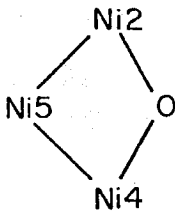
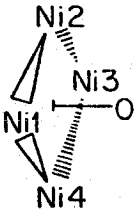
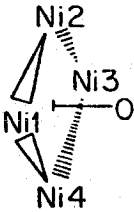
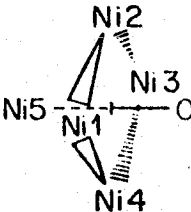
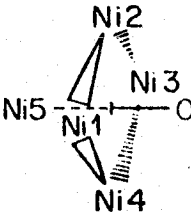
contraction [7] of the Huzinaga (9s,5p) set [8]. This contraction is double zeta valence but uses a single 1s-like contracted function and leads to energies within 0.0001h of those obtained with the double zeta contraction [9]. For the NiO cluster a single set of d-functions ($\alpha = 1.04$) was used on the O, while for the Ni₂O cluster the geometry was optimized without d-functions but d-functions were added at the optimum geometry. d-functions were omitted for the larger clusters.

We solved for the states of the finite clusters using the ab initio generalized valence bond (GVB) method [10] which differs from the usual Hartree-Fock (HF) method in that it includes the dominant electron correlation effects necessary to describe bond formation.

3. Qualitative Discussion

Table 1 summarizes the results for bonding an O atom to the various Ni clusters. For the (100) surface, the surface unit cell contains four surface Ni atoms at the corners of a square (which we refer to as Ni1, Ni2, Ni3, and Ni4) and one atom below the center of the square in the next layer down (which we refer to as Ni5). For S on the Ni (100) surface, we found that only the four surface Ni atoms (1-4) had to be included to describe the geometry. However, for the O case the higher electronegativity of O leads to a positive ion state of the cluster being consistent with the charge distribution for the full O overlayer and we find that Ni5 must be included to describe polarization effects in the direction perpendicular to the surface. Thus, we used a Ni₅⁺O model for O on Ni (100). This model

Table 1 Summary of Results for Bonding of Oxygen to the Ni Clusters

Cluster	Geometry	Model for	Distance above Plane(Å)	R_{NiO} (Å)	D (eV)
NiO	Ni—O	-	1.60	1.60	3.95
Ni ₂ O		(110)	0.31	1.79	4.37
Ni ₃ O		(110)	0.08	1.76	3.32 ^a
Ni ₄ O		-	0.56	1.85	3.22
Ni ₄ ⁺ O		(100)	(0.75) ^b	-	-
Ni ₅ O		-	0.65	1.88	1.93
Ni ₅ ⁺ O		(100)	0.96	2.01	3.09

^aThe NiO and Ni₂O calculations used a [3s,1p,2d/3s,2p,1d] basis, while a [2s,1p,1d/3s,2p] basis was used for the larger clusters. From comparisons of both types of calculations for Ni₂O we estimate that this basis leads to an error in D_e of 0.24 eV, but does not have a significant ef-

Footnotes for Table 1 (continued)

fect on the geometry. Thus, we have added 0.24 eV to the D_e values for the Ni_3O , Ni_4O , and Ni_5O clusters in order to compare with the NiO and Ni_2O calculations.

^bThis value is estimated from Koopmans' theorem by assuming that the error in the geometry from Koopmans' theorem for Ni_5^+O (0.25Å) will also be the same in Ni_4^+O .

leads to a distance above the surface of 0.96\AA in excellent agreement with the value from dynamic LEED intensity analysis, $0.90 \pm 0.10\text{\AA}$ [5].

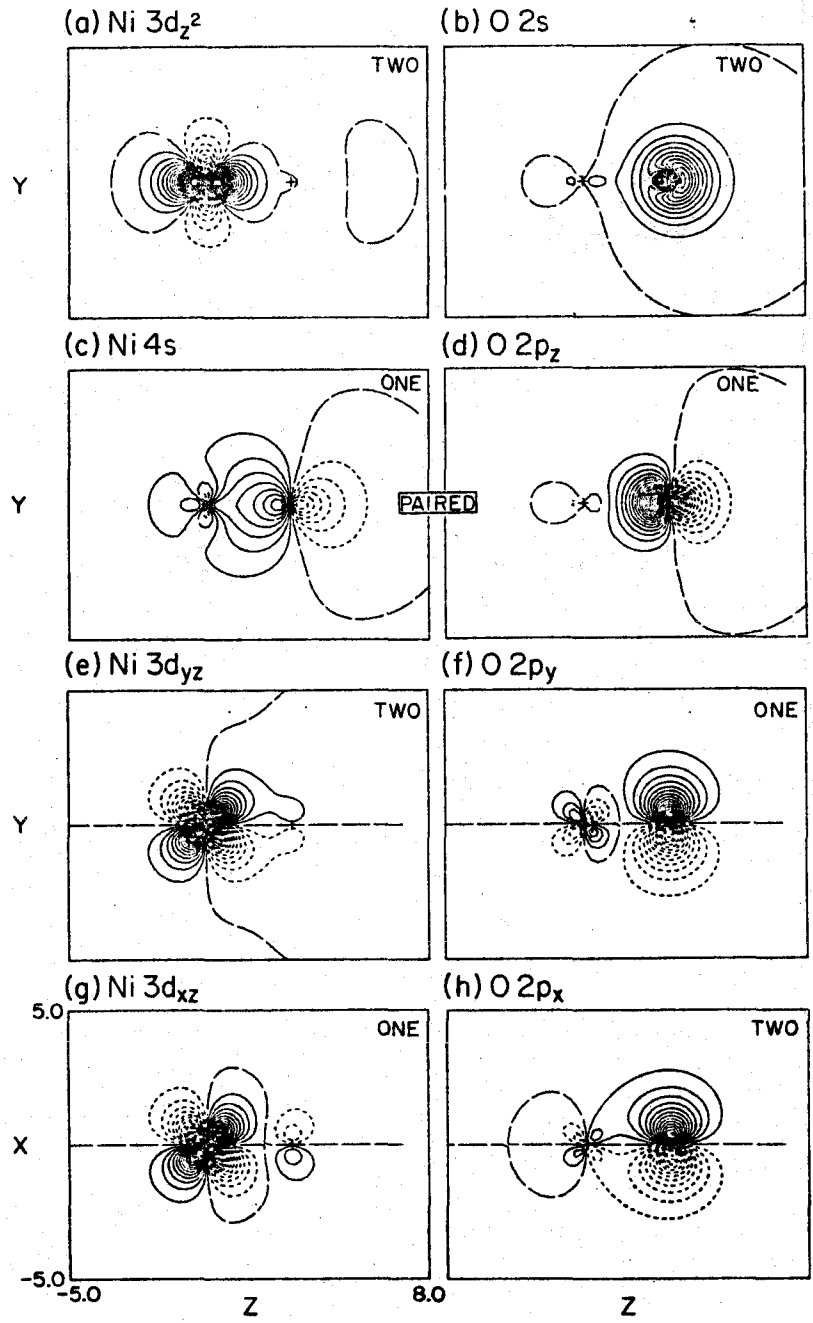
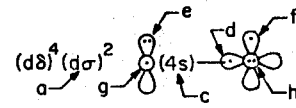
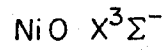
In the following, we discuss qualitatively the essential features of the wavefunctions for the various clusters shown in Table 1. For all the clusters considered here, we find that the Ni atom has the character of the $4s^1 3d^9$ configuration and the bonding is dominated by the 4s orbital, while the orientation of the hole in the 3d shell leads to small energy effects.

The simplest model which contains the qualitative features of the bonding to the (100) surface is the Ni_2O cluster, which corresponds to bridging across a pair of surface Ni atoms (say Ni2 and Ni4) along the diagonal of the square.

3.1 NiO and Ni_2O

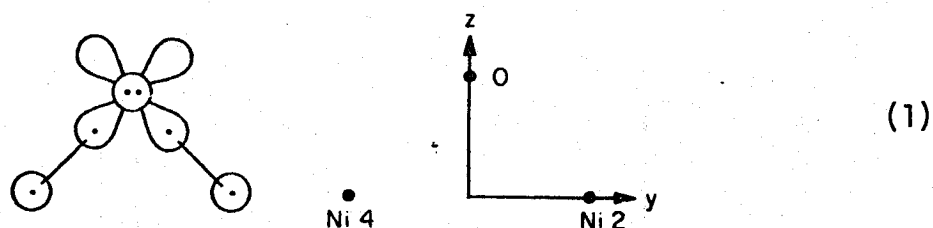
Wavefunctions for numerous electronic states of NiO have been discussed in detail elsewhere [11]. The bonding in NiO is dominated by the sigma bond which may be described qualitatively as a Ni(4s) orbital singlet paired with an O ($2p\sigma$) orbital. The orbitals of the bond pair are shown in Fig. 1cd; as expected from the relative electronegativities (1.8 for Ni, 3.5 for O [4a]) there is a substantial amount of charge transfer [12] to the O atom (0.55 electrons). For the ground state of NiO, the 3d hole of the Ni $3d^9$ configuration is $3d\pi$, leading to a $^3\Sigma^-$ ground state which is quite analogous to the ground states of NiS [3] and of O_2 [13]. As indicated in Fig. 1aeg, the Ni(3d) orbitals are only slightly affected by the bond. The major difference between

Fig. 1 The GVB orbitals of $X^3\Sigma^-$ ground state of NiO. Unless otherwise noted, all plots have uniformly spaced contours of 0.05 a.u. Solid lines indicate positive contours, short dashes indicate negative contours, and long dashes indicate nodal lines. The same conventions are used for other figures.

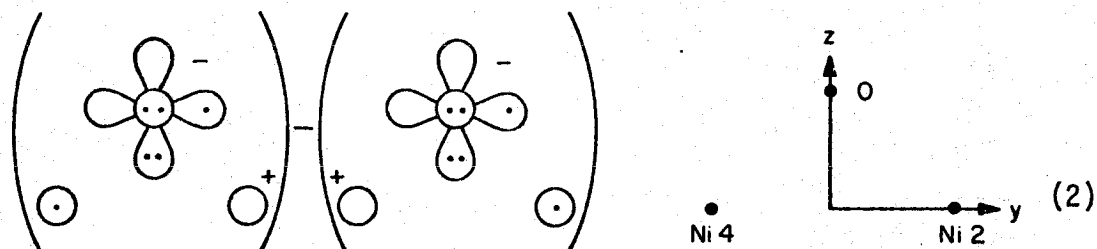


NiO and NiS is the greater charge transfer (0.55 electrons for NiO as compared with 0.38 electrons for NiS [12]).

Bonding a second Ni atom to the singly occupied $0(2p_y)$ orbital (Fig. 1f) leads (after readjustment effects) to a structure with two equivalent sigma bonds (i.e., the Ni_2O cluster).



Solving for a wavefunction of the form (1) leads to a total charge transfer to the oxygen of 0.91 electrons, which is consistent with incorporating a substantial component of the ionic configuration (2) [14].



Covalent bonding as in (1) favors 90° bond angles, whereas bonding to 0^- as in (2) favors 180° bond angles. Thus, incorporation of ionic character leads to large bond angles and small vertical displacements of the O atom (relative to the surface). For the Ni_2O cluster,

the optimum geometry is with the O atom 0.31\AA above the surface, which is consistent with the overall charge transfer (0.91 electrons).

The orbitals corresponding to (1) are shown in Fig. 2. The bond pairs (Fig. 2abcd) show a substantial amount of charge transfer to the oxygen. For one bond pair (Fig. 2ab), one component (Fig. 2b) is essentially $O(2p)$ -like, while the other component (Fig. 2a) corresponds approximately to a $Ni(4s)$ orbital which contains a large amount of $O(2p)$ character. (Thus, the covalent bond has an appropriate amount of ionic character.) The $O(2s)$ -like orbital (Fig. 2e) has hybridized away from the bond pairs.

We find that bridged bonding as in the Ni_2O cluster is more favorable ($D_e = 4.37\text{ eV}$) than bonding directly above a surface Ni atom as in NiO ($D_e = 3.95\text{ eV}$). The small difference in bond energies here reflects the fact that the Ni_2O cluster contains a large component of (2) which involves only a single sigma bond.

3.2 Ni_4O , Ni_4^+O

Including the nonbonded surface Ni atoms (Ni1 and Ni3) leads to the Ni_4O cluster. Qualitatively the electronic configuration of the Ni_4O cluster is

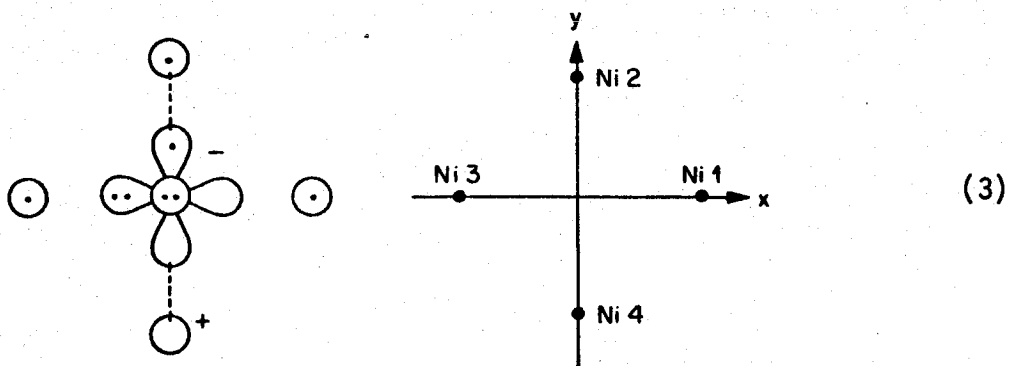
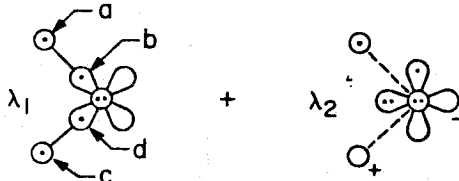
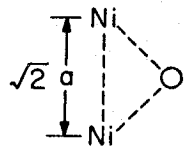
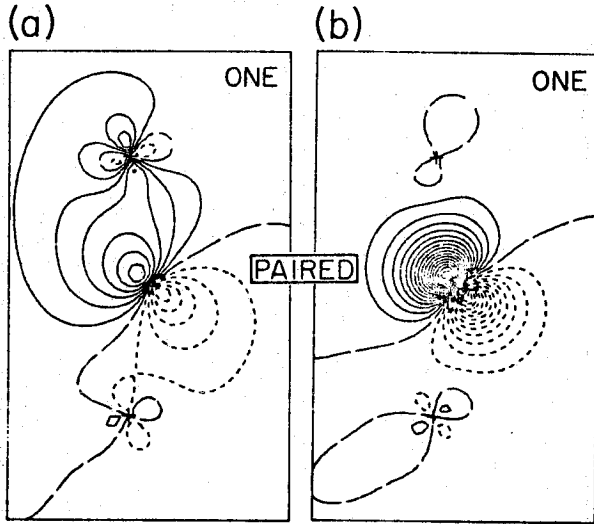


Fig. 2 Selected orbitals of the Ni₂O cluster.

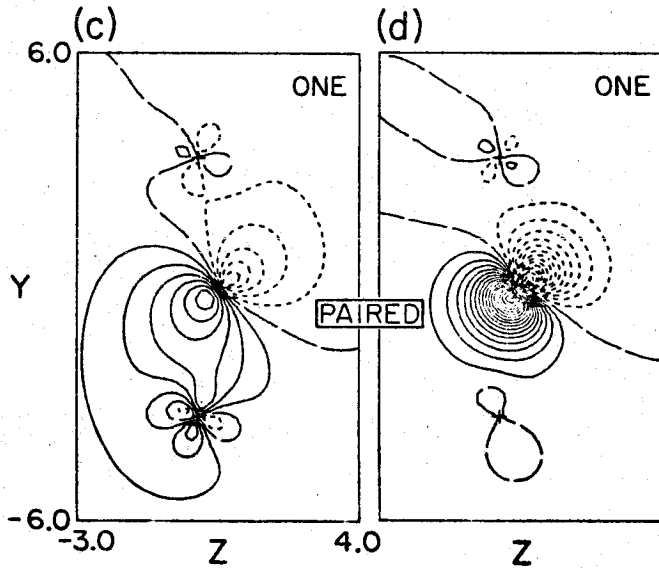
Ni₂O GVB (2/PP)



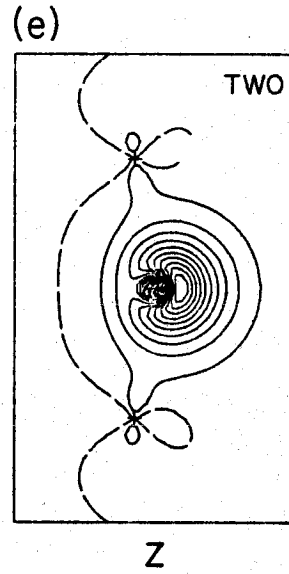
UPPER NiO BOND



LOWER NiO BOND



O 2s PAIR



The bonding orbitals (shown in the yz plane) are analogous to the orbitals of (2). We find (as for Ni_4S) that there are repulsive interactions between the doubly occupied $O(2p_x)$ orbital and the other two surface Ni atoms ($Ni1$ and $Ni3$) which lead to an optimum geometry with the O atom 0.56\AA above the surface, 0.25\AA higher than for the Ni_2O calculation.

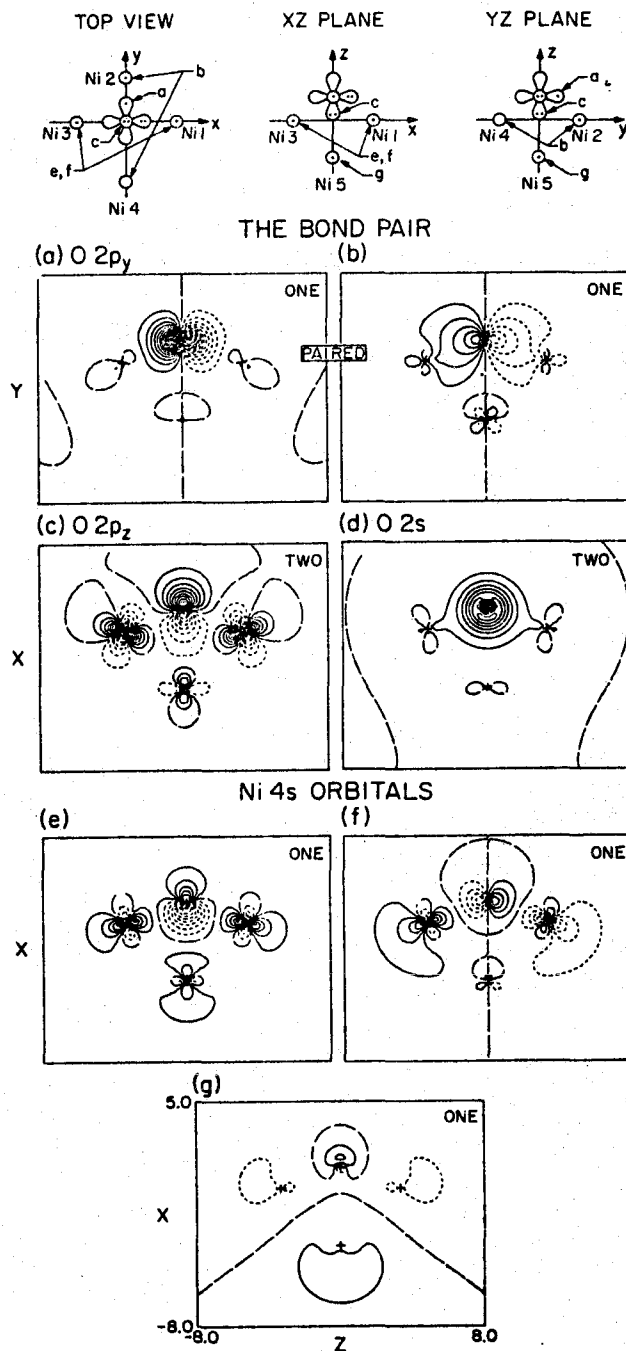
For the full oxygen overlayer, $Ni1$ and $Ni3$ are involved in bonds to other O atoms. Considering the charge transfer involved in the bonds leads to a charge of ~ 0.9 distributed between $Ni1$ and $Ni3$ (based on Ni_2O). Thus, the overall charge is more accurately represented by an ion state of the Ni_4 cluster involving removal of one electron from among the orbitals corresponding to $Ni1$ and $Ni3$. It was anticipated that for the positively charged cluster polarization effects involving $Ni5$ would be important, thus we used a Ni_5^+O cluster as the model for O on $Ni(100)$.

3.3 Ni_5O , Ni_5^+O

Here we consider first the neutral Ni_5O cluster. For Ni_5O we find that $Ni5$ is nonbonding and the remaining electronic configuration is similar to (3) for Ni_4O . The orbitals of the neutral Ni_5O cluster are shown in Fig. 3. Looking first at the bond pair (Fig. 3ab), one sees that one component (Fig. 3a) is essentially an $O(2p_y)$ orbital, while the other component (Fig. 3b) corresponds approximately to $Ni2(4s)$ - $Ni4(4s)$ but contains a substantial amount of $O(2p_y)$ character (indicating an ionic bond). The $O(2p_z)$ pair (Fig. 3c) has delocalized somewhat onto the Ni, but the overall populations correspond most

Fig. 3 Selected orbitals of the Ni₅O cluster.

Ni_5O GVB (I/PP)

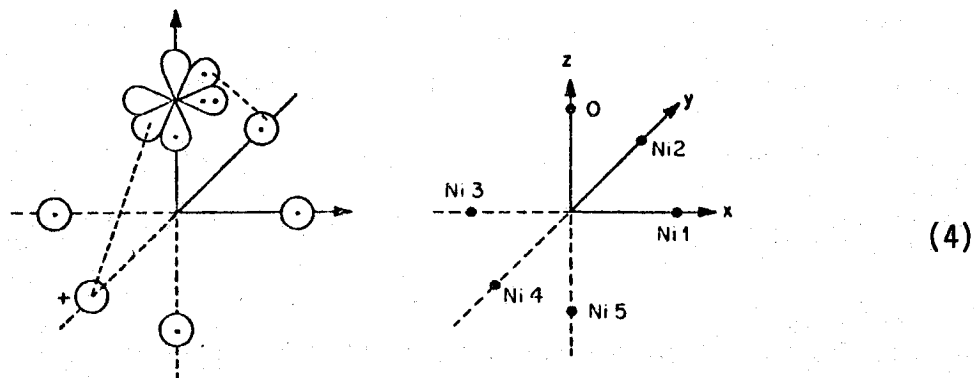


closely to an O^- configuration for the O atom as in (3). The $O(2s)$ pair (Fig. 3d) is essentially atomic-like, but has built in a small amount of 3d character on the surface Ni atoms. The singly occupied orbitals (Fig. 3efg) are all derived from Ni(4s) orbitals (mainly on Ni1, Ni3, and Ni5). The orbitals in Fig. 3ef correspond approximately to $Ni1(4s) + Ni3(4s)$ and $Ni1(4s) - Ni3(4s)$, respectively; note however, that the symmetric combination (Fig. 3e) has delocalized onto Ni5, leading to bonding character on all three centers. The other singly occupied orbital (Fig. 3g) corresponds to a 4s orbital on Ni5 and is antibonding in character. The optimum geometry for this cluster is with the O 0.65\AA above the surface, only 0.09\AA higher than for the Ni_4O cluster. Thus Ni5 has only a small effect on the geometry of the neutral cluster (as was predicted for bonding S to this cluster [3]).

Now we consider the Ni_5^+O cluster. The lowest ion state of the Ni_5O cluster involves ionizing the singly occupied orbital in Fig. 3g. At the equilibrium geometry for Ni_5O neutral, the orbitals of Ni_5^+O are very similar to the corresponding Ni_5O orbitals shown in Fig. 3. However, the Ni_5^+ cluster has a higher effective electronegativity than the Ni_5 cluster which leads to more covalent bonding in Ni_5^+O and an equilibrium geometry with the O atom further from the surface. Moving the O atom away from the surface, the doubly occupied $O(2p_z)$ orbital delocalizes more onto the Ni while the singly occupied Ni-Ni bonding orbital (Fig. 3e) localizes on the O atom; leading (at the equilibrium geometry for Ni_5^+O) to a singly occupied $O(2p_z)$ orbital

and a doubly occupied Ni-Ni bonding orbital (i.e., an electron has been transferred from O back to the metal).

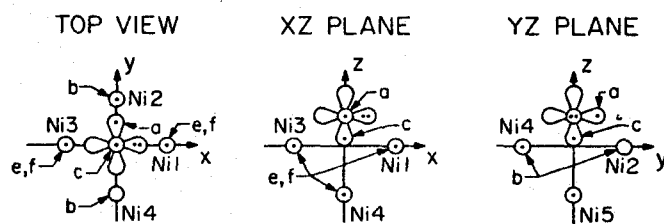
The overall electronic configuration is



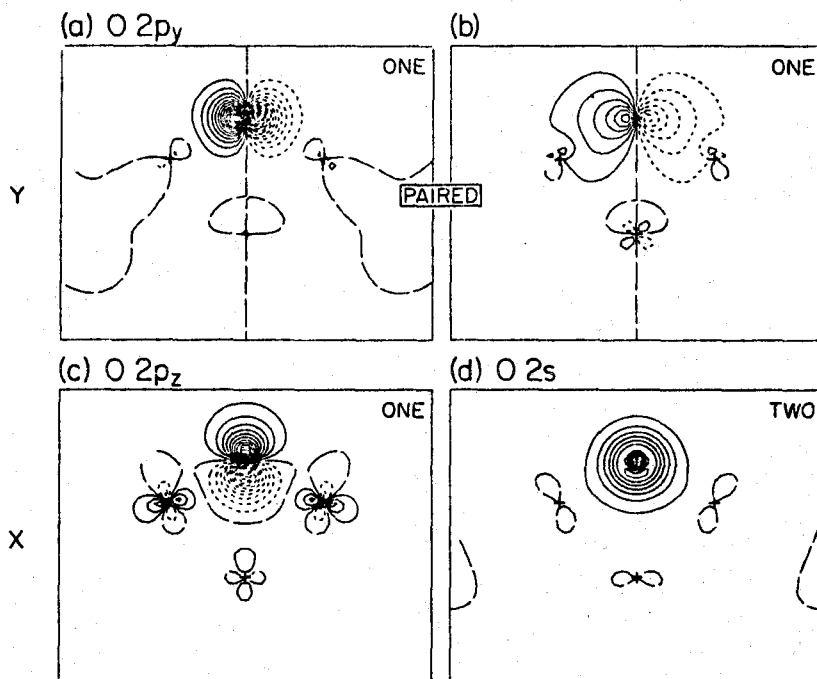
We show the orbitals corresponding to (4) in Fig. 4. The bond pair (Fig. 4ab) is very similar to the bond pair for Ni_5O neutral (Fig. 3ab). The $\text{O}(2p_z)$ orbital (Fig. 4c) is now singly occupied and localized, while the orbital corresponding to the bonding combination of the $\text{Ni}(4s)$ orbitals (Fig. 4e) is doubly occupied. The remaining singly occupied orbital (Fig. 4f) corresponds to $\text{Ni}1(4s)\text{-Ni}3(4s)$ and has not changed significantly from the corresponding orbital for Ni_5O neutral (Fig. 3f).

Thus, the overall configuration for the Ni_5^+O cluster corresponds to a neutral oxygen atom configuration [but with about 0.5 electrons transferred in the bond pair (Fig. 4ab) leading to a total charge on the oxygen of 0.61 electrons as compared to 0.82 electrons for Ni_5O neutral]. The net effect of the more covalent bonding is an equilibrium geometry with the O atom 0.96\AA above the surface, 0.31\AA higher than for Ni_5O neutral. This value is in good agreement with the results of dynamic LEED intensity analysis, $0.90 \pm 0.10\text{\AA}$ [5].

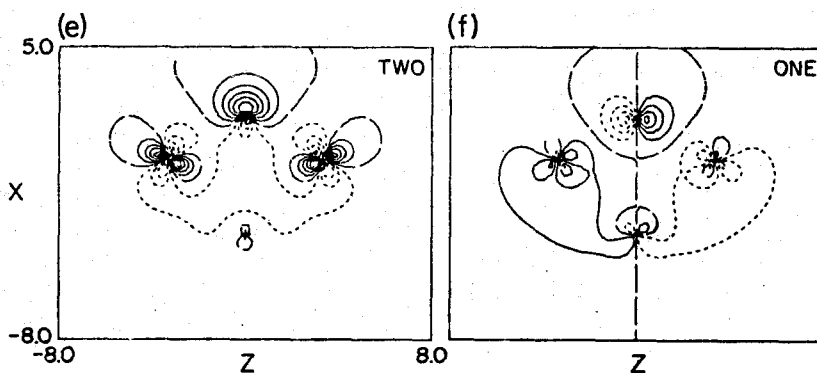
Fig. 4 Selected orbitals of the Ni_5^+O cluster.

Ni_5^+O GVB(I/PP)


THE BOND PAIR



Ni 4s ORBITALS



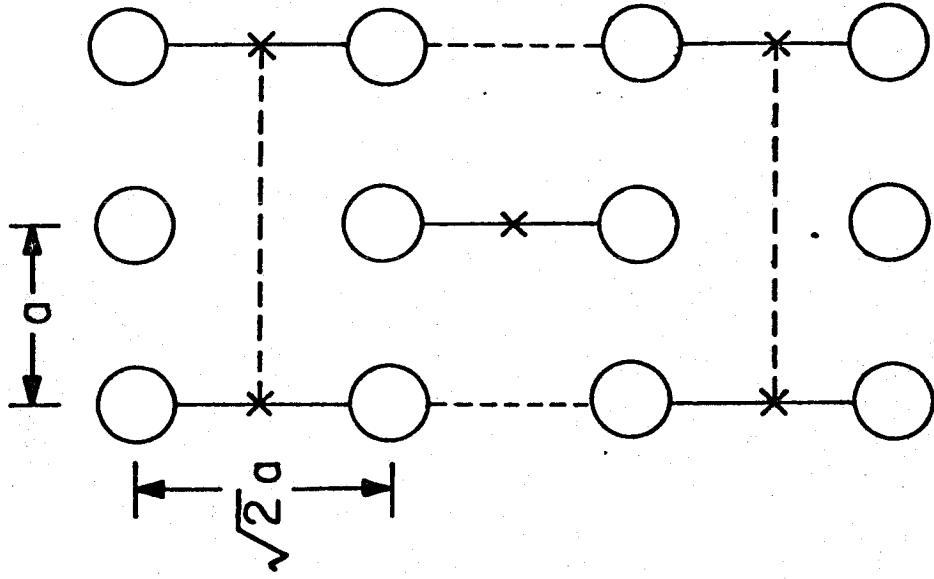
From Table 1 we see that the Ni_5^+O cluster leads to a substantially larger bond energy 3.09 eV than for Ni_5O neutral (1.93 eV). This effect derives largely from the antibonding character of the ionized orbital (Fig. 3g). Thus, withdrawal of charge by adjacent O atoms on the surface leads to stronger bonding of O to the surface. This effect should lead to island formation at low coverages and formation of ordered overlayers at higher coverages.

Figure 5a shows the bonding expected for $c(2 \times 2)$ overlayers on the Ni(100) surface. The localized bonds shown in Fig. 5a suggest a $p(2 \times 2)$ structure with the center and corner Ni atoms connected by a glide plane. However, there is a degenerate structure rotated by 90° and these two structures are expected to have a strong interaction (resonance) leading to all the O atoms being equivalent. This leads to $c(2 \times 2)$ as is observed [5].

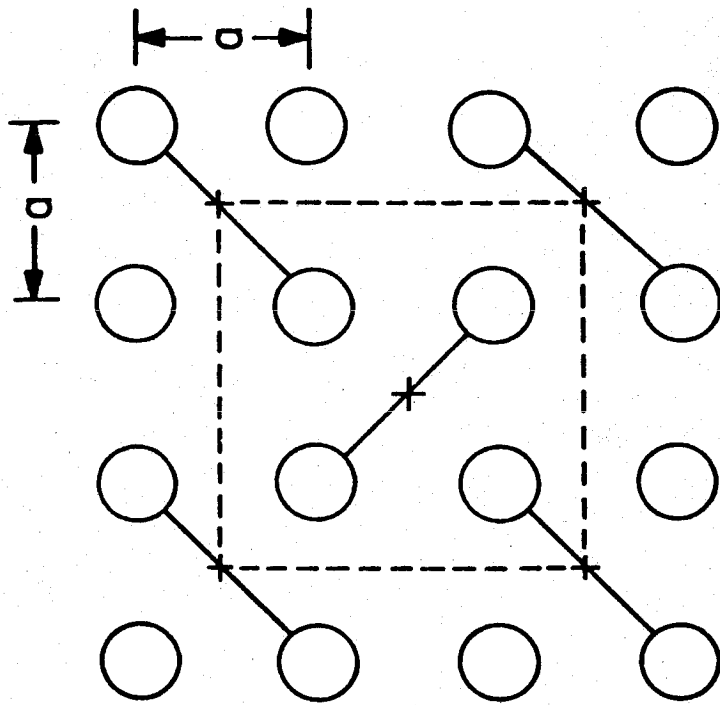
As shown in Fig. 5a, bonding the 4s orbital of each Ni to one O leads to an O atom in only half the four-fold sites. Thus, this bonding picture suggests that the $c(2 \times 2)$ overlayer is particularly stable. The van der Waals radius of the O atom is 1.40\AA [4b], considerably smaller than half the O-O distance for the $c(2 \times 2)$ structure (1.76\AA) but somewhat larger than half the O-O distance if an O atom were in each four-fold site (1.25\AA). Thus, it seems that nonbonded repulsions between the O atoms alone would not account for the $c(2 \times 2)$ structure, while the bonding picture in Fig. 5a does.

Fig. 5 The $c(2 \times 2)$ structure for O on (a) Ni(100) and (b) Ni(110), respectively. Circles represent surface Ni atoms, crosses represent O atoms, heavy lines represent Ni-O bonds, and dashed lines outline the unit cell.

(110) SURFACE



(100) SURFACE

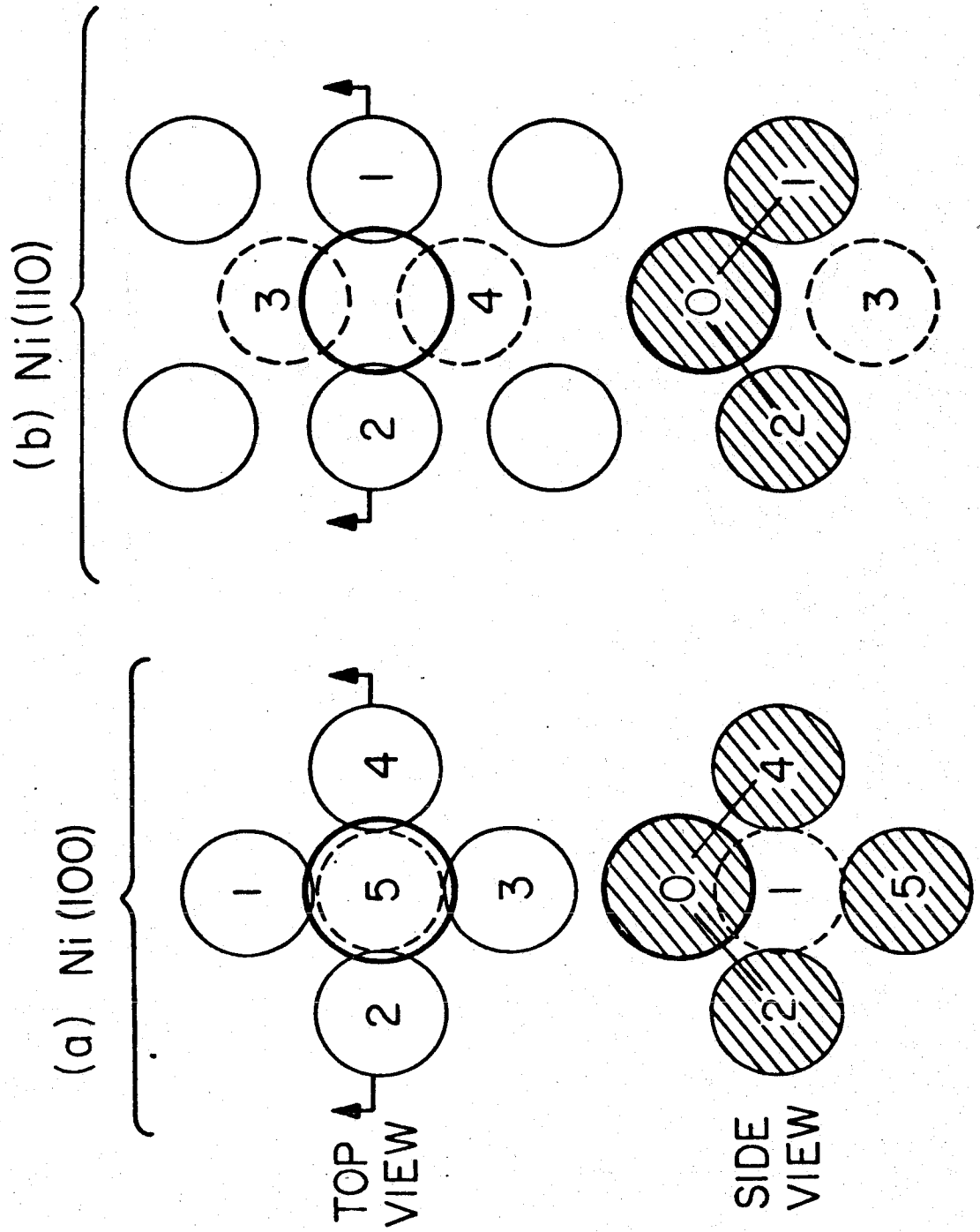


3.5 The (110) Surface

The simplest model for the (110) surface is the Ni_2O cluster. Figure 5b illustrates the bonding expected for a $c(2 \times 2)$ overlayer on the Ni(110) surface for bonding consistent with our Ni_2O model. As shown in table 1, this model leads to a distance above the surface of 0.31\AA . However, for the O this close to the surface, there should be interactions with the two Ni atoms in the next layer down. Figure 6b shows the locations of these atoms relative to the surface atoms and the O atom. While we have not solved for the Ni_4O cluster which includes the effects of these second layer atoms, we have solved for a Ni_3O cluster which includes the two surface Ni atoms and one of the atoms in the second layer. As indicated in table 1, the third Ni atom has an attractive interaction with the O atom leading to a decrease by 0.23\AA in the distance between the O and the third Ni atom (this distance is not normal to the (110) surface).

Putting these effects together, we would expect that the optimum geometry for the (110) surface is with the O bridged across next nearest neighbor surface Ni atoms and approximately in the plane of the surface. While there has been no dynamic LEED intensity analysis reported for O on Ni(110), for O on Fe(100) [which involves a more open structure (BCC lattice with $a = 2.87\text{\AA}$ as compared with FCC with $a = 2.49\text{\AA}$ for Ni), possibly intermediate between Ni(100) and Ni(110)] the O is found to be closer to the surface ($0.53 \pm 0.06\text{\AA}$) [15]. Thus, it is not surprising that for the (110) surface of Ni the O is predicted to be very close to the surface.

Fig. 6 The geometry of the O atom and nearest neighbor Ni atoms for the Ni(100) and Ni(110) surfaces. Ni atoms in the plane of the paper are illustrated by light circles, while those below the paper are illustrated by dashed circles and the O atom is illustrated by a somewhat larger heavy circle.



4. Further Discussion of the Wavefunctions

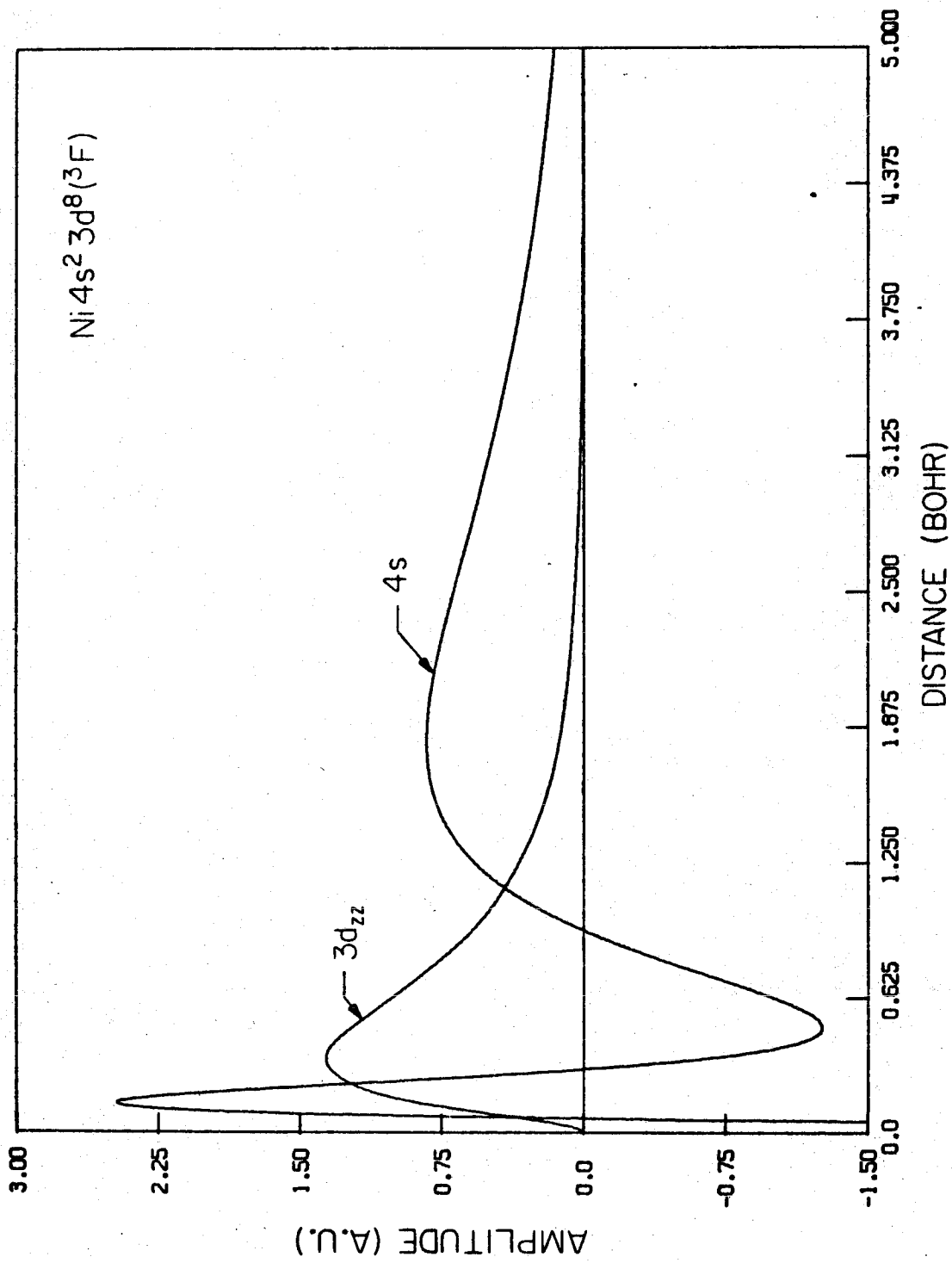
Before discussing the bonding of an O atom to the various Ni clusters, we first consider the bonding in NiH and Ni₂, since these simple cases illustrate the basic characteristics of the bonding between Ni atoms and the bonding to an O atom.

The Ni atom has two low-lying states $4s^1 3d^9 (^3D)$ and $4s^2 3d^8 (^3F)$. Ignoring spin-orbit coupling effects, the ground state is 3D with the 3F state only 0.03 eV higher [16]. Thus, both states could play a role in the bonding. However, the Ni(4s) orbital is $\sim 2-1/2$ times as large as the Ni(3d) orbitals (see Fig. 7); thus, the 4s orbital dominates the bonding. Bringing up an H atom to the $4s^2 3d^8$ state of Ni leads to repulsive interactions much as for the case of HeH. The $4s^1 3d^9$ state of Ni, on the other hand, leads to a sigma bond between the Ni(4s) and H(1s) orbitals and, hence, an attractive potential curve as for H₂.

The remaining $3d^9$ configuration on the Ni then leads to $^2\Sigma^+$, $^2\Pi$, and $^2\Delta$ states depending on whether the singly occupied 3d orbital is taken as a $3d\sigma$, $3d\pi$, or $3d\delta$ orbital respectively. As discussed elsewhere [18], while the Ni configuration is basically $4s^1 3d^9$ there is some mixing in of components of $4s^3 3d^8$ character, the energy of which varies over a range of several eV depending on whether the $4s^1 3d^9$ configuration has a singly occupied $3d\sigma$, $3d\pi$, or $3d\delta$ orbital. The net effect (referred to as the interatomic coupling effect) leads to the ordering $^2\Delta < ^2\Pi < ^2\Sigma^+$ with $^2\Delta$ 0.346 eV below $^2\Pi$ which in turn is 0.095 eV below $^2\Sigma^+$ (at R_e for the $X^2\Delta$ state) [19]. We find that these

Fig. 7 Comparison of the 4s and 3d orbital sizes of the Ni atom.

These orbitals are for the $s^2d^8(^3F)$ state, the orbitals for the $s^1d^9(^3D)$ state are quite similar. The 3d orbital shown is $3z^2-r^2$.



results are quite general for sigma bonds to the Ni(4s) orbital leading to an increased stability associated with having a 3d hole which is δ -like with respect to the bond axis.

From the discussion of NiH, it is not surprising that the bonding in Ni₂ [20] involves a 4s¹3d⁹ configuration on each Ni leading to a sigma bond between the 4s orbitals, and the lowest 3d occupation has both 3d holes taken in 3d δ orbitals (other 3d orbital occupancies lead to numerous low-lying excited states).

As a generalization of these cases, we find that the bonding in the various Ni clusters involves the 4s¹3d⁹ Ni configuration and is dominated by the Ni(4s) electrons, while the most favorable 3d⁹ configuration has the hole in the 3d shell taken to be delta-like with respect to the bond axis (axes). (See the discussion in reference [3].)

4.1 Ni₂O

From the above discussion, given (1) we expect the lowest 3d orbital occupancy to correspond to taking the 3d holes to be δ -like with respect to the NiO bond axes [21].

In these calculations we fixed the Ni-Ni distance at $\sqrt{2}a$ (where a is the nearest neighbor distance 2.49⁰Å in Ni metal), as appropriate for next nearest neighbors on the Ni(100) and Ni(110) surfaces. We then varied the NiO distance (retaining C_{2v} symmetry). The resulting potential curve is shown in Fig. 8, while the energies used to construct the curve are given in Table 2. The optimum geometry from the potential curve corresponds to a distance above the surface of 0.31⁸Å

Fig. 8 Ni₂O geometry optimization. The calculated points are indicated.

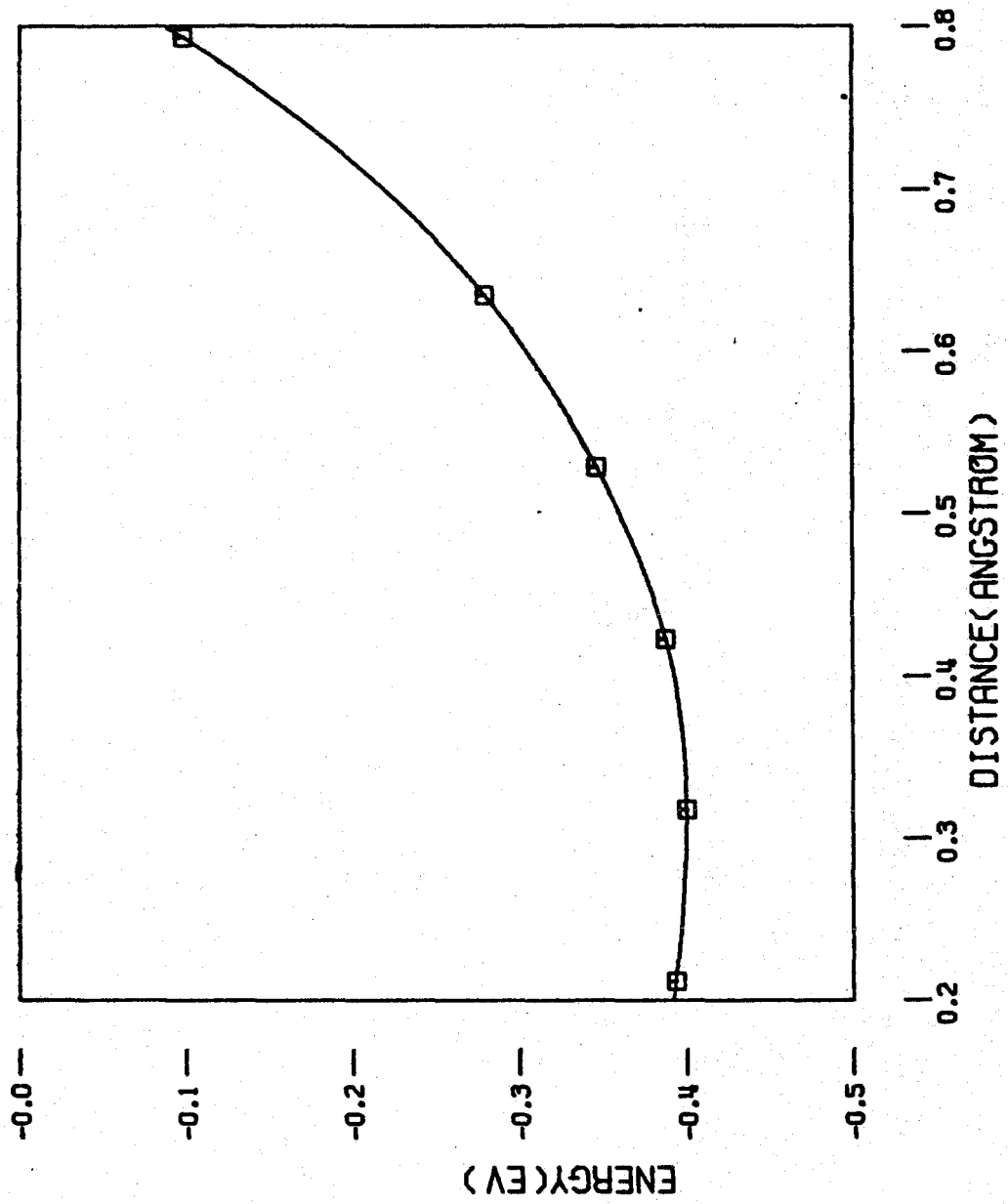
NI₂O GEOMETRY OPTIMIZATION

Table 2 Ni₂O Geometry Variation

d ^a	Energy	
	GVB(2/pp) ^b	GVB(1/pp) ^c
1.5	-155.91732	-
1.2	-155.92398	-
1.0	-155.92644	-
0.8	-155.92797	-155.90678
0.6	-155.92842	-155.90909
0.4	-155.92818	-155.91034

^a d is the perpendicular distance (in a.u.) from the O to a line between the two Ni atoms.

^b This corresponds to wavefunction (5). The optimum geometry corresponds to a d value of 0.31 Å which gives a NiO distance of 1.79 Å and a NiONi angle of 160.0°. The D_e values are 3.87 eV and 4.37 eV for GVB and CI wavefunctions respectively.

^c This corresponds to wavefunction (8).

which leads to a NiO bond length of 1.79\AA and a NiONi angle of 160.0° .

Including only the two bond pairs [in the following discussion we include only the 4s electrons of each Ni atom], the GVB wavefunction corresponding to (1) is written in terms of natural orbitals as

$$(\phi_\ell^2 - \lambda\phi_\ell^{*2})(\phi_r^2 - \lambda\phi_r^{*2}) \quad (5)$$

where the two GVB pairs correspond to the localized bond pairs shown in Fig. 2. An alternative way to correlate this wavefunction using symmetry orbitals is

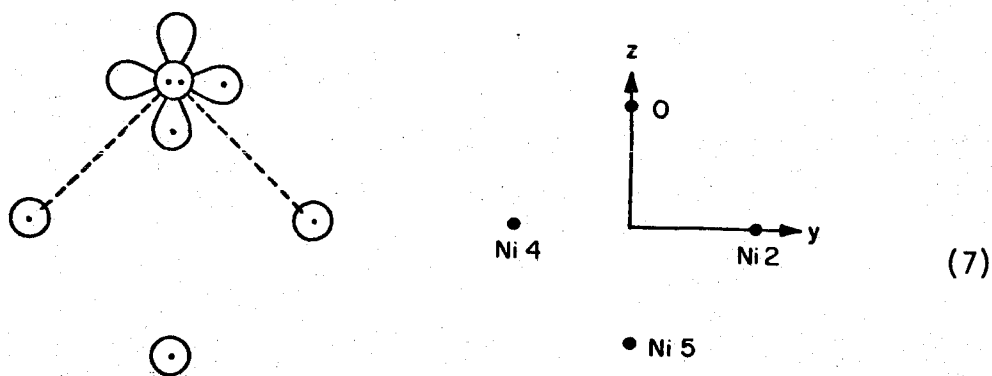
$$(1a_1^2 - \lambda 2a_1^2)(1b_2^2 - \lambda 2b_2^2) \quad (6)$$

where

$$1a_1 = \phi_\ell + \phi_r, \quad 1b_2 = \phi_\ell - \phi_r$$

$$2a_1 = \phi_\ell^* + \phi_r^*, \quad \text{and} \quad 2b_2 = \phi_\ell^* - \phi_r^*$$

One may imagine (6) to correspond to bonding the O atom in the following orientation



The bond pairs may then be qualitatively described as (1) an a_1 pair

with one component essentially $0(2p_z)$ -like and the other component corresponding to $Ni2(4s) + Ni4(4s)$; (2) a b_2 pair with one component essentially $0(2p_y)$ -like and the other component corresponding to $Ni2(4s)-Ni4(4s)$. However, because of the ionic character of Ni_2O , we find that the a_1 pair corresponds essentially to an $0(2p_z)$ doubly occupied orbital, leading to a wavefunction of the form

$$1a_1^2(1b_2^2 - \lambda 2b_2^2) \quad (8)$$

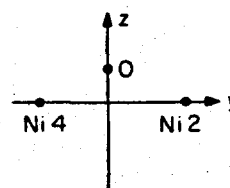
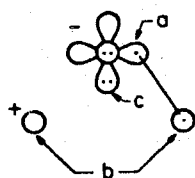
which corresponds to the ionic configuration (2).

For Ni_2O (5) is lower in energy than (8) (see table 2). Thus, we optimized the geometry based on (5). However, from the populations it is clear that there is a large ionic component corresponding to (8). For larger clusters, we find that the presence of nearby Ni atoms restricts the correlation effects leading to a wavefunction of the form (8) being lower.

We show the orbitals of (8) in Fig. 9. From Fig. 9 one sees that the $1a_1$ orbital (Fig. 9c) is essentially an $0(2p_z)$ orbital, while the b_2 pair has one component (Fig. 9a) which is essentially $0(2p_y)$ -like, while the other component (Fig. 9b) corresponds to $Ni2(4s)-Ni4(4s)$ but has built in a substantial amount of $0(2p_y)$ character (indicating an ionic bond).

To calculate the D_e for the Ni_2O cluster, we carried out a small configuration interaction (CI) calculation using the orbitals of (5). Here, we projected these orbitals onto (6), leading to basis functions which have the C_{2v} symmetry of the molecule. In addition to these four

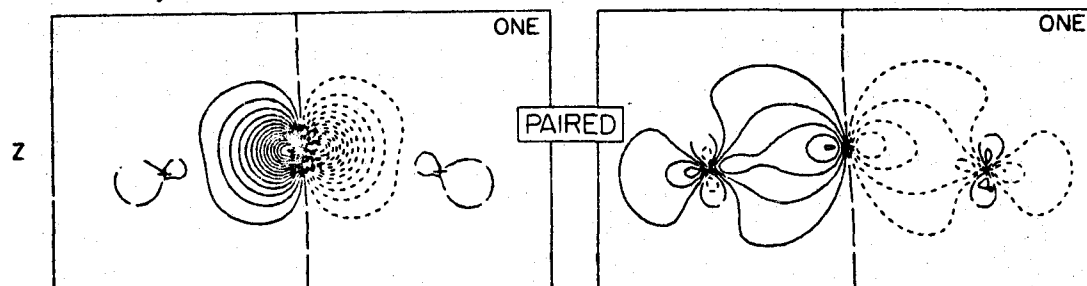
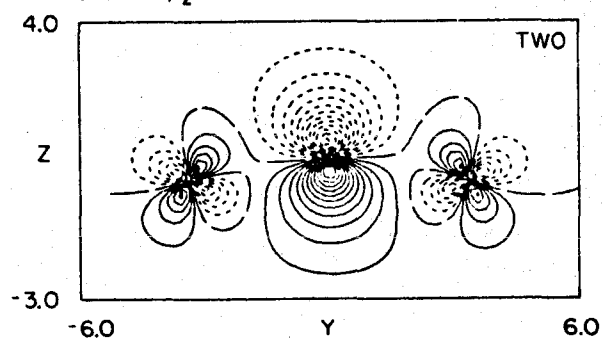
Fig. 9 The GVB orbitals for Ni_2O using the wavefunction (8).

Ni_2O GVB(1/pp), C_{2v} SYMMETRY


THE BOND PAIR

(a) $\text{O}2p_y$

(b)

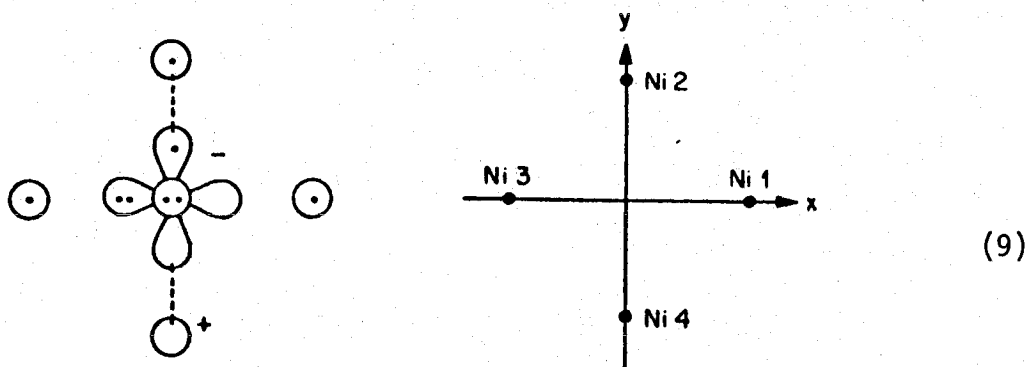
(c) $\text{O}2p_z$ 

orbitals, all the remaining occupied orbitals were included in the CI, leading to 17 basis functions (including the $O(1s)$ -like orbital which was kept doubly occupied in all configurations). The configurations were generated by allowing all single excitations from the set of generating configurations in table 3.

The resulting D_e value is 4.37 eV as compared with a D_e of 3.95 eV for a comparable CI treatment for NiO (see reference [11]) indicating that O prefers bridged sites on the Ni(100) surface as compared with bonding positions directly above a surface Ni atom.

4.2 Ni_4O

Adding Ni atoms 1 and 3 leads to the Ni_4O cluster. The electronic configuration is



where the bond orbitals (shown in the yz plane) correspond to the orbitals of (8). Adding to (8) the doubly-occupied O $2p_x$ orbital ($1b_1^2$) and the $4s$ orbitals of Ni1 and Ni3 which are triplet-coupled ($2a_1^1 2b_1^1$) leads to the overall configuration [22],

$$1a_1^2(1b_2^2 - \lambda 2b_2^2) 1b_1^2 2a_1^1 2b_1^1 \quad (10)$$

Table 3 Generating Configurations for the
 Ni_2O CI Calculation

$1a_1$	$2a_1$	$1b_2$	$2b_2^a$
$\begin{pmatrix} 2 \\ 1 \end{pmatrix}$	$\begin{pmatrix} 0 \\ 1 \end{pmatrix}^b$	$\begin{pmatrix} 2 \\ 1 \end{pmatrix}$	$\begin{pmatrix} 0 \\ 1 \end{pmatrix}$

^aThese orbitals correspond to the bond orbitals of Ni_2O projected on C_{2v} symmetry.

^bThe parentheses indicate that we take products of the configurations in the left parentheses with those in the right parentheses, resulting in four configurations.

Repulsive nonbonded interactions between the $O(2p_x)$ pair and Ni atoms 1 and 3 lead to an equilibrium geometry with the O 0.56\AA above the surface, 0.25\AA higher than for Ni_2O . The resulting potential curve is shown in Fig. 10, while the energies are given in Table 4.

In Table 5, we show Mulliken populations for the various clusters. Here we see that, for Ni_2O and Ni_4O Ni atoms 2 and 4 have populations corresponding to charges of $\sim +0.5$ electrons. From Fig. 5 we see that, considering the other oxygen atoms in the overlayer, the overall charge distribution is approximately described by an ion state where one 4s electron has been ionized from among the 4s orbitals of Ni1 and Ni3 [i.e., ionizing an electron from the $2a_1$ or $2b_1$ orbital of (10)]. For the positively charged clusters, we anticipated that polarization effects in a direction perpendicular to the surface would be important. Therefore, we added the Ni atom beneath the surface, leading to the Ni_5^+O cluster as the model for O on Ni(100).

4.3 Ni_5O, Ni_5^+O

We find for the neutral Ni_5O cluster that Ni5 is nonbonding, leading to a wavefunction [23]

$$1a_1^2(1b_2^2 - \lambda 2b_2^2) 1b_1^2 2a_1^1 3a_1^1 2b_1^1 \quad (11)$$

We show the orbitals corresponding to (11) in Fig. 3. The orbitals of the GVB pair $(1b_1^2 - \lambda 2b_2^2)$ are shown in Fig. 3ab, where one sees that they are similar to the corresponding orbitals of (8) (Fig. 9ab). The $1a_1^2$ pair (Fig. 3c) is essentially a doubly occupied $O(2p_z)$ orbital. The $2a_1$ orbital (Fig. 3e) has bonding character on all three Ni atoms,

Fig. 10 Ni_4O geometry variation. The calculated points are indicated.

NI₄O GEOMETRY OPTIMIZATION

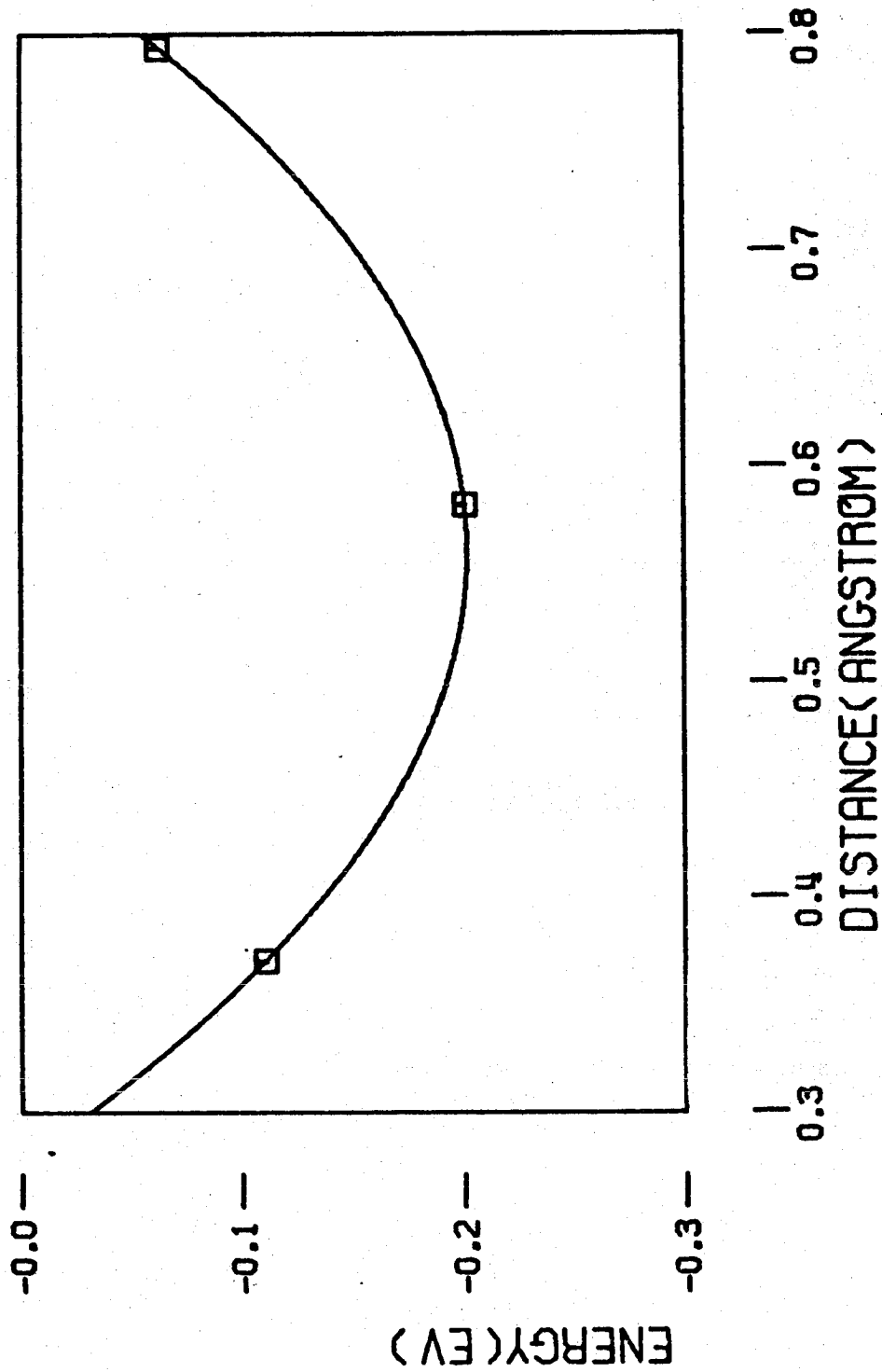


Table 4 Ni_4O Geometry Variation

d^a	Energy ^b
1.5	-237.02681
1.1	-237.03187
0.7	-237.02857

^a d is the perpendicular distance (in a.u.) from the O to the plane containing the four Ni atoms.

^b For a GVB(1/pp) wavefunction. The optimum geometry corresponds to a d of 0.56\AA which corresponds to a NiO distance of 1.85\AA and a NiONi angle of 144.7° . The D_e value is 2.98 eV for a GVB(1/pp) wavefunction. The basis set used here is [2s,1p,1d/3s,2p] which we estimate to lead to an error in the energy of 0.239 eV (from comparison of Ni_2O calculations using these basis sets) as compared with the [3s,1p,2d/3s,2p,1d] basis used for the NiO and Ni_2O calculations. Thus, this correction should be added to the D_e value to compare with the NiO and Ni_2O calculations, leading to 3.22 eV as our best estimate for D_e .

Table 5 Mulliken Populations for the Ni_nO Clusters^{a,b}

	Ni ₂ O	Ni ₃ O	Ni ₄ O	Ni ₅ O	Ni ₅ ⁺ O
Ni1 ^c	-	-	10.02	10.00	9.75
Ni2	9.55	9.57	9.54	9.55	9.52
Ni3	-	-	10.02	10.00	9.75
Ni4	9.55	9.57	9.54	9.55	9.52
Ni5	-	9.99	-	10.08	9.85
0	8.91	8.87	8.88	8.82	8.61

^aNear the optimum geometry in each case, which corresponds to vertical displacements of 0.6, 0.1, 1.1, 1.2, and 1.8 a.u. for Ni₂O, Ni₃O, Ni₄O, Ni₅O and Ni₅⁺O, respectively.

^bSee footnote 12 in the text.

^cThe numbering of the Ni atoms is as shown in Fig. 6a [Ni(100)].

while the $3a_1$ orbital (Fig. 3g) is essentially a 4s orbital on Ni5 and is antibonding in character. The $2b_1$ orbital (Fig. 3f) corresponds approximately to Ni1(4s)-Ni3(4s).

The lowest ion state of the Ni_5O cluster corresponds to ionizing the $3a_1$ orbital leading to the wavefunction

$$1a_1^2(1b_2^2 - \lambda 2b_2^2) 1b_1^2 2a_1^1 2b_1^1 \quad (12)$$

Near the equilibrium geometry for the neutral Ni_5O cluster, the orbitals of (12) are very similar to the corresponding orbitals of (11) (as assumed in using Koopmans' theorem). However, the Ni_5^+ cluster has a larger effective electronegativity than the Ni_5 neutral cluster, which leads to more covalent bonding for Ni_5^+O than for Ni_5O neutral. As expected from the discussion in section 4.1, this leads to an equilibrium geometry with the O further from the surface than for the Ni_5^+O cluster.

As the O atom moves from the equilibrium geometry for Ni_5O neutral toward the equilibrium geometry for the Ni_5^+O cluster, an electron is transferred from O back to the metal leading to the $1a_1^2$ pair being mainly on the Ni (bonding orbital) while the $2a_1$ orbital becomes a singly occupied O($2p_z$) orbital.

The resulting orbitals for the Ni_5^+O cluster near its equilibrium geometry are shown in Fig. 4. Here one sees that the orbitals of the GVB pair (Fig. 4ab) are very similar to the corresponding orbitals of the Ni_5^+O neutral cluster (Fig. 3ab). The doubly occupied $1a_1$ orbital (Fig. 4e) has bonding character on all three Ni atoms and also shows

NiO bonding character. The singly occupied $2a_1$ orbital (Fig. 4c) is essentially an $O(2p_z)$ orbital and the $2b_1$ orbital (Fig. 4f) is similar to the corresponding orbital of (11).

The Mulliken populations (Table 5) indicate that the Ni atoms involved in NiO bonds (Ni2 and Ni4) have Mulliken populations consistent with charges of ~ 0.5 electrons. From Table 5 we see that the Ni_5^+O cluster has a positive charge of ~ 0.5 electron distributed between Ni1 and Ni3 as compared with ~ 1.0 electron expected for Ni_4^+O . Thus, we expect larger nonbonded repulsions between the $O(2p_x)$ pair and the surface Ni atoms (1 and 3) for Ni_5^+O than for Ni_4^+O . This effect, which derives from polarization effects involving Ni5, leads to an equilibrium geometry for Ni_5^+O with the O atom 0.23\AA further from the surface than for Ni_4^+O .

In Fig. 11 we show the potential curves for the Ni_5O and Ni_5^+O clusters, while the energies are given in Table 6. As indicated in Table 1, the Ni_5^+O cluster leads to a distance above the surface of 0.96\AA which is in excellent agreement with the results of dynamic LEED intensity analysis, $0.90 \pm 0.10\text{\AA}$ [5].

4.4 Ni_3O

Starting with the wavefunction (8) for Ni_2O and adding the atom beneath the surface (Ni5) leads to the Ni_3O cluster. We find that Ni5 is nonbonding, leading to the qualitative description for Ni_3O :

Fig. 11 $\text{Ni}_5\text{O}, \text{Ni}_5^+\text{O}$ geometry variation. The calculated points are indicated.

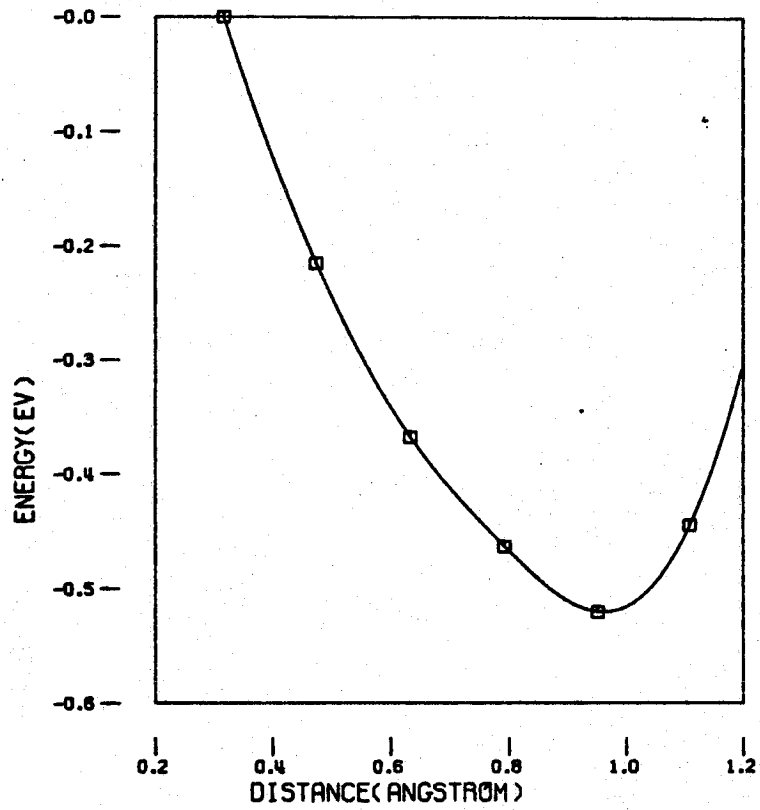
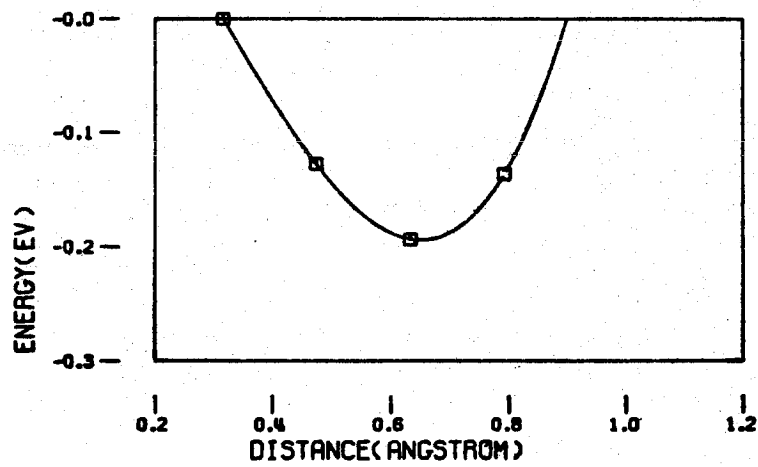
Ni₅O GEOMETRY OPTIMIZATIONNi₅O GEOMETRY OPTIMIZATION

Table 6 Ni_5O and Ni_5^+O Geometry Variation

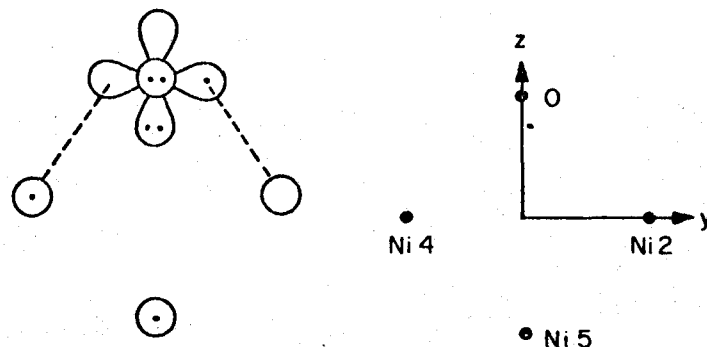
d ^a	Energy		
	$\text{Ni}_5\text{O}^{\text{b}}$	Ni_5^+O	
	GVB	GVB ^c	Koopmans' Theorem
2.1	-	-277.4016	-
1.8	-	-277.4044	-
1.5	-277.5567	-277.4023	-277.3854 ^d
1.2	-277.5588	-277.3988	-277.3857
0.9	-277.5564	-277.3932	-277.3794
0.6	-277.5517	-277.3853	-

^a d is the perpendicular distance (in a.u.) from the O to the plane containing the four surface Ni atoms.

^b For a GVB(1/pp) wavefunction. The optimum geometry corresponds to a d value of 0.65 \AA which leads to NiO distance of 1.88 \AA and a NiONi angle of 139.5°. The D_e value is 1.69 eV (see footnote b of Table 4).

^c For a GVB(1/pp) wavefunction. The optimum geometry corresponds to a d value of 0.96 \AA which leads to a NiO distance of 2.01 \AA and a NiONi angle of 122.8°. The D_e value is 2.85 eV (see footnote b of Table 4).

^d The Koopmans' theorem energies lead to an optimum geometry with the O atom 0.71 \AA above the surface.



which corresponds to the GVB wavefunction [24]

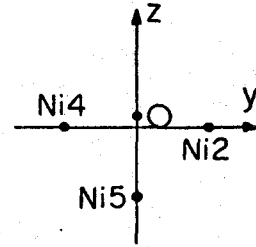
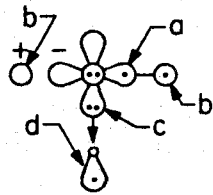
$$1a_1^2 2a_1^1 (1b_2^2 - \lambda 2b_2^2) \quad (13)$$

We show the orbitals of (13) in Fig. 12. Here one sees that the b_2 bond pair (Fig. 12ab) is qualitatively similar to the corresponding pair in Ni_2O (Fig. 9ab), Ni_5O (Fig. 3ab), and Ni_5^+O (Fig. 4ab). The $2a_1$ orbital (Fig. 12d) corresponds approximately to a 4s orbital on Ni5 but has hybridized away from the O atom. This leaves a partially exposed $3d^9$ core on Ni5 which we expect to have an attractive interaction with the doubly occupied $\text{O}(2p_z)$ orbital (as for the 5σ orbital of CO upon bonding to Ni [18]). It is apparently this effect that leads to an equilibrium geometry for the Ni_3O cluster with the O atom only 0.08\AA above the surface, 0.23\AA closer than for the Ni_2O cluster [25]. The resulting potential curve is shown in Fig. 13, while the energies used to construct Fig. 13 are given in Table 7.

Comparing to the (110) surface, from Fig. 6b we see that there are two Ni atoms below the surface (atoms 3 and 4 for geometry A),

Fig. 12 Selected orbitals of the Ni₃O cluster.

Ni₃O GVB (I/PP)



THE BOND PAIR

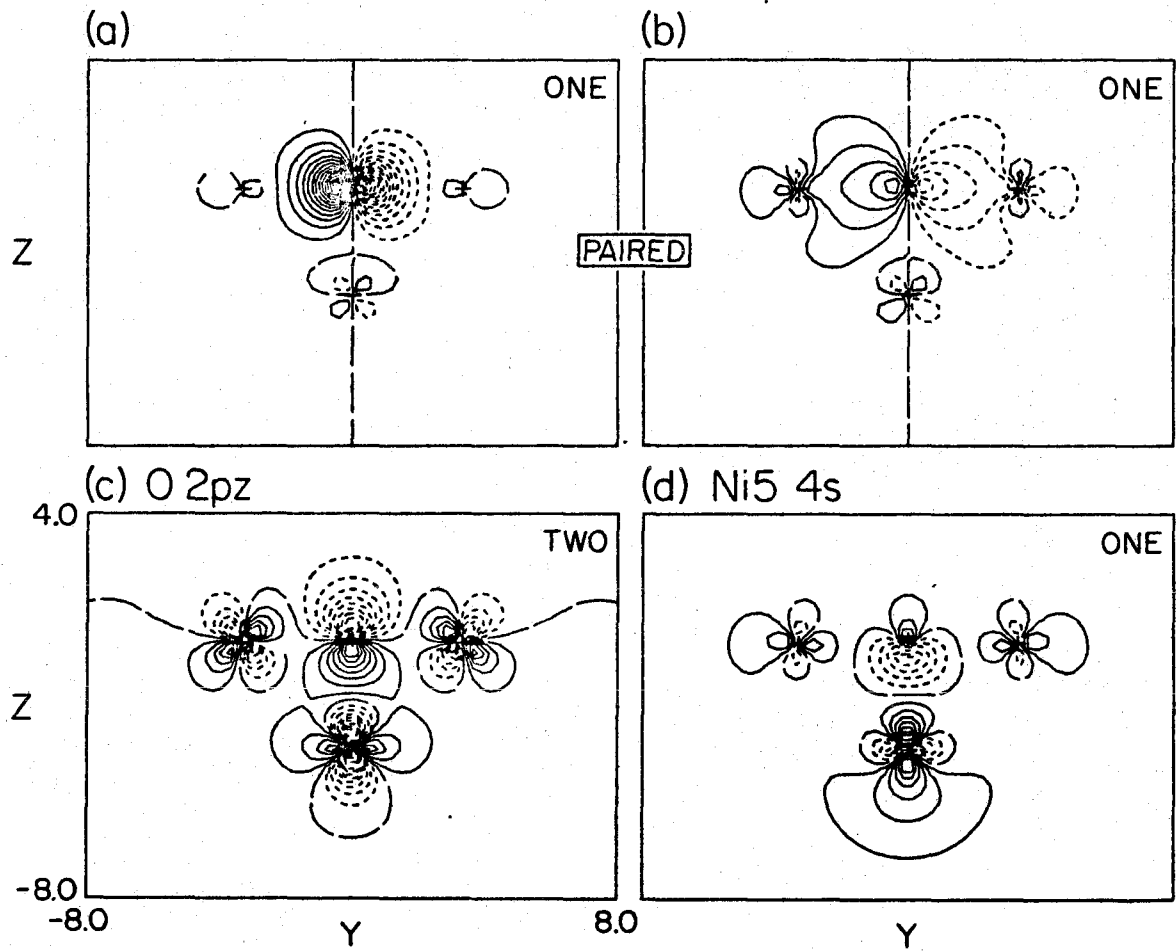


Fig. 13 Ni_3O geometry variation. The calculated points are indicated.

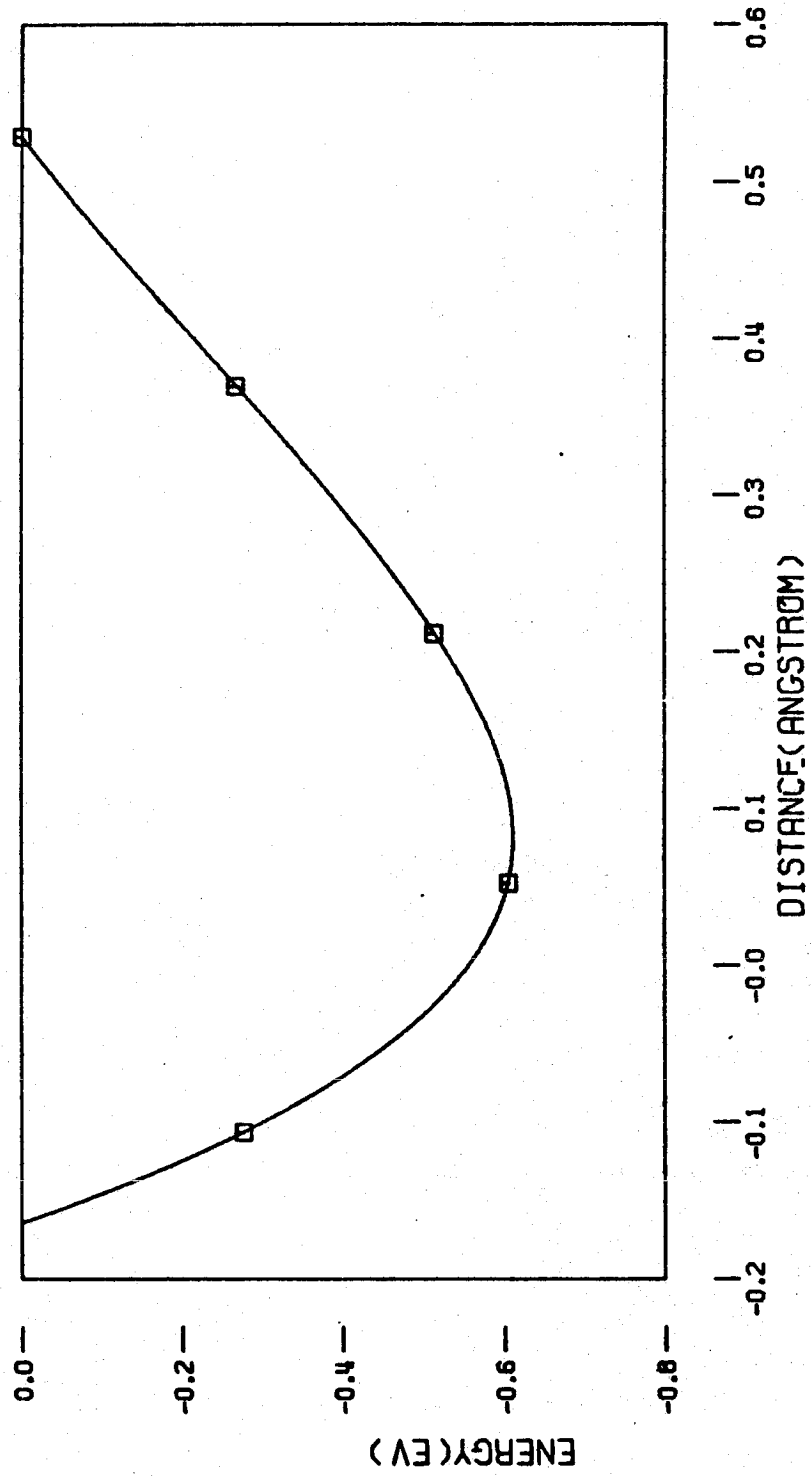
NI₃O GEOMETRY OPTIMIZATION

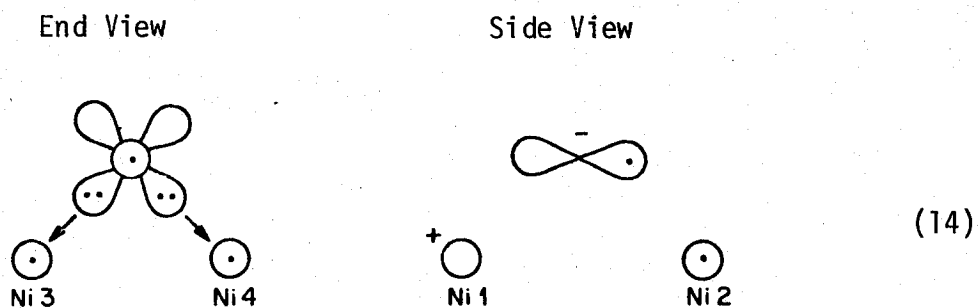
Table 7 Ni₃O Geometry Variation

d ^a	Energy ^b
1.0	-196.46073
0.7	-196.47057
0.4	-196.47960
0.1	-196.48297
-0.2	-196.47092

^ad is the perpendicular distance (in a.u.) from the O to a line connecting Ni2 and Ni4.

^bFor a GVB(1/pp) wavefunction. The optimum geometry corresponds to a d value of 0.08⁰Å which gives a NiO distance of 1.76⁰Å and a NiONi angle of 174.8°. The D_e value is 3.08 eV (see footnote b of Table 4).

which can interact in the manner that Ni5 did for the Ni₃O cluster. This leads to the expectation that, for the O bridging Ni atoms 1 and 2 of Fig. 6b, there will be attractive interactions between the two doubly occupied p orbitals of the O atom and Ni atoms 3 and 4.



In this picture, the oxygen would be expected to lie approximately in the plane of the surface (not more than 0.1\AA above the surface) and along the long edge of the surface unit cell. As indicated in Fig.5b, this leads to a $c(2 \times 2)$ overlayer.

References

- [1] Partially supported by a grant (DMR74-04965) from the National Science Foundation.
- [2] Partially supported by a grant (EX-76-G-03-1305) from the Energy Research and Development Administration.
- [3] S. P. Walch and W. A. Goddard III, *Surface Science*, to be published.
- [4] (a) L. Pauling, *The Nature of the Chemical Bond* (Cornell University Press, New York, 1972), 3rd ed., p. 93; (b) *ibid*, p. 260.
- [5] J. E. Demuth, D. W. Jepsen and P. M. Marcus, *Phys. Rev. Lett.* 31(8) (1973) 540.
- [6] A.J.H. Wachters, *J. Chem. Phys.* 52 (1970) 1033.
- [7] T. H. Dunning, Jr. and P. J. Hay, *Gaussian Basis Sets for Molecular Calculations*, in *Modern Theoretical Chemistry*, Vol. 2, ed. H. F. Schaefer III, Plenum Press, to be published. The p functions are the same as in Ref. 9, the tightest seven s functions are contracted into a single s function based on the 1s HF orbital, the second and third most diffuse are contracted into a basis function based on the 2s HF orbital; the most diffuse function is uncontracted.
- [8] S. Huzinaga, unpublished.
- [9] T. H. Dunning, Jr., *J. Chem. Phys.*, 53 (1970) 2823.
- [10] W. A. Goddard III, T. H. Dunning, Jr., W. J. Hunt and P. J. Hay, *Accts. Chem. Res.* 6 (1973) 368.
- [11] S. P. Walch and W. A. Goddard, III, *J. Amer. Chem. Soc.*, to be published.

- [12] This is from Mulliken populations. Generally, these populations indicate a greater charge transfer than would be indicated, for example, by the dipole moment. Thus, the populations although indicative of charge transfer should not be taken too literally.
- [13] (a) B. J. Moss and W. A. Goddard III, *J. Chem. Phys.* 63 (1975) 3523; (b) B. J. Moss, F. W. Bobrowicz and W. A. Goddard III, *ibid.* 63 (1975) 4632.
- [14] A wavefunction of the form (1) leads to an energy ~ 0.5 eV below a wavefunction of the form (2). However, the qualitative description is like (2).
- [15] K. O. Legg, F. P. Jona, D. W. Jepsen and P. M. Marcus, *J. Phys.* C8 (1975) L492.
- [16] The quoted atomic separations are obtained by taking a weighted average over the spectral levels corresponding to a given L and S (spin-orbit interactions are not included in our calculations). The values are from Ref. 17.
- [17] C. E. Moore, "Atomic Energy Levels", Vol. II, National Bureau of Standards (1952).
- [18] S. P. Walch and W. A. Goddard III, *J. Amer. Chem. Soc.* 98 (1976) 7908.
- [19] M. J. Sollenberger, M. S. thesis, California Institute of Technology, 1975.
- [20] T. H. Upton, W. A. Goddard III and C. F. Melius, *J. Amer. Chem. Soc.*, to be submitted.

- [21] There are two possible choices for the delta-like orbitals on each Ni. Their energies are within ~ 0.04 eV and we chose to solve self-consistently for the case where each Ni 3d hole is asymmetric with respect to the molecular plane, since this choice simplifies the SCF calculations.
- [22] The Ni(3d) holes for Ni atoms 2 and 4 (involved in Ni-O bonds) were taken to be delta-like with respect to the NiS bond axis and asymmetric with respect to the yz plane (containing Ni2, Ni4, and the S) which is the same orientation as for the Ni₂O calculation. The Ni(3d) holes for Ni1 and Ni3 were taken in 3d_{yz} orbitals which are delta-like with respect to the x axis, which passes through Ni1 and Ni3.
- [23] The Ni(3d) holes for Ni atoms 1-4 are the same as for the Ni₄O cluster (see Ref. 22). The 3d hole for Ni5 is taken in a 3d_{xy} orbital which is thus delta-like with respect to the z axis (regarded as the bond axis for bonding Ni5 to the surface Ni atoms).
- [24] The Ni(3d) holes for Ni atoms 2 and 4 are the same as for the Ni₂O calculation (see Ref. 21). The 3d hole for Ni5 is the same as for the Ni₅O calculation (see Ref. 23).
- [25] For the Ni₅O cluster repulsive effects between the nonbonded Ni atoms (1 and 3) and the O(2p_π) pair lead to a geometry with the O atom further above the surface than for Ni₂O. Apparently, at larger distances stabilization of the O(2p_z) pair is less significant than nonbonded repulsion due to the Ni5(4s) orbital, leading to a slightly repulsive effect due to Ni5.

PART F: THE ELECTRONIC STATES OF THE NiO MOLECULE^{1,2}

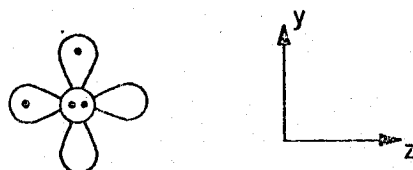
I. Introduction

A great deal of attention is currently being directed toward the study of heterogeneous catalysis of various reactions by metal surfaces and homogeneous catalysis using transition metal complexes. A major difficulty in designing and interpreting experimental studies of such systems is that the electronic structure and bonding of unsaturated ligands to transition metals is poorly understood (even at a qualitative level) with very little in the way of quantitative thermochemical data. Indeed, there is currently only very sketchy experimental (or theoretical) information about such simple diatomic systems as transition metal oxides.³ As part of a project aimed at providing both qualitative and quantitative information about chemisorption and reactions of atoms and molecules on metal surfaces, we carried out a rather extensive study of numerous electronic states of NiO as described herein.

In section II we present the qualitative description of the various states of NiO as obtained from the generalized valence bond (GVB)⁶ calculations. Various calculational details are outlined in section III, while section IV describes the details of the configuration interaction (CI calculations). Finally, section V contains a summary of the main results obtained.

II. Qualitative Description

The ground state of $O(^3p)$ has the configuration $(1s)^2(2s)^2(2p)^4$ and can be visualized as



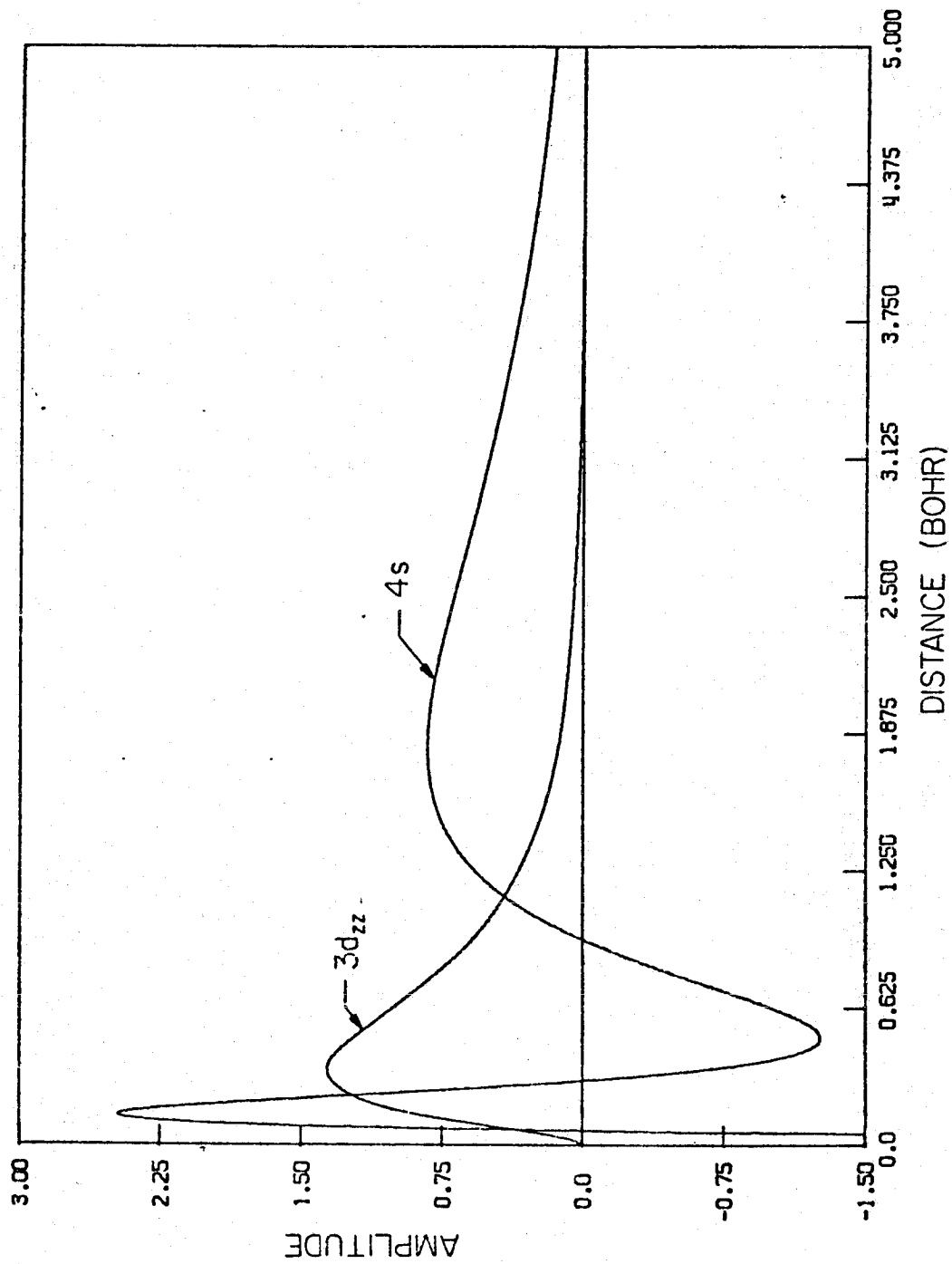
where ∞ indicates a $2p_z$ orbital in the plane and \odot indicates a $2p_x$ orbital pointing out of the plane.

Ni is a bit more complicated. Neglecting spin-orbit coupling, the ground state is $^3D(4s^1 3d^9)$ while the $^3F(4s^2 3d^8)$ state is at 0.03 eV.⁷ Thus, both states could well play a role in the bonding. However, as shown in Fig. 1, the 4s orbital of Ni is $\sim 2\frac{1}{2}$ times larger than the 3d orbitals, so that the bonding is dominated by the 4s orbital. In consequence, the lower bound states of NiO all have essentially $(4s)^1(3d)^9$ character on the Ni.

Before examining the states of NiO we will consider NiH^9 since it illustrates the sigma bonding without the complications of the π bonds.

Coupling the $Ni(s^1 d^9)$ state to the H leads to an attractive interaction much as in H_2 , whereas at large R, coupling the $Ni(s^2 d^8)$ state to the H leads to repulsive interactions (arising from the Pauli principle) somewhat analogous to the case of HeH or BeH. At small R the $s^2 d^8$ state can lead to bonding (the atomic state is promoted by splitting the 4s pair into two sp hybrids, one of which overlaps the H);

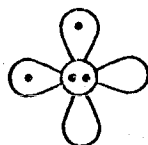
Figure 1. Comparison of the 4s and 3d orbital sizes of the Ni atom.

NICKEL ATOM $4s^2 3d^8 (^3F)$ 

however, the ground state of NiH has the s^1d^9 configuration on the Ni. Allowing the orbitals to readjust, as in the GVB wavefunction, leads to mixing of small amounts of Ni $4p\sigma$, Ni $3d\sigma$, and H $1s$ character into the Ni($4s$) orbital; however, the qualitative description is as above.

Given that the ground state of NiH has $4s^13d^9$ character on the Ni with the $4s$ orbital coupled to the H, we expect five low-lying states ($^2\Delta$, $^2\Pi$, and $^2\Sigma^+$) depending on which of the five d orbitals is singly occupied (i.e., which one has the hole). As discussed elsewhere⁹ the best state has a δ hole, the next best has a π hole, while the case with a σ hole is worst. The separations here are $\delta \rightarrow \pi$ 0.346 eV and $\delta \rightarrow \sigma$ 0.441 eV. (The effect leading to this ordering is referred to as the intra-atomic coupling.)¹⁰

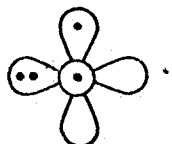
Now we consider NiO. Again we find the lower states to involve a Ni($4s^13d^9$) configuration. Assuming this and pairing the Ni($4s$) orbital with a singly occupied O($2p\sigma$) orbital



(1)

leads to five possible Ni $3d^9$ configurations, each of which can be coupled with two O($2p\pi$)³ configurations. Each of these ten spatial configurations leads to a singlet and a triplet, resulting in 20 states (some of which are degenerate) that we will refer to collectively as the group I states.

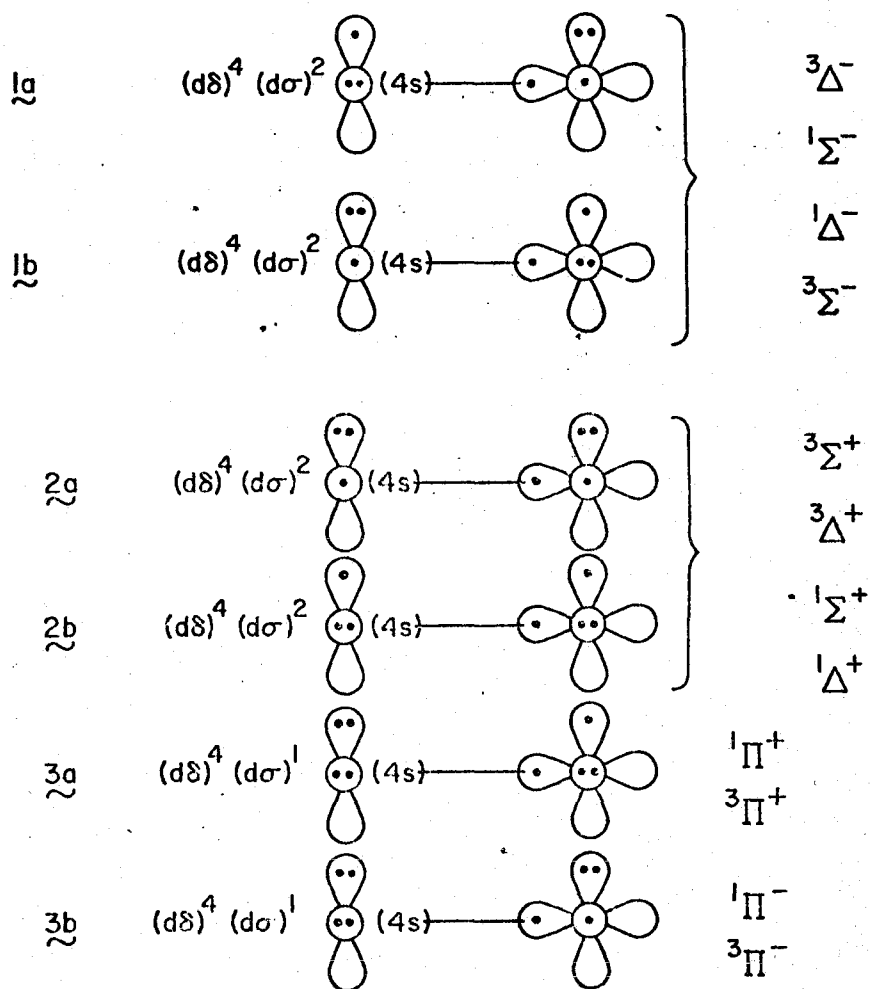
Pairing the Ni($4s^1 3d^9$) configuration with the oxygen configuration

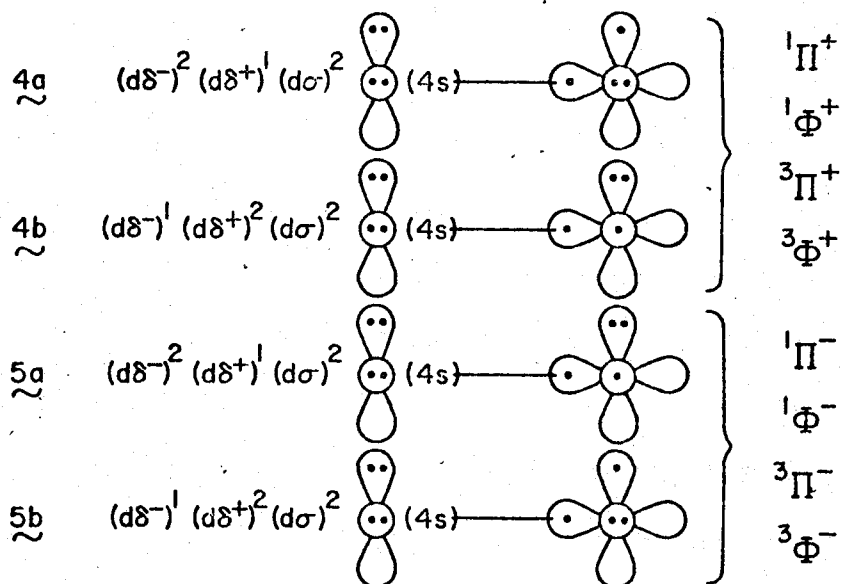


(2)

leads to a number of additional states which generally have a weaker bond due to repulsive interactions of the $O(2p\sigma)$ doubly occupied orbital with the Ni($4s$) orbital. These states lead to bonding because the $O(2p\sigma)$ pair is attracted by the Ni core somewhat as for the CO lone pair in NiCO.¹⁰ The set of states resulting from (2) are denoted as group II states.

A. The Group I States. The ten group I configurations corresponding to (1) and the electronic states arising from these configurations are shown below. Each of these configurations involves a sigma bond between the Ni($4s$) and $O(2p\sigma)$ orbitals, and the ordering of the states is controlled mainly by differences in the π interactions. Thus, we indicate the Ni($3d\pi$) and $O(2p\pi)$ orbitals schematically (for simplicity we use the same notation for Ni($3d\pi$) orbitals as for $O(2p\pi)$ orbitals) and include the remaining Ni atom configuration in an abbreviated form (e.g., $(d\delta)^4(d\sigma)^2$). In 1-5 the symmetries resulting from each configuration are listed at the right in order of the energy (highest state at the top).





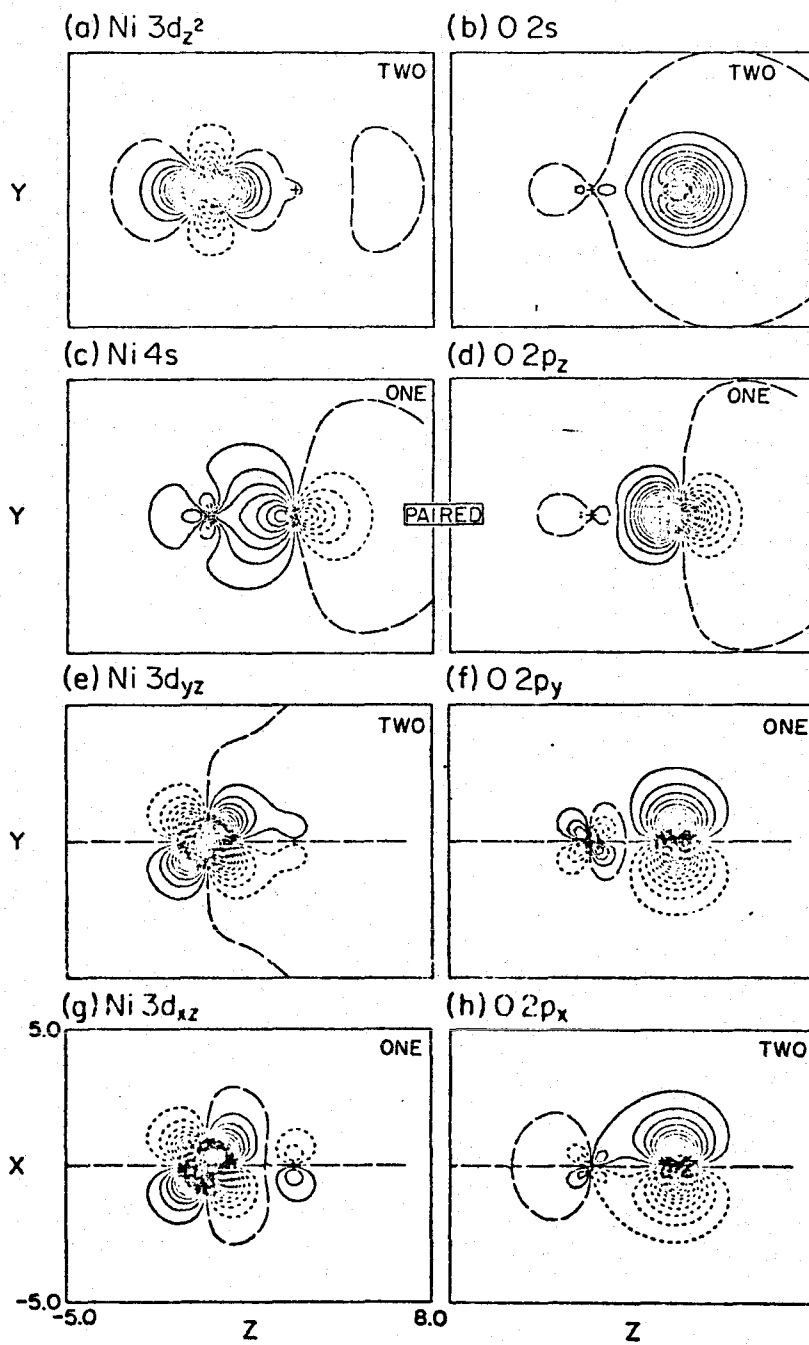
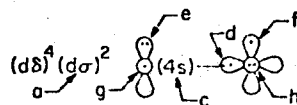
Configurations $\tilde{1}$ and $\tilde{2}$ have a $3d\pi$ hole and lead to states $3\Sigma^-$, 1Δ , $1\Sigma^+$, $1\Sigma^-$, 3Δ , and $3\Sigma^+$ just as for the analogous case of O_2 (where these six states are the lowest six states). Indeed, the ordering of these states is exactly as in O_2 ,¹¹ and we find that the ground state of NiO is the $3\Sigma^-$ state.

Configurations $\tilde{3}$ have a $3d\sigma$ hole and lead to $1,3\Pi$ states. Configurations $\tilde{4}$ and $\tilde{5}$ (which involve a $3d\delta$ hole) lead to $1,3\Pi$ and $1,3\Phi$ states.

Figure 2 shows the GVB orbitals of configuration $\tilde{1a}$ (which together with configuration $\tilde{1b}$ leads to the $X^3\Sigma^-$ ground state of NiO). Concentrating first on the sigma bond (Fig. 2cd) we see that the $O(2p\sigma)$ component (Fig. 2d) of the bond pair is essentially atomic-like, while the $Ni(4s)$ component (Fig. 2c) is significantly distorted toward the O. This indicates a somewhat ionic bond (toward the oxygen). These effects

Figure 2. The GVB orbitals of the $X^3\Sigma^-$ state of NiO (at $R = 1.63\text{\AA}$).

Unless otherwise noted, all orbital plots have uniformly spaced contours with increments of 0.05 a.u. Positive contours are indicated by solid lines, negative contours are indicated by dashed lines, and nodal lines are indicated by long dashes. The same conventions are used for the other figures.

NiO $X^3\Sigma^-$ 

are reflected in the Mulliken populations (Table I) which show 0.57 electron transferred from Ni to O.¹² The Ni(4s)-like component of the NiO sigma bond pair has incorporated some 3d σ character.

The relatively large size of the Ni(4s) orbital favors formation of the sigma bond at an R much larger than the size of the 3d orbital, leading to small Ni3d π -O2p π overlaps. This is reflected in the localized character of the π orbitals. The doubly occupied O(2p π) orbital (Fig. 2h) delocalizes somewhat more onto the Ni than does the doubly occupied Ni(3d π) orbital (Fig. 2e) onto O, leading to a slight net charge transfer back onto the Ni (0.08 electrons) in response to the charge flow from Ni to O in the sigma system (0.65 electrons).

We now consider the ordering of the group I states. Here we first examine the ordering of the covalent configurations $\underline{1}$ - $\underline{5}$ and then consider modifications to this ordering due to additional configuration interaction (CI) effects.

Consider first configurations $\underline{1}$ and $\underline{2}$, which lead to states whose ordering is the same as the ordering of the analogous states of the O₂ molecule.¹¹

In the case of configurations $\underline{1}$, the singly occupied orbitals are orthogonal leading to the triplet coupling being lower; whereas, for configurations $\underline{2}$ the singly occupied orbitals overlap, which leads to the singlet pairing (π bonding) being lower. We now compare the triplet coupling of $\underline{1}$ and the singlet coupling of $\underline{2}$. Configurations $\underline{2}$ have a single π bond in one direction which is partially counterbalanced by non-bonded interactions between the adjacent doubly

Table I Mulliken Populations for the $X^3\Sigma^-$ and $5\Sigma^-$ States of NiO^a

STATE	Ni													Totals			
	x^2-y^2	$2z^2-x^2-y^2$	xy	xz	yz	4s	x	y	z	1s	2s	x	y	z	d	N1	0
$5\Sigma^-(6)$	2.00	0.92	2.00	1.93	1.93	1.04	0.01	0.01	0.15	2.00	1.94	1.06	1.06	1.94	0.02	9.98	8.02
$X^3\Sigma^-(1)$	2.00	1.76	2.00	1.03	1.97	0.55	0.06	0.02	0.04	2.00	1.92	1.90	1.00	1.73	0.00	9.43	8.57

^aAt R = 1.626Å which is close to the equilibrium internuclear separation for the $X^3\Sigma^-$ state of NiO.

occupied orbitals in the other direction. At small R , these repulsive interactions dominate and make $\underline{2}$ unfavorable; whereas, at large R the π bond dominates, favoring $\underline{2}$. In the case of $\underline{1}$, there is no π bonding at large R , but at small R the doubly occupied π orbital can delocalize onto the opposite center. This leads to stabilization of the doubly occupied orbital which is partially counterbalanced by antibonding character being introduced into the singly occupied orbitals. The net effect, however, is bonding and is referred to as a three-electron bond.¹¹

Thus, $\underline{1}$ should be favorable at large overlap while $\underline{2}$ is favored at small overlap. For O_2 , $\underline{1}$ is lower near R_e but the ordering is reversed at large R .¹¹ Since the $3d\pi-2p\pi$ overlap in NiO is small even at R_e (for configuration $\underline{2}$ with a π bond the π overlap is only 0.250 at $R = 1.64\text{\AA}$), we find that for NiO $\underline{2}$ is below $\underline{1}$ for the distances considered here.

Configurations $\underline{3}-\underline{5}$ each involve one three-electron bond, whereas $\underline{1}$ had two three-electron bonds. Thus, based only on the π bonding involved, one expects the ordering

$$\underline{2} < \underline{1} < \underline{3} \approx \underline{4} \approx \underline{5}$$

However, just as for NiH we expect the states with a $3d\delta$ hole to lead to a stronger sigma bond than the states with a $3d\pi$ hole which in turn is more favorable than the states with a $3d\sigma$ hole. Thus, $\underline{4}$ and $\underline{5}$ are stabilized relative to $\underline{1}$ and $\underline{2}$ which in turn are stabilized relative to $\underline{3}$, leading to the calculated ordering

$$\underline{\underline{2a}} < \underline{\underline{5b}} < \underline{\underline{1a}} < \underline{\underline{3a}}$$

with relative energies of 0.0, 0.064, 0.177, and 0.248 eV, respectively (at $R = 1.64\text{\AA}$).

Thus, the single configurations $\underline{1}$ - $\underline{5}$ are close in energy, and the final ordering is determined by additional CI effects. (In the following we first discuss the states which arise from $\underline{1}$ and $\underline{2}$.)

Figure 3 shows how configurations $\underline{1}$ and $\underline{2}$ are combined into the $^3\Sigma^-$, $^1\Delta$, $^1\Sigma^+$, $^1\Sigma^-$, $^3\Delta$, and $^3\Sigma^+$ states of NiO and the resultant orderings for SCF and CI wavefunctions. The left side of Fig. 3 shows the ordering of the singlet and triplet couplings of configurations $\underline{1}$ and $\underline{2}$, while the right side shows the CI ordering and the dominant covalent and ionic configurations involved in the CI wavefunctions for the various states.

First we consider the SCF ordering. As previously discussed, the singlet coupling of $\underline{2}$ is below the triplet coupling of $\underline{1}$. We now consider the magnitude of the singlet-triplet splittings for $\underline{1}$ and $\underline{2}$.

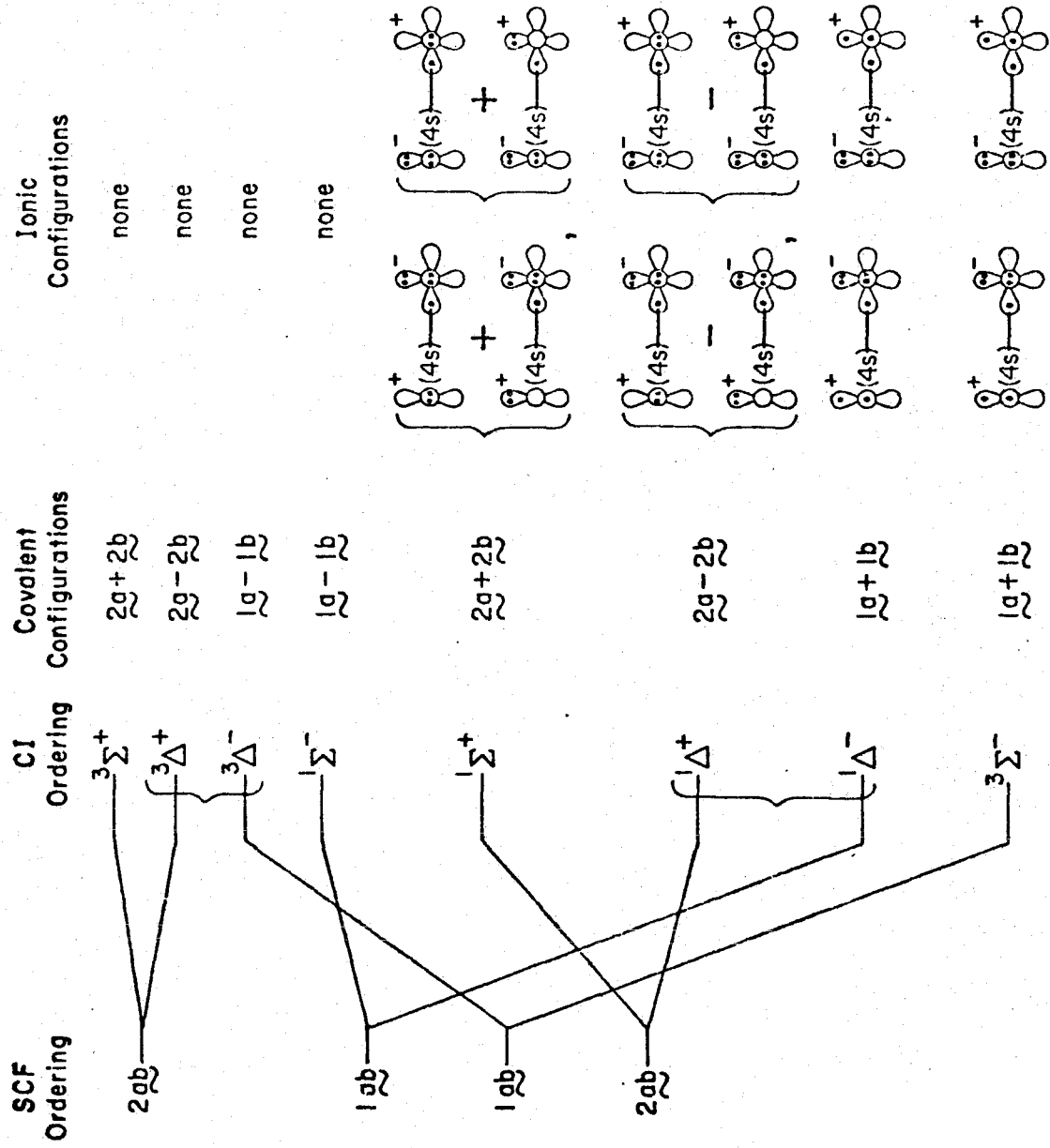
Covalent coupling of two singly occupied orbitals on different centers ϕ_l and ϕ_r , leads to singlet and triplet states with energies given by¹³

$$\begin{aligned} E_S &= E_{lr} + \frac{\bar{\tau}}{1 + S^2} \\ E_T &= E_{lr} + \frac{-\bar{\tau}}{1 - S^2} \end{aligned} \quad (3)$$

where

$$\begin{aligned} E_{lr} &= h_{ll} + h_{rr} + J_{lr} \\ \bar{\tau} &= 2S\tau + (K_{lr} - S^2J_{lr}) \\ \tau &= h_{lr} - \frac{1}{2}S(h_{ll} + h_{rr}) \end{aligned}$$

Figure 3. The ordering of the group I states of NiO arising from configurations 1 and 2. The left side indicates the SCF ordering while the right side indicates the CI ordering and the dominant ionic and covalent configurations for each state.



Here $E_{\ell r}$ is the energy of the product wavefunction and the ordering of the singlet and triplet states is determined by the sign of $\bar{\tau}$. If $S = 0$, then $\bar{\tau} = K_{\ell r} > 0$ and the triplet state is lower (e.g., Hund's rule). If $S \neq 0$, then τ is large and negative and $\bar{\tau}$ is generally negative, leading to a singlet ground state (e.g., H_2 at large R). For $\tilde{1}$, ϕ_ℓ and ϕ_r are orthogonal and the singlet-triplet splitting is given by $2K_{\ell r}$, which is small. For $\tilde{2}$, ϕ_ℓ and ϕ_r overlap, leading to a large singlet-triplet splitting with singlet lower. Thus we obtain the SCF ordering given in the first column of Fig. 3.

The next two columns of Fig. 3 show how the covalent configurations $\tilde{1}$ and $\tilde{2}$ are combined in the various states and the CI ordering of these states (at R_e of the $X^3\Sigma^-$ state).

As shown in the last column of Fig. 3, important ionic configurations arise for some states but are excluded (by symmetry) from others; this leads to a large effect upon the relative splittings of the states. Considering first the singlet and triplet couplings of $\tilde{1}$, we see from Fig. 3 that the $^1\Delta^-$ and $X^3\Sigma^-$ states have important ionic contributions to the wavefunction which are not present for the $^3\Delta^-$ and $^1\Sigma^-$ states. Thus, the $X^3\Sigma^-$ and $^1\Delta^-$ states are substantially stabilized with respect to $^3\Delta^-$ and $^1\Sigma^-$. For the singlet coupling of $\tilde{2}$, ionic terms are involved for both the $^1\Sigma^+$ and $^1\Delta^+$ states, leading to comparable energy lowerings for these states and a small splitting, while the states arising from the triplet coupling of $\tilde{2}$ do not have important ionic terms.

For the $X^3\Sigma^-$ state the ionic terms have the effect of allowing delocalization of the doubly occupied π orbitals of $\tilde{1}$ onto the other center (i.e., formation of three-electron π bonds). This effect is especially favorable here since the delocalization is in opposite directions in the π_x and π_y systems leading to little net charge transfer. The

result is an $X^3\Sigma^-$ ground state for NiO.

For the $^3\Phi$ and $^3\Pi$ states arising from 3-5, ionic configurations involving transfer of a single electron from a Ni(3d π) to an O(2p π) orbital contribute to the wavefunction. These configurations involve charge transfer from Ni to O which is unfavorable given the ionic NiO sigma bond. In addition, they contribute equally to both the $^3\Phi$ and $^3\Pi$ states and thus lead to no net splittings of these states.

Figure 4 shows the potential curves for the group I states of NiO (obtained from CI calculations based on the GVB orbitals of the $X^3\Sigma^-$ state). The CI energies used to construct these curves are given in Table III, while Table II contains the GVB energies of $1a$ for comparison. As indicated also in Fig. 3, the ordering of the six states with a 3d π hole is the same as for the corresponding states of O₂. (From the preceding discussion this is expected, since the factors affecting the ordering of these states are analogous to those determining the ordering of the O₂ states.)

Examining now the states arising from a 3d σ or 3d δ hole, one sees that at small R the $1^3\Pi$ state (which involves a 3d hole) is below the $2^3\Pi$ and $^3\Phi$ states (which involve 3d holes); whereas, at larger R the ordering is reversed. The ordering at large R is expected since the 3d δ hole is better than the 3d σ hole for sigma bonding. The reversal of 3d δ and 3d σ at small R seems to arise from a smaller repulsive interaction of the oxygen sigma orbitals with the Ni 3d σ state (one 3d σ electron) than with the Ni 3d δ state (two 3d σ electrons); this effect is of negligible importance at large R.

Figure 4. Potential curves for the group I states of NiO based on CI calculations using the $^3\Sigma^-$ basis. The dominant configuration(s) for each state are indicated in parentheses. The singlet states corresponding to $\underline{3}$, $\underline{4}$, and $\underline{5}$ were not included in this calculation.

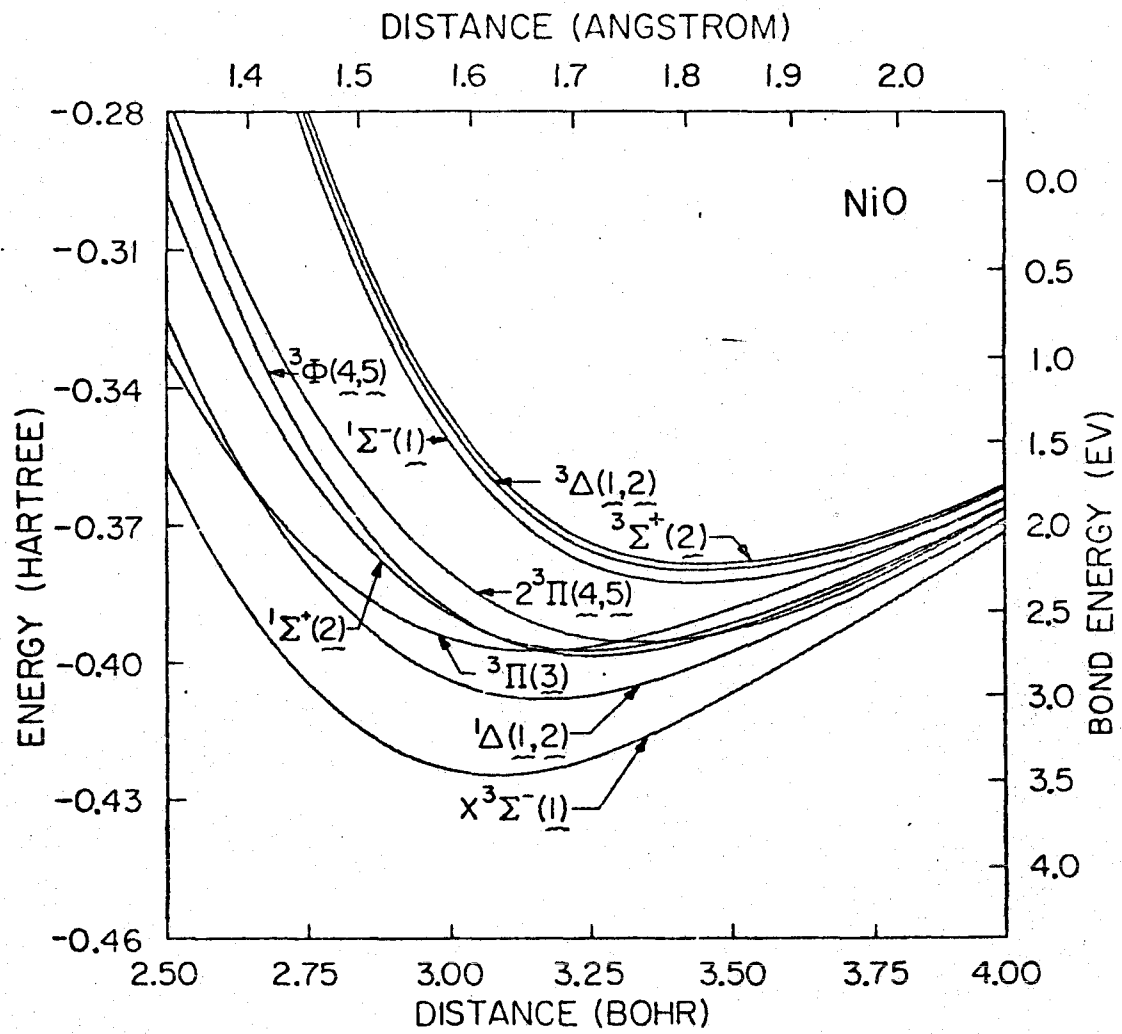


Table II GVB Energies for the $X^3\Sigma^-$ and $5\Sigma^-$ States of NiO. The quoted number should be subtracted from -115.0 to yield the total energy in hartrees.

STATE	R = 2.7 a_0	3.0727 a_0	3.5 a_0	4.0 a_0	5.0 a_0
$5\Sigma^-$ (6)	0.23702	0.29640	0.31416	0.31154	0.29929
$X^3\Sigma^-$ (1)	0.29042	0.35321	0.36004	0.33875	0.29524

Table III CI Energies for Group I States Using the $3\Sigma^-$ Basis (The energies are presented in the same form as Table II)

SYMMETRY	$R = 2.7 a_0$	$3.0727 a_0$	$3.5 a_0$	$4.0 a_0$	$5.0 a_0$
$3\Sigma^+(2)^a$	0.25922	0.35735	0.37979	0.36252	0.31600
$3\Delta(1,2)$	0.26247	0.35957	0.38114	0.36323	0.31616
$1\Sigma^-(1)$	0.26728	0.36314	0.38382	0.36551	0.31895
$2^3\Pi(4,5)$	0.33219	0.38768	0.39503	0.36767	--- b
$3\phi(4,5)$	0.34150	0.39504	0.39492	0.36762	--- b
$1\Sigma^+(2)$	0.34930	0.39507	0.39355	0.36748	0.31881
$1^3\Pi(3)$	0.36954	0.39836	0.39038	0.36574	0.31625
$1\Delta(1,2)$	0.37128	0.40841	0.40007	0.37002	0.31912
$X^3\Sigma^-(1)$	0.39865	0.42654	0.40935	0.37299	0.31707

^aThe numbers in parentheses indicate the dominant configuration(s) corresponding to each root.

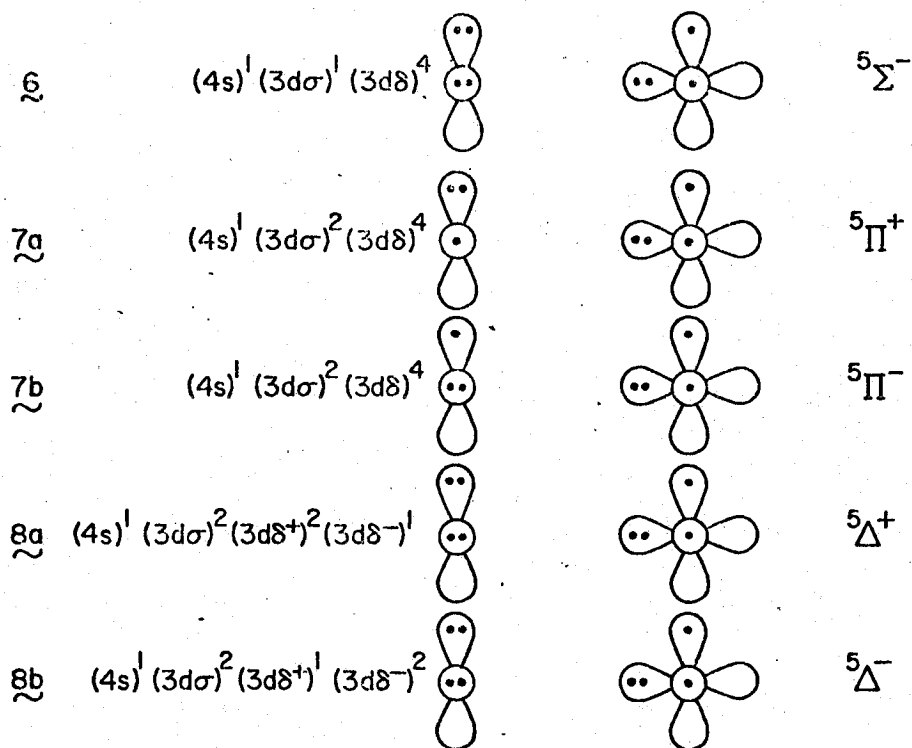
^bFor these cases the Shavitt diagonalization did not converge because the roots are too closely spaced.

The crossing of the $1^3\Pi$ and $2^3\Pi$ states¹⁴ induces a crossing of the $3^3\Phi$ and $2^3\Pi$ states (which each involve a $3d\delta$ hole). At small R the $1^3\Pi$ state is below the $2^3\Pi$ state (although these curves cross we use the $1^3\Pi$ and $2^3\Pi$ designations as useful neumonics), hence the lower $1^3\Pi$ state is stabilized, the upper $2^3\Pi$ state is destabilized, while the $3^3\Phi$ state is not affected, leading to $3^3\Phi$ below $2^3\Pi$. At large R the $2^3\Pi$ state is below the $1^3\Pi$ state and hence $2^3\Pi$ is stabilized, leading to $2^3\Pi$ below $3^3\Phi$.

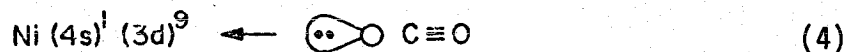
As discussed in section IIC, there are group II states which overlap the group I $3^3\Sigma^-$, $1^1\Delta$, and $1^1\Sigma^+$ states, leading to incorporation of character of these upper states and further stabilization of these group I states. Including these additional effects leads to a D_0 for the $X^3\Sigma^-$ state of NiO of 89.9 Kcal/mole (the D_e value is 91.1 Kcal/mole) in good agreement with the experimental bond energy of 86.5 ± 5 Kcal/mole.⁵ We calculate a NiO bond length of 1.60\AA which, as expected, is a good deal shorter than for bulk NiO (2.08\AA).¹⁵ The bond length for the NiO molecule is not known experimentally.

B. The Group II Quintet States. Group II configurations lead to quintet ($S = 2$), triplet ($S = 1$), and singlet ($S = 0$) states. In this section we discuss the simplest of these, the group II quintet states. [The group II singlets and triplets are more complex due to strong couplings with the group I states.]

Combining the five possible $Ni(4s^1 3d^9)$ configurations with the 0 atom configuration (2) leads to the five group II quintet configurations, 6, 7, and 8, shown below.



For the group II states the Ni(4s) orbital is non-bonding and simply builds in 4p character to move out of the way of the oxygen orbitals. Since this situation is formally analogous to the bonding of CO to Ni, we compare the bonding here to that in NiCO.¹⁰ In the case of NiCO we found that there was very little delocalization of the C(2s) lone pair of the CO onto the Ni (sigma donation), and very little delocalization of the Ni(3d) orbitals onto the CO (π back-bonding).



Thus, for CO, the bonding mainly involves stabilization of the C(2s) orbital by interaction with the partially exposed Ni(3d)⁹ core. Sigma donation and π backbonding effects are of the same order of magnitude as the splittings induced by the intra-atomic coupling effect; thus, the lowest state of

NiCO has a $3d\delta$ hole and the state having a $3d\sigma$ hole is 0.240 eV higher.

For NiO, however, the high electronegativity of oxygen leads to significant delocalization of the Ni($3d\pi$) orbitals into the singly occupied O($2p\pi$) orbitals. This delocalization is most favorable if it is coupled with delocalization of the doubly occupied O($2p\sigma$) orbital onto Ni in the sigma system. Thus, there are important sigma-donation π back-bonding effects for the group II NiO states which lead to $\underline{6}$ being the lowest group II quintet state, while $\underline{8}$ is ~ 1.2 eV higher and $\underline{7}$ should be even higher.

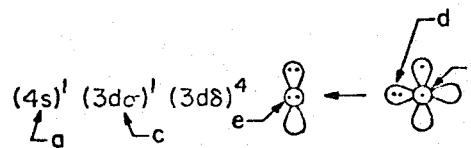
These effects are evident in the orbitals of the $^5\Sigma^-$ state ($\underline{6}$) which are shown in Fig. 5. Here one sees that the Ni($4s$) orbital (Fig. 5a) has hybridized away from the oxygen while the Ni($3d\pi$) orbitals (Fig. 5e) have delocalized substantially onto the oxygen and the doubly occupied O($2p_z$) orbital has delocalized onto the Ni.

The Mulliken populations (Table I) show that the delocalization of the Ni($3d\pi$) orbitals onto O leads to an increase in the total $2p\pi$ population of 0.12, an effect which is counterbalanced by a decrease in the O($2p_z$) population of 0.06, leading overall to a nearly neutral molecule.¹²

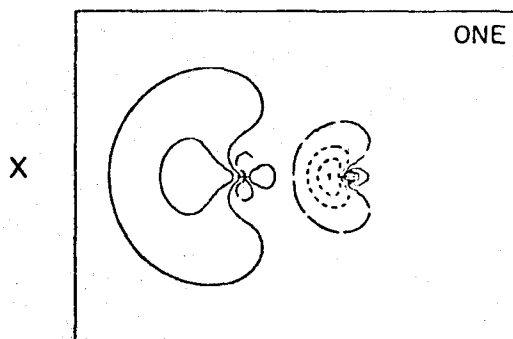
In addition to $\underline{6}$ - $\underline{8}$ there are other important group II quintet states involving ionic configurations. Of these, the states involving a Ni($3d\sigma$) hole are lowest and lead to configurations $\underline{9}$ and $\underline{10}$, shown below:

Figure 5. The GVB orbitals of the ${}^5\Sigma^-$ state of NiO (at $R = 1.63\text{\AA}$)

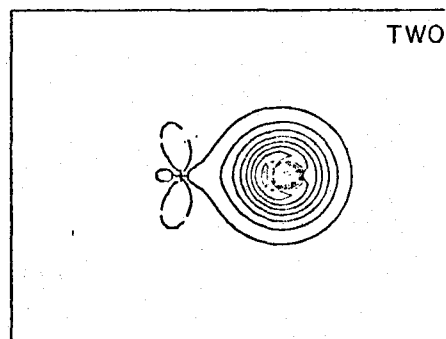
NiO $5\Sigma^-$



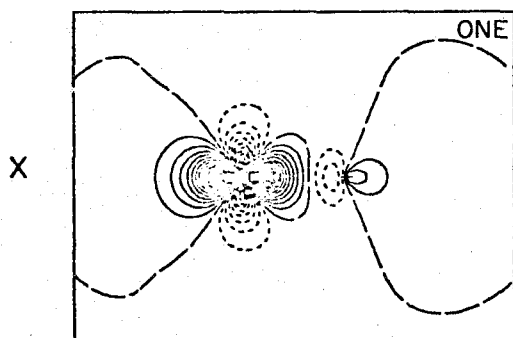
(a) Ni 4s-4p HYBRID



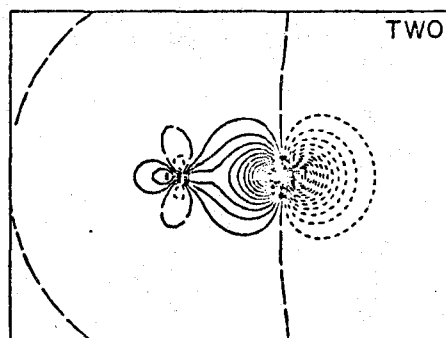
(b) O 2s



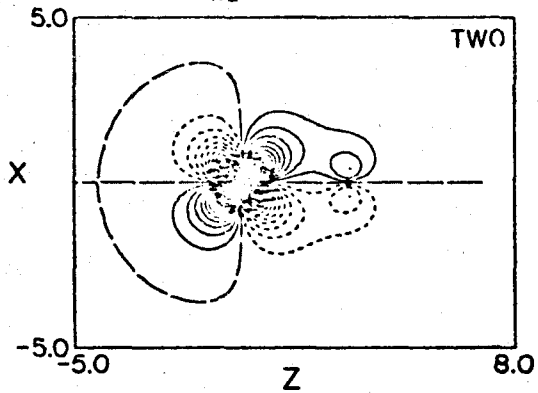
(c) Ni 3d_{z²}



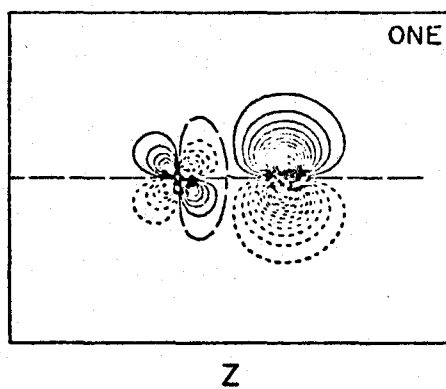
(d) O 2p_z



(e) Ni 3d_{xz}



(f) O 2p_x



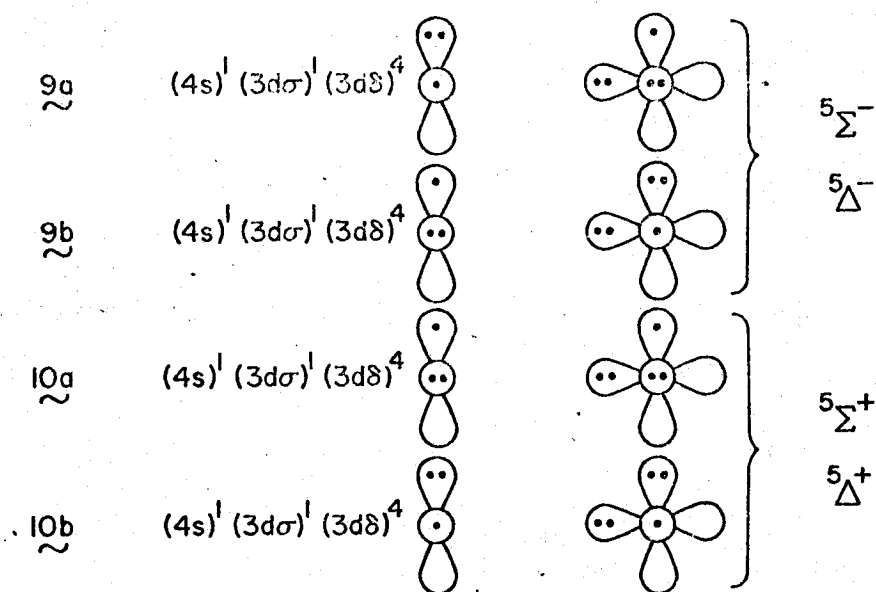


Table IV shows the CI energies for the group II quintet states. These energies are based on CI calculations using the orbitals of 6. The potential curves for the group II quintet states are shown in Fig. 6, along with the potential curves for the group I and group II singlet and triplet states.

C. Group II Singlet and Triplet States. The remaining group II states correspond to singlet and triplet couplings of the orbitals in 6-10. Since some of these states couple strongly with the group I states, the potential curves for these states are based on CI calculations designed to provide a good description of both the group I and group II states (see section IV for a discussion of the details of the CI calculations). The resulting potential curves are those shown in

Table IV CI Energies for Group II Quintet States Using the $5\Sigma^-$ Basis (The energies are presented in the same form as Table II)

SYMMETRY	R = 2.7 a_0	3.0727 a_0	3.5 a_0	4.0 a_0	5.0 a_0
$2^5\Delta(9,10)^a$	0.20807	0.28996	0.29799	0.28701	-
$5^5\Sigma^+(10)$	0.21106	0.29478	0.30160	0.28760	0.28201
$1^5\Delta(8)$	0.28630	0.33958	0.33189	0.31040	0.29394
$5^5\Sigma^-(6)$	0.35879	0.37768	0.35349	0.32307	0.30071

^aSee footnote a of Table III

Fig. 6 and the energies used to construct these potential curves are tabulated in Tables V and VI.

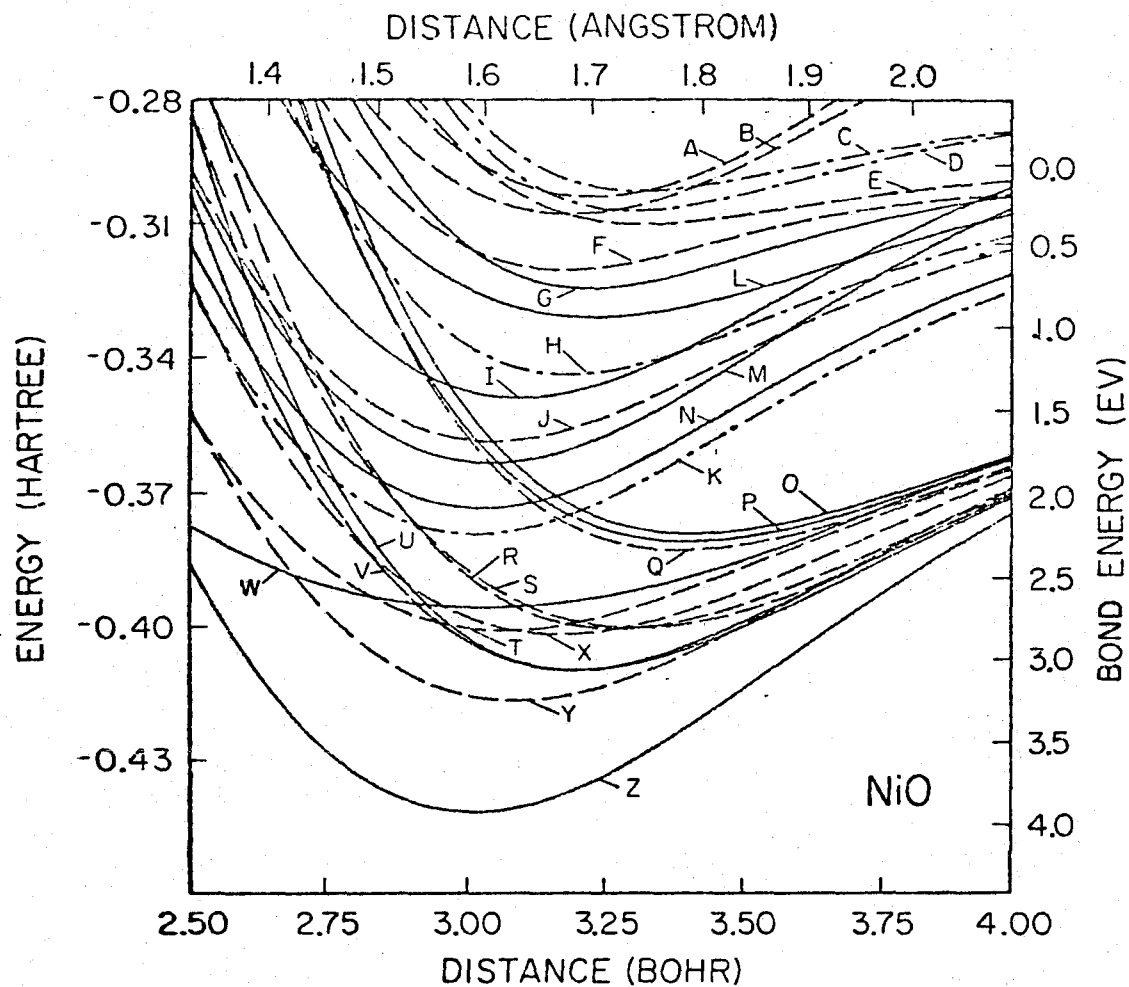
For the $^5\Sigma^-$ state (6), the singly occupied orbitals [Ni(4s), Ni(3d σ), 0(2p $_x$), and 0(2p $_y$)] are all orthogonal, thus the quintet coupling is lowest. Given these four orthogonal orbitals one can also form three linearly independent triplet states and two linearly independent singlet states,¹⁶ some of which interact strongly with the group I states.

We consider first the triplet states. Singlet coupling the 0(2p $_x$) and 0(2p $_y$) orbitals leads to the $^3\Delta^-$ state; two other spin functions can be constructed, both of which have these orbitals triplet coupled, leading to $^3\Sigma^-$ states. Since the exchange integral between the 0(2p $_x$) and 0(2p $_y$) orbitals is 1.10 eV, whereas the exchange integral between the Ni(3d σ) and Ni(4s) orbitals is only 0.39 eV, the $^3\Delta^-$ state should be highest. This spin-coupling is schematically indicated as



where vertically adjacent positions indicate high-spin coupling and horizontally adjacent positions indicate singlet coupling (see also Ref. 16). Using the same notation, the two $^3\Sigma^-$ states are denoted by

Figure 6. Potential curves for the group I and group II states of NiO based on CI calculations using the $^5\Sigma^-$ POL basis. Singlet states are indicated by dashed lines, triplet states are indicated by solid lines, and quintet states are shown with dot-dashed lines. The dominant configuration(s) for each state are indicated in parentheses.



A. $2^1\Sigma^+(\underline{11})$	H. $5\Delta(\underline{8})$	O. $3\Sigma^+(\underline{2})$	V. $3\Phi(\underline{4,5})$
B. $2^1\Delta(\underline{6,11})$	I. $2^3\Sigma^+(\underline{11})$	P. $3\Delta(\underline{1,2})$	W. $3\Pi(\underline{3})$
C. $2^5\Delta(\underline{9,10})$	J. $2^1\Sigma^-(\underline{6})$	Q. $1^1\Sigma^-(\underline{1})$	X. $1^1\Sigma^+(\underline{2})$
D. $5\Sigma^+(\underline{10})$	K. $5\Sigma^-(\underline{6})$	R. $1^1\Phi(\underline{4,5})$	Y. $1^1\Delta(\underline{1,2})$
E. $3^1\Delta(\underline{8})$	L. $3^3\Sigma^-(\underline{6})$	S. $2^1\Pi(\underline{4,5})$	Z. $X^3\Sigma^-(\underline{1})$
F. $3^1\Pi(\underline{7})$	M. $2^3\Delta(\underline{6,11})$	T. $1^1\Pi(\underline{3})$	
G. $3^3\Delta(\underline{9,10})$	N. $2^3\Sigma^-(\underline{6})$	U. $2^3\Pi(\underline{4,5})$	

Table V CI Energies for Group I and Group II Triplet States Using the $5\Sigma^-$ POL Basis
(The energies are presented in the same form as in Table II)

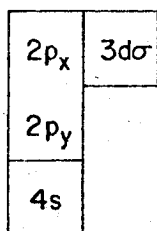
Group	Symmetry	$R = 2.7 a_0$	$3.0727 a_0$	$3.5 a_0$	$4.0 a_0$
II	$3^3\Delta(9,10)^a$	0.25584	0.31828	0.31571	0.30155
II	$3^3\Sigma^-(6)$	0.28719	0.32604	0.32384	0.30560
II	$2^3\Sigma^+(11)$	0.31635	0.34716	0.33004	0.29962
II	$2^3\Delta(6,11)$	0.33834	0.36196	0.33915	0.30431
II	$2^3\Sigma^-(6)$	0.35099	0.37198	0.34888	0.31914
I	$1^3\Sigma^+(2)$	0.27117	0.35974	0.37714	0.36027
I	$1^3\Delta(1,2)$	0.28160	0.36322	0.37877	0.36105
I	$2^3\Pi(4,5)$	0.35039	0.40580	0.39831	0.36915
I	$1^3\Phi(4,5)$	0.35869	0.40612	0.39944	0.36974
I	$1^3\Pi(3)$	0.38800	0.39459	0.38430	0.36040
I	$X^3\Sigma^-(1)$	0.42129	0.44038	0.41378	0.37331

^aSee footnote a of Table III

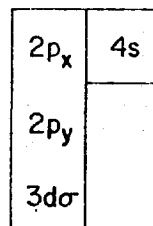
TABLE VI CI Energies for Group I and Group II Singlet States Using the $5\Sigma^-$ POL Basis
(The energies are presented in the same form as in Table II)

Group	Symmetry	R = 2.7 a_0	3.0727 a_0	3.5 a_0	4.0 a_0
II	$2^1\Sigma^+(1,1)^a$	0.24402	0.29750	0.29292	0.25646
II	$3^1\Pi(7)$	0.27240	0.31660	0.31081	0.30124
II	$2^1\Delta(6,11)$	0.25996	0.30356	0.29540	0.26359
II	$2^1\Sigma^-(6)$	0.33426	0.35708	0.33754	0.31361
I	$2^1\Pi(4,5)$	0.33863	0.39159	0.39573	0.36902
I	$1^1\Phi(4,5)$	0.33340	0.39308	0.39421	0.36852
I	$1^1\Pi(3)$	0.38079	0.39989	0.38597	0.36328
I	$1^1\Sigma^-(1)$	0.27929	0.36526	0.38052	0.36259
I	$1^1\Sigma^+(2)$	0.36456	0.39940	0.39116	0.36467
I	$1^1\Delta(1,2)$	0.38908	0.41564	0.39930	0.36770

^aSee footnote a of Table III

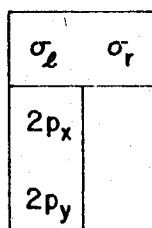


(6)



(7)

while the $X^3\Sigma^-$ state (1) has the coupling



(8)

(Here σ_ℓ and σ_r are the GVB orbitals of the bond pair.) Recombining (6) and (7) we can form one combination (9) which is orthogonal¹⁷ to the ground state

$$2^3\Sigma^- = \sqrt{\frac{2}{3}} \begin{array}{|c|c|} \hline 2p_x & 3d\sigma \\ \hline 2p_y & \\ \hline 4s & \\ \hline \end{array} + \frac{1}{\sqrt{3}} \begin{array}{|c|c|} \hline 2p_x & 4s \\ \hline 2p_y & \\ \hline 3d\sigma & \\ \hline \end{array} \quad (9)$$

and another orthogonal component (10) which overlaps the ground state,

$$3^3\Sigma^- = \begin{array}{|c|c|} \hline 3d\sigma & 4s \\ \hline 2p_x & \\ \hline 2p_y & \\ \hline \end{array} = -\frac{1}{\sqrt{3}} \begin{array}{|c|c|} \hline 2p_x & 3d\sigma \\ \hline 2p_y & \\ \hline 4s & \\ \hline \end{array} + \sqrt{\frac{2}{3}} \begin{array}{|c|c|} \hline 2p_x & 4s \\ \hline 2p_y & \\ \hline 3d\sigma & \\ \hline \end{array} \quad (10)$$

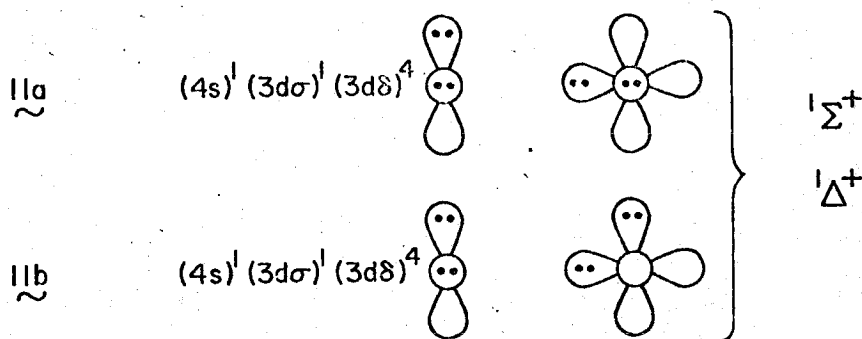
The ground state incorporates a component of (10) (there is a large matrix element connecting these states since they differ by a single excitation), leading to increased stability and a shorter bond length

for the $\chi^3_{\Sigma^-}$ state, while the upper state (10) is pushed up in energy (see Fig. 6) thereby rising above the other $^3_{\Sigma^-}$ component (9).¹⁷ The remaining component (5) of $^3_{\Delta^-}$ symmetry is orthogonal to the $1^3_{\Delta^-}$ state, since it involves singlet pairing of the π orbitals; whereas, the $1^3_{\Delta^-}$ state has these orbitals triplet coupled.

Consider now the singlet states. The two possible spin-couplings of 6 are

$$2^1_{\Delta^-} = \begin{array}{|c|c|} \hline 4s & 3d\sigma \\ \hline \pi_x & \pi_y \\ \hline \end{array} \quad 2^1_{\Sigma^-} = \begin{array}{|c|c|} \hline 4s & \pi_x \\ \hline 3d\sigma & \pi_y \\ \hline \end{array} \quad (11)$$

(where the $2^1_{\Sigma^-}$ state is expected to be below the $2^1_{\Delta^-}$ state). In addition, configuration $\underline{11}$ leads to $2^1_{\Sigma^+}$ and $2^1_{\Delta^+}$ states



The spin function for the $2^1_{\Sigma^+}$ and $2^1_{\Delta^+}$ states is the same as for the $2^1_{\Delta^-}$ state (these are, of course, degenerate components of the same state) and the $1^1_{\Sigma^+}$ and 1^1_{Δ} group I states. Thus, just as for the $\chi^3_{\Sigma^-}$ state these group I states are stabilized by building in components of the group II states and the corresponding group II states are pushed up in energy (see Fig. 6). The $2^1_{\Sigma^-}$ state, on the other hand, is orthogonal to the $1^1_{\Sigma^-}$ group I state, because its spin-function is orthogonal and thus its potential curve is not modified by interaction with the group I states.

D. Allowed Electronic Transitions and Properties of the Potential Curves. Energies were calculated at five points over the range 2.7 to $5a_0$ (e.g., see Table III). Cubic splines were fitted to these points for plotting Fig. 6, and the resulting R_e , D_e , and ω_e are tabulated in Table VII.

Transitions between group I states or between group II states are expected to be weak, since these are $3d \leftrightarrow 3d$ transitions, however symmetry allowed transitions between the two groups of states should be strong, since the group II states are charge transfer states relative to the group I states. Table VIII shows the calculated energies of the $0 \leftrightarrow 0$ bands for the allowed group I to group II singlet-singlet and triplet-triplet transitions.

Unfortunately, only very sketchy experimental information is available for NiO. The available spectroscopic data comes from emission spectra observed in flames or following the explosion of nickel wires in the presence of oxygen.⁴ The vibrational structure of three bands has been analyzed leading to zero-zero bands at 1.569, 2.036, and 2.620 eV. Numerous other bands are observed between 1.844 and 2.991 eV. This information is not adequate to make any specific assignments; however, given the transition energies in Table VIII, one would expect a complicated spectrum in the region from about 1.0 to 3.0 eV, as is observed. The vibrational frequencies for those states which have been analyzed fall in the range of $\sim 560 \text{ cm}^{-1}$ to $\sim 825 \text{ cm}^{-1}$, in the same range as the values calculated.

Table VII Spectroscopic Parameters for the States of NiO
 (Note that within each spin the most strongly
 bound state is listed at the bottom.)

Singlets			
State	D_e (eV)	R_e^0 (Å)	ω_e^b (cm ⁻¹)
$2^1\Sigma^+(\underline{11})^a$	0.16	1.71	800
$3^1\Pi(7)$	0.50	1.69	737
$2^1\Delta(\underline{6},\underline{11})$	0.27	1.69	770
$2^1\Sigma^-(\underline{6})$	1.67	1.61	806
$2^1\Pi(\underline{4},\underline{5})$	2.81	1.75	695
$1^1\Phi(\underline{4},\underline{5})$	2.82	1.73	746
$1^1\Pi(\underline{3})$	2.83	1.62	691
$1^1\Sigma^-(\underline{1})$	2.33	1.79	684
$1^1\Sigma^+(\underline{2})$	2.85	1.68	714
$1^1\Delta(\underline{1},\underline{2})$	3.26	1.64	771
Quintets			
$2^5\Delta(\underline{9},\underline{10})$	0.13	1.85	713
$5^5\Sigma^+(\underline{10})$	0.25	1.83	756
$1^5\Delta(\underline{8})$	1.26	1.72	819
$5^5\Sigma^-(\underline{6})$	2.24	1.63	827
Triplets			
$3^3\Delta(\underline{9},\underline{10})$	0.73	1.71	788
$3^3\Sigma^-(\underline{6})$	0.91	1.71	649
$2^3\Sigma^+(\underline{11})$	1.40	1.64	809
$2^3\Delta(\underline{6},\underline{11})$	1.80	1.61	830
$2^3\Sigma^-(\underline{6})$	2.08	1.60	829

Table VII - Continued

State	D_e (eV)	R_e^0 (Å)	ω_e^b (cm ⁻¹)
$1^3\Sigma^+(2)$	2.23	1.81	667
$1^3\Delta(1,2)$	2.28	1.80	668
$2^3\Pi(4,5)$	3.07	1.69	831
$1^3\Phi(4,5)$	3.07	1.69	775
$1^3\Pi(3)$	2.69	1.60	480
$X^3\Sigma^-(1)$	3.95	1.60	841

^aSee footnote a of Table III

^b ω_e is computed using masses of 16 for O and 58 for Ni.

Table VIII Allowed Transitions for NiO (The quoted excitation energies are adiabatic)

Transition ^c	Energy (eV) ^b
singlet ↔ singlet transitions	
$1^1_{\Delta}(\underline{1}, \underline{2}) \leftrightarrow 2^1_{\Delta}(\underline{6}, \underline{11})^a$	2.99
$1^1_{\Delta}(\underline{1}, \underline{2}) \leftrightarrow 3^1_{\Pi}(\underline{7})$	2.65
$1^1_{\Sigma^+}(\underline{2}) \leftrightarrow 2^1_{\Sigma^+}(\underline{11})$	2.69
$1^1_{\Sigma^+}(\underline{2}) \leftrightarrow 3^1_{\Pi}(\underline{7})$	2.24
$1^1_{\Pi}(\underline{3}) \leftrightarrow 2^1_{\Delta}(\underline{6}, \underline{11})$	2.56
$1^1_{\Pi}(\underline{3}) \leftrightarrow 2^1_{\Sigma^+}(\underline{11})$	2.67
$1^1_{\Pi}(\underline{3}) \leftrightarrow 3^1_{\Pi}(\underline{7})$	2.22
$1^1_{\Pi}(\underline{3}) \leftrightarrow 2^1_{\Sigma^-}(\underline{6})$	1.16
$1^1_{\Phi}(\underline{4}, \underline{5}) \leftrightarrow 2^1_{\Delta}(\underline{6}, \underline{11})$	2.55
$1^1_{\Phi}(\underline{4}, \underline{5}) \leftrightarrow 3^1_{\Pi}(\underline{7})$	2.21
$2^1_{\Pi}(\underline{4}, \underline{5}) \leftrightarrow 2^1_{\Delta}(\underline{6}, \underline{11})$	2.54
$2^1_{\Pi}(\underline{4}, \underline{5}) \leftrightarrow 2^1_{\Sigma^+}(\underline{11})$	2.65
$2^1_{\Pi}(\underline{4}, \underline{5}) \leftrightarrow 3^1_{\Pi}(\underline{7})$	2.20
$2^1_{\Pi}(\underline{4}, \underline{5}) \leftrightarrow 2^1_{\Sigma^-}(\underline{6})$	1.15
triplet ↔ triplet transitions	
$X^3_{\Sigma^-}(\underline{1}) \leftrightarrow 3^3_{\Sigma^-}(\underline{6})$	3.04
$1^3_{\Pi}(\underline{3}) \leftrightarrow 2^3_{\Sigma^-}(\underline{6})$	0.61
$1^3_{\Pi}(\underline{3}) \leftrightarrow 2^3_{\Delta}(\underline{6}, \underline{11})$	0.89
$1^3_{\Pi}(\underline{3}) \leftrightarrow 2^3_{\Sigma^+}(\underline{11})$	1.29
$1^3_{\Pi}(\underline{3}) \leftrightarrow 3^3_{\Sigma^-}(\underline{6})$	1.78
$1^3_{\Pi}(\underline{3}) \leftrightarrow 3^3_{\Delta}(\underline{9}, \underline{10})$	1.96

Table VIII - Continued

Transition ^c	Energy (eV) ^b
$2^3\Pi(\underline{4},\underline{5}) \leftrightarrow 2^3\Sigma^-(6)$	0.99
$2^3\Pi(\underline{4},\underline{5}) \leftrightarrow 2^3\Delta(\underline{6},\underline{11})$	1.27
$2^3\Pi(\underline{4},\underline{5}) \leftrightarrow 2^3\Sigma^+(\underline{11})$	1.67
$2^3\Pi(\underline{4},\underline{5}) \leftrightarrow 3^3\Sigma^-(6)$	2.17
$2^3\Pi(\underline{4},\underline{5}) \leftrightarrow 3^3\Delta(\underline{9},\underline{10})$	2.35
$1^3\Phi(\underline{4},\underline{5}) \leftrightarrow 2^3\Delta(\underline{6},\underline{11})$	1.27
$1^3\Phi(\underline{4},\underline{5}) \leftrightarrow 3^3\Delta(\underline{9},\underline{10})$	2.35
$1^3\Delta(\underline{1},\underline{2}) \leftrightarrow 3^3\Delta(\underline{9},\underline{10})$	1.55
quintet \leftrightarrow quintet transitions	
$1^5\Delta(\underline{8}) \leftrightarrow 2^5\Delta(\underline{9},\underline{10})$	1.11

^aSee footnote a of Table III

^bThe transition energies correspond to the difference in D_e values, thus they are not corrected for differences in zero point vibrational energy.

^cThe following transitions are not allowed because the integral over spin coordinates is zero:



III. Calculation Details

A. The Modified Effective Potential. In order to carry out calculations of the type described here at reasonable cost, it is expedient to use an effective potential to replace the 18-electron Ar core of the transition metal. Toward this end, Melius, Olafson, and Goddard¹⁸ developed an effective potential, referred to as the ab initio effective potential (AIEP). This AIEP leads to near ab initio accuracy with errors < 0.1 eV in excitation energies. However, for the Ni atom ab initio calculations carried out with the usual basis and level of correlation lead to very large errors (2 eV) in the separations of the states. For example, using the Wachters basis,¹⁹ the $s^1 d^9(^3D)$ state is calculated in the Hartree-Fock (HF) description to be 2.29 eV above the $s^2 d^8(^3F)$ state; whereas, the experimental separation is 0.03 eV.^{7,8}

The error involved in the usual HF description of the atoms is found to result from: 1) a bias in the d basis toward the $s^2 d^8$ state, and 2) differential correlation effects. The basis set problem can be alleviated by addition of another set of 3d primitives ($\alpha = \sim 0.15$) leading to a 3D - 3F separation of only 1.16 eV. Inclusion of CI effects among the ten valence electrons (but without using f functions) leads to a final energy separation of 0.28 eV.²⁰ Thus, one approach to obtaining a proper description of molecules involving the Ni atom is to include the extra 3d functions and the CI effects necessary to obtain the proper atomic separations. This is a very expensive and cumbersome procedure for molecules and we have attempted to avoid it. The extra effects

necessary to get the correct atomic separations do not lead to significant changes in the shapes of the orbitals in the valence region,²⁰ and furthermore the necessary correlation effects are intra-atomic in nature and should be modified only slightly due to bond formation. Thus a simpler but nearly equivalent procedure is to add additional terms to the ab initio effective potential in such a way as to reproduce the atomic separations for HF calculations using the usual Wachter basis, but without significantly altering the orbital shapes. This procedure has been developed by Sollenberger, Goddard, and Melius⁹ and the resulting potential is referred to as the modified effective potential (MEP).

The MEP leads to reasonable bond lengths and bond energies for NiH and FeH,⁹ and for NiCO,¹⁰ whereas corresponding ab initio calculations lead to very poor results (e.g., no bonding in NiCO). This MEP was used for the calculations described here.

B. Basis Set and Geometry. The basis for Ni was selected from the set optimized for the ground states of the third-row atoms by Wachters.¹⁹ We have used all five d primitives for each of the five types, but as discussed in Ref. 18, only the outer four s-functions are needed for describing the coreless Hartree-Fock orbital. The inner four d-primitives were contracted together and the inner two s-functions were contracted together with the relative coefficients based on Hartree-Fock calculations for the $s^2d^8(^3F)$ state of the Ni atom.⁹ In addition, a single p primitive with $\alpha = 0.12$ was added in each direction (to allow polarization effects involving the 4s orbital). The final basis for Ni is identical to that used for the NiCO calculations¹⁰

previously reported.

The basis for oxygen is the Dunning (3s,2p) contraction²² of the Huzinaga (9s,5p) basis. This contraction is double zeta for the valence region but uses a single 1s-like contracted function and leads to energies which are generally within 0.0001 h of those obtained with the "double zeta" contraction.²³ The oxygen basis was augmented with a single set of d-primitives (orbital exponent $\alpha = 1.04$).

The Ni-O distance was varied from 2.7 to 5.0 bohr.

IV. The CI Calculations

As discussed in section II, there are no group I quintet states, thus we were able to describe the group II quintet states by CI calculations using the $^5\Sigma^-$ vectors as a basis. On the other hand, for the group II singlet and triplet states a similar approach leads to two problems: 1) In order for the group II states to be true upper bounds, the lower roots corresponding to the group I states must be adequately represented, and 2) couplings between the group I and group II states are important and are expected to modify both sets of potential curves.

The solution to these problems is to use in the CI an orbital basis capable of describing both sets of states. This approach is developed below. For the group I states, the problem is less serious, in the sense that calculations using the vectors of the X^3^- state as a basis do lead to upper bounds to the energy and such calculations were carried out for comparison. (Of course inclusion of the additional group II basis functions and configurations leads to a better

description of the group I states and alters the potential curves.)

For the group I CI calculations, the starting point for the CI orbital basis was the set of GVB orbitals for configuration $1a$. Because configuration $1a$ is only one of two degenerate configurations describing the $X^3\Sigma^-$ state, the π_x and π_y orbitals were not equivalent. In order to generate an equivalent set of π orbitals for the CI, the π_x orbitals were rotated by 90° and combined with the π_y orbitals to obtain two π_x orbitals and two π_y orbitals. To provide sufficient flexibility to describe the excited states, this π space was augmented by adding the more diffuse components of the Ni $3d\pi$ and O $2p\pi$ -like functions after orthogonalizing to the previous two π functions. For similar reasons the GVB δ orbitals were augmented by adding the more diffuse δ -like functions (suitably orthonormalized). The resulting basis (referred to hereafter as the $^3\Sigma^-$ basis) consists of 17 functions [including the O(1s)-like function which was kept doubly occupied in all configurations].

The basis for the quintet states was constructed using the GVB orbitals of the $^5\Sigma^-$ state (configuration 6) and similar procedures for generating the virtuals. This basis (again 17 functions) is referred to hereafter as the $^5\Sigma^-$ basis.

For describing the group I and group II singlet and triplet states simultaneously, the $^5\Sigma^-$ basis was augmented by adding to the basis the $3d\sigma$ -like orbital and the GVB natural orbitals of the bond pair from the $X^3\Sigma^-$ state as polarization functions. This basis of 20 functions is referred to

as the $5\Sigma^-$ POL basis. In addition to leading to a good description of the group II singlet and triplet states (as was expected given the origin of the basis), the $5\Sigma^-$ POL basis was found to lead to better energies for some of the group I states (due to a better description of the ionic group II-like components in those states). The other group I states are described equally well with either this basis or with the $3\Sigma^-$ basis. Since the $5\Sigma^-$ POL basis leads to a good description of the potential curves for both sets of states, it was used to generate the potential curves of Fig. 6.

The procedure for selecting configurations consisted of selecting first a set of reference configurations consisting of (essentially) the dominant configurations for all states of interest, and using these to define a set of generating configurations from which all single excitations were included in the CI. For example, to describe the group I states the configurations 1-5 could be used as the reference configurations. At this point, the configurations were partitioned by symmetry (using the C_{2v} point group). From the reference configurations a set of generating configurations was obtained which consisted of all excitations within the GVB space (here defined to include the π orbitals and for the group I states the natural orbitals of the sigma bond pair) with the restriction that single excitations were allowed within subsets of symmetry sigma, π_x , and π_y but not between subsets, and all products were included in the final list. Given the set of generating configurations, all single excitations (singles) were then allowed from these into the GVB space plus

virtual space. The final list of configurations thus included singles and doubles within the GVB space relative to the reference configurations plus readjustment effects over all the generating configurations. This approach provides, we believe, an effective and relatively simple method for consistently treating a large number of excited states simultaneously.

Table IX shows the generating configurations for the group I states over the $^3\Sigma^-$ basis. Allowing single excitations from the generating configurations into the full CI basis led to (130, 232), (92, 208), (122, 326), (92, 324), (158, 626) [(spatials, spin-eigenfunctions)] for the 1A_1 , 1A_2 , 3A_1 , 3A_2 , and 3B_1 CI's, respectively.

Table X shows the generating configurations for the group II quintet states over the $^5\Sigma^-$ basis. Allowing all singles from the generating configurations into the full CI basis led to (106, 242) and (128, 280) [(spatials, spin eigenfunctions)] for the 5A_1 and 5A_2 CI's respectively.

Table XI shows the generating configurations used for the singlet and triplet group I and group II states using the $^5\Sigma^-$ POL basis. From these generating configurations all singles were allowed among the GVB orbitals plus the π - and δ -like virtuals. For the starred configurations (which have group I character) we also allowed all singles into the sigma virtuals (obtained from the group I orbitals). This led to (410, 852), (320, 826), (278, 982), (398, 1282), (320, 1332), and (378, 1586) [(spatials, spin-eigenfunctions)] for the 1A_1 , 1A_2 , 1B_1 , 3A_1 , 3A_2 , 3B_1 CI's, respectively.

Table IX Generating Configurations for Group I States over the $3\Sigma^-$ Basis

		Configuration ^a															
Ni(3d σ)	σ	σ^*	Ni(3d π_x)	O(2p π_x)	Ni(3d π_y)	O(2p π_y)	Ni(3d δ_{xy})	Ni(3d $\delta_{x^2-y^2}$)									
2	$\begin{pmatrix} 2 \\ 1 \end{pmatrix}$	$\begin{pmatrix} 0 \\ 1 \end{pmatrix}$	$\begin{pmatrix} 2 \\ 1 \\ 2 \\ 2 \\ 0 \\ 2 \end{pmatrix}$	$\begin{pmatrix} 2 \\ 1 \\ 2 \\ 0 \\ 2 \\ 2 \end{pmatrix}$	$\begin{pmatrix} 1 \\ 2 \\ 2 \\ 2 \\ 2 \\ 0 \end{pmatrix}$	$\begin{pmatrix} 1 \\ 2 \\ 0 \\ 2 \\ 2 \\ 2 \end{pmatrix}$	2	2									
									A1	2	2	2	2				
														2	2	2	2
2	$\begin{pmatrix} 2 \\ 1 \end{pmatrix}$	$\begin{pmatrix} 0 \\ 1 \end{pmatrix}$	$\begin{pmatrix} 2 \\ 1 \\ 2 \\ 2 \\ 0 \\ 2 \end{pmatrix}$	$\begin{pmatrix} 2 \\ 1 \\ 2 \\ 0 \\ 2 \\ 2 \end{pmatrix}$	$\begin{pmatrix} 1 \\ 2 \\ 2 \\ 2 \\ 2 \\ 0 \end{pmatrix}$	$\begin{pmatrix} 1 \\ 2 \\ 2 \\ 2 \\ 2 \\ 0 \end{pmatrix}$	2	2									
									A2	2	2	2	2				
														2	2	2	2
2	$\begin{pmatrix} 2 \\ 1 \end{pmatrix}$	$\begin{pmatrix} 0 \\ 1 \end{pmatrix}$	$\begin{pmatrix} 2 \\ 1 \\ 2 \\ 2 \\ 0 \\ 2 \end{pmatrix}$	$\begin{pmatrix} 2 \\ 1 \\ 2 \\ 0 \\ 2 \\ 2 \end{pmatrix}$	$\begin{pmatrix} 1 \\ 2 \\ 2 \\ 2 \\ 2 \\ 0 \end{pmatrix}$	$\begin{pmatrix} 1 \\ 2 \\ 2 \\ 2 \\ 2 \\ 0 \end{pmatrix}$	2	2									
									B1	2	2	2	2				
														2	2	2	2
1	$\begin{pmatrix} 2 \\ 1 \end{pmatrix}$	$\begin{pmatrix} 0 \\ 1 \end{pmatrix}$	$\begin{pmatrix} 2 \\ 1 \\ 2 \\ 2 \\ 0 \\ 2 \end{pmatrix}$	$\begin{pmatrix} 2 \\ 1 \\ 2 \\ 0 \\ 2 \\ 2 \end{pmatrix}$	$\begin{pmatrix} 1 \\ 2 \\ 2 \\ 2 \\ 2 \\ 0 \end{pmatrix}$	$\begin{pmatrix} 1 \\ 2 \\ 2 \\ 2 \\ 2 \\ 0 \end{pmatrix}$	2	2									

^a σ and σ^* are the natural orbitals of the sigma bond pair

^b The parentheses indicate that we take products of the configurations in the left parentheses with those in the right parentheses (e.g., for the A1 case there are $2 \times 6 = 12$ configurations).

Table X Generating Configurations for Group II Quintets over the $5\Gamma^-$ Basis

		Configuration									
		Ni(3d _z)	Ni(4s)	Ni(3d _{π_x)}	O(2p _{π_x)}	Ni(3d _{π_y)}	O(2p _{π_y)}	Ni(3d _{xy})	Ni(3d _{z²-y²)}		
A1	1	1	1	(1 1)	1	2	2	2	2	2	2
				(2 2)	2	1	1				
	2	1	(2 1)	1	2	1	1	1	2	2	2
			(1 2)	2	1	2					
A2	1	1	(1 2)	1	2	1	1	1	2	2	2
			(2 1)	2	1	2					
	2	1	(2 2)	2	1	1	1	1	2	2	2
			(1 1)	1	2	1	2				
B1	1	1	(2 1)	1	2	1	1	1	2	2	2
			(1 2)	2	1	2					
	2	1	(2 2)	2	1	1	1	1	2	2	2
			(1 1)	1	2	1	2				

V. Summary

We find that the low lying states of NiO all involve the s^1d^9 (3D) configuration of the Ni atom and lead to two groups of states (denoted as group I and group II respectively). The group I states involve O atom configurations with a singly occupied O ($2p\sigma$) orbital leading to formation of a covalent sigma bond with the singly occupied Ni($4s$) orbital. The remaining 3d hole may be taken in a $3d\sigma$, $3d\pi$, or $3d\delta$ orbital respectively. The $3d\pi$ hole leads to $^3\Sigma^-$, $^1\Delta$, $^1\Sigma^+$, $^1\Sigma^-$, $^3\Delta$, and $^3\Sigma^+$ states, analogous to the corresponding states of O_2 , while the $3d\sigma$ hole leads to $^1,^3\Pi$ states and the $3d\delta$ hole leads to $^1,^3\Pi$ and $^1,^3\Phi$ states. We find that the ground state of NiO is the $^3\Sigma^-$ state which has an electronic structure analogous to the ground state of O_2 . The D_0 and R_e values for the ground state are 89.9 Kcal/mole and 1.60\AA respectively. The D_0 value is in good agreement with the experimental value of 86.5 ± 5 Kcal/mole, while the R_e value for NiO is not known experimentally.

The group II states involve an O atom configuration where the O($2p\sigma$) orbital is doubly occupied. The Ni($4s$) orbital here is non-bonding and builds in 4p character to move away from the oxygen orbitals. The bonding is somewhat analogous to the bonding in NiCO, but the high electronegativity of oxygen leads to substantial delocalization of the doubly occupied Ni($3d\pi$) orbitals onto oxygen simultaneous with delocalization of the doubly occupied O($2p\sigma$) orbital onto Ni. Thus the $^5\Sigma^-$ state with a $3d\sigma$ hole is lowest.

Taking the singlet and triplet couplings of the orbitals of the group II quintet states leads to other group II states some of which are strongly coupled with the group I states, leading to stabilization of certain group I states and concomitant destabilization of certain group II states. Since the group II states are charge transfer states relative to the group I states, allowed transitions between the two sets of states should be strong leading to the prediction of numerous allowed transitions in the energy range of ~ 1.0 to ~ 3.0 eV (in the range where emission bands are observed).

References

1. Partially supported by a grant (DMR74-04965) from the National Science Foundation.
2. Acknowledgment is made to the donors of The Petroleum Research Fund, administered by the ACS, for partial support of this research. (PRF#7683-AC6).
3. For NiO some spectroscopic information is available from the analysis of emission spectra, as summarized in Ref. 4. The bond energy is known (Ref. 5).
4. B. Rosen, Tables of Constants and Numerical Data, Simone Bourcier, Ed. (Pergamon Press, London 1970).
5. R. T. Grimley, R. P. Burns, and Mark G. Ingraham, J. Chem. Phys., 35(2), 551 (1961).
6. W. A. Goddard III, T. H. Dunning, Jr., W. J. Hunt, and P. J. Hay, Accts. Chem. Res., 6, 368 (1973).
7. The quoted atomic separations are obtained by taking a weighted average over the spectral levels corresponding to a given L and S (spin-orbit interactions are not included in our calculations). The values are from Ref. 8.
8. C. E. Moore, "Atomic Energy Levels", Vol. II, National Bureau of Standards, 1952.
9. M. J. Sollenberger, Masters Thesis, California Institute of Technology, 1975; C. F. Melius, W. A. Goddard III and M. J. Sollenberger, to be published.
10. S. P. Walch and W. A. Goddard III, J. Amer. Chem. Soc., 98, 7908 (1976).

11. For a discussion of the states of O_2 see B. J. Moss and W. A. Goddard III, *J. Chem. Phys.*, 63, 3523 (1975); and B. J. Moss, F. W. Bobrowicz, and W. A. Goddard III, *ibid*, 63, 4632 (1975).
12. This is from Mulliken populations. Generally, these populations indicate a greater charge transfer than would be indicated, for example, by the dipole moment. Thus, the populations although indicative of relative charge transfer should not be taken too literally.
13. The discussion here is related to the approach used by C. W. Wilson, Jr. and W. A. Goddard III, *Chem. Phys. Lett.*, 5, 45 (1970); *Theor. Chim. Acta*, 26, 195,211 (1972)
14. In Fig. 4 and Fig. 6 we draw the $1^3\Pi$ and $2^3\Pi$ states as crossing. Actually, there is a matrix element connecting them which leads to a small energy gap and adiabatic states which do not cross.
15. E. I. Alessandrini and J. F. Freedman, *Acta Crystallogr.*, 16, 54 (1963); G.W.C. Wyckoff, *Crystal Structures* (Interscience, New York, 1964), 2nd ed.
16. The spin-eigenfunctions (SEF's) used are as follows:

For the 4-electron singlet:

$$G1 = a[\phi_1\phi_2\phi_3\phi_4 \frac{1}{\sqrt{4}} \{(\alpha\beta-\beta\alpha)(\alpha\beta-\beta\alpha)\}] =$$

ϕ_1	ϕ_2
ϕ_3	ϕ_4

$$G2 = a[\phi_1\phi_2\phi_3\phi_4 \frac{1}{\sqrt{12}} \{2\alpha\alpha\beta\beta + 2\beta\beta\alpha\alpha - (\alpha\beta+\beta\alpha)(\alpha\beta+\beta\alpha)\}] =$$

ϕ_1	ϕ_3
ϕ_2	ϕ_4

For the 4-electron triplet

$$G1 = a[\phi_1\phi_2\phi_3\phi_4 \frac{1}{\sqrt{2}} \{(\alpha\beta-\beta\alpha)\alpha\alpha\}] =$$

ϕ_1	ϕ_2
ϕ_3	
ϕ_4	

$$G2 = \mathcal{A}[\phi_1\phi_2\phi_3\phi_4 \frac{1}{\sqrt{6}} \{2\alpha\alpha\beta\alpha - (\alpha\beta+\beta\alpha)\alpha\alpha\}] = \begin{array}{|c|c|} \hline \phi_1 & \phi_3 \\ \hline \phi_2 & \\ \hline \phi_4 & \\ \hline \end{array}$$

$$G3 = \mathcal{A}[\phi_1\phi_2\phi_3\phi_4 \frac{1}{\sqrt{12}} \{3\alpha\alpha\alpha\beta - (\beta\alpha\alpha+\alpha\beta\alpha+\alpha\alpha\beta)\alpha\}] = \begin{array}{|c|c|} \hline \phi_1 & \phi_4 \\ \hline \phi_2 & \\ \hline \phi_3 & \\ \hline \end{array}$$

where horizontally coupled orbitals (i.e., $\begin{array}{|c|c|} \hline a & b \\ \hline \end{array}$) indicate that the spin-function is asymmetric under interchange of a and b, while vertically coupled orbitals (i.e., $\begin{array}{|c|} \hline a \\ \hline b \\ \hline \end{array}$) indicate that the spin-function is symmetric under interchange of a and b.

17. Since the SEF's are orthogonal, states corresponding to different spin-eigenfunctions (SEF's) can at most be coupled by transpositions arising from the antisymmetrizer. The resulting matrix elements involve two-electron exchange integrals and are generally smaller than for cases where the two states have the same SEF (in which case they can have one-electron terms connecting them, if they differ by only a single excitation).
18. C. F. Melius, B. D. Olafson, and W. A. Goddard III, Chem. Phys. Lett., 28, 457 (1974); C. F. Melius and W. A. Goddard III, Phys. Rev. A, 10, 1528 (1974).
19. A.J.H. Wachters, J. Chem. Phys., 52, 1033 (1970).
20. T. A. Smedley and W. A. Goddard III, unpublished calculations. Similar effects have been observed by Brooks and Schaefer for the Mn atom (Ref. 21).

21. B. R. Brooks and H. F. Schaefer III, "A Model Transition Metal-Carbene System $MnCH_2$ ", to be published.
22. T. H. Dunning, Jr. and P. J. Hay, Gaussian Basis Sets for Molecular Calculations, in Modern Theoretical Chemistry, Vol. 2, ed. H. F. Schaefer III, Plenum Press, to be published. The p functions are the same as in Ref. 23, the tightest seven s functions are contracted into a single s function based on the 1s HF orbital, the second and third most diffuse are contracted into a basis function based on the 2s HF orbital; the most diffuse function is uncontracted.
23. T. H. Dunning, Jr., J. Chem. Phys., 53, 2823 (1970).

Appendix A. Bond Energies for Bridged and Linear Sites

In this appendix we tabulate geometry and bond energy results for the bonding of various atoms and molecules at (i) linear sites which involve bonding directly above a surface Ni atom (here we use a single Ni atom to represent the surface), and (ii) at bridged sites involving second nearest neighbor Ni atoms (here we use two Ni atoms separated by $\sqrt{2}$ times the nearest neighbor separation to represent the surface).

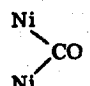
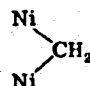
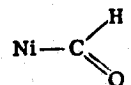
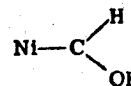
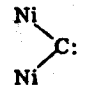
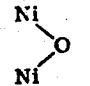
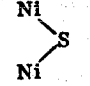
While the bond energies are not directly comparable between linear and bridged sites (since the bridged sites are expected to involve greater disruption of metal-metal bonds), we expect that comparing different species for the same site should give correct relative bond energies. This information on bond energies is not available experimentally and is essential for establishing mechanisms for reactions on Ni surfaces [1].

The results are summarized in Table 1. Except as noted the calculations are by the author. The NiCO, NiO, NiS, Ni₂O, and Ni₂S calculations have been described elsewhere in this thesis. The Ni₂CO, Ni₂CH₂, NiCHO, and Ni₂C calculations are discussed below.

I. Basis Sets

The Ni basis and effective potential have been described previously [2]. The C and O basis sets are valence double zeta and are the same as for the NiCO calculations [2]. The H basis is a (3,1) contraction of a GTO-4 expansion of an H(1s)-like Slater function with exponent $\zeta = 1.2$ [3]. For certain calculations the C basis was

TABLE 1. Results from GVB-CI calculations. D_0 is the bond energy, ΔH_f is the standard heat of formation of the chemisorbed intermediate, R_{NiX} is the bond length to the Ni, Q is the charge transfer,^a and ν_{MX} is the calculated vibrational frequency.

	D_0 (kcal/mole)	ΔH_f (kcal/mole)	R_{NiX} Å	Q electrons	ν_{MX} (cm^{-1})
Ni-H ^b	64	-12	1.45	0.12	1911
Ni-CO	26	-52	1.90	-0.05	428
	32	-58	1.94	0.59	287
Ni=CH ₂ ^c	65	27	1.78	0.56	1181
	122	-30	1.91	0.70	
Ni-CH ₃ ^c	60	-25	1.87	0.42	1066
	57	-47		0.30	
	56	-4		0.36	
	91	80			
Ni=O	89	-29	1.60	0.55	841
	101	-41	1.79	0.91	170
Ni-O _H ^d	50	-41	1.72		
Ni=S	76	-9	1.91	0.38	483
	123	-56	2.04	0.57	298

^a This is from Mulliken populations and need not be a good measure of total charge transfer.

^b M. J. Sollenberger, M. S. Thesis, California Institute of Technology, 1975.

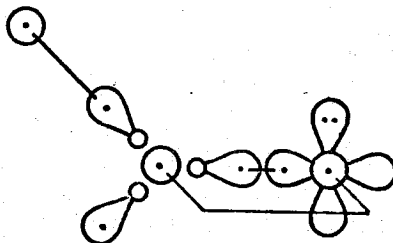
^c A. K. Rappé and W. A. Goddard III, J. Amer. Chem. Soc., in press.

^d C. F. Melius, unpublished calculations.

augmented with a set of d functions ($\alpha = 0.6769$).

II. NiHCO

Qualitatively the HCO radical has the electronic configuration

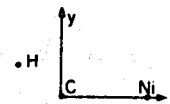
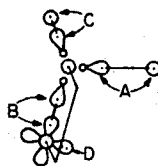
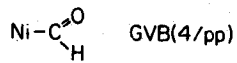


which we may think of in terms of bonding an H atom to one of the lobes of CO, leaving a singly occupied lobe orbital. Since the lobes of the CO lone pair have a large overlap (~ 0.792) in free CO unpairing them costs a substantial amount of energy and hence the HC bond energy in HCO is small (only 16.9 Kcal/mole) [4].

Coupling the 4s orbital of the $4s^1 3d^9$ Ni atom configuration with the singly occupied orbital of HCO leads to the ground state of NiHCO. We find that the most favorable orientation of the hole in the 3d shell of the Ni atom is in an orbital which is delta-like with respect to the NiC bond axis. In the calculations we correlated the CC sigma and pi pairs, the CH bond, and the NiC bond [i.e., a GVB(4/pp) wavefunction].

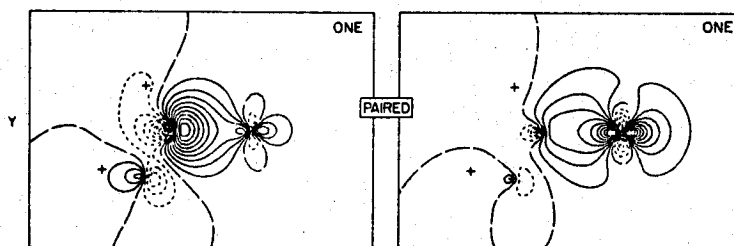
Selected orbitals of the GVB(4/pp) wavefunction for NiHCO are shown in Figure 1. The NiC bond (Fig. 1a) has one component which is basically Ni(4s)-like, while the other component corresponds to one of the lobes of the CO lone pair. The other lobe of the CO lone pair is coupled to a H(1s)-like orbital, leading to the CH bond (Fig. 1c). The CO bond pair (Fig. 1b) is similar to the sigma bond pair in CO. The O lone pair (Fig. 1d) corresponds to a doubly occupied O(2p) orbital. In

Fig. 1. Selected orbitals of the GVB(4/pp) wavefunction of NiHCO. Unless otherwise noted, all plots have uniformly spaced contours with increments of 0.05 a.u. Positive contours are indicated by solid lines, negative contours are indicated by short dashes, and nodal lines are indicated by long dashes. The same conventions are used for other figures.

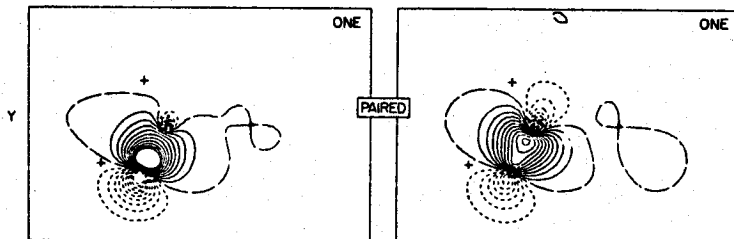


•O

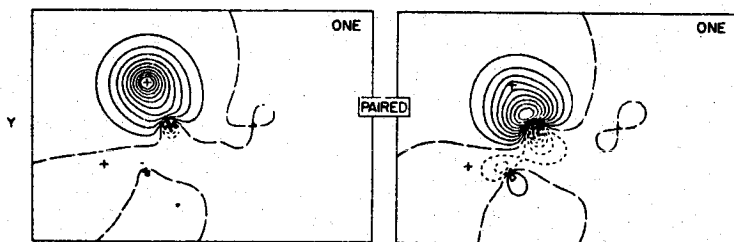
A. NiC BOND PAIR



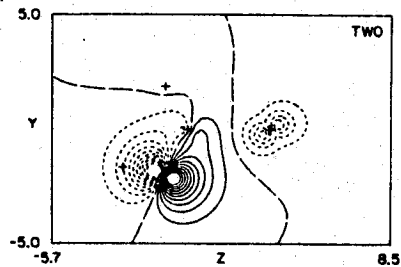
B. CO BOND PAIR



C. CH BOND PAIR



D. O LONE PAIR



addition to the orbitals shown, there is a π bond perpendicular to the plane of the paper as indicated in the drawing at the top of Figure 1.

The geometry for the HCO part of the molecule was taken to be the experimental geometry for free HCO ($r_{\text{CH}} = 1.11\text{\AA}$, $r_{\text{CO}} = 1.17\text{\AA}$, $\angle \text{HCO} = 127^\circ$) [5]. The Ni-C distance was taken as 1.84\AA (from $\text{Ni}(\text{CO})_4$); this is probably a bit short for a Ni-C sigma bond (1.87\AA is optimum for NiCH_3). The OC Ni angle was taken as 116.5° which corresponds to positioning the Ni atom approximately in the direction of maximum overlap with the radical orbital of the free HCO molecule.

The calculated $D_e(\text{Ni-HCO})$ is 57 Kcal/mole. (This calculation did not include d functions on the carbon, which we estimate would contribute about 3 Kcal/mole, leading to 60 Kcal/mole as our best estimate of D_e .)

III. Ni_2CH_2

The ground state of CH_2 [6] is the 3B_1 state which has the electronic configuration



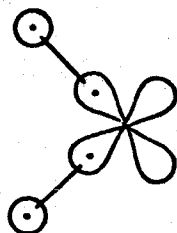
(1)

Bonding the CH_2 to two Ni atoms at the $\sqrt{2}a$ separation leads to two equivalent NiC bonds in the xz plane (i.e., the carbon has a tetrahedral geometry as in CH_4). Here the holes in the 3d shells of the two Ni atoms were taken to be delta-like with respect to the NiC bond axes, and we correlated both NiC bonds and both CH bonds [GVB(4/pp) wavefunction].

The CH distance was fixed at 1.10\AA , while the NiC distance and HCH angle were optimized. The Ni-C distance was optimized first for a fixed HCH angle of 110° . This led to an optimum NiC distance of 1.913\AA (see Table 2). The HCH angle was then optimized using the optimum NiC distance, leading to an optimum angle of 107.6° (quite close to the angle originally assumed). For the optimum geometry a set of d functions ($\alpha = 0.6769$) was added and the bond energy was calculated relative to a comparable calculation for the 3B_1 ground state of CH_2 at the experimental geometry ($r_{\text{CH}} = 1.071\text{\AA}$, $\angle \text{HCH} = 135^\circ$) [6]. The resulting D_e value is 122 Kcal/mole (d functions here contributed ~ 3 Kcal/mole) or about twice a typical NiC bond energy (60 Kcal/mole for NiCH_3).

IV. Ni_2C

Here we solved for the state corresponding to the singlet state (1A_1) of CH_2



(2)

using the optimum geometry from the Ni_2CH_2 calculation. The two NiC bond pairs were correlated [GVB(2/pp) wavefunction]. The resulting D_e is 91 Kcal/mole.

V. Ni_2CO

In bonding CO to a single Ni atom we found that the CO molecule could be thought of as a triple bond with a lone pair on the carbon

Table 2. Ni_2CH_2 Geometry Optimization (Subtract the quoted value from -120.0 to get the total energy in hartrees)^a

$d_{\text{Ni-C}}(\text{\AA})$	HCH Angle		
	105°	110°	115°
1.8884		0.11713	
1.9130 ^b	0.11755	0.11758	0.11653
1.9295		0.11741	
2.0000		0.11315	

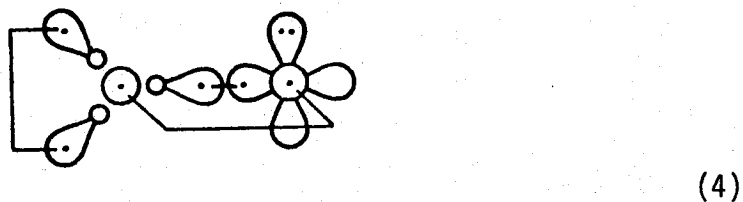
^aThe optimum geometry corresponds to a Ni-C distance of 1.9130^oÅ, a NiCNi angle of 133.7° and an HCH angle of 107.6°. (A C-H bond length of 1.10^oÅ was assumed.) The D_e value is 122 Kcal/mole with respect to two Ni atoms and the 3B_1 ground state of CH_2 in the same basis.

^bThis is the optimum NiC distance.

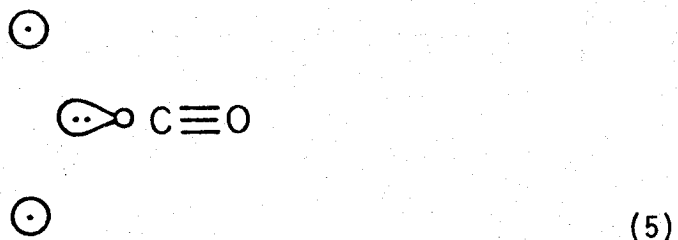


Here the 4s orbital of the Ni atom hybridizes away from the CO and the main bonding effect involves interaction between the lone pair of the CO (5σ orbital) and the partially exposed $3d^9$ core of the Ni.

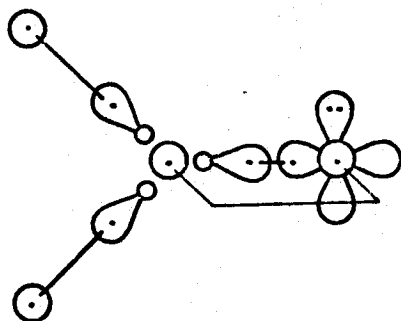
However, for the free CO molecule there is an important angular correlation effect involving the lone pair, and (3) may be thought of as a superposition of two degenerate structures, one of which is



This leads to two possible modes of bonding CO to a pair of Ni atoms at the second nearest neighbor separation (i) a structure analogous to the bonding of CO to a single Ni atom in which the lone pair of (3) inserts between the two Ni atoms



and (ii) a structure involving two sigma bonds between the Ni(4s) orbitals and the lobes of (4) as in formaldehyde



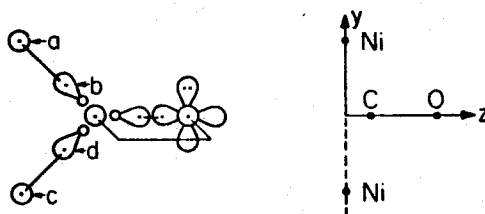
(6)

(5) and (6) both correspond to the same Hartree-Fock (HF) configuration, and thus have a large overlap with each other [an analogous situation exists for (3) and (4)]. However, when correlation effects are included we may solve for either (5) or (6). Doing this we find that (6) is 0.45 eV below (5). Thus, we optimized the geometry and calculated the D_e value based on (6).

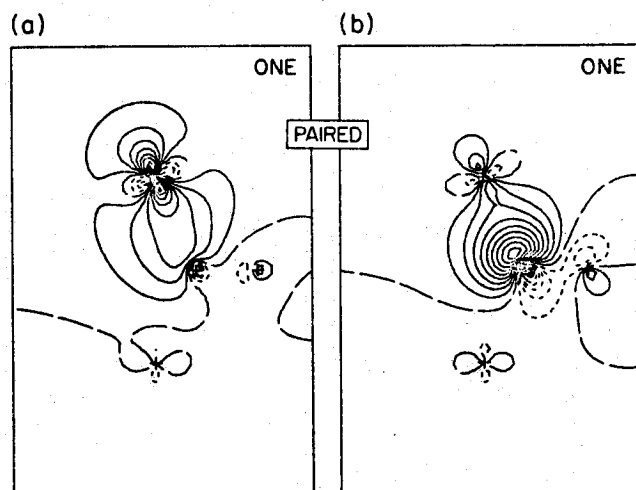
In solving for the GVB wavefunction corresponding to (6), we correlated the two NiC bonds and the CO sigma and pi bonds [GVB(4/pp) wavefunction]. The holes in the 3d shells of the two Ni atoms were taken to be delta-like with respect to the NiC bond axes (as for Ni_2CH_2).

We show the bond orbitals of the GVB(4/pp) wavefunction of (6) in Figure 2. The orbitals corresponding to the lobes of the CO lone pair are shown in Figure 2b and Figure 2d. The two bond pairs correspond to bonds between one of the lobes and a 4s-like orbital on one Ni atom. Looking at one bond pair (Fig. 1ab) we see that the Ni(4s)-like component has distorted in the direction of the C indicating a somewhat ionic bond. The total charge transfer here is 0.60 electrons from Ni to CO as compared with a slight charge transfer from CO to Ni (0.05 electrons) for NiCO.

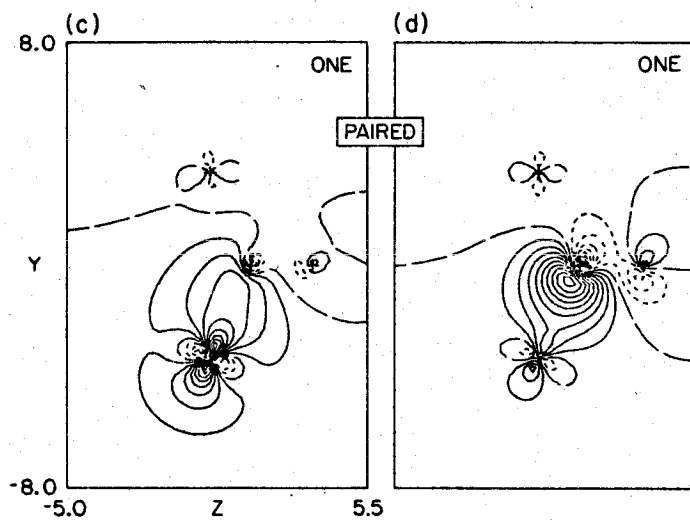
Fig. 2. The NiC bond orbitals of the GVB(4/pp) wavefunction of Ni_2CO .

Ni₂CO BOND ORBITALS

UPPER Ni-C BOND



LOWER Ni-C BOND



The CO distance was fixed at $2.17 a_0$ which is close to the optimum CO distance in $\text{Ni}(\text{CO})_4$ and is the same distance used for the NiCO calculations [2]. The NiC distance was optimized (see Table 3), leading to an optimum NiC distance of 1.942 \AA (slightly larger than for the Ni_2CH_2 case) which corresponds to a NiCNi angle of 130.1° . The calculated D_e value is 1.42 eV (33 Kcal/mole), while the ω_e value is 287 cm^{-1} [somewhat smaller than for the NiCO case (428 cm^{-1})].

Table 3. Ni_2CO Geometry Optimization ($\text{Ni-Ni} = \sqrt{2}a$)

$d(a_0)$ ^a	Energy (hartree) ^{b,c}
1.2	-193.78467
1.4224	-193.78813
1.6	-193.78860
1.8	-193.78638

^a d is the distance from the C to a line connecting Ni1 and Ni2.

^b For a GVB(4/pp) wavefunction. See text.

^c The optimum d is 0.819\AA which corresponds to a Ni-C distance of 1.942\AA and a NiCNi angle of 130.1° . The ω_e value is 287 cm^{-1} , somewhat smaller than for the NiCO case (428 cm^{-1}). The D_e value is 1.42 eV ($\sim 33\text{ Kcal/mole}$).

References

1. For an application of these results to the mechanism of methanation of CO over a Ni catalyst, see W. A. Goddard III, S. P. Walch, A. K. Rappé, T. H. Upton, and C. F. Melius, J. Vac. Sci. Tech. 14, 416 (1977).
2. S. P. Walch and W. A. Goddard III, J. Amer. Chem. Soc. 98, 7908 (1976).
3. T. H. Dunning, Jr., J. Chem. Phys. 53, 2823 (1970).
4. L. B. Harding and W. A. Goddard III, unpublished calculations.
5. J. A. Austin, D. H. Levy, C. A. Gottlieb, and H. E. Radford, J. Chem. Phys. 60(1), 207 (1974).
6. P. J. Hay, W. J. Hunt, and W. A. Goddard III, Chem. Phys. Lett. 13, 30 (1972).

Appendix B

Other Publications by the Author

The Generalized Valence Bond Description of the Low-Lying States of Diazomethane¹

Stephen P. Walch² and William A. Goddard III*

Contribution No. 5030 from the Arthur Amos Noyes Laboratory of Chemical Physics, California Institute of Technology, Pasadena, California 91125.

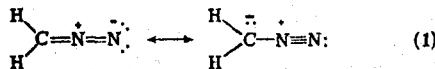
Received December 23, 1974

Abstract: We report ab initio generalized valence bond (GVB) and configuration interaction (CI) calculations (using a double- ζ basis) on the ground and low-lying excited states of diazomethane. We find that the ground state is more accurately described as a singlet biradical (somewhat as in ozone) than as a zwitterion. The calculated vertical excitation energies are 2.65 eV (³A₂), 2.93 eV (¹A₂), 3.66 eV (³A₁), and 5.90 eV (²A₁). The singlet excitation energies are in good agreement with the observed absorptions, broad continuum bands with peaks at 3.14 and 5.70 eV, leading hence to assignments of these transitions. Studies of the higher Rydberg states are also reported.

I. Introduction

The bond of the N₂ molecule is one of the strongest known bonds ($D_0 = 9.756$ eV) and is usually pictured as a triple bond involving two electrons in a σ bond and four electrons in two π bonds. This bond is so strong that atmospheric nitrogen is essentially unavailable to living organisms except for the fact that certain bacteria in the soil are able to convert N₂ into a more active form (no NN bonds). Indeed, an active and potentially important area of modern chemical research is the search for proper substrates and catalysts to first bond N₂ and then to break the NN bonds. Although several transition metal compounds have been found that bond N₂, it is generally not known whether the σ or π bonds are weakened by the bonding to the metal.³

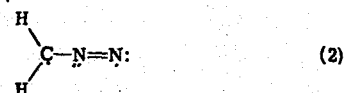
As a first step into the investigation of such phenomena, we have considered the end-on bonding of N₂ to CH₂, that is the molecule diazomethane. The bonding in diazomethane is usually represented by the resonance structures



A peculiar fact about this system is that both of these structures involve charge separation. In fact, one cannot write a proper resonance structure for diazomethane without allowing charge separation.⁴

In this paper we present the results of generalized valence bond (GVB) calculations on the ground and excited states of diazomethane. This approach corresponds to a generalization of the valence bond method in which all orbitals are solved for self-consistently. The resulting wave function for

diazomethane is basically that of a singlet biradical with strong bonding between the radical π orbitals on the C and



terminal N resulting from the interaction with the π pair on the central N.

The basic form of the wave function and other calculational details are discussed in section II. The wave function for the ground state of diazomethane is analyzed in section III and the excited states are discussed in section IV. The CI calculations are described in section V and some of the implications of these results for understanding the chemistry of diazomethane are presented in section VI.

II. The Wave Functions

A. The Perfect Pairing GVB Wave Functions. The generalized valence bond method (GVB) is described in some detail elsewhere.^{5a} Here we will review some of the ideas important for presentation of our results.

The simple closed-shell Hartree-Fock (HF) wave function can be written as

$$\alpha \{ [\varphi_1(1)\varphi_1(2)\alpha(1)\beta(2)] [\varphi_2(3)\varphi_2(4)\alpha(3)\beta(4)] \dots \} \quad (3)$$

where each HF molecular orbital φ_i is doubly occupied. [For simplicity we discuss the case of singlet states.] This restriction that the orbitals be doubly occupied leads to a number of difficulties in describing excited states and reac-

tions of molecules. To remove this restriction we replace the paired function

$$\varphi_i(1)\varphi_i(2) \quad (4)$$

in (3) by the pair function

$$\varphi_{ia}(1)\varphi_{ib}(2) + \varphi_{ib}(1)\varphi_{ia}(2) \quad (5)$$

leading then to

$$\alpha \{ [\varphi_{1a}(1)\varphi_{1b}(2) + \varphi_{1b}(1)\varphi_{1a}(2)] [\varphi_{2a}(3)\varphi_{2b}(4) + \varphi_{2b}(3)\varphi_{2a}(4)] \dots \chi \} \quad (6)$$

where

$$\chi = \alpha(1)\beta(2)\alpha(3)\beta(4)\dots \quad (7)$$

[In the following, expressions such as (6) and (7) will have the electron numbers deleted, the orbitals being ordered with increasing electron number for each term.] The orbitals of (6) are then solved for self-consistently to obtain the GVB wave function.

In the GVB wave function no restrictions are made on the orbitals or on the spin function χ .⁶ However, for computational convenience we have placed some restrictions on the orbitals of (6), namely, although the orbitals of a pair are allowed to have whatever overlap

$$\langle \varphi_{ia} | \varphi_{ib} \rangle$$

results from the variational principle, orbitals of different pairs are taken as orthogonal, that is

$$\langle \varphi_{ia} | \varphi_{jb} \rangle = 0 \quad (8)$$

$$\langle \varphi_{ia} | \varphi_{ja} \rangle = 0$$

if $i \neq j$. In addition, the spin function χ of (6) is restricted so that each pair is singlet coupled.⁷ The resulting wave function is denoted as GVB-PP to indicate that these restrictions have been made (PP denotes "perfect pairing"). These restrictions are later relaxed and found to be of little consequence for the cases considered herein.

In solving for the GVB-PP wave function it is convenient to define natural orbitals, ϕ_{i1} and ϕ_{i2} , for each pair such that

$$C_i [\varphi_{i1}\varphi_{i1} - \lambda_i^2 \varphi_{i2}\varphi_{i2}] = \phi_{ia}\phi_{ib} + \phi_{ib}\phi_{ia} \quad (9)$$

where

$$\begin{aligned} \phi_{ia} &= N_i [\varphi_{i1} + \lambda_i \varphi_{i2}] \\ \phi_{ib} &= N_i [\varphi_{i1} - \lambda_i \varphi_{i2}] \end{aligned} \quad (10)$$

The natural orbitals are orthogonal and lead to more convenient variational equations than do the GVB orbitals, φ_{ia} and φ_{ib} .

In the full GVB wave function every doubly occupied orbital of the HF wave function is replaced by two GVB orbitals. Although the GVB description of a pair leads to lower energies than the HF description, there are many cases where the same potential curves and excitation energies are obtained whether a particular pair is split or not. Examples are the 1s orbitals of first row atoms such as C and N and the 2s orbitals of O and F. Generally, it is only the bonding pairs that have to be described as GVB pairs (eq 5). As a result, we will often describe only a limited number of pairs in the GVB form (5), the others being described with doubly occupied orbitals, as in (4). Of course, all orbitals are solved for self-consistently. When only n pairs are split [that is, described as in (5)], we will use the notation GVB(n) or GVB(n /PP). For example, GVB(3) is

quite sufficient for N₂ and GVB(6) is quite sufficient for diazomethane.

For triplet states we use GVB(n) to indicate that all but n pairs are doubly occupied. For perfect pairing a triplet state requires two orbitals to be antisymmetrically coupled

$$\phi_{ia}\phi_{ib} - \phi_{ib}\phi_{ia} \quad (5')$$

rather than symmetrically coupled as in (5). Thus for a triplet state GVB(n /PP) implies $n - 1$ singlet pairs as (5) and one triplet pair as (5'). With this notation singlet and triplet states described to a comparable quality are denoted with the same n . (Note that for a triplet state GVB(1) is just the Hartree-Fock wave function.)

B. Computational Details. All calculations presented here (ground and excited states) use the experimental geometry for the ground state:⁸ $R_{CH} = 1.077 \text{ \AA}$, $R_{CN} = 1.300 \text{ \AA}$, $R_{NN} = 1.139 \text{ \AA}$, and $\angle HCH = 126.1^\circ$. The axes are chosen so that the z direction coincides with the rotation axis and the yz plane is the molecular plane. With this convention, the B₁ and A₂ symmetries indicate orbitals antisymmetric with respect to the molecular plane (denoted collectively as $\bar{\pi}$) while the A₁ and B₂ symmetries indicate orbitals symmetric with respect to the molecular plane (denoted collectively as $\bar{\sigma}$). Note the bar in $\bar{\sigma}$ and $\bar{\pi}$; this is to distinguish these symmetries from the σ and π symmetries of diatomic molecules.

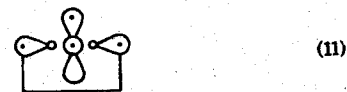
Three basis sets were used for the valence states. (1) MBS: a (7s,3p/3s) set of Gaussian primitive basis functions was contracted to a minimal basis set (2s,1p/1s) using a scale factor of 1.17 for the hydrogens.^{9a} (2) DZ: the (9s,5p/4s) primitive set of Huzinaga was contracted to the double zeta basis (4s,2p/2s) of Dunning^{9b} using a scale factor of 1.20 for the hydrogens. (3) DZR_x: the DZ basis was augmented with a single diffuse p_x primitive function on each N and C ($\xi_N = 0.05153$ and $\xi_C = 0.03650$).

For describing the Rydberg states we used the DZ basis and added on each N and C the following diffuse functions (all primitive Gaussians). (a) Two s functions chosen by scaling down the valence basis functions (orbital exponents: $\xi_C = 0.04736$, $\xi_C' = 0.01460$, $\xi_N = 0.0650$, and $\xi_N' = 0.0198$). (b) Two sets of p basis functions chosen in a similar manner (orbital exponents: $\xi_C = 0.03654$, $\xi_C' = 0.01165$, $\xi_N = 0.05148$, and $\xi_N' = 0.01602$).

The GVB(PP) calculations were carried out with the Bobrowicz-Wadt-Goddard program (GVBTWO)^{10a} based on the Hunt, Hay, and Goddard^{5b} fully self-consistent variational procedures. The CI calculations were carried out with the Caltech spin-eigenfunction CI program.^{10b} The molecular integrals were calculated with a version of the POLYATOM integrals program and the properties were calculated using a version of the J. Moskowitz Gaussian properties program. The CI properties were obtained with a program written by T. H. Dunning, Jr., and S. P. Walch. The IVO calculations were carried out using a specialized version (W. R. Wadt) of the GVBTWO program.

III. The Ground State

A. Introduction. For the ground state of carbon the GVB wave function yields orbitals that can be schematically represented^{5a,c} as



where



THE GVB ORBITALS OF DIAZOMETHANE

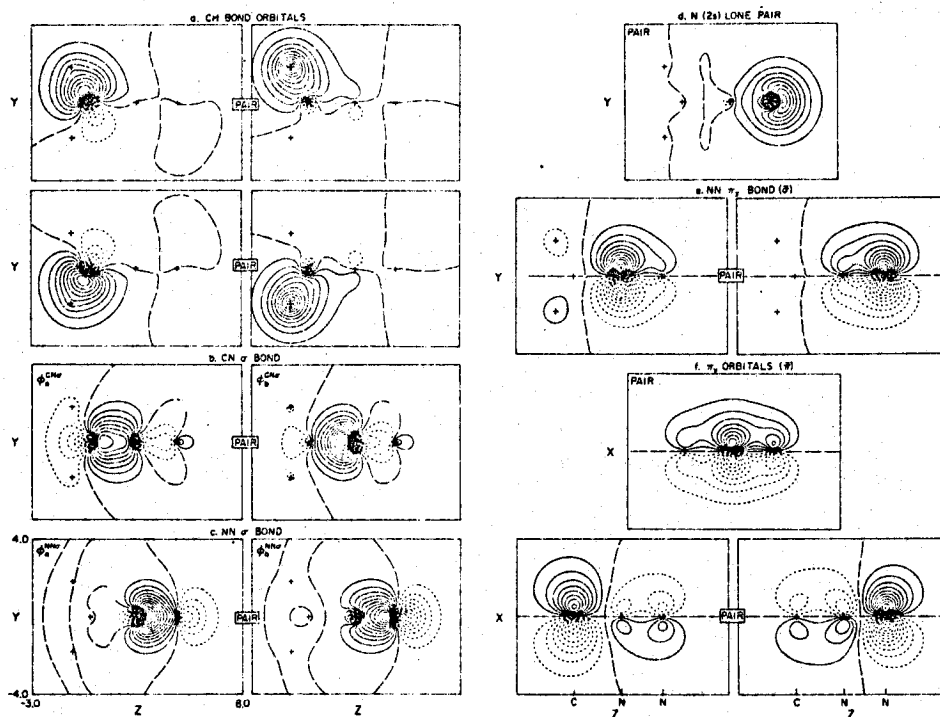
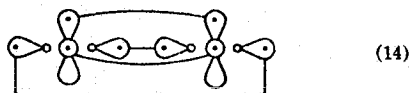


Figure 1. The GVB(6/PP) orbitals of the $X(^1A_1)$ state of diazomethane. The molecule is in the yz plane. Long dashes indicate zero amplitude. The contours represent constant amplitudes with a difference of 0.05 au between contours. The positions of the nuclei are denoted by +. The same conventions are used for all other plots (unless otherwise noted).

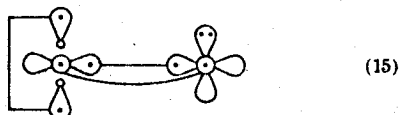
indicate singly occupied orbitals perpendicular and parallel to the paper, respectively, and



indicates the angularly correlated 2s pair. Studies of various carbon containing molecules⁵ have shown that the geometries and ordering of states can be simply understood in terms of coupling the orbitals of the other atoms to the orbitals of (11). Thus, the ground state of C_2 is^{5c} ($^1\Sigma_g^+$)



and the ground state of CO is^{5d}



where the lines between singly occupied orbitals indicate bond (singlet coupled) pairs. The tetravalent character of carbon can thus be understood in terms of the four GVB orbitals of the ground state of carbon.⁵

For the ground state of the nitrogen atom (4S), the presence of a singly occupied orbital in each direction restricts

the angular correlation of the 2s pairs, leading to just three orbitals that can form bonding pairs (the 2s doubly occupied orbital is omitted).¹¹



Thus, the trivalent character of nitrogen follows directly from (16). The $(2s)^2(2p)^3$ configuration of N also leads to 2D and 2P states and for the 2P state there is a strong angular correlation effect just as in $C(^3P)$. The 2P wave function is schematically represented as



Starting with (17) for the central nitrogen atom, bringing up a $N(^4S)$ on the right [as in (16)] and the ground state (3B_1) of methylene [as in (18)]

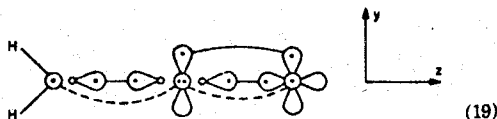


on the left leads to a description of diazomethane

Table I. Dipole Moment Breakdown for the X^1A_1 and 1^1A_2 states of H_2CINN^a

State	Pair	Orbital contribution, au ^c	Occupation no.	Pair contribution, D	
X^1A_1	N 2s	0.3973	0000	2.018	
	NN σ	0.1426	1.994	0.7245	
	NN σ^*	0.1571	0.0062		
	CN σ	0.1958	1.992	0.9858	
	CN σ^*	-0.2221	0.0083		
	CH σ_l	-0.0733	1.987	-0.3744	
	CH σ_l^*	-0.1393	0.0126		
	CH σ_r	-0.733	1.987	-0.3744	
	CH σ_r^*	-0.1393	0.0126		
	NN π_y (b_2)	-0.2372	1.925	-1.1437	
	NN π_y^* (b_2)	0.0839	0.0750		
		$1\pi_x$	0.1631	2.000	0.8287
		$2\pi_x$	-0.1366	1.884	
	$3\pi_x$	-0.0971	0.116	-0.6821	
	Total =		1.9824		1.9824 D
1^1A_2	N 2s	0.453	2.000	2.3012	
	NN σ	0.0617	2.000	0.3134	
	CN σ	0.163	1.991	0.8199	
	CN σ^*	-0.196	0.0089		
	CH (a_1)	-0.234	2.000	-1.1887	
	CH (b_2) ^b	-0.234	2.000	-1.1887	
	$2b_2$	0.967	2.000	4.9124	
	$3b_2$	-0.826	1.000	-2.0980	
	$1\pi_x$	-0.319	1.952	-1.5979	
	$1\pi_x^*$	-0.133	0.04798		
		$2\pi_x$	0.327	1.000	0.8306
		Total =		3.104	3.104 D

^a The nuclear charge is partitioned in a manner consistent with (10) for the X^1A_1 state and consistent with (25) in the case of the 1^1A_2 state. ^b Since the $1b_2$, $2b_2$ orbitals are in the same shell, the energy and other properties are invariant to a nonsingular transformation among them. We have used this freedom to fix the orbital contribution for the CH (b_2) orbital to that for the CH (a_1) orbital. The value for the $2b_2$ orbital was then determined by requiring that the total dipole moment remain constant. ^c 1 au of dipole moment equals 2.54158 D.



close to that found from the GVB calculations on H_2CINN .

B. The GVB Orbitals. The GVB orbitals of the ground state of diazomethane are shown in Figure 1. In describing these orbitals we will find it useful to discuss the contribution to the dipole moment for each pair and to compare with the value expected from the GVB model. To make this comparison we partition the nuclear contributions among the orbital pairs just as suggested by (19). [Thus the NN σ pair has associated with it one nuclear charge on each N.] The results are shown in Table I, where a positive dipole moment indicates extra electrons have moved toward the terminal N.

Of the four orbitals involved in the CN and NN σ bonds, two ($\phi_b^{CN\sigma}$ and $\phi_a^{NN\sigma}$) are concentrated on the nitrogen. These orbitals correspond to the lobe orbitals of (17) [the

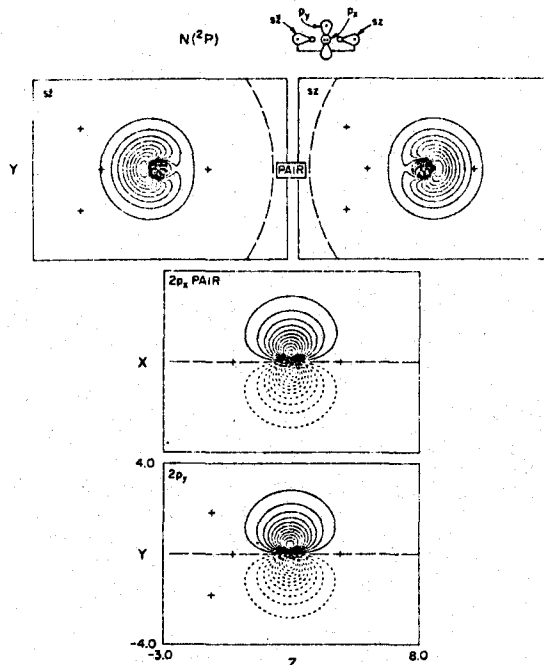


Figure 2. The GVB(1/PP) orbitals of the $2P$ state of the N atom.

self-consistent orbitals of (17) are shown in Figure 2] and as expected are very similar to each other. Note that $\phi_b^{CN\sigma}$ is slightly delocalized onto the N whereas $\phi_a^{CN\sigma}$ is more atomic like; this is typical of a slightly ionic bond (toward the N) and indeed this pair contributes +0.986 D to the dipole moment. The $\phi_b^{NN\sigma}$ orbital in Figure 1c corresponds to the p_z orbital of (16) but delocalized slightly onto the central N. The NN pair contributes +0.724 D to the dipole moment indicating a slightly ionic bond toward the terminal N.

The orbital in Figure 1d is doubly occupied and corresponds to the 2s pair of $N(^4S)$. As is typical of the 2s pairs of N, O, and F, it has shifted away from the bonding pairs. This effect derives essentially from the repulsive interaction between the 2s pairs and the bond pairs (arising from the Pauli principle). This pair contributes +2.018 D to the dipole moment, the dominant contribution.

The orbitals in Figure 1e correspond to a π_y bond between the nitrogens but in the plane of the molecule (that is, the π bond orbitals of N_2 are $\bar{\sigma}$ orbitals for H_2CINN). This π bond is quite similar to that of N_2 . It is delocalized to the left, contributing -1.144 D to the dipole moment. This shift is probably in response to the shift in the σ orbitals to the right.

The orbitals corresponding to the two CH bonds (Figure 1a) correspond closely to the CH bond orbitals of CH_2^{5c} and of H_2CO .¹² The total dipole moment contribution for a CH pair in CH_2N_2 is 1.577 D ($H-C^+$) directed at an angle of 76.3° with the z axis as compared to the internuclear angle of 63.1° . However, only the z component contributes to the net dipole, leading to a contribution of -0.374 D per CH pair. The slight delocalization of the H like orbitals onto the near nitrogen probably explains the fact that the dipole contribution is not directed along the bond.

The remaining orbitals (Figure 1f) are $\bar{\pi}$ type (we will denote these as π_x) and exhibit some unusual characteristics. We find that this four-electron system is described by

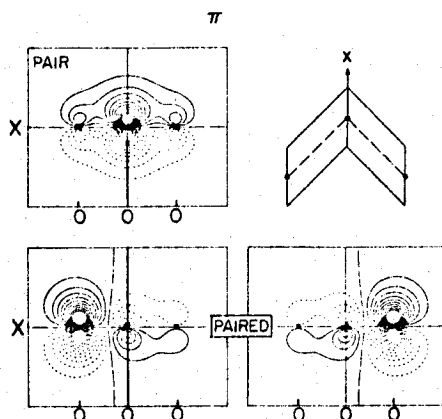


Figure 3. The GVB(3/PP) π orbitals of ozone.

one doubly occupied pair (denoted as ϕ_c) consisting of components localized mainly on the center nitrogen and a GVB pair consisting of components localized mainly on the carbon and on the end nitrogen (denoted as ϕ_l and ϕ_r , respectively),

$$(\phi_c)^2(\phi_l\phi_r + \phi_r\phi_l) \quad (20)$$

This four-electron π_x system in diazomethane bears a formal resemblance to the π^4 system of ozone.^{5a} However, in the case of diazomethane the $\phi_l\phi_r$ GVB pair has a much higher overlap ($S_{lr} = 0.60$) than is the case in ozone ($S_{lr} = 0.28$). Thus, while ozone is represented as a biradical with weak coupling between the biradical orbitals (single-triplet separation of 1.4 eV), such a description is less appropriate to CH_2N_2 . The singlet-triplet splitting here is 3.7 eV (vertical), which is comparable to the vertical singlet-triplet separation for a normal π bond (4.2 eV for ethylene, 3.5 eV for formaldehyde).

The π orbitals of the ground state of ozone are shown in Figure 3. A close comparison between these orbitals and the π_x orbitals of diazomethane provides some insight into the difference between the two systems. The reason for the moderate overlap of the $\phi_l\phi_r$ pair of ozone is that each component of the pair builds in a nodal plane in the region of the center O in order to remain orthogonal to the doubly occupied orbital. This results in a moderate amplitude for both ϕ_l and ϕ_r near the center O and a moderate overlap for the pair. However, in the case of diazomethane the doubly occupied orbital is asymmetric with the center of density shifted toward the end nitrogen. Thus the ϕ_l component of the GVB pair has its nodal plane shifted toward the right. This results in a moderate amplitude for this orbital in the

vicinity of the end nitrogen, where the ϕ_r orbital has its maximum. At the same time the ϕ_r orbital becomes more antibonding due to the higher overlap with the ϕ_c orbital, causing increased density near the C where the ϕ_l orbital is maximum. The overall result is a much higher overlap for the GVB π_x pair than occurs in ozone.

The ϕ_c pair leads to a contribution of +0.829 D to the dipole moment (as expected from its delocalization onto the terminal N). However, the other pair contributes -0.682 D to the dipole moment leading to a net contribution of +0.147 D due to the π_x orbitals.

Summarizing the trends in the dipole moments, we find that the CNN σ orbitals all shift to the right (a net shift of +3.728 D), the π_y and CH orbitals shift in the opposite direction (-1.892 D), while the π orbitals lead to little net shift (0.147 D). Thus, the large positive dipole moment of the ground state is dominated by effects in the σ system. The most important single contribution to the dipole moment arises from the N(2s) pair. This effect is a result of the hybridization of the N(2s) pair away from the bonding orbitals (an effect arising from the Pauli principle and which is not reflected in the Mulliken population analysis). Additionally, the CH and CN σ bonds as a whole give a net positive contribution as expected from electronegativity. However, the NN $\pi_y(\bar{\sigma})$ pair contributes negatively. (This complicated effect derives from the flow of charge onto the end nitrogen in the π_x system which was in turn a response to the polarity of the CN bonding pair.) This result serves to emphasize the point that electronegativity differences alone are not sufficient for predicting dipole moments (e.g., CO,¹³ NO,^{14,15} and CF¹⁴ all have "reversed" dipole moments).

Most of the small discrepancy (~ 0.3 D) of the CI dipole moment with experiment is probably due to a need for d polarization functions not included in our DZ basis.

C. Mulliken Populations. Since Hartree-Fock and MO wave functions are often analyzed in terms of Mulliken populations, we have also evaluated the Mulliken populations from the GVB(6/PP) wave function for comparison (see Table II).

In the $\bar{\sigma}$ system the polarity of the CH and CN σ leads to a small negative charge (-0.148) on the carbon and a rather large negative charge (-0.372) on the center N. The buildup of charge on the center N in the $\bar{\sigma}$ system is compensated for in the π system by a movement of charge from the center N onto the C and end N. This leads in the π system to a negative charge on the C (-0.335) and end N (-0.264) and a large positive charge on the center N (+0.599). In the $\pi_y(\bar{\sigma})$ system the shift of charge toward the end nitrogen occurring in the π system is compensated for by charge flow from the end N to the center N.

The Mulliken populations are in rough accord with the contributions to dipole moment. However, use of Mulliken

Table II. Mulliken Populations and Net Charges for the Ground State of H_2CNN^a

	1s	1s'	2s	2s'	x	x'	y	y'	z	z'
Mulliken Populations										
NA	1.1605	0.8335	0.9131	0.9011	1.0454	0.2895	0.6546	0.1536	0.9749	0.1312
NB	1.1594	0.8346	0.8910	0.4841	1.0062	0.3945	0.9233	0.2974	1.0797	-0.0765
C	1.1739	0.8201	0.7121	0.5254	0.9321	0.3323	0.9676	0.1795	0.7391	0.0305
HA	0.5090	0.2592								
HB	0.5090	0.2592								
			C	NA	NB	HA	HB			
			Net Charges ^b							
			The π_x system	-0.335	+0.599	-0.264				
			The π_y pair		-0.221	+0.192				
			The $\bar{\sigma}$ system	-0.148	-0.372	+0.086	+0.232		+0.232	

^a GVB(3/PP). ^b Net charges are relative to (19).

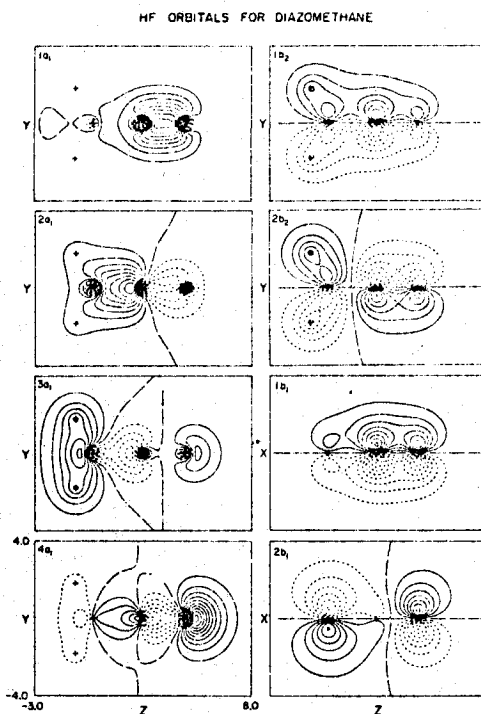


Figure 4. The HF orbitals of the $X(^1A_1)$ state of diazomethane.

populations to predict dipole moments would be suspect since the $N(2s)$ term dominating the dipole moment would be ignored.

D. The Hartree-Fock Orbitals. The HF orbitals for the ground state of diazomethane are shown in Figure 4. Comparing with the GVB orbitals of Figure 1 there are only slight resemblances. On the other hand, from (9) and (10) we see that a GVB pair can be reduced to a doubly occupied HF-like pair by merely deleting the second configuration ($\phi_{12}\phi_{12}$). This corresponds to just averaging the two GVB orbitals together in order to obtain the HF orbital. Doing this for all six pairs of Figure 1 leads to a Slater determinant of doubly occupied orbitals in (21) with an energy only 0.00696 hartree = 0.189 eV above the self-consistent HF wave function of H_2CNN .

$$\alpha \{[\phi_{11}\phi_{11}][\phi_{21}\phi_{21}] \dots \chi\} \quad (21)$$

However, despite the close correspondence in energies we see that the HF orbitals (Figure 4) are quite different from averages of the GVB orbitals. Averaging the GVB orbitals leads to doubly occupied orbitals corresponding to localized CH bonds, CN σ bonds, NN π bonds, etc., whereas the HF orbitals are much more delocalized.

What is the problem here; why are the HF orbitals so delocalized? Basically, the problem is that the HF orbitals are not unique. With a Slater determinant of doubly occupied orbitals we can take any nonsingular linear transformation among the occupied orbitals without making any change in the energy or any property of the molecule. The usual choice of the HF orbitals is to use the eigenfunctions of the HF one-electron Hamiltonian

$$H^{HF}\varphi_i = \epsilon_i\varphi_i$$

$$H^{HF} = h + \sum_i (2J_i - K_i) \quad (22)$$

Table III. Energies for the Ground State of Diazomethane (Energies in hartrees, Relative to HF)

	MBS		DZ
HF (ref 17)	+0.29687	HF (ref 18)	+0.01328
HF (this work)	+0.00000 ^a	HF (this work)	0.00000 ^b
GVB(3/PP)	-0.07374	GVB(3/PP)	-0.07844
GVB(6/PP)	-0.09080 ^c	GVB(6/PP)	-0.11422
GVB(3)-CI	-0.12651	GVB(3)-CI	-0.12811

^a -147.30687 hartrees. The other energies in this column are relative to this energy. ^b -147.78348 hartrees. The other energies in this column are relative to this energy. ^c In the MBS GVB(6/PP) wave function we restricted the CH pairs to be symmetry functions. While the description in terms of symmetry functions is equivalent to a localized orbital description at the HF level, at the GVB level the two are not equivalent. For the DZ basis the GVB(6/PP) energy was lower for localized CH orbitals and the same is probably true for MBS.

Table IV. Overlaps and Pair Splittings^a

Pair	Diazomethane		CH_2^b and N_2^c	
	Energy lowering, hartrees	Overlap	Energy lowering, hartrees	Overlap
CH σ left	0.01292	0.8524	0.0139	0.842
CH σ right	0.01292	0.8524	0.0139	0.842
CN σ	0.01098	0.8786		
NN σ	0.01011	0.8946	0.0123	0.8940
π_x GVB pair	0.03838	-0.6023	0.03182	0.6969
π_y GVB pair	0.03593	0.6703	0.03182	0.6969

^a DZ basis, GVB(6/PP). ^b Reference 5c. ^c T. H. Dunning, Jr., and D. C. Cartwright, to be published.

which does indeed lead to a unique set of orbitals (ignoring trivial flexibility for degenerate orbitals). Should the particular orbitals obtained from (22) lead to more useful interpretations than the other choices? There is some reason to believe so. In fact, Koopmans showed that the orbitals from (22) are optimally adjusted for describing the *positive ion* (within the restriction that the orbitals of the ground state are unchanged upon ionization). The usual HF MO's, or rather their energies, are indeed quite useful for interpreting the photoelectron spectra of molecules, as would be expected from Koopmans' theorem. However, it does not follow from this that these same orbitals would be particularly useful for understanding the chemical or physical properties of the neutral molecule.

The inappropriateness of the HF canonical orbitals as a basis for chemical concepts of molecules has long been noted and a number of techniques for obtaining more localized forms of the HF orbitals have been suggested. The GVB method provides yet another way of obtaining localized HF orbitals. Essentially, the set of HF-like orbitals obtained from (20) is that combination of the HF orbitals that is optimal for correlating the wave function. Thus viewing each GVB pair as

$$\varphi_a\varphi_b + \varphi_b\varphi_a = C(\varphi_a\varphi_b - \lambda\varphi_b\varphi_a)$$

the set of first natural orbitals spans essentially the same space as is spanned by the HF orbitals and the set of second natural orbitals φ_u provides the correlation effects. Applying the variation principle we find that the correlation correction effects are largest when both φ_b and φ_u are localized in the same region.¹⁶

E. Energies. Energies for the GVB and HF wave function for the ground state of diazomethane are listed in Table III. Table IV contains some of the special parameters of the GVB(6/PP) wave function. Note that most of the energy lowering in the GVB(6/PP) wave function as compared

Table V. CI Energies for Diazomethane Excited States

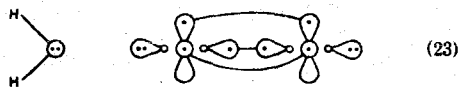
State	DZ basis		DZRx basis		Expt, ^e eV
	MBS, eV	Ground state core, eV	SCF core, eV	Ground state core, eV	
$X(^1A_1)$	0.0 ^a	0.0 ^b			
3A_2	2.84		2.65 ^d		
1A_2	3.23	3.31	2.93 ^c		3.14
3A_1	3.68	3.66			
$2(^1A_1)$	7.85	7.39		6.89 ^c	5.70

^a MBS GVB(3)-CI energy = -147.43338 hartrees. ^b DZ GVB(3)-CI energy = -147.91159 hartrees. ^c Energy relative to DZ GVB(3)-CI. ^d An SCF core appropriate to the singlet state was used. ^e Absorption maximum.

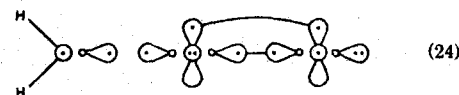
with HF comes from correlation of the $\pi_x(\bar{\pi})$ and $\pi_y(\bar{\sigma})$ pairs.

As a test of the perfect pairing assumption we carried out configuration interaction (CI) calculations using the orbitals from the GVB(3/PP) wave function. We find that the GVB-PP wave function contains about two-thirds of the correlation energy in the GVB(3)-CI. The additional energy lowering in the CI was primarily due to $\sigma \rightarrow \sigma^* \pi \rightarrow \pi^*$ double excitations, and we conclude that the perfect pairing restriction had little effect on the shapes of the orbitals. This is generally the case for closed shell systems near the equilibrium geometry.

F. The Separated Limits and the Nature of the Bond. Starting with the GVB wave function for the ground state of diazomethane and pulling off the N_2 along a linear path (C_{2v} symmetry) the lowest limit (about 3.4 eV above the ground state) would be the ground state of $N_2(X^1\Sigma_g^+)$ and the $2^1A_1^{19}$ state of CH_2



A higher energy limit (about 7.4 eV above the ground state) would be the ground state of methylene (X^3B_1) and the $^3\Pi$ excited state of N_2



Although (24) is considerably higher (~4 eV) than (23) the orbitals of the ground state of diazomethane are very similar to (24). In fact, bringing methylene (X^3B_1) up to N_2 ($^3\Pi_g$) as shown so as to form a CN σ bond, we would expect the doubly occupied π_{ux} orbital of N_2 to delocalize somewhat onto the carbon and concomitantly the singly occupied N_2 π_{gx} orbital to localize toward the terminal nitrogen. At the same time, the singly occupied methylene $1b_1$ orbital (π_x) must build in a nodal plane to become orthogonal to the double occupied N_2 π_{ux} orbital. In fact, at the equilibrium geometry the ϕ_c orbital still resembles the π_{ux} orbital of N_2 while the ϕ_r and ϕ_t orbitals resemble the $1b_1$ orbital of CH_2 and the π_{gx} orbital of N_2 , respectively. Either limit in (23) or (24) involves a large promotion energy and hence we expect a weak CN bond in diazomethane, as found experimentally and in our calculations.^{20,21}

IV. The Excited States

A. The 3A_2 and 1A_2 States. To find low-lying excited states of diazomethane we will start with (19) and search for other ways of distributing the electrons over the valence orbitals of the atoms without disrupting the σ bonds. As-

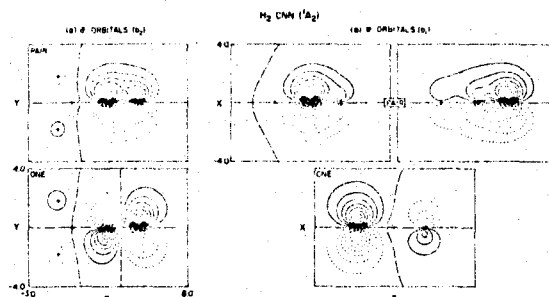
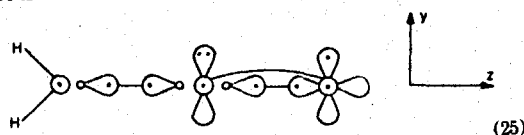


Figure 5. The GVB(3/PP) $\pi_x(\bar{\pi})$ and $\pi_y(\bar{\sigma})$ orbitals of the 1A_2 state of diazomethane.

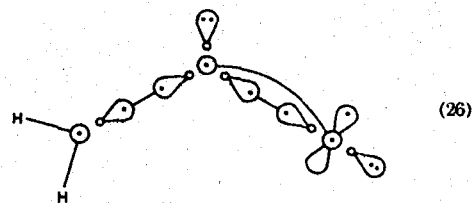
suming the linear CCN configuration the most favorable case is



which leads to 3A_2 and 1A_2 states. This has the same atomic configuration on each atom and the same number of σ and π bonds. However, in (25) the doubly occupied p_y orbital on the central N cannot delocalize onto the carbon (because of the CH bonds), whereas the corresponding (p_x) orbital of (19) can. As a result the singly occupied p_y orbital on the terminal atom of (25) is much more antibonding than the corresponding (p_x) orbital of (19). In addition, in (19) the singlet state is stabilized by the $\phi_r\phi_t$ pairing, an effect lost in (25) where the singly occupied orbitals are orthogonal. Given these differences it is not surprising that the vertical excitation energies to the 3A_2 and 1A_2 states are 2.65 and 2.93 eV, respectively (see Table V). Since the singly occupied orbitals are orthogonal, the 3A_2 state should be below the 1A_2 state and since the singly occupied orbitals are concentrated at opposite ends of the molecule, the exchange integral should be small and hence the triplet-singlet splitting small.

In Figure 5 we show the DZ $\bar{\pi}$ and in-plane π -like ($\bar{\sigma}$) orbitals of the 1A_2 state.

Looking first at the three-electron π_x system, we see that this system corresponds closely to that of allyl radical. However, here one of the resonance structures is far lower in energy than the other. The system is thus well described by a $\bar{\pi}_x$ pair (with components on the center nitrogen and end nitrogen) and a singly occupied orbital on carbon. Comparing the doubly occupied $N(^2P)\bar{\sigma}$ orbital on the center nitrogen with (25), we see that it has delocalized strongly toward the end nitrogen concomitantly with the singly occupied $2p$ $\bar{\sigma}$ orbital on the end nitrogen building in a nodal plane to remain orthogonal. The decrease in energy associated with the delocalization of the doubly occupied $\bar{\sigma}$ orbital is thus somewhat offset by the now highly antibonding singly occupied $\bar{\sigma}$ orbital. In order to decrease these interactions we expect the molecule to bend within the yz plane toward (26). However, the configuration in (26) is



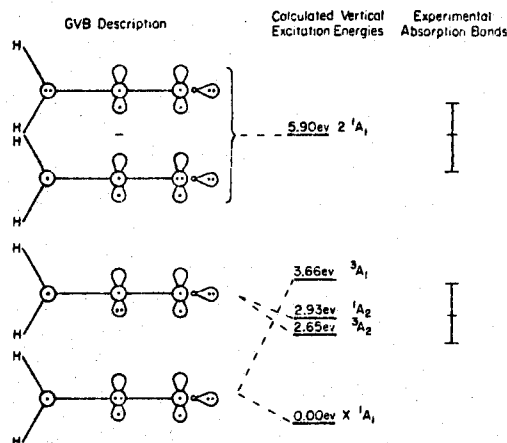
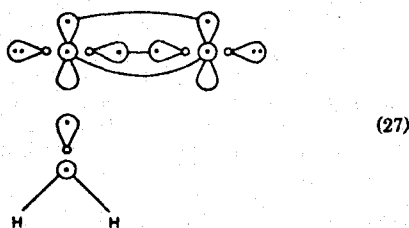


Figure 6. The GVB descriptions of the low-lying states of diazomethane.

compatible with dissociation to



leading to the formation of $\text{CH}_2(^3B_1)$ and $\text{N}_2(^1\Sigma_g^+)$. For the 1A_2 state, however, the corresponding limit $\text{CH}_2(^1B_1)$ and $\text{N}_2(^1\Sigma_g^+)$ is 1.9 eV higher. Since the $^1A_1 \rightarrow ^1A_2$ excitation energy is 2.9 eV and the ground state is bound by ~ 1.5 eV with respect to $\text{CH}_2(^3B_1)$ and $\text{N}_2(^1\Sigma_g^+)$, the $^1A''$ state of (25) is bound by ~ 0.5 eV with respect to products in (26). [Dissociation to $\text{N}_2(^1\Sigma_g^+) + \text{CH}_2(^1A_1)$ should be exothermic by ~ 1 eV.]

Excitation to the 1A_2 state is dipole forbidden but vibronically allowed. We identify the 1A_2 state with the diffuse weak absorption with maximum at 3.14 eV (see Figure 6).

The delocalization of the π_y orbital on the central N (corresponding to the p pair of the 2P state) also leads to a large increase in the dipole moment of this state as compared with the ground state (see Table VI). In fact the dipole moment of the 1A_2 state is calculated to be +3.62 D [GVB(3)-CI] as compared with the ground state dipole moment of +1.86 D [GVB(3)-CI]. The charge distribution in the 3A_2 state is expected to be quite close to that in the singlet state and indeed the dipole moment of the 3A_2 state is +3.54 D [GVB(3)-CI]. A detailed breakdown of the dipole moment of the 1A_2 state into orbital contributions is given in Table I.

B. The 3A_1 State. Starting with the $\bar{\pi}$ orbitals of the X^1A_1 ground state (19) and (20) and coupling the ϕ_1 and ϕ_r orbitals antisymmetrically

$$\phi_s^2(\phi_r\phi_1 - \phi_1\phi_r) \quad (28)$$

leads to the 3A_1 state of H_2CNN . In the simple approximation in which the same orbitals are used for both states, the excitation energy is

$$\Delta E = -A/(1 - S^2) \quad (29)$$

Table VI. Dipole Moments (in Debye) for the Valence States of H_2CNN ^a

	X^1A_1	3A_1	2^1A_1	1A_2	3A_2
HF	+1.69				
GVB(3/PP)	+1.99			3.11	
GVB(6/PP)	+1.98				
CI	+1.86	2.64	0.21	3.62	3.54
Exptl	$\pm 1.50^b$				

^a All calculations use the DZ basis. A positive dipole moment implies that the terminal nitrogen is negative. ^b Reference 8.

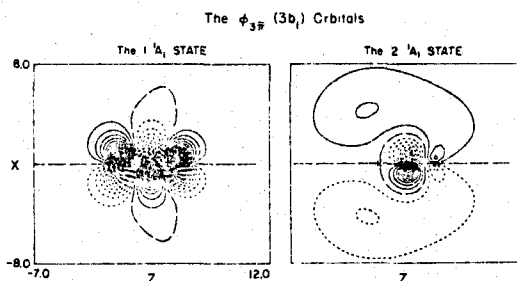


Figure 7. The $3b_1(\pi^*)$ orbitals for the 2^1A_1 and X^1A_1 states. (Contour interval = 0.02 a.u.)

where A is a (negative) quantity approximately proportional to the square of the overlap, S , of the ϕ_1 and ϕ_r orbitals.²² For ozone $S = -0.28$ and $\delta E = 1.4$ eV, for H_2 molecule $S = 0.80$ and $\Delta E = 10$ eV, and for ethylene $S = 0.64$ and $\Delta E = 4.2$ eV (all vertical excitation energies). Thus for H_2CNN with $S = -0.60$ the calculated $\Delta E = 3.66$ eV is reasonable.

Defining delocalized orbitals (MO's) $\phi_{2\bar{r}}$ and $\phi_{3\bar{r}}$ as

$$\begin{aligned} \phi_{2\bar{r}} &= (\phi_1 - \phi_r)/\sqrt{2(1-S)} \\ \phi_{3\bar{r}} &= (\phi_1 + \phi_r)/\sqrt{2(1+S)} \end{aligned} \quad (30)$$

where the constant factors ensure normalization, the $\bar{\pi}$ part of the singlet state (20) becomes

$$\psi_S = \phi_C^2\{(1-S)\phi_{2\bar{r}}\phi_{2\bar{r}} - (1+S)\phi_{3\bar{r}}\phi_{3\bar{r}}\} \quad (31)$$

while the triplet state (28) becomes

$$\psi_T = \phi_C^2(\phi_{2\bar{r}}\phi_{3\bar{r}} - \phi_{3\bar{r}}\phi_{2\bar{r}}) \quad (32)$$

For the self-consistent orbitals of the ground state, S is negative (see Figure 1), hence (31) may be written

$$\psi_S = \phi_C^2(a\phi_{2\bar{r}} - b\phi_{3\bar{r}}) \quad (33)$$

where for the self-consistent wave function a is 0.9705 and b is 0.2410. The MO description of the singlet state has the form (33) except that the $\phi_{3\bar{r}}\phi_{3\bar{r}}$ term is deleted, while the MO description of the triplet state is (32). Thus, in the MO description the $^3A_1 \leftarrow ^1A_1$ transition is described as $3\bar{\pi} \leftarrow 2\bar{\pi}$ and these states appear to be quite different [The MO excitation energy will be low by 1.044 eV (the π_x splitting energy) because the triplet state is correctly described, while for the singlet state the second configuration $\phi_{3\bar{r}}\phi_{3\bar{r}}$ is neglected.] On the other hand, the GVB wave functions [(20) and (28)] for the two states involve similar orbitals and differ mainly in the way in which the orbitals are coupled. We thus expect somewhat similar charge distributions in the two states and in fact the calculated dipole moment of the 3A_1 state is 2.64 D [GVB(3)-CI], a value not drastically different from the dipole moment of the ground state.

D. Rydberg States. In the above sections we discussed the low-lying excited states expected to arise from excitations among the valence orbitals. Other low-lying excited states are expected to correspond to excitation into diffuse Rydberg-like orbitals. To examine such states diffuse basis functions were added to our basis (see section IB). Rather than solving self-consistently for each excited state, we used the IVO approach of Hunt and Goddard²⁵ in which the correct variational Hamiltonian for the excited orbital is set up and diagonalized over the orbitals orthogonal to the occupied orbitals of the ground state. Thus, with one diagonalization, one gets all excited orbitals (out of a particular ground state orbital and for a particular total spin).

The calculated excitation energies^{25b} and oscillator strengths are given in Table VII and plots of the Rydberg orbitals are given in Figure 8.

The Orbitals. The assignment and calculated energy of each Rydberg orbital is given in Figure 8.

As expected the three 3p orbitals have similar energies as do the three 3d orbitals solved for. There is a 0.9 eV separation between the 3s and 3p states and a 0.8 eV separation between the 3p and 3d states, reasonable results given the different abilities of these orbitals to penetrate the H₂CNN⁺ core.

Looking more closely we see that the 3s orbital is squished away from the CH bonds and N lone pair, apparently due to repulsive effects with these pairs. This change in shape can be described as subtraction of d_{z²} character (2z² - x² - y²) from the 3s wave function.

The 3p_z orbital corresponds closely to the shape expected for a 3p orbital. The 3p_x orbital deviates somewhat, concentrating more on the H₂C end of the molecule. This is apparently in response to the shift of the σ system to the right making the N end less attractive for the Rydberg state.

The 3p_y orbital corresponds closely to the shape expected for a 3p orbital. However, there are complications here. This orbital leads to the second A₁ state of H₂CNN, discussed in section IVC. Carrying out a CI calculation leads to the introduction of valence character in the wave function and a decrease in the energy of this state to 5.9 eV.

Since diffuse s and p functions were placed on each atom, we expect a good description of the 3s and 3p Rydberg states. Although diffuse d functions were not included we expect moderately good descriptions of the 3d_{z²}, 3d_{x²-y²}, and 3d_{xy} excited orbitals from combining the diffuse function on various centers. A much poorer description of 4s, 4p, and higher states is expected since sufficiently diffuse functions were not included.

The 3d orbitals being the highest of the n = 3 orbitals are distorted in the unfavorable directions (e.g., toward the end N). The exception is 3db₁, which has a large amount of carbon valence character.

The Energies. Rydberg states are often characterized in terms of a quantum defect, δ defined as

$$\text{IP(hartrees)} = 1/2(n - \delta)^2 \quad (40)$$

in terms of the ionization potential of the excited state (in hartrees). Thus, δ is the correction to the principle quantum number that would lead to an energy expression like that of the hydrogen atom.

The calculated quantum defects are listed in Table V. The average values $\delta_{3s} = 0.905$, $\delta_{3p} = 0.500$, and $\delta_{3d} = -0.113$ are all a bit smaller than for smaller molecules, indicating extra repulsive interactions due to the core.

The calculated excitation energy into the 3s orbital (¹B₁ state) is 5.89 eV. However, the calculated oscillator strength is 5.4×10^{-3} and this transition is probably bur-

ied under the strong absorption due to the 2¹A₁ state (calculated $f = 0.376$).

At shorter wavelengths, Merer²⁶ has observed an extensive series of perpendicular bands near 1900 Å (6.51 eV). At 1585 Å (7.65 eV) there is a similar series of perpendicular bands. Herzberg²⁷ has pointed out that these two-band systems fit reasonably well as the first two members of an np series with $\delta = 0.67$ leading to an IP of 9.06 eV.

Our calculations show a ¹B₁ state at 6.87 eV and also a ¹A₂ state at 6.65 eV corresponding to excitation to 3p_x and 3p_z orbitals, respectively. However, Merer's analysis of the 1900 Å group indicated three very closely spaced states, two of B₁ symmetry and a third which did not seem to have "any intensity of its own in absorption" (which Merer tentatively assigned as a B₂ state). It seems reasonable that our ¹B₁ state is one of Merer's B₁ states. The ¹A₂ state is not dipole allowed but becomes vibronically allowed for B₁, B₂, and A₂ vibrations. We suggest that the remaining states analyzed by Merer (B₁ and B₂) may correspond to vibronically induced transitions ¹A₂ ← X¹A₁.

Since we did not include sufficiently diffuse basis functions to describe 4p orbitals, our results cannot be used to verify the assignment of the 1585 Å group to 4p Rydberg levels.

We find three states of 3d character near 7.6 eV. Without d functions explicitly in our basis we may expect to be a bit high on these states (as evidenced by negative quantum defects) and hence it appears reasonable to associate the ¹A₁ 3d Rydberg state with the first member of the parallel nd Rydberg series observed by Herzberg (7.37 eV). To obtain a good description of these Rydberg levels d functions should be included, a calculation we intend to pursue later.

V. Details of the CI Calculations

While the GVB(6/PP) wave function for the ground state of diazomethane is highly useful for interpretation purposes, it is clear from Table IV that the major part of the ground state correlation energy is contained within a two-pair wave function in which the π_x and π_y pairs are split. For our CI studies we have used the orbitals of GVB(3/PP) wave functions in which the π_x , π_y , and CN σ pairs are split.

In all the CI calculations the three 1s-like orbitals were kept doubly occupied (this allows these electrons to be eliminated from all calculations by appropriately modifying the one-electron integrals). For the MBS-CI calculations there are 14 additional basis functions for describing 11 occupied GVB orbitals. For each state we started with the dominant configuration for that state and included all single and double excitations among the 11 GVB orbitals.

For the DZ and DZR_x bases we carried out self-consistent GVB(3/PP) calculations for the X¹A₁, 1¹A₂, and 2¹A₁ states. These self-consistent vectors were then used in the corresponding CI calculations (for the ³A₁ state we used X¹A₁ vectors and for ³A₂ we used ¹A₂ vectors). In each case the doubly occupied σ orbitals of the GVB(3/PP) calculations were kept paired in the CI. Based on the results from MBS-CI, we also made the following restriction in the CI. The orbitals for the CI were partitioned into subspaces corresponding to a₁, b₁, and b₂ symmetries, respectively, and only excitations within these symmetry types were allowed. Within this restriction all single and double excitations were taken from the appropriate dominant configurations. This procedure leads to a significant reduction in the number of configurations while allowing a good description of the excitation energies.

We also solved for the various states using the GVB vectors of the ground state. In these calculations we included

configurations involving single excitations from the π GVB orbitals into the remaining π virtuals (a procedure referred to as polarization CI). This latter calculation leads to errors for the excited 1A_2 and 2^1A_1 states of 0.4 to 1.5 eV which can be attributed to two effects: (1) lack of relaxation of the unexcited orbitals and (2) a restricted description of the excited orbital. Probably (2) is the most important for 1A_2 but core relaxation is responsible for lowering the excitation energy of 2^1A_1 by about 1 eV (for the DZR_x basis). This large effect is due to the diffuse nature of the excited orbital of the 2^1A_1 state, leading to significant contraction of the other orbitals upon excitation.

A. The 1A_2 and 3A_2 CI Calculations. We used the 1A_2 DZ GVB(2) orbitals as a basis for π -electron CI calculations on the 1A_2 and 3A_2 states. We also carried out polarization CI calculations using the GVB(3) ground state orbitals.

B. The 3A_1 and 2^1A_1 CI Calculations. The 3A_1 and 2^1A_1 states both arise from the π_x electron configuration.



However, as has been previously shown (sections IVB and IVC), the 3A_1 state corresponds basically to the triplet coupling of the GVB π_x pair, whereas the 2^1A_1 state is a charge transfer state. Thus, the 3A_1 state should be well described with orbitals much like the ground state GVB π_x natural orbitals, whereas we expect the 2^1A_1 state to have a diffuse $3b_1$ orbital in agreement with the ionic character of the state.

We carried out π electron polarization CI calculations on the 3A_1 state using the DZ GVB(3) natural orbitals as a basis. From an examination of the single excitations, it is clear that the DZ basis is adequate to describe this state and that the π_x orbitals are not much different from those for the singlet state.

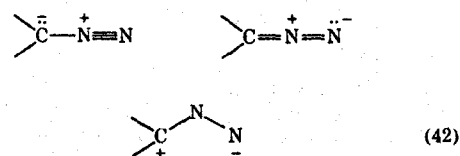
For the 2^1A_1 state we used the configurations for polarization CI plus additional configurations from allowing all double excitations within the b_1 space. Using the DZ GVB(3) orbitals and the above configurations, we find a sizable improvement over the MBS results. Examination of the single excitations indicates that the variationally correct $3b_1$ orbital would have large amplitudes on the more diffuse p_x basis functions. Augmenting the basis with a single diffuse p_x function on each center (DZR_x) and repeating the CI with a similar set of configurations resulted in another decrease in the energy, with the $3b_1$ orbital again showing large amplitudes on the most diffuse functions. However, this calculation still used a frozen σ core appropriate to the ground state. In order to obtain a more contracted σ core appropriate to the diffuse $3b_1$ orbital, we carried out CI calculations using the GVB(3/PP) vectors from the pseudo-SCF calculation described in section IVC. The $3b_1$ orbital from this calculation was found to have large amplitudes on the most diffuse p_x basis functions and to have a small orbital energy (-0.077111 hartree) consistent with a Rydberg-like orbital. Using the σ core from this calculation in a π electron CI calculation on the 2^1A_1 state and using the same spatial configurations as in the previous CI with ground state core an energy only 0.2 eV above the experimental λ_{\max} was obtained.

Examining the CI results for the 2^1A_1 state, we see that the best CI energy (DZR_x, SCF core) is a full 2.0 eV below the MBS CI, whereas for the other states the MBS CI gave excitation energies essentially the same as were obtained with the more extensive DZ basis. This is, of course, strong evidence for the ionic character of the 2^1A_1 state. It is interesting to note that 1.0 eV of the difference between our final CI result for the 2^1A_1 state and the MBS result is due

to a σ core contraction in response to excitation into a diffuse $3b_1$ orbital.

VI. Ground State Chemistry of Diazomethane

Diazomethane belongs to a class of compounds commonly referred to as 1,3 dipoles because the principal resonance structures drawn to describe the bonding are zwitterion structures. For example for diazomethane these structures are



However, we find that the ground state is more accurately described as biradical-like, although, as discussed earlier, there is a fairly large overlap between the $\phi_1\phi_r$ components of the π_x GVB pair.

Roberts²⁸ has pointed out that the GVB description yields a simple consistent rationalization of the facile 1,3 addition of diazomethane to olefins. Usually the dipolar nature of diazomethane

is considered as the dominant influence. However, abundant experimental evidence suggests that this reaction occurs in a one-step process not involving charge separation.²⁹

On the other hand, the GVB model of diazomethane suggests a biradical attack analogous to that in ozone. In particular we note that cycloaddition of diazomethane to ethylene does preserve orbital phase continuity.³⁰ This follows from the fact that the overlap between the $\phi_1\phi_r$ components of the GVB π_x pair results from a through-bond coupling rather than a direct coupling as for ethylene. Thus, to get a positive S_{ir} the orbitals must be oriented as in (43).

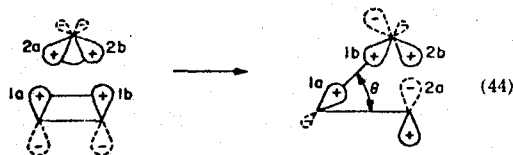


Therefore, the phases are preserved in the cycloaddition, so that the reaction is expected to be concerted.

Addition of Methylene to N_2 . Recently several investigators have observed recombination of $CH_2(^1A_1)$ and $N_2(^1\Sigma_g^+)$ to give diazomethane. Moore and Pimentel³¹ have observed recombination of N_2 and methylene in an N_2 matrix at liquid He temperatures. In line with this observation, Bass et al.³² have had to postulate reaction between methylene singlet and N_2 to explain their kinetic studies of N_2/CH_2N_2 mixtures following flash excitation. Based on the rate constant for the N_2 -methylene recombination derived by Bass et al., Laufer and Okabe²¹ estimate an activation energy of ≤ 3 kcal/mol. Moore and Pimentel conclude that recombination of CH_2 and N_2 to give diazine has a much higher activation energy, since they do not observe diazine formation. In fact, they show that formation of diazomethane in diazine photolysis is a result of recombination of CH_2 (produced in the diazine photolysis) with matrix N_2 .

The formation of diazomethane with a small activation energy and the failure to observe diazine in the reaction between $CH_2(^1A_1)$ and $N_2(X^1\Sigma_g^+)$ may be understood using the orbital phase continuity principle and concepts from the GVB description of diazomethane.

Consider the following reaction path 44. For this orientation closure to the symmetric diazine is not favored. However, using large θ ($> 120^\circ$) leads to orbitals with the same



phase orientation as in (43), thus we expect the energy to decrease monotonically as the molecule opens to diazomethane and hence a predominance of diazomethane, as is observed.

References and Notes

- (1) Partially supported by a grant (GP-40783X) from the National Science Foundation.
- (2) National Defense Education Act Fellow.
- (3) For an interesting example and further references, see J. E. Bercaw, E. Rosenberg, and J. D. Roberts, *J. Am. Chem. Soc.*, **96**, 612 (1974).
- (4) See D. J. Cram and G. S. Hammond, "Organic Chemistry", McGraw-Hill, New York, N.Y., 1964.
- (5) (a) W. A. Goddard III, T. H. Dunning, Jr., W. J. Hunt, and P. J. Hay, *Acc. Chem. Res.*, **6**, 368 (1973); (b) W. J. Hunt, P. J. Hay, and W. A. Goddard III, *J. Chem. Phys.*, **57**, 738 (1972); (c) P. J. Hay, W. J. Hunt, and W. A. Goddard III, *J. Am. Chem. Soc.*, **94**, 8293 (1972); (d) A. P. Mortola and W. A. Goddard, *ibid.*, **96**, 1 (1974).
- (6) As an example, consider a four-electron singlet. There are two possible spin couplings: $\chi_1 = 0.5(\alpha\beta - \beta\alpha)(\alpha\beta - \beta\alpha)$ and $\chi_2 = (3^{1/2}/6)[2(\alpha\alpha\beta\beta - \beta\beta\alpha\alpha) - (\alpha\beta + \beta\alpha)(\alpha\beta + \beta\alpha)]$. We may define a general spin eigenfunction (SEF) by $\chi = \cos \theta \chi_1 + \sin \theta \chi_2$ and then solve for the spin coupling simultaneously with obtaining the optimum orbitals.
- (7) In many cases solving for χ as above results in only the χ_1 coupling being important, $\chi = (\alpha\beta - \beta\alpha)(\alpha\beta - \beta\alpha) \dots (\alpha\beta - \beta\alpha)$. When we force χ to have this form, the wave function is denoted by PP for "perfect pairing". We may then write our GVB wave function as $G\{[\varphi_{1a}\varphi_{1b}\varphi_{2a}\varphi_{2b} \dots \varphi_{m\alpha}\varphi_{m\beta}]\chi_{PP}$, which is equivalent to $G\{[\varphi_{1a}\varphi_{1b} + \varphi_{1b}\varphi_{1a}][\varphi_{2a}\varphi_{2b} + \varphi_{2b}\varphi_{2a}] \dots [\alpha\beta\alpha\beta \dots \alpha\beta]\}$.
- (8) A. P. Cox, L. F. Thomas, and J. Sheridan, *Nature (London)*, **181**, 1000 (1958); J. Sheridan, *Adv. Mol. Spectrosc., Proc. Int. Meet.*, **4th 1959**, **1**, 139 (1962).
- (9) (a) S. Huzinaga, D. McWilliams, and B. Domskey, *J. Chem. Phys.*, **54**, 2283 (1972); (b) T. H. Dunning, Jr., *ibid.*, **53**, 2823 (1970).
- (10) (a) See F. W. Bobrowicz, Ph.D. Thesis, California Institute of Technology, March 1974. (b) Written by F. W. Bobrowicz (vide sup.a) and N. W. Winter utilizing spin eigenfunction techniques of R. C. Ladner (see Ph.D. Thesis, California Institute of Technology, November 1971). Modifications due to L. A. Harding, S. P. Walch, B. J. Moss, and W. A. Goddard III.
- (11) Taking our wave function for the $N(^4S)$ state as $\psi = G\{\varphi_{1a}\varphi_{1b}\varphi_{2a}\varphi_{2b} + \varphi_{1a}\varphi_{1b}\varphi_{2b}\varphi_{2a} + \varphi_{1a}\varphi_{2a}\varphi_{1b}\varphi_{2b} + \varphi_{1a}\varphi_{2a}\varphi_{2b}\varphi_{1b} + \varphi_{1a}\varphi_{2b}\varphi_{1b}\varphi_{2a} + \varphi_{1a}\varphi_{2b}\varphi_{2a}\varphi_{1b} + \varphi_{1b}\varphi_{2a}\varphi_{1a}\varphi_{2b} + \varphi_{1b}\varphi_{2a}\varphi_{2b}\varphi_{1a} + \varphi_{1b}\varphi_{2b}\varphi_{1a}\varphi_{2a} + \varphi_{1b}\varphi_{2b}\varphi_{2a}\varphi_{1a}\}$, where $\varphi_{1a} = \varphi_{2a} + \lambda\varphi_{2b}$ and $\varphi_{1b} = \varphi_{2b} - \lambda\varphi_{2a}$, we see that this is equivalent to $G\{\varphi_{2a}^2 - \lambda\varphi_{2b}^2\}2\varphi_{1a}\varphi_{1b}\varphi_{2a}\varphi_{2b}$, which reduces to $G\{\varphi_{2a}^2 - \lambda\varphi_{2b}^2\}2\varphi_{1a}\varphi_{1b}$ due to the antisymmetrizer.
- (12) L. Harding and W. A. Goddard III, *J. Am. Chem. Soc.*, in press.
- (13) F. Grimaldi, A. Lecourt, and C. Moser, *Int. J. Quantum Chem.*, **15**, 153 (1967).
- (14) S. Green, *Chem. Phys. Lett.*, **23**, 115 (1973).
- (15) S. P. Walch and W. A. Goddard III, *Chem. Phys. Lett.*, **33**, 18 (1975).
- (16) The energy change due to the $\phi_a\phi_b$ configuration is approximately $\Delta E = -K_{ab}^2/(E_a - E_b)$, and thus the correlation effected by ϕ_a favors maximizing K_{ab} . To maximize K_{ab} , one needs to concentrate ϕ_a and ϕ_b both in the same regions of space.
- (17) J.-M. André, M. Cl. André, G. Leroy, and J. Weiler, *Int. J. Quantum Chem.*, **3**, 1013 (1969).
- (18) L. Snyder and H. Basch, "Molecular Wave Functions and Properties Tabulated from SCF Calculations in a Gaussian Basis Set", Wiley, New York, N.Y., 1972.
- (19) This corresponds to the $^1\Sigma_g^+$ state of linear CH_2 or to the MO occupancy $1a_1^2 2a_1^2 2b_1^2 2b_2^2$ of bent CH_2 .
- (20) Using the GVB(3/PP) energy of $CH_2(^1A_1)$ (ref 5c) and estimating the GVB(3/PP) energy of N_2 by adding the pair lowerings for each pair (Table IV) to the HF energy (ref 9b) leads to an H_2C-N_2 bond energy of 0.88 eV for diazomethane in the DZ basis. The best experimental estimate (ref 21) of this quantity is 2.31 eV. Since we did not include d functions in the basis, errors of the order of 1 eV are expected in bond dissociation energies, approximately the value obtained.
- (21) A. H. Laufer and H. Okabe, *J. Am. Chem. Soc.*, **93**, 4137 (1971). We use their value relative to 3B_1 methylene and add 0.50 eV as the $^1A_1 \leftarrow ^3B_1$ excitation energy for methylene (ref 5c).
- (22) (a) C. W. Wilson, Jr., and W. A. Goddard III, *Theor. Chem. Acta*, **26**, 195 (1972); (b) W. A. Goddard III and C. W. Wilson, Jr., *ibid.*, **26**, 211 (1972); (c) C. W. Wilson, Jr., and W. A. Goddard III, *Chem. Phys. Lett.*, **5**, 45 (1970).
- (23) T. H. Dunning, Jr., W. J. Hunt, and W. A. Goddard III, *Chem. Phys. Lett.*, **4**, 147 (1969).
- (24) G. Herzberg, *Proc. R. Soc. London, Ser. A*, **262**, 291 (1961).
- (25) (a) W. J. Hunt and W. A. Goddard III, *Chem. Phys. Lett.*, **3**, 414 (1969); see also W. J. Hunt, Ph.D. Thesis, California Institute of Technology, September 1971. (b) In the IVO procedure it is the ionization potential (IP) of the excited (Rydberg) orbital that is calculated. To obtain excitation energies, this is subtracted from the experimental IP, 8.99 eV for H_2CNN .
- (26) A. J. Merer, *Can. J. Phys.*, **42**, 1242 (1964).
- (27) G. Herzberg, "Electronic Spectra and Electronic Structure of Polyatomic Molecules", Van Nostrand-Reinhold, New York, N.Y., 1966.
- (28) J. D. Roberts, private communication.
- (29) R. Husigan, *Angew. Chem.*, **2**, 633 (1963).
- (30) W. A. Goddard III, *J. Am. Chem. Soc.*, **94**, 793 (1972).
- (31) C. B. Moore and G. C. Pimentel, *J. Chem. Phys.*, **41**, 3504 (1964).
- (32) W. Braun, A. M. Bass, and M. Pilling, *J. Chem. Phys.*, **52**, 5131 (1970).

DIPOLE MOMENTS AND ELECTRIC FIELD GRADIENTS
FOR CORRELATED WAVEFUNCTIONS OF NO: THE $X^2\Pi$, $A^2\Sigma^+$, AND $D^2\Sigma^+$ STATES*

Stephen P. WALCH** and William A. GODDARD III
*Arthur Amos Noyes Laboratory of Chemical Physics[†], California Institute of Technology,
Pasadena, California 91109, USA*

Received 10 February 1975

Recent experiments by Bergeman and Zare led to a dipole moment of $|\mu| = 1.10 \pm 0.03$ D for the $v = 3$ vibrational level of the $A^2\Sigma^+$ state of NO, whereas configuration interaction (CI) studies by Green led to $\mu = 0.39$ D (N^+O^-), a serious discrepancy. We report herein ab initio generalized valence bond (GVB) and GVB CI calculations resulting in a dipole moment of +1.36 at R_e for the $A^2\Sigma^+$ state; considering the expected decrease of μ for increasing v , this is in reasonable agreement with experiment. Theoretical values of the dipole moment, electric field gradient, and excitation energies are reported for the $X^2\Pi$, $A^2\Sigma^+$, and $D^2\Sigma^+$ states of NO.

1. Introduction

Recently Bergeman and Zare [1] reported the first experiments determining the dipole moment of a Rydberg state of a molecule. They found the dipole moment for the $v = 3$ vibrational level of the $A^2\Sigma^+$ state of NO to be

$$|\mu| = 1.10 \pm 0.03 \text{ debye,}$$

where the quoted uncertainty was estimated as three standard deviations. They pointed out that this value differs quite significantly from that determined by Green [2] from configuration interaction (CI) calculations:

$$\mu = 0.47 \pm 0.03 \text{ debye (N}^+O^-)$$

for $R = 1.06 a_0$ and an estimated value [based on the variation of μ with R for the Hartree-Fock (HF) wavefunction] of

$$\mu = 0.39 \pm 0.10 \text{ debye}$$

for the $v = 3$ level. Bergeman and Zare suggested two

possible explanations for the difficulty: (1) An R -dependent "dipole borrowing" from the D state that would come in differently with CI than for HF and (2) nonadiabatic coupling of the A and D states. They analyzed the second effect and found the correction to be small.

We felt that the theoretical results deserved re-evaluation and carried out extensive generalized valence bond [3] (GVB) and GVB CI calculations on the X state at R_e (2.1747 bohr) and the A and D states at R_e (2.0101 bohr). The results for the dipole moment are (all CI wavefunctions)

$$\begin{aligned} \mu &= -0.10 \text{ debye for } X^2\Pi, \\ \mu &= +1.36 \text{ debye for } A^2\Sigma, \\ \mu &= -2.21 \text{ debye for } D^2\Sigma. \end{aligned}$$

The value for the ground state is in good agreement with the experimental value $|\mu| = 0.16$ D [4] and the value for the A state is in reasonable agreement with the value obtained by Bergeman and Zare (especially considering that our value for μ should decrease in magnitude when averaged over the $v = 3$ vibrational level).

We find that the Hartree-Fock wavefunctions lead to a significant error (-0.67 D) in the dipole moment. The reason is as follows: (1) due to the doubly-occupied orbital restrictions of HF the π orbitals of the NO^+ core

* Partially supported by a grant (GP-40783X) from the National Science Foundation.

** NDEA Fellow, 1967-69, 1973-74.

[†] Contribution No. 5018.

tend to concentrate too much on the oxygen; (2) as a result the Rydberg orbital polarizes toward the N; however the resulting relatively small changes in the Rydberg orbital lead to large changes in the dipole moment. Correlating the NO bonds as in GVB removes this problem. The CI calculations of Green were based on HF wavefunctions and apparently sufficiently high orders of excitation to overcome the deficiencies of HF were not included.

Thus there is no reason to presume particularly large nonadiabatic corrections in the dipole moments for Rydberg excited states of molecules.

2. Theoretical details

We used three basis sets for these calculations. The first (32 basis functions) consisted of the "double zeta" (DZ) set of contracted cartesian gaussian functions of Dunning and Huzinaga [5], augmented by a set of d functions on the N and O (orbital exponents $\alpha_N = 0.80$ and $\alpha_O = 1.04$). This is the type of basis (denoted DZd) we would normally use for describing potential curves of valence states and it was used for the $X^2\Pi$ state. In order to describe the Rydberg states ($A^2\Sigma^+$ and $D^2\Sigma^+$), the DZd basis was augmented by diffuse s and p_o functions on the N and O (N exponents: $\alpha_s = 0.0650$ and 0.0198 , $\alpha_p = 0.0515$ and 0.0160 ; O exponents: $\alpha_s = 0.0862$ and 0.0261 , $\alpha_p = 0.0637$ and 0.0190). (The exponents for the diffuse functions were obtained by scaling down from the exponents of the valence primitives, a procedure that has worked well for the Rydberg states of a number of molecules [6-8].) This leads to a total of 40 basis functions for this second basis set (denoted as DZdR). As a check on the validity of our results for the A state we also carried out calculations using a more extensive basis set (denoted as Big) in which the (9s5p1d) primitive basis set was contracted to [5s, 3p, 1d] [5], and in addition to the diffuse functions of the DZdR set we added more diffuse s and p_z functions (N exponents $\alpha_s = 0.0060$ and $\alpha_p = 0.0050$; O exponents $\alpha_s = 0.0079$ and $\alpha_p = 0.0057$) and diffuse d functions ($2d_{z^2} - d_{x^2} - d_{y^2}$; N exponent $\alpha = 0.03$ and O exponent $\alpha = 0.04$). The Big basis involves 58 basis functions.

For each state we carried out self-consistent generalized valence bond (GVB) calculations followed by appropriate CI calculations. For the $A^2\Sigma$ state the

GVB wavefunction differs from the HF wavefunction by having the σ bond and each of the π bonds correlated [referred to as GVB(3/PP)]. Thus we solve for 11 orbitals self-consistently rather than eight as in HF. Since the orbitals are optimized for the dominant correlation effects, one can account for most of the residual correlation effects remaining in the GVB wavefunction by including other configurations involving the 11 GVB orbitals, rather than using the full basis (40 basis functions). To describe the D state we also included the 3p-like orbital obtained as the lowest variational orbital from the GVB variational solution of the $A^2\Sigma^+$ state (this leads to the optimum excited orbital for the D state within the restriction that the NO^+ core orbitals from the $A^2\Sigma^+$ state are not readjusted).

For the ground state wavefunction we carried out GVB(2/PP) calculations (splitting the σ and π_y bonds, with a singly-occupied π_x orbital in addition to the π_x bond pair) using the DZd basis. This procedure leads to different orbitals in the x and y directions. To generate an equivalent set for the CI calculations, we rotated the π_y correlating orbital and orthogonalized to the first two π_x orbitals. The resulting three orbitals were then used in both directions.

In the CI calculations we initially allowed only configurations involving excitations among the GVB orbitals. However, after preliminary calculations we found that a good description of the $^2\Pi$ state required additional configurations involving excitation from the GVB π orbitals into the remaining virtual orbitals of the π space. (These configurations were more important for the X state than for the excited states.) We also allowed up to double excitations from the GVB π orbitals into the four virtual orbitals of delta symmetry. This procedure yielded 202 spatial configurations (483 spin eigenfunctions or 908 determinants) for the $X^2\Pi$ state and 190 spatial configurations (532 spin eigenfunctions or 939 determinants) for the $^2\Sigma^+$ states (A and D).

The GVB calculations used the Bobrowicz-Wadt-Goddard program incorporating the full variational treatment of open shell systems [9] and the GVB variational methods [10]. The Caltech CI program (Bobrowicz, Winter, Ladner, Goddard, Hay, Moss, Walch, and Harding) was used for the CI calculations. The CI properties were evaluated with a program written by Walch and Dunning using the NYU (Moskowitz)

Table 1

Calculated and experimental properties for X, A, and D states of NO (in the DZd basis for X $^2\Pi$ and the DZdR basis for $^2\Sigma^+$ unless noted otherwise)

		X $^2\Pi$	A $^2\Sigma^+$	D $^2\Sigma^+$
Excitation energy (eV)				
	HF ^{a)}	0.0	5.45	(6.59) ^{g)}
	GVB	0.0	4.60 ^{b)}	(5.69) ^{g)}
	CI	0.0	5.05 ^{d)}	6.39 ^{d)}
	exper.	0.0	3.92	-
			5.42 ^{c,d)}	6.55 ^{c,d)}
Dipole moment (D)				
	HF	+0.36	+0.66	(-2.10)
			+0.74 ^{h)}	
	ref. [2]	+0.26	+0.63	-
	GVB	0.0	1.36	(-2.20)
			+1.41	
	CI	-0.10	+1.36	-2.21
	ref. [2]	-0.25	+0.39	-
	exper.	± 0.16 [4]	$\pm 1.10 \pm 0.03$ ^{e)}	-
Quadrupole coupling constants at N (MHz)				
eQ_Nq_N	HF	-1.79	-6.35	(-4.49)
			-5.29 ⁱ⁾	
	GVB	-1.20	-5.26	(-4.23)
			-4.27	
	CI	-1.10	-4.36	-4.38
	ref. [2]	-1.63	-5.62	-
	exper.	-1.876 ± 0.008 [4]	-2.88 ± 0.17 ^{e)}	-
$eQ_N\bar{q}_N$	HF	29.35		
	ref. [2]	21.03		
	GVB	21.75		
	CI	26.76		
	exper.	23.04 ± 0.05 [4]		

a) The calculated total energies for the X $^2\Pi$ state are -129.26934 H, -129.32614 H, and -129.43055 H for HF, GVB, and CI, respectively.

b) The Big basis leads to a drop in the energy of 0.206 eV for HF and 0.218 eV for GVB. This basis would also lead to a similar drop for $^2\Pi$ and hence little change in the excitation energy is expected.

c) Includes a correction of 0.03 eV for the difference in zero-point energies for the ground and Rydberg states. Excitation energies are taken from ref. [11].

d) The calculated oscillator strength (f) for A \leftrightarrow D is 0.324, the experimental value [13] is 0.18.

e) Ref. [1], this is for the $v = 3$ vibrational level.

f) Parentheses for an HF quantity indicate that the HF wavefunction was obtained by deleting the second natural orbitals of the GVB wavefunction.

g) Parentheses for a GVB quantity for the D state indicate that the core orbitals were restricted to be those of the A state.

h) Using the GVB wavefunction and the approximate HF-type wavefunction described in footnote f leads to +1.54 D.

i) Using the GVB wavefunction and the approximate HF-type wavefunction described in footnote f leads to -4.33 MHz.

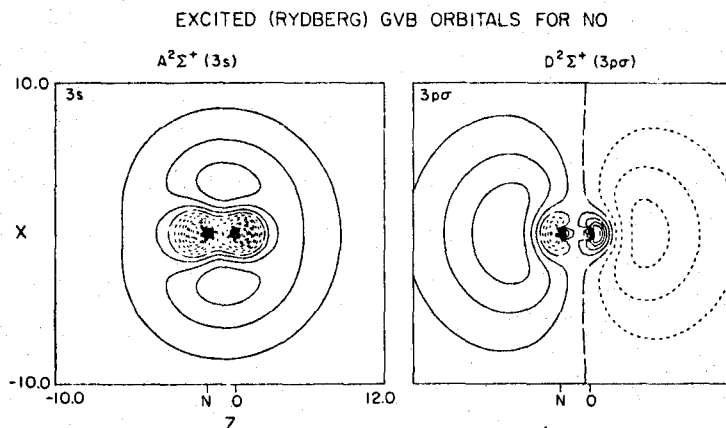


Fig. 1. The Rydberg orbitals from GVB wavefunctions of the $A^2\Sigma^+$ and $D^2\Sigma^+$ states of NO. The long dashes indicate nodal planes. Solid and dotted lines indicate positive and negative amplitudes. Contour intervals are 0.01 au.

integrals program. The molecular integrals were evaluated with a version of the POLYATOM (Basch and Snyder) integrals program.

3. Results and comparison with experiment

The calculated energies and properties are compared with experiment in table 1. The shapes of the excited orbitals for the A and D states of NO are shown in fig. 1 (using the DZdR basis). As expected, these orbitals have basically the character of 3s and 3p σ orbitals, respectively, and are well described as Rydberg orbitals. For simplicity we will refer to these self-consistent GVB orbitals as 3s and 3p σ .

3.1. Energies and oscillator strength

The calculated excitation energies (CI) are 5.05 eV for $A \leftarrow X$ and 6.39 eV for $D \leftarrow X$, which are 0.37 eV and 0.18 eV lower, respectively, than the experimental values [11] (errors of 7% and 3%, respectively).

The calculated bond dissociation energy D_e (NO) is 6.41 eV which is 97% of the experimental value[†] of 6.60 eV.

[†] We have taken the energies of the separated atoms as $O(^3P) = -74.80087$ H from a DZd HF calculation [12] and that for $N(^4S)$ as -54.39439 H [5] from a DZ HF calculation. [For the $N(^2S)$ state the d functions do not mix into the HF wavefunction.] The experimental dissociation energy $D(NO)$ was corrected for the zero-point vibrational energy $\frac{1}{2} h\nu_0$ for comparison with the calculated value.

We calculated the oscillator strength, f , only for $D \leftrightarrow A$. The result is $f = 0.324$ which is 80% larger than the experimental value of 0.18 from the $D^2\Sigma^+ \rightarrow A^2\Sigma^+$ 0-0 emission band [13].

3.2. Dipole moment

For the $X^2\Pi$ ground state, the calculated dipole moment is $\mu = -0.10$ D, whereas the experimental value [4] is $|\mu| = 0.159$ D. Thus, just as for CO [14], the ground state of NO has the electron charge distribution distorted slightly from the oxygen to the more electropositive element.

Using the DZdR basis we calculated a dipole moment for the $A^2\Sigma^+$ state of $\mu = 1.41$ D with GVB and $\mu = 1.36$ D with GVB CI while the Big basis yields $\mu = 1.36$ D for GVB. Thus our best estimate of the theoretical μ is

$$\mu = 1.31 \text{ D.}$$

The experimental value is $|\mu| = 1.10 \pm 0.03$ D for $v = 3$ [1]. The dipole moment is expected to decrease in magnitude for larger R and hence should decrease for larger v . Thus the calculated value is in reasonable agreement with experiment.

We find that the $D^2\Sigma^+$ state leads to $\mu = -2.21$ D, even larger in magnitude than for the A state but directed in the opposite direction. The reason for this oscillation is understood as follows.

From the GVB(3/PP) wavefunction for the $A^2\Sigma^+$ state, we find that the dipole moment of the NO^+ core (evaluated about the nitrogen) is +0.999 au (N^+O^+). Thus if the 3s or 3p σ orbitals of the Rydberg state were centered at +0.999 au (50% of the bond length) from the N (toward the O), the dipole moment would be zero. In fact the GVB 3s orbital is pulled significantly toward the O, leading to a total μ of 1.41 D (N^+O^-) [this corresponds to a centering of the 3s orbital at 1.553 a_0 (77% of the bond length) with respect to the N]. Since the GVB Rydberg orbital for the A state has a component of 3p σ character pushing it toward the O

$$\phi_{3s} + \lambda\phi_{3p\sigma},$$

the GVB Rydberg orbital for the D state is expected (and observed) to be pushed toward the N (see fig. 1)

$$\phi_{3p\sigma} - \lambda\phi_{3s}.$$

The center of charge of the GVB 3p σ orbital is at +0.119 a_0 (6% of the bond length) relative to the N, leading to a large dipole moment in the opposite direction (N^-O^+). This effect leads to wildly different dipole moments for alternate Rydberg states. Similar results were found earlier by Hunt and Goddard for I_2O [6] and can be expected to be general.

3.3. Quadrupole coupling constants

The experimental quadrupole coupling constant (at the nitrogen), denoted as eQ_Nq_N , is a measure of both the nuclear quadrupole moment, Q_N , and the electric field gradient,

$$q_N = 2\xi_0/R^3 - \langle \sum_i \{ (3z_i^2 - r_i^2)/r_i^5 \} \rangle_N \equiv F_{zz}$$

(coordinates centered at the N) where ξ_0 and R are the oxygen atom nuclear charge and NO bond distance, respectively. For the $^2\Pi$ state there is also a second (perpendicular) component $eQ\bar{q}_N$ where

$$\bar{q}_N = 9 \langle \sum_i \{ (x_i^2 - y_i^2)/r_i^5 \} \rangle \equiv 3(F_{xx} - F_{yy}).$$

Since only the product of Q and q is experimentally accessible, the values of Q must be obtained by comparison of calculated electric field gradients q and measured values of eQq . We chose $Q_N = 1.56 \times 10^{-26}$ cm², the value suggested by O'Konski and Ha [15] based on a comparison of HF values for q and experimental eQq

for a number of molecules. Using this value for Q , one atomic unit of field gradient results in an eQq of 3.6657 MHz.

The calculated CI values of eQq for the X and A states are off by -41% and +51% from the experimental values and the calculated $eQ\bar{q}$ of the X state is off by +16%. These are much larger errors than for the other properties (our value for eQq for the A state is somewhat better than the value obtained by Green, 95% error). One should bear in mind here that the basis set used was designed solely on the basis of energy considerations. This basis is, we believe, quite adequate for global properties such as the dipole moment but may be deficient for describing properties at the nucleus. For example, one should include high exponent d functions (and perhaps high exponent p functions) to describe polarization of the N 1s pair and in addition f functions could lead to changes in the field gradients due to the p-like orbitals.

4. Comparison of theoretical results

4.1. Energies

The energy of the $X^2\Pi$ and $A^2\Sigma$ states drops 1.55 eV and 2.45 eV, respectively, in going from HF to GVB and drops an additional 2.84 and 2.39 eV, respectively, in going to the CI wavefunction. The net result is that the HF excitation energy is 0.03 eV above the experimental value while the CI result is 0.37 eV below experiment. We believe that the good result obtained here for HF is accidental.

Generally for excitation of a doubly-occupied valence orbital to a Rydberg orbital, HF leads to an excitation energy too small by ≈ 1 eV, corresponding to the correlation error of a valence pair. In NO the $A \leftrightarrow X$ excitation is out of a singly-occupied orbital and the above argument does not apply. However relaxing the spin restriction on the HF wavefunction of the $^2\Pi$ state leads to a decrease in the energy of 0.41 eV hence an increase in the excitation energy to 5.91 eV. Such a value, larger than experiment, is reasonable since the correlation error in the π_x pair is expected to be greater in the $^2\Sigma$ state than in the $^2\Pi_x$ states (where there is also a singly-occupied $2\pi_x$ orbital). The GVB(PP) wavefunction leads then to too small a value because this pair is still uncorrelated in the $^2\Pi$ state although correlated in the $^2\Sigma$ state.

Green obtained an HF excitation energy of 5.23 eV in reasonable agreement with our value; however, his CI wavefunctions led to an excitation energy 1.50 eV lower than experiment and 1.13 eV lower than for our wavefunction. As expected, we find that the A state has more correlation energy than the X state (4.84 eV and 4.39 eV, respectively, within the restriction that the 1s and 2s pairs remain uncorrelated). However in our CI for the X state, 25 configurations produce CI lowerings greater than 0.001 H, whereas for the A state only nine do. Thus the correlation energy for the X state is more difficult to describe in the CI and we suspect that the low excitation energy obtained by Green may be a result of using too restrictive a set of configurations.

4.2. Dipole moment

For the X state the dipole moments for the HF, GVB, and CI wavefunctions are +0.36 D, 0.00 D, and -0.10 D. Thus just as for CO the HF wavefunction leads to a dipole moment with the extra charge on the more electro-negative member while the CI wavefunctions reverse the sign. For NO the principal effect of electron correlation on the dipole moment is a decrease in the contribution of the π_y pair (-0.592 debye) partially balanced by an increased contribution due to the three electrons in the π_x orbitals (+0.183 debye).

For the A state the HF, GVB, and CI wavefunctions lead to $\mu = +0.74$ D, +1.41 D, and +1.36 D, respectively, for the DZdR basis and $\mu = 0.66$ D and +1.36 D for the HF and GVB wavefunctions with the Big basis. Thus the HF wavefunction leads to a small dipole moment in agreement with the value reported by Green (0.63 D with optimized exponents). However, when simple correlation effects are included within the positive ion core, we find significant changes, resulting in a calculated dipole moment in reasonable agreement with the experimental value.

As expected, the primary effect of correlation is a decrease in the ionic character of the core (NO^+) orbitals. (The dipole moment contribution of the core decreases by 0.398 D.) However, the resultant flow of charge from O to N in the core results in a large shift of the Rydberg orbital toward O, leading to an increased contribution for the Rydberg orbital of 1.098 D. Thus the HF wavefunction, which neglects these important correlation effects, leads to a low dipole moment.

For the GVB wavefunction, since the orbitals are solved for with the dominant correlation effects already present, only a small CI necessary to account for the remaining small effects and the CI dipole moment is little changed from the GVB value. On the other hand, for the HF wavefunction a rather extensive CI is necessary to allow correlation of the core orbitals and simultaneous reoptimization of the Rydberg orbital.

Green carried out restricted Hartree-Fock calculations, constructed a limited CI expansion, and carried out iterative natural orbital calculations to obtain the optimum orbitals. Since Green reports that the dipole moment *decreased* with CI, it would appear that the configurations selected described the correlation of the core, but were not sufficiently flexible to allow simultaneous readjustment of the 3s orbitals.

As a further check on the validity of our results for the A state, we repeated the HF and GVB calculations with the more extensive Big basis set. With the Big basis we obtain $\mu = +0.66$ D and +1.36 D for the HF and GVB(3/PP) wavefunctions, respectively, in good agreement with the results for the smaller basis (and in slightly better agreement with experiment).

4.3. The electric field gradients

For the ground state we find a large change in the electric field gradient between HF and GVB while the GVB and CI values are similar. The change of this property upon correlation is essentially related to the shift of the π_y pair toward the N (which also led to a significant decrease in the dipole moment).

Our value for q of the A state is closer to experiment than Green's values (41% error as compared with 95%). For the X state properties our values are in poorer agreement with experiment. It is likely that high exponent d functions are needed to obtain a good description of the field gradients [16].

5. Conclusion

We find that the GVB procedure of solving for the optimum orbitals with the dominant correlation terms present allows a good description of the energies and properties of both the valence and Rydberg states of NO. As a result the additional correlation effects are

small and the properties of the states can be interpreted in terms of the simple orbital description of GVB.

Acknowledgement

We thank Professor R.N. Zare for bringing to our attention the disagreement between the theoretical and experimental values of μ for the A state of NO.

References

- [1] T. Bergeman and R.N. Zare, *J. Chem. Phys.*, to be published.
- [2] S. Green, *Chem. Phys. Letters* 13 (1972) 552; 23 (1973) 115.
- [3] W.A. Goddard III, T.H. Dunning Jr., W.J. Hunt and P.J. Hay, *Accounts Chem. Res.* 6 (1973) 368, and references therein.
- [4] R.M. Neumann, *Astrophys. J.* 161 (1970) 779.
- [5] T.H. Dunning Jr., *J. Chem. Phys.* 53 (1970) 2823.
- [6] W.J. Hunt and W.A. Goddard III, *Chem. Phys. Letters* 3 (1969) 414; W.A. Goddard III and W.J. Hunt, *Chem. Phys. Letters* 24 (1974) 464.
- [7] D.C. Cartwright, W.J. Hunt, W. Williams, S. Trajmar and W.A. Goddard III, *Phys. Rev. A* 8 (1973) 2436.
- [8] W.J. Hunt, Ph.D. Thesis, California Institute of Technology, September 1971.
- [9] W.J. Hunt, W.A. Goddard III and T.H. Dunning Jr., *Chem. Phys. Letters* 6 (1970) 147.
- [10] W.J. Hunt, P.J. Hay and W.A. Goddard III, *J. Chem. Phys.* 57 (1972) 738.
- [11] B. Rosen, in: *Tables of constants and numerical data*, ed. S. Bourcier (Pergamon Press, London, 1970).
- [12] W.A. Goddard III, P.J. Hay and T.H. Dunning Jr., *J. Am. Chem. Soc.*, submitted for publication.
- [13] K.L. Wray, *J. Quant. Spectry. Radiative Transfer* 9 (1969) 255.
- [14] F. Grimaldi, A. Lecourt and C. Moser, *Intern. J. Quantum Chem.* 1S (1967) 153.
- [15] C.T. O'Konski and T.-K. Ha, *J. Chem. Phys.* 49 (1968) 5354.
- [16] P.J. Hay and W.A. Goddard III, *Chem. Phys. Letters* 9 (1971) 356.